DEVELOPMENT OF SELF-ADAPTIVE PVD COATINGS FOR MACHINING TI6AL4V ALLOY

DEVELOPMENT OF SELF-ADAPTIVE PVD COATINGS FOR MACHINING TI6AL4V ALLOY

By

MOHAMMAD SHARIFUL ISLAM CHOWDHURY

B.Sc., M.Sc., M.A.Sc.

A Thesis Submitted to the School of Graduate Studies in Partial Fulfilment of the Requirements for the Degree Doctor of Philosophy

DOCTOR OF PHILOSOPHY (2021) McMaster University

(Mechanical Engineering) Hamilton, Ontario

TITLE	Development of self-adaptive PVD coatings for machining Ti6Al4V alloy
AUTHOR	Mohammad Shariful Islam Chowdhury, B.Sc., M.Sc., M.A.Sc.
SUPERVISOR	Dr. Stephen C. Veldhuis Department of Mechanical Engineering
SUPERVISORY COMITTEE	Dr. Tohid Didar Department of Mechanical Engineering
	Dr. Nabil Bassim Department of Materials Science and Engineering
Page Count	xx, 202

To my wife, children, parents, and sister, for their unconditional love and support. I am truly thankful for having you all in my life.

Acknowledgements

First and foremost, I would like to express my deepest gratitude to my supervisor, Dr. Stephen C. Veldhuis. I am thankful to him for giving me the opportunity to be a part of the McMaster Manufacturing Research Institute (MMRI). Without his continuous guidance and support, helpful suggestions, and supervision, this research work would not be possible. I am also grateful to my committee members, Dr. Tohid Didar and Dr. Nabil Bassim for their valuable comments and advice throughout this research work.

I need to thank all my mentors, friends, and colleagues at the McMaster Manufacturing Research Institute (MMRI), especially Dr. Bipasha Bose, Dr. German Fox-Rabinovich, Dr. Abul Fazal Arif, and Dr. Sushant Rawal, for their continuous support and guidance along the journey. I would also like to extend my special thanks to Dr. Kenji Yamamoto, Senior Researcher at Kobe Steel Ltd., for all his help and suggestions with the coating selection. I feel extremely fortunate to have worked alongside so many talented and amazing individuals, and I will always cherish the knowledge, experience, and memories I have gained at the MMRI over the years.

Finally, I thank my wife, Sadeka, my children, Aayan and Aafreen, and my family for their understanding, patience, and support. None of this would have been possible without their endless love, sacrifice, and support over the years.

I also acknowledge that this research was supported by the Natural Sciences and Engineering Research Council of Canada (NSERC) under the CANRIMT Strategic Research Network Grant NETGP 479639-15.

Although I have completed this thesis paper to the best of my ability, I acknowledge the possibility that it may contain mistakes and ask the reader to excuse any they may find.

Lay Abstract

Titanium alloys are increasingly becoming the material of choice for many industrial applications due to their superior properties. However, they are very difficult to machine since they have high chemical affinity towards tool materials, low thermal conductivity, and high temperature strength. These properties cause rapid failure of the tool. The objective of the current research is to address machinability issues during Ti6Al4V machining and improve tool performance. One effective strategy to minimize tool wear is to apply self-adaptive PVD tool coatings that can form beneficial tribo-films through their interaction with the environment and provide enhanced lubricity, hardness, strength, and thermal barrier characteristics to the cutting tool. In the current research, two self-adaptive PVD coatings were developed that offset the dominant tool wear mechanisms prevalent during the rough and finish turning of Ti6Al4V alloy and reduced the tool wear rate by more than 60% compared to the current industrial standard.

Abstract

The usage of titanium alloys in many industries has increased significantly over the years due to their superior properties. However, they are extremely difficult to machine because of their distinctive characteristics such as their high temperature strength, low thermal conductivity, and high chemical affinity for tool materials. Hence, despite their increased usage, they are still expensive to machine when compared to other metals.

The current research aims to address the machinability issues of titanium alloys by developing novel compositions of a new generation of self-adaptive Physical Vapor Deposition (PVD) coatings that function by forming beneficial tribo-films through their interaction with the environment. These tribo-films form during cutting and provide enhanced lubricity, hardness, strength, and thermal barrier characteristics to the cutting tool. It was found that during Ti6Al4V machining, significant BUE and crater wear formation occurs; however, one is dominant over the other depending on the cutting conditions. Therefore, the coatings investigated were designed by taking into consideration the dominant tool wear mechanisms and the complex tribological phenomena that occur in the cutting zone.

The current research investigated monolayer TiB_2 and CrN self-adaptive PVD coatings for the rough (cutting speed - 45 m/min, feed -0.15 mm/rev, and depth of cut – 2 mm) and finish (cutting speed - 150 m/min, feed -0.1225 mm/rev, and depth of cut – 0.25 mm) turning of Ti6Al4V alloy. Detailed experimental studies were performed to study the

effectiveness of the coatings during machining. Micro-mechanical characteristics of the coatings were also studied to understand how coating properties affect the coatings performance in machining and tribo-film formation. The results obtained show that both the TiB_2 and CrN coatings significantly improve tool performance during the rough turning of Ti6Al4V alloy compared to the current industrial standard, which is due to certain micro-mechanical coating properties and the beneficial tribo-films formed. A coating of CrN coating was found to increase tool life during finish turning. It was also established that for machining applications where intensive adhesive interaction occurs at the tool-chip interface, coatings with lower hardness values perform significantly better than harder ones.

Table of Contents

Lay Abstract v
Abstract vi
Table of Contents vii
List of Figures ix
List of Tables xii
Abbreviations xiii
Chapter 1. Introduction 1
1.1. Background 1
1.2. Literature Review 2
1.2.1. Machining 2
1.2.2. Tool wear and tool wear mechanisms 3
1.2.3. Cutting tool coatings 7
1.2.3.1 PVD Coatings 8
1.2.4. Titanium alloys 9
1.2.4.1 Machinability issues of titanium alloys 10
1.2.4.2 Cutting tools and substrate material 13
1.2.4.3 Wear mechanisms of cemented carbide tools in titanium machining 15
1.2.4.4 Application of coated carbide tools in titanium machining 17
1.3. Research Gaps 19
1.4. Motivation and Research Objectives 20
1.5. Thesis Organization 21
1.6. Note to Reader 25
1.7. References 26
Chapter 2. Development of Coating for Finish Turning Operation 32
2.1. Introduction 34
2.2. Experimental Details 35
2.2.1. Coating deposition 35

2.2.2. Coating characterization 36
2.2.3. Machining studies 39
2.3. Results and discussion 40
2.3.1. Structural and mechanical properties of the coatings 40
2.3.2. Tool wear studies 45
2.3.3. Tribological analysis 49
2.4. Conclusions 54
2.5. References 55
Chapter 3. Development of Coating for Rough Turning Operation 61
3.1. Introduction 63
3.2. Experimental Methods 66
3.2.1. Coating Deposition and Characterization 66
3.2.2. Cutting Tests and Chip Morphology Analysis 70
3.3. Results and Discussions 72
3.3.1. Tool Wear Performance Studies 72
3.3.2. Coating Characterization 76
3.3.3. Assessment of Tribological Performance 82
3.4. Conclusions 87
3.5. References 88
Chapter 4. Effect of Coating Hardness and Thickness 95
4.1. Introduction 97
4.2. Experimental Procedure 99
4.2.1. Coating Deposition and Characterization Analyses 99
4.2.2. Experimental Setup and Tool Wear Analyses 103
4.3. Results and Discussions 105
4.3.1. Machining Performance Analysis 105
4.3.2. Coating Characterization 110
4.4. Conclusions 125

4.5. References 127
Chapter 5. Conclusions and Future Work 134
5.1. General Conclusion 134
5.2. Research Contributions 137
5.3. Recommendations for Future Research 139
Appendix A: Tool Wear Mechanism During Rough and Finish Turning of Ti6Al4V Alloy 142
A.1. Preface 142
A.2. Part A: Wear performance of TiB_2 coated carbide tools under varying machining conditions of TiAl6V4 alloy 144
A.2.1 Finite Element Process Modeling 144
A.2.2 Experimental Procedure 148
A.2.3 Results and discussion 151
A.2.3.1 Rough turning operation at low speed 151
A.2.3.2 Finish turning operation. 155
A.2.4 Conclusions 161
A.3. Part B: Comparison of wear performance of TiB_2 and CrN coated carbide tools 162
A.3.1 Tool wear performance 162
A.3.2 Tribo-film formation and coating characterization 165
A.3.3 Conclusions 170
A.4. References 171
Appendix B: Effect of Deposition Parameters on CrN Coating Properties and Performance. 174
B.1. Preface 174
B.2. Experimental Details 175
B.3. Results and Discussions 177
B.3.1 Tool Wear performance studies 177
B.3.1.1 Tuning of Nitrogen Gas pressure 177

B.3.1.2 Tuning of bias voltage 181
B.3.1.3 Tuning of coating thickness 184
B.3.2 Coating Characterization 187
B.4. Conclusions 200
B.5. References 201

List of Figures

Figure 1.1. Cross-sectional view of the machining process. 3
Figure 1.2. Types of tool wear [based on [10]]. 4
Figure 1.3. Typical stages in flank wear 5
Figure 1.4. Flank wear and crater wear definition [based on [12]]. 5
Figure 1.5. Causes of tool wear in cutting operations [based on [13]. 7
Figure 2.1. SEM images of fracture sections of coatings: a) AlTiN; b) CrN. 41
Figure 2.2. XRD data of monolayer CrN coating. 42
Figure 2.3. Scratch track data for AlTiN coating. 43
Figure 2.4. Scratch track data for CrN coating. 44
Figure 2.5. Flank wear vs. length of cut data under wet conditions at 150 m/min for coated and uncoated tools. 45
Figure 2.6. 3D progressive wear data for uncoated tool after every 600 m length of cut: (a) 600 m; (b) 1200 m; (c) 1800 m; (d) 2400 m. 46
Figure 2.7. 3D progressive wear data for CrN coated tool after every 600 m length of cut: (a) 600 m; (b) 1200 m; (c) 1800 m; (d) 2400 m. 47
Figure 2.8. Built up volume for coated and uncoated tools considering the peaks above reference surface of the original tool. 48
Figure 2.9. Crater wear volume for coated and uncoated tools considering the peaks below reference surface of the original tool. 48
Figure 2.10. High resolution XPS data of worn rake surface of CrN coated insert, Cr2p spectrum. 51
Figure 2.11. Coefficient of friction, shear strength and normal contact stress vs. temperature data for uncoated and coated tools. 52
Figure 2.12. EBSD analysis of chip cross section showing orientation and phase map: (a) AlTiN; (b) CrN. 53
Figure 3.1. Experimental setup for turning operation. 71
Figure 3.2. Flank wear vs. length of cut data of wet rough turning for uncoated, AlTiN and CrN coated tools showing significant tool life improvement for CrN coated tool. 73
Figure 3.3. 3D progressive wear data for uncoated tool highlighting progression of built up layer and crater wear after different length of cut: (a) 600 m; (b) 1200 m; (c) 1800 m. ... 74
Figure 3.4. 3D progressive wear data for AlTiN coated tool highlighting progression of built up layer and crater wear after different length of cut: (a) 600 m; (b) 1200 m; (c) 1800 m. 74
Figure 3.5. 3D progressive wear data for CrN coated tool highlighting progression of built up layer and crater wear after different length of cut: (a) 600 m; (b) 1200 m; (c) 1800 m. 75

Figure 3.6. Built up volume progression vs. length of cut for uncoated, AlTiN and CrN coated tools considering the peaks above reference surface of the original tool. 75
Figure 3.7. Crater wear volume progression vs. length of cut for uncoated, AlTiN and CrN coated tools considering the peaks below reference surface of the original tool. 75
Figure 3.8. SEM images of fracture sections of the studied PVD coatings highlighting coating thickness: (a) AlTiN; (b) CrN. 77
Figure 3.9. X-ray diffraction patterns of monolayered AlTiN and CrN coatings. 78
Figure 3.10. X-ray diffraction patterns of monolayered AlTiN and CrN coatings. 78
Figure 3.11. Atomic force microscope (AFM) images of surface topography of the coatings with arithmetic mean height (Sa) values: (a) AlTiN; (b) CrN. 81
Figure 3.12. Evolution of coefficient of friction at different passes during repetitive wear test at 0.75 N for AlTiN and CrN coatings. 81
Figure 3.13. Optical images of the ramped load scratch test track with coefficient of friction and acoustic emission data for the AlTiN coating. 82
Figure 3.14. Optical images of the ramped load scratch test track with coefficient of friction and acoustic emission data for the CrN coating. 82
Figure 3.15. Coefficient of friction vs. temperature data for uncoated, AlTiN and CrN coated tools obtained from high temperature/heavy load tribometer. 84
Figure 3.16. High resolution XPS data (Cr 2p spectrum) of worn rake surface of CrN coated insert confirming formation of Cr_2O_3 tribo-oxides. 85
Figure 3.17. EBSD orientation, chip cross sections and phase map of chip cross sections: (a) AlTiN; (b) CrN. 86
Figure 4.1. Flank wear vs. cutting length data for the three TiB_2 coatings during wet rough turning of Ti6Al4V alloy. 105
Figure 4.2. 3D progressive wear difference measurement of the coated tools highlighting evolution of built-up layer and crater wear during machining. 108
Figure 4.3. Built-up volume progression vs length of cut for the three TiB_2 coated tools considering the peaks above reference surface of the original tool. 108
Figure 4.4. Crater wear volume progression vs length of cut for the three TiB_2 coated tools considering the peaks below reference surface of the original tool. 109
Figure 4.5. Variation of cutting forces for the three TiB_2 coated tools. 109
Figure 4.6. X-ray diffraction patterns of the three TiB_2 coatings. 111
Figure 4.7. SEM surface morphology of the three TiB_2 coatings: (a,c,e) at low magnification, (b,d,f) at high magnification. 113
Figure 4.8. SEM images of FIB cross-sections of the three TiB_2 coatings showing coating thickness and structure: (a,c,e) at low magnification, (b,d,f) at high magnification. 114
Figure 4.9. AFM images of surface topography and column boundaries of the different TiB_2 coatings with arithmetic mean height (S_a) values. 115

Figure 4.10. Ramped load scratch test data with optical images of the scratch track for Coating A. 119
Figure 4.11. Ramped load scratch test data with optical images of the scratch track for Coating B. 119
Figure 4.12. Ramped load scratch test data with optical images of the scratch track for Coating C. 119
Figure 4.13. Evolution of coefficient of friction at different passes during repetitive wear test at 0.75 N for the three TiB_2 coatings after: (a) 1 pass, (b) 3 passes and (c) 5 passes. 120
Figure 4.14. SEM images of Vickers indentation and cracks of the three TiB_2 coatings from modified Palmqvist toughness test: (a,c,e) SE images, (b,d,f) BSE images. 122
Figure 4.15. First 150 s depth of penetration obtained from nano-impact testing at a load of 20 mN for the TiB_2 coatings. 123
Figure 4.16. Temperature dependent data of (a) thermal diffusivity and (b) thermal conductivity for the three TiB_2 coatings. 123
Figure 4.17. High resolution XPS data (B 1s spectrum) of worn rake surface of the three TiB_2 coatings confirming B_2O_3 tribo-oxide formation. 124
Figure A.1. FEM temperature profile at: a) 45 m/min and b) 150 m/min. 147
Figure A.2. Flank wear data vs. length of cut for the uncoated and TiB_2 coating carbide turning inserts with SEM images of the worn surface (after length of cut of 4000 m). .. 152
Figure A.3. HR XPS data on the worn rake (a,b) and flank surfaces (c) after rough turning of Ti6Al4V alloy: (a) Ti2p;(b,c) B1s spectra. 153
Figure A.4. Coefficient of friction vs. temperature data for the uncoated and TiB_2 coated inserts: (1) uncoated; (2) TiB_2 coated. 154
Figure A.5. Flank wear data vs. length of cut for the uncoated and TiB_2 coated carbide turning inserts under finishing operations at 150 m/min. 155
Figure A.6. 3D progressive wear volume data on uncoated (a–d) and TiB_2-coated (e–h) inserts, finish turning at 150 m/min. (a,e) 600 m length of cut; (b,f) 1200 m length of cut; (c,g) 1800 m length of cut; (d,h) 2400 m length of cut. 156
Figure A.7. Numerical data on the volumetric 3D wear measurement for uncoated and TiB_2 coated inserts, finish turning at 150 m/min: a) rake surface square covered by buildup; b) volumetric 3D wear data. 157
Figure A.8. SEM images of the Coated tool worn surface at 150 m/min. 158
Figure A.9. HR XPS data on the worn surfaces after finish turning of TiAl6V4 alloy (cutting edge area) at 150 m/min: (a,b) Ti2p spectra at rake and flank surface respectively, and (c,d) O1s spectra at rake and flank surface respectively. 159
Figure A.10. Chip undersurface morphology evaluated by Alicona 3D microscope: a) uncoated; b) TiB_2 coated and c) surface roughness values, (μm). 160

Figure A.11. Flank wear vs. cutting length data during the wet rough turning of Ti6Al4V alloy.....163
Figure A.12. 3D progressive wear difference measurement of the uncoated and coated tools, highlighting evolution of built-up layer and crater wear during the rough turning of Ti6Al4V alloy. 164
Figure A.13. Flank wear vs. cutting length data during the wet finish turning of Ti6Al4V alloy.....164
Figure A.14. 3D progressive wear difference measurement of the uncoated and coated tools, highlighting evolution of built-up layer and crater wear during the finish turning of Ti6Al4V alloy. 165
Figure A.15. Coefficient of friction vs. temperature data for uncoated, TiB_2, and CrN coated tools. 167
Figure A.16. Optical images of the ramped load scratch test track with coefficient of friction and acoustic emission data for the AlTiN coating 168
Figure A.17. Optical images of the ramped load scratch test track with coefficient of friction and acoustic emission data for the TiB_2 coating 168
Figure A.18. Optical images of the ramped load scratch test track with coefficient of friction and acoustic emission data for the CrN coating.....169
Figure B.1. Flank wear vs. cutting length data during the wet finish turning of Ti6Al4V alloy with a CrN coating deposited under varying nitrogen gas pressures. 178
Figure B.2. 3D progressive wear difference measurement of the CrN coated tools deposited under varying nitrogen gas pressures, highlighting the evolution of built−up layers and crater wear during machining. 179
Figure B.3. Built up volume progression vs. length of cut for the CrN coated tools deposited under varying nitrogen gas pressures, considering the peaks above the reference surface of the original tool. 180
Figure B.4. Crater wear volume progression vs. length of cut for the CrN coated tools deposited under varying nitrogen gas pressures, considering the peaks below the reference surface of the original tool. 180
Figure B.5. Flank wear vs. cutting length data during the wet finish turning of Ti6Al4V alloy with a CrN coating deposited under varying bias voltages.....181
Figure B.6. 3D progressive wear difference measurement of the CrN coated tools deposited under varying bias voltages, highlighting the evolution of built−up layers and crater wear during machining. 182
Figure B.7. Built up volume progression vs. length of cut for the CrN coated tools deposited under varying bias voltages, considering the peaks above the reference surface of the original tool. 183

Figure B.8. Crater wear volume progression vs. length of cut for the CrN coated tools deposited under varying bias voltages, considering the peaks below the reference surface of the original tool. 183
Figure B.9. Flank wear vs. cutting length data during the wet finish turning of Ti6Al4V alloy with a CrN coating deposited with varying coating thicknesses. 184
Figure B.10. 3D progressive wear difference measurement of the CrN coated tools deposited with varying coating thicknesses, highlighting the evolution of built−up layer and crater wear during machining. 185
Figure B.11. Built up volume progression vs. length of cut for the CrN coated tools deposited with varying coating thicknesses, considering the peaks above the reference surface of the original tool. 186
Figure B.12. Crater wear volume progression vs. length of cut for the CrN coated tools deposited with varying coating thicknesses, considering the peaks below the reference surface of the original tool. 186
Figure B.13. Variation of micromechanical properties of the CrN coatings deposited with varying nitrogen gas pressure: (a) hardness, (b) elastic modulus, (c) plasticity index, (d) H/E ratio, and (e) H^3/E^2 ratio. 189
Figure B.14. Variation of micromechanical properties of the CrN coatings deposited with varying bias voltage: (a) hardness, (b) elastic modulus, (c) plasticity index, (d) H/E ratio, and (e) H^3/E^2 ratio. 190
Figure B.15. Variation of micromechanical properties of the CrN coatings deposited with varying coating thickness: (a) hardness, (b) elastic modulus, (c) plasticity index, (d) H/E ratio, and (e) H^3/E^2 ratio. 191
Figure B.16. Variation of yield stress of the CrN coatings deposited with varying: (a) nitrogen gas pressure, (b) bias voltage, and (c) coating thickness. 192
Figure B.17. Micro-scratch test data with optical images of the scratch track for CrN coating deposited at 1.33 Pa nitrogen gas pressure, -50 V bias voltage and with approximately 1.8 µm coating thickness. 194
Figure B.18. Micro-scratch test data with optical images of the scratch track for CrN coating deposited at 4 Pa nitrogen gas pressure, -50 V bias voltage and with 1.81 µm coating thickness. 195
Figure B.19. Micro-scratch test data with optical images of the scratch track for CrN coating deposited at 5.5 Pa nitrogen gas pressure, -50 V bias voltage and with approximately 1.8 µm coating thickness. 195
Figure B.20. Micro-scratch test data with optical images of the scratch track for CrN coating deposited at -20 V bias voltage, 4 Pa nitrogen gas pressure and with approximately 1.8 µm coating thickness 196

Figure B.21. Micro-scratch test data with optical images of the scratch track for CrN coating deposited at -50 V bias voltage, 4 Pa nitrogen gas pressure and with 1.81 µm coating thickness. 196
Figure B.22. Micro-scratch test data with optical images of the scratch track for CrN coating deposited at -100 V bias voltage, 4 Pa nitrogen gas pressure and with approximately 1.8 µm coating thickness. 197
Figure B.23. Micro-scratch test data with optical images of the scratch track for CrN coating deposited at -150 V bias voltage, 4 Pa nitrogen gas pressure and with approximately 1.8 µm coating thickness. 197
Figure B.24. Micro-scratch test data with optical images of the scratch track for CrN coating deposited with 1.21 µm coating thickness at 4 Pa nitrogen gas pressure and -20 V bias voltage. 198
Figure B.25. Micro-scratch test data with optical images of the scratch track for CrN coating deposited with 1.81 µm coating thickness at 4 Pa nitrogen gas pressure and -20 V bias voltage. 198
Figure B.26. Micro-scratch test data with optical images of the scratch track for CrN coating deposited with 5.74 µm coating thickness at 4 Pa nitrogen gas pressure and -20 V bias voltage. 199
Figure B.27. Micro-scratch test data with optical images of the scratch track for CrN coating deposited with 7.52 µm coating thickness at 4 Pa nitrogen gas pressure and -20 V bias voltage. 199

List of tables

Table 2.1. Cutting data for the experiments performed. 40
Table 2.2. Micro-mechanical properties of the coatings. 42
Table 2.3. Tribological performance evaluated through chip characteristics. 53
Table 3.1. Cutting parameters for machining of Ti6Al4V alloy. 71
Table 3.1. Micromechanical properties of AlTiN and CrN coatings. 77
Table 3.3. Tribological performance evaluation through chip characteristics for AlTiN and CrN coatings. 84
Table 4.1. Micro-mechanical properties of the three monolayer TiB_2 coatings. 100
Table 4.2. Cutting parameters for machining of Ti6Al4V alloy. 104
Table 4.3. Tribological performance evaluated through chip characteristics for the TiB_2 coatings. 109
Table 4.4. Critical load for crack initiation in coating, LC_1 and critical load for coating failure, LC_2 obtained from ramped load scratch test for the three TiB_2 coatings. 120
Table 4.5. Relative percentages of the B_2O_3 phase present on the rake surface of the three TiB_2 coated tools after approximately 100 m cut obtained from High Resolution XPS. 125
Table A.1. Workpiece, tool and coolant material properties and cutting contact conditions [10-12]. 145
Table A.2. Cutting data for the experiments performed. 147
Table A.3. Properties of the TiB_2 coating [1]. 148
Table A.4. Coating properties of the three coatings. 169
Table B.1. Variation of deposition parameters. 175
Table B.2. Cutting data for the experiments performed. 176
Table B.3. Critical loads, LC_1 and LC_2, obtained from micro- scratch test for the coatings. 194

Abbreviations

BUE	Built up edge
CVD	Chemical vapor deposition
FC	Fine cathode
FIB	Focused ion beam
MQL	Minimum quantity lubrication
PVD	Physical vapor deposition
SEM	Scanning electron microscopy
SFC	Super fine cathode
WC	Tungsten carbide
XRD	X-Ray diffraction
XPS	X-Ray photoelectron spectroscopy

Chapter 1. Introduction

1.1. Background

Over the years, the use of titanium and its alloys has increased significantly in various industries. Titanium alloys possess a unique combination of mechanical and chemical properties (high ductility, excellent toughness and corrosion resistance, high-temperature strength, good strength-to-weight ratio, etc.) that make them suitable for many industrial applications especially for aerospace and automobile industries [1-5]. However, they are extremely difficult to cut due to certain distinctive characteristics such as high temperature strength, low thermal conductivity and high chemical affinity for tool materials, low modulus of elasticity, etc. Researchers have yet to find an effective strategy to overcome these challenges and improve the tool life during the machining of titanium alloys. As a result, the costs of finished titanium products are high, limiting the use of titanium despite its beneficial characteristics.

For nearly all machining applications, tool coatings are applied that have been demonstrated to reduce tool wear rates and improve productivity. For this reason, almost 80% of all tools used for machining are coated tools. However, for titanium machining, coatings have yet to achieve the desired success. In many cases, coated tools perform worse than straight grade cemented carbides, thereby making straight grade carbides the preferable choice for titanium machining [6]. However, coating deposition technologies have advanced considerably in recent years, and with a better understanding of the unique

tribological requirements of machining titanium, new coating designs are now being proposed [7].

Current research aims to develop novel compositions of adaptive Physical Vapor Deposition (PVD) coatings for turning of TiAl6V4 alloys, thereby reducing production cost, and improving product quality. The focus is on a new generation of self-lubricating and self-adaptive PVD coating designs to address the machinability issues of titanium alloy machining. Self-lubricating or self-adaptive coatings function by forming beneficial tribo-films through interaction with their environment. The coating system reacts with elements from the environment (mostly oxygen) to form lubricating films or tribo-ceramics with enhanced hardness, strength, and thermal barrier characteristics [8]. Selection of coatings should be made, however, considering the tribological compatibility of the tool and the workpiece and the local conditions of heavy load and high temperature under which they are operating. Typically, cemented carbide tools face rapid tool wear during machining due to high heat generation, poor thermal conductivity, and high chemical affinity of titanium. Both crater wear and flank wear are observed with intensive built-up edge formation. However, the severity and rate of these cutting phenomena vary widely based on machining conditions spanning roughing and finishing operations.

1.2. Literature Review

1.2.1. Machining

Machining or metal cutting refers to numerous controlled metal removal processes that remove unwanted material in the form of chips from a given block of metal to attain

the desired geometry. Turning, milling, and drilling are the most common machining operations. Figure 1.1 shows a cross-sectional view of the machining process. In the present research, turning operations were used. Turning refers to the machining operation that produces cylindrical parts by feeding a single-point cutting tool into a rotating workpiece.

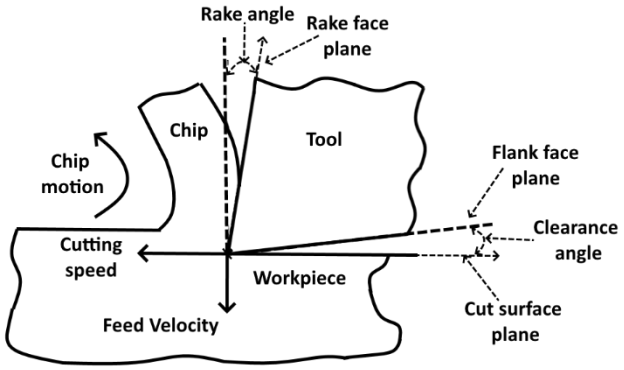

Figure 1.1. *Cross-sectional view of the machining process.*

1.2.2. Tool wear and tool wear mechanisms

Tool wear refers to the change of the shape of a tool from its original shape due to the gradual loss of tool material or deformation of the tool during cutting [9]. Tool wear is inevitable in all machining processes. It adversely affects product quality, dimensional accuracy, and overall productivity. So, it is of utmost importance to reduce tool wear in any machining process.

According to the ISO standard 3685:1993 [10], there are multiple types of wear namely flank wear, crater wear, built up edge (BUE) formation, notch wear, plastic deformation, thermal and mechanical fatigue, chipping and fracture. The most important wear types are flank wear and crater wear.

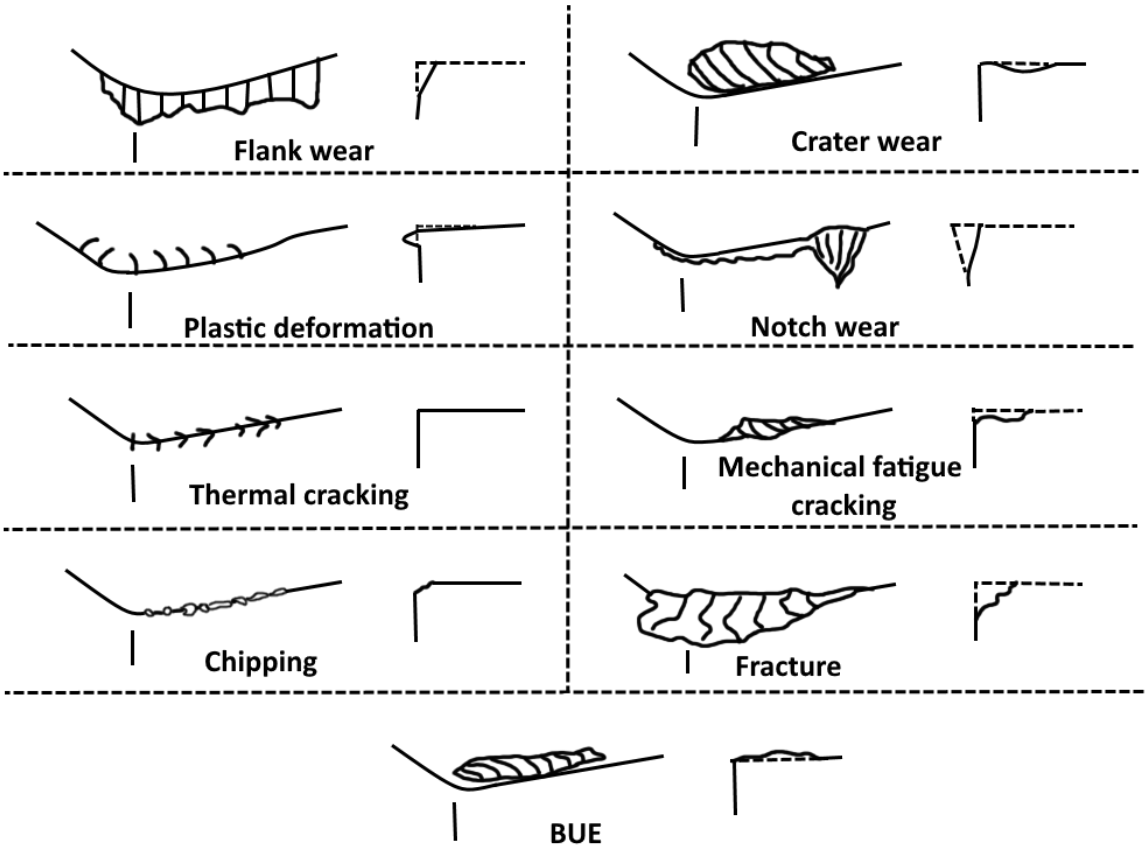

Figure 1.2. *Types of tool wear [based on [11]].*

Flank wear is observed in the form of wear land on the flank face of the tool. Flank wear decreases the relief angle of the tool and increases frictional resistance [12]. Flank wear reduces dimensional accuracy and gives poor surface integrity of the machined part. According to ISO 3685:1993 [10], tool life criterion is set to be 300 μm of flank wear. Figure 1.3 shows the characteristic tool wear curve.

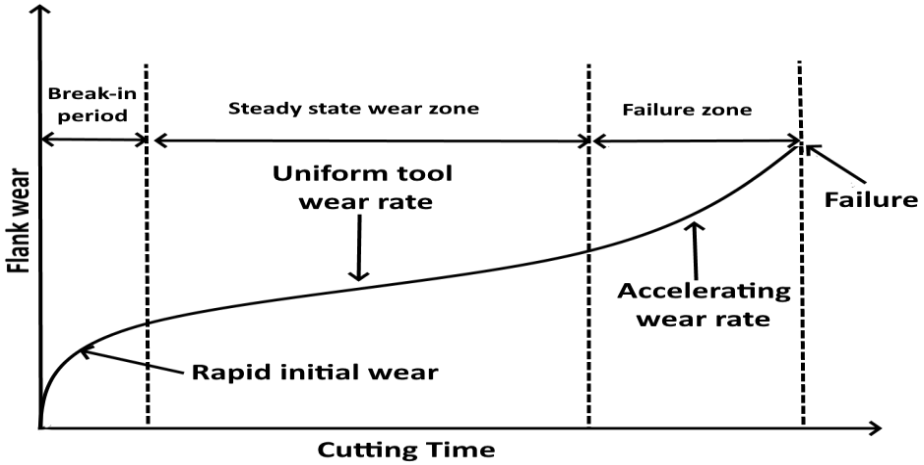

Figure 1.3. *Typical stages in flank wear*.

Crater wear results on the rake face of the tool because of the sticking and sliding motion of the chips as they travel over the rake face of the tool at high stress and temperature. Crater wear causes the strength of the cutting edge to decrease and increases the probability of tool breakage. The crater depth, KT, is most widely used to evaluate crater wear.

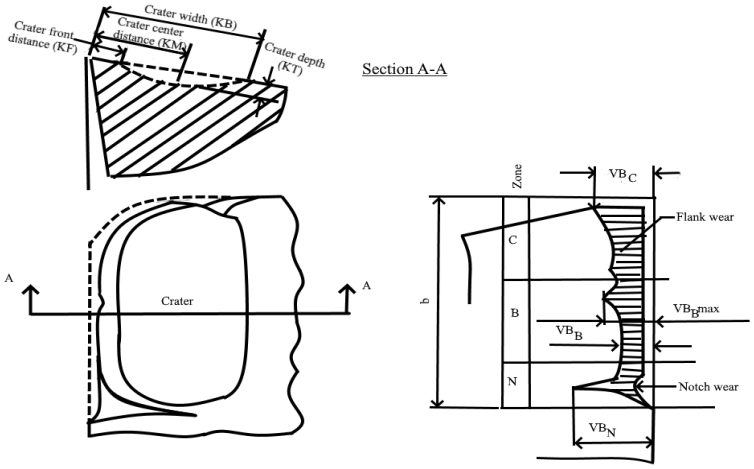

Figure 1.4. *Flank wear and crater wear definition [based on [10]].*

There are different types of tool wear mechanisms. The most typical mechanisms of tool wear are briefly discussed below. Most cutting processes are influenced by one or

more of these wear mechanisms and are dependent on the specifics of the cutting process (workpiece material, cutting zone temperature and stress, tool material, etc.)

• Abrasive Wear: Abrasive wear occurs due to scratching or scoring of the workpiece material by hard abrasive particles present in the workpiece. Abrasion occurs mainly on the flank face of the tool. Abrasive wear is not a uniform form of wear and appears at various positions across the tool wear land. Depending on the material being machined, abrasive wear volume is typically higher compared to other wear mechanisms.

• Adhesion Wear: Adhesion or attrition wear occurs when workpiece material adheres to the tool surface and breaks off at intervals taking cutting tool fragments along with it. This adhesion of workpiece material is referred to as built up edge (BUE) and forms due to high temperatures and pressures generated during cutting. It is prevalent on both flank and rake faces. Adhesion wear volume is generally low unless the workpiece materials are sticky in nature.

• Diffusion Wear: During cutting, high temperatures are generated. Often at high temperatures, diffusion of tool constituents into the workpiece or vice versa takes place. This results in a smooth type of wear referred to as diffusion wear. The rate of diffusion is dictated by the chemical affinity between the tool and workpiece, concentration gradient, and the cutting temperature. With an increase in cutting temperature, diffusion rate increases exponentially.

• Oxidation Wear: Oxidation wear occurs due to oxidation of tool materials. Binder materials that hold the carbide particles in place are particularly susceptible. High cutting temperatures and pressures increase oxidation. Oxidation wear typically results in localized

notch wear that takes place at a maximum depth of cut where the cutting zone is exposed to the environment.

• Fatigue Wear: There are two types of fatigue wear, namely, mechanical and thermal fatigue wear. Alternative compressive and tensile stresses during machining give rise to mechanical fatigue, whereas thermal fatigue occurs due to cyclic heating and cooling of the cutting tool. Crack propagation is promoted by such cyclic loadings.

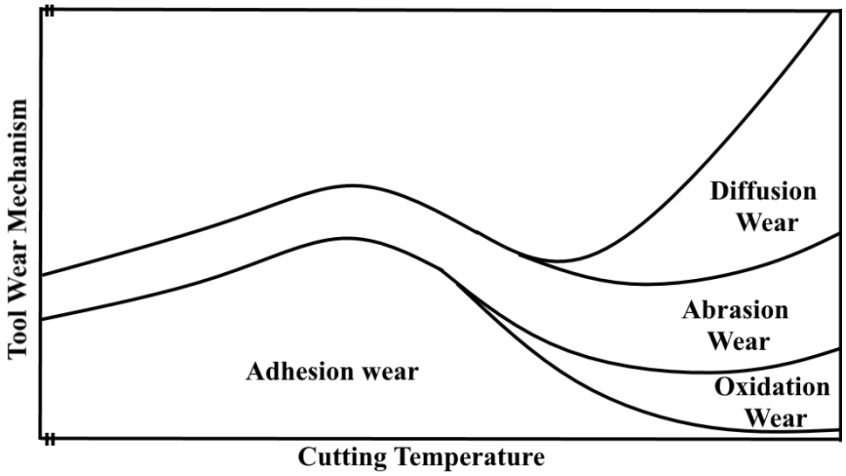

Figure 1.5. *Causes of tool wear in cutting operations [based on [13]].*

1.2.3. Cutting tool coatings

During machining, high temperatures are generated. The heat generated dissipates into the chip, tool, and workpiece. To minimize cutting temperature generation, coatings have been applied on cutting tools to reduce friction at the tool-chip-workpiece interfaces. Detailed understanding of coating behaviour in relation to the different tool and workpiece material combination and how it affects cutting temperature generation is required for tool design. Coatings must be designed in such a way that it can withstand the harsh machining

conditions. It should also be able to reduce friction, provide wear resistance, and serve as a thermal barrier.

The two most common coating techniques used for cutting tools are Chemical Vapor Deposition (CVD) and Physical Vapor Deposition (PVD) with the latter being more common in the industry due to the wide range of materials that can be deposited at lower temperatures than typically used for CVD processes. All the coated tools used in the present research are PVD coated.

1.2.3.1 PVD Coatings

PVD is a vacuum coating process. In this process, the material to be deposited is separated from the target by evaporation or sputtering. The vapor particles are then condensed onto a substrate. Vapor particles are transported and condensed, forming a film on suitably placed parts. Coating thicknesses deposited by PVD process typically ranges from a few nanometers up to several microns. Chemical compounds can also be deposited by using a similar source (target) material or by introducing reactive gases (nitrogen, oxygen or hydrocarbons) containing desired reactants into the chamber causing them to react with the metal from the PVD source [7].

PVD coating process produces a sharp coated edge. PVD coating provides high intrinsic hardness and gives beneficial compressive stresses that resist crack initiation. PVD coated tools can also be de-coated, making re-sharpening of tools much easier, reducing production costs.

Self-adaptive PVD coatings are a new generation of coatings that respond in a selective way to cutting conditions. Self-adaptive coatings function by forming beneficial

tribo-films through interacting with their environment. Tribo-films are thin films that form on the interface or worn surface of the tool as the coating system reacts with elements from the environment (mostly oxygen). They are dynamic structures and have different chemical composition, structure, and tribological behaviour compared to the underlying bulk material [14-15]. They have a notable influence on frictional characteristics at the interface regions and thus the wear performance of tools. Tribo-films can provide enhanced hardness, strength, and thermal barrier characteristics to the surface of a tool [8].

1.2.4. Titanium alloys

Titanium and its alloys are increasingly becoming the material of choice for a wide range of applications. They have found their way into numerous industries due to their superior properties. Their major application, however, is still the aerospace industry, where they are used in engine parts and airframes [4], [16-18]. They have exceptional corrosion resistance, high wear resistance and fracture resistance, biocompatibility, and high strength-to-weight ratio, which they can retain even at elevated temperatures [19-21]. Titanium alloys are approximately 40% lighter compared to steel while only around 60% heavier compared to aluminum [22]. Ti6Al4V contribute to about 45-60% of total titanium production. Ti6Al4V has been chosen as the workpiece material in the present research due to its high usage in the industry [6], [19], [23].

Titanium is an allotropic metal and has two crystallographic forms. It has a hexagonal close packed (hcp) crystal structure at temperatures below 882°C and referred to as α-phase. This structure has a limited number of shear or slip planes. At temperatures above 882°C, it exists in β-phase and has a body-centered cubic (bcc) structure. β-phase is

stable until about 1677°C, which is the melting point of titanium. β-phase also has more shear or slip planes and allows more local deformations. The allotropic transformation temperature of titanium can be increased or decreased by adding various alloying elements. These alloying elements also give distinct mechanical properties. Alloying elements that increase the allotropic transformation temperature are referred to as α-stabilizers, whereas elements that decrease the allotropic transformation temperature are called β-stabilizers. Common α-stabilizers are aluminum (Al), nitrogen (N), oxygen (O), gallium (Ga) and carbon (C). Al increases the strength of the α-phase at room temperature and elevated temperatures up to about 550°C. Al also gives high strength to weight ratio due to its low density. Common β-stabilizers are molybdenum (Mo), vanadium (V), nickel (Ni), copper (Cu), manganese (Mn), tantalum (Ta), iron (Fe), cobalt (Co), chromium (Cr) and hydrogen (H). β-stabilizers makes the β-phase stable even at low temperatures, including room temperature. Ti6Al4V is the most commonly used α+β alloy [23].

1.2.4.1 Machinability issues of titanium alloys

Machinability generally refers to the ease or difficulty faced during machining a particular material for a certain set of operating conditions. Machinability of a certain material depends not only on the mechanical properties of the material but also on the machining processes, cutting tools, and cutting condition. Machinability is mainly evaluated by assessing tool life, forces generated during cutting, and surface finish of the machined part [6, 24].

Titanium alloys are considered difficult-to-cut materials owing to their inherent properties. As a result, the costs of finished titanium products are high, limiting the use of

titanium despite its beneficial characteristics. Most of the tool materials that perform well when machining other materials show relatively poor performance in machining titanium and its alloys [6, 25]. The problems associated with titanium machining are discussed below and have been summarized from references [6], [25-27]:

- Poor Thermal Conductivity: During machining, energy is consumed to overcome the friction between the tool-chip or tool-workpiece interface and to plastically deform the workpiece to form chips. Nearly all the energy is converted to heat, which in turn raises the cutting zone temperature. Generally, a significant portion of the heat generated is dissipated into the chip, with a small amount dissipating into the workpiece and tool. However, because of the poor thermal conductivity of titanium and its alloys (about 1/6 that of steel), the fast-flowing chip and the workpiece are not able to dissipate the heat thereby trapping and intensifying the heat in the cutting zone. Consequently, almost 80% of the heat is conducted into the tool and as such can reach temperatures as high as 1100°C, causing rapid tool wear.

- Low Modulus of Elasticity: Titanium has high elasticity making it ideal for use in applications requiring flexibility while limiting crack formation. However, this characteristic is problematic during machining. Titanium has a low modulus of elasticity compared to other metals, meaning that it deflects more per unit force/stress. Thus, when subjected to pressure from a contacting cutting tool edge, titanium has a greater spring-back effect causing rubbing of the cutting edge instigating premature flank wear and chipping. Titanium deflects nearly twice as much as steel under the same cutting pressure. The presence of built up edge (BUE) at the tool edge, a common occurrence when

machining titanium, increases the perpendicular forces acting on the workpiece by at least three to four times. This high thrust force, coupled with low modulus of elasticity causes the workpiece to deflect and spring away from the tool. This results in tool chatter and rubbing, causing poor dimensional accuracy and surface quality of the finished product.

- Chemical Reactivity: Titanium and its alloys are relatively chemically inert, making them suitable for medical implant applications. However, at temperatures above 500°C, they become very reactive and react with almost all tool materials. Due to the high chemical reactivity and adhesive characteristics of titanium at high temperatures, intensive sticking on the tool is commonly observed in the form of built up edge. Diffusion of particles between tool and workpiece material also takes place causing rapid tool wear.

- Hardening due to Diffusion and Plastic Deformation: Titanium work hardens, or strain hardens during machining and is also hardened due to the diffusion of oxygen and nitrogen. At high temperature, most materials experience thermal softening and undergo a reduction in strength. However, titanium retains its strength even at high temperatures requiring higher cutting power to plastically deform titanium to produce chips. This high cutting power and its resultant plastic deformation harden the machined surface; a phenomenon commonly referred to as strain hardening or work hardening.

- Mechanism of Chip Formation: Chip formation during titanium machining is somewhat unique. The distinct characteristics of titanium chips are that they are serrated, cyclic and of segmented geometry with shear-localized zones. Titanium chips generally show lower deformation than other metals and are consequently thinner. In accordance with cutting kinematics, a thin chip flows over the rake face of the tool faster than does a thick

chip, for the same cutting speed, which will trigger higher temperatures at the tool-chip interface. Thin chips also curl easier which mean that the tool-chip contact area is small, thereby concentrating the heat generated over a small region and raising contact stress near the cutting edge.

1.2.4.2 Cutting tools and substrate material

Over the years, different types of cutting tool materials have been applied in titanium machining in an attempt to obtain higher tool life [6], [16], [28-30] with little success. High cutting zone temperatures during titanium machining results in a reduction in strength of their inter-particle bonds for a majority of the tool substrates which ultimately leads to accelerated wear and failure of the cutting tool [19], [31]. Tool materials tested for titanium machining are high-speed steels (HSS), cemented carbides (WC), cubic boron nitrides (CBN), polycrystalline cubic boron nitrides (PCBN), polycrystalline diamond (PCD) and ceramic. However, the behaviour and wear pattern vary and is unique to each tool material. The use of each type depends on the process requirements, tool cost, and machining conditions [16], [23].

PCD tools are the most effective commercially available tool for machining titanium and its alloys [17]. Several researchers [6], [17], [32] have confirmed that PCD outperforms CBN, PCBN, uncoated, and coated carbide tools for titanium machining, yielding the lowest wear rate and best workpiece surface finish. However, their relatively high cost prevents their widespread use in industry [6].

CBN tools have the highest hardness next to diamond tools. They sustain their high hardness characteristics even at elevated temperatures. They also remain oxidation-

resistant up to 2000°C. However, their high hardness and corresponding low toughness make them susceptible to chipping and fracture, especially if larger depths of cuts are used. This restricts their application to finishing operations during titanium machining. Furthermore, they are approximately 10-20 times more expensive than carbide tools making them economically infeasible [6], [16].

Ceramic tools are hard cutting tool materials and have high hot hardness, good oxidation resistance, chemical inertness, and high compressive strength. Their high melting point prevents thermal softening from taking place under extreme machining conditions. However, they are brittle and have low fracture strength and toughness, making them susceptible to thermal and mechanical shock during machining, particularly milling [16], [17], [33]. Compared to cemented carbide tools, ceramic tools show higher flank and rake wear rates [4]. Thus, ceramic tools are inappropriate for machining titanium and its alloys [6], [16].

HSS tools were extensively used for machining various materials in the past and still used in special applications like drilling. They have higher toughness compared to other materials. However, HSS has a softening temperature of about 600°C. Hence, they are not suitable for machining at working temperatures over 500°C rendering HSS tools incompatible for this application [6], [16], [19], [34].

Cemented carbide tools are the most accepted and widely used tools for titanium machining. Commercially available cemented carbide tools fall under two categories: straight grade carbides and mixed grade carbides (also referred to as steel cutting grades). Researchers [6], [16], [18] have found that straight tungsten grade carbide tools are superior

to mixed grade carbide tools. Both attrition and diffusion wear are more prominent in mixed carbide grade tools [18]. Cutting speeds over 60 m/min is not recommended for tungsten carbide tools due to the intense heat produced at higher cutting speeds, which often leads to plastic deformation of the tools. Coated carbide tools have also been used for titanium machining. However, most coated tools perform worse in comparison to the straight grade carbides due to the reactivity of titanium with the coating materials. Therefore, uncoated straight grade cemented carbides are still the preferred choice for titanium machining [6], [16].

1.2.4.3 Wear mechanisms of cemented carbide tools in titanium machining

Cemented carbide tools encounter rapid tool wear during titanium machining due to the high temperatures generated, the high chemical affinity of titanium, high cutting stresses, and short chip-tool contact length. Typically, both crater wear and flank wear are observed, as is a substantial built-up edge formation extending over both rake and flank faces. Surface damage and failure by chipping at the tool nose are also commonly reported. Surface speed of about 45 m/min is typically adopted in industry, with attempts at higher cutting speeds typically resulting in plastic deformation of the cutting edge due to the intense heat generated [4], [6].

Tool wear in cemented carbide tools during titanium machining is dictated mainly by two wear mechanisms: Dissolution-diffusion and adhesion. Dissolution-diffusion normally produces smooth worn surfaces, whereas adhesion results in irregular worn surfaces [17], [18]. Both types of wear are prevalent on rake and flank faces of the tool.

Dearnley et al. [4] found that adhesion or attrition played a significant role in flank wear. Due to high chemical reactivity and adhesive characteristics of titanium, significant material transfer from the workpiece to the tool is observed in both flank and rake surfaces [6], [35]. This adhered material builds up, forming a layer referred to as a built-up edge (BUE). Attrition wear results from the adhered particles breaking off on reaching a critical size tearing away fragments of tool material.

The high cutting temperature during titanium machining provides an ideal environment for the dissolution-diffusion wear mechanism to take place. It has been reported [4] that the dissolution-diffusion wear mechanism dictates tool wear on the rake surface of uncoated cemented carbides. It was suggested that [36-37] crater wear occurred due to tool material diffusing into the workpiece material which passes over the tool surface and not by mechanical fracture of the tool surface into fragments. This diffusion, however, may alter the tool structure, thereby weakening the tool cutting edge and causing possible mechanical removal of the tool fragments by the moving chips [38].

Plastic deformation of tools occurs at higher cutting speeds during titanium machining. Higher cutting speeds during machining generates very high temperatures and gives rise to high compressive stresses near the cutting edge resulting in plastic deformation at the cutting edge or/and at the tool nose consequently leading to tool failure [17], [23], [39]. During machining titanium and its alloys with straight grade carbides, the cutting speed is limited to 60 m/min due to plastic deformation [4], [6].

1.2.4.4 Application of coated carbide tools in titanium machining

Almost 80% of all tools used in industries for machining are coated tools. Coatings, being hard materials, offer better resistance to abrasion. They provide superior high-temperature characteristics such as high hot hardness, increased resistance to oxidation wear, and diffusion wear. They can reduce friction between the tool-chip or tool-workpiece interfaces because of their high lubricating abilities, thereby minimizing cutting temperature. They also reduce cutting forces during machining in comparison to uncoated tools [40].

Although coated carbide tools have had significant success in machining cast irons, steels and many super alloys, they are yet to achieve the same level of success when it comes to titanium machining. In many cases, coated tools perform worse than straight grade cemented carbides, thereby making straight grade carbides the preferable choice still for titanium machining [6]. Many researchers [4], [41] have found that coatings such as TiN, TiC, TiCN, TiN-TiC, TiN–Ti(C,N)–TiC, Al_2O_3/TiC, Al_2O_3, HfN, and TiB_2 show higher tool wear rates than straight grade WC/Co cemented carbides when machining titanium alloys.

Jawaid et al. [41] investigated the wear mechanism and performance of PVD-TiN, and CVD-TiCN + Al_2O_3 coated carbide tools for face milling operations under various operating conditions. They found that CVD-coated inserts performed better than PVD-coated inserts in most cases which can be attributed to the greater coating thickness, its better wear resistance and greater adhesion strength of the coating onto the substrate for the CVD coated tools.

Ezugwu and co-workers [42-43] observed that PVD coated tools outperform straight WC fine-grain carbide inserts. They found that single layer PVD TiN coated tools gave higher flank wear as compared to the multilayer PVD TiN/TiCN/TiN coated tool at low feed rates whereas the phenomenon is exactly opposite at higher feed rates for turning operations. Ozel and co-workers [44] found that the TiAlN coating slightly outperforms uncoated WC/Co tools in terms of cutting forces and tool wear rate.

Corduan et al. [45] recommended TiB_2 coated carbide tools for high-speed machining of Ti6Al4V at cutting speeds lower than 100 m/min. The wear pattern of the coated tool progressed in two stages: coating delamination followed by substrate damage. They suggested further research into refining the deposition techniques of the TiB_2 coatings as well as research into coatings which exhibit better thermal fatigue resistance. However, they did not conduct any tool life studies and no comparison with other coated or uncoated carbide tools. Their study also lacks an explanation regarding why TiB_2 coated carbide tools experience wear progression in the manner as they reported. Their investigation also revealed that PCD inserts showed better performance than CBN and coated tools and that CBN tools are better suited for finishing operations.

Liang Jin [46] investigated the adhesion characteristics of the Ti6Al4V alloy to various nitride coatings (TiN, AlTiN, CrN) and AISI 52100 steel. COF and adhesion behaviour was evaluated by adhesion tests and ball-on-disk tests with uncoated and coated (AlTiN, TiN, CrN) AISI 52100 steel as counter face materials. It was found that the CrN coating had the lowest amount of material transferred during the initial stage of sliding, resulting in a lower wear rate. However, the COF for the CrN coating reached its threshold

value within a shorter distance as compared to others. It was observed that in the transfer layer on steel TiO and V_2O_3 is present in the high oxygen content region whereas only TiO is present in the case of the PVD coatings. This suggested that Ti6Al4V is less severely oxidized during sliding against PVD coatings. The author concluded that TiN and CrN coating show better performance in terms of oxidation and adhesion reduction of Ti6Al4V under a dry sliding condition.

1.3. Research Gaps

Available literature provides very limited information regarding the tribological interaction occurring at the tool/chip/workpiece interface for Ti6Al4V machining. A suitable and effective tool coating is yet to be identified or developed to address machinability issues of Ti6Al4V machining. Thus, the current research aims to address the following research gaps not yet explored in the literature:

1. Although some work has been done in this area, the manufacturing industry still faces problems in terms of machinability of Ti6Al4V alloy. Tool wear of cemented carbide tools is dictated by adhesion (with BUE formation) and diffusion wear mechanisms. No solution has yet been found to address the tool wear mechanisms and minimize tool wear during Ti6Al4V machining.

2. The performance of the cutting tool is strongly associated with the conditions of the machining process. No research has been done to understand how the tool wear mechanisms change with various machining conditions such as rough turning or finish turning.

3. Industries still use uncoated cemented carbide tools for titanium machining due to lack of effective tool coating. Current research aims to develop PVD coatings to reduce tool wear during rough and finish turning.

4. Mostly comparison data of different industrial coatings are provided in the literature with a detailed systematic approach with regards to coating design still lacking in the literature for machining of Ti6Al4V alloy.

5. The potential of a new generation of self-adaptive PVD coatings to address machinability issues of Ti6Al4V is yet to be explored.

6. Detailed study regarding tribo-films formation during Ti6Al4V machining and how it effects tool wear is required.

7. No attempt at how the coating properties like hardness effects coating performance during Ti6AlV machining has been made.

1.4. Motivation and Research Objectives

PCD tools are the most effective tool material for machining titanium alloys. However, their relatively high cost prevents their widespread use in industry making cemented carbide tools still the most preferred tools in industry to machine titanium alloys. Due to the lack of an effective tool coating, uncoated straight grade cemented carbide tools are still being used to machine titanium alloys. However, coating deposition technology has significantly advanced in recent years and new coating design considering the unique tribological requirements of machining titanium are now possible.

During titanium machining with cemented carbide tools, significant BUE and crater wear formation is observed. However, one is dominant over the other depending on the

machining conditions, such as during roughing and finishing operations. Hence, the present research focuses on the general direction of identifying, developing, and characterizing coatings that would further improve the tool life of cemented carbide tools catering to the specific wear mechanisms that takes place during rough turning and finish turning of Ti6Al4V alloy thereby reducing manufacturing cost and improving product quality. The main objectives of the current research are:

1. Study and identify the dominant tool wear mechanism associated with rough and finish turning of Ti6Al4V alloys.
2. Study the tribo-films formed on coatings during machining and their effect on tool wear.
3. Develop a new adaptive coating for rough turning of Ti6Al4V alloys.
4. Develop a new adaptive coating for finish turning of Ti6Al4V alloys.
5. Establish an adaptive coating for both rough and finish turning of Ti6Al4V alloys.

1.5. Thesis Organization

The main body of this dissertation has been arranged in a sandwich thesis format with the following chapters composed of published journal articles that address multiple objectives of the research study outlined in section 1.4. The appendices provided at the end of the dissertation contain the preliminary study conducted at the start of this research project and other relevant studies that complement the current research and address specific objectives. Part of the content of the appendices has been published in journals (details provided in the appendices) while the rest consists of unpublished work. The final chapter

of this dissertation provides an overall conclusion and summarizes the major findings of the current research.

The ultimate goal of this research was to understand the underlying tool wear mechanisms associated with the rough and finish turning of Ti6Al4V alloy and develop self-lubricating PVD coatings to counteract them. Two self-adaptive PVD coatings, TiB_2 and CrN, were chosen based on the expected formation of beneficial tribo-films that cater to specific wear mechanisms during the rough and finish turning operations. A preliminary study revealed that the adhesion wear mechanism, which leads to BUE formation and crater wear formation due to high cutting temperature generation, dictates tool performance during rough and finish turning operations, respectively. It was found that both the TiB_2 and CrN coatings significantly outperformed the uncoated cemented carbide tool and industrially recommended AlTiN coated tool for rough turning operations, with the TiB_2 coated tool giving the best performance. On the other hand, the CrN coated tool gave the best tool performance during finish turning operations, with the TiB_2 coated tool performing almost identically to the uncoated and AlTiN coated tools. These findings are discussed in detail in Appendix A. Since the CrN coating provided significant tool life improvement for both roughing and finishing, further tuning of the CrN coating was done by varying the deposition process parameters to improve its performance. This is discussed in detail in Appendix B.

The unique micro-mechanical properties and adaptive tribological characteristics of the CrN coated tool which lead to improved tool performance during finish and rough turning operations are discussed in Chapter 2 and Chapter 3, respectively. While conducting this

research, it was also found that for machining applications where BUE formation is observed, lower hardness coatings perform better than higher hardness coatings. This finding is highlighted in Chapter 4 where it is shown that a TiB_2 coating with a lower hardness and thinner coating thickness performs better than a harder, thicker TiB_2 coating.

A summary of each chapter of this dissertation is given below.

Chapter 1 provides a general background and literature review of machinability issues and PVD coatings. This chapter also highlights the research gaps in the literature and the main objectives of the current research.

Chapter 2 presents the tool performance of CrN coated tools during finish turning operations as contrasted with uncoated and industrially recommended AlTiN coated tools. The wear characteristics of the tools were investigated by SEM and 3D wear volume measurements. Detailed micro-mechanical characteristics of the coatings were also studied in detail. This chapter addresses the first, second, third, and fifth objective of this research and resulted in the following publication: M.S.I. Chowdhury, B. Bose, K. Yamamoto, L.S. Shuster, J. Paiva, G.S. Fox-Rabinovich, and S.C. Veldhuis, “Wear performance investigation of PVD coated and uncoated carbide tools during high-speed machining of TiAl6V4 aerospace alloy”, Wear, V. 446-447, 2020.

Chapter 3 studies the tool performance of CrN coated tools during rough turning operations compared to uncoated and AlTiN coated tools. The micro-mechanical properties of the coatings were also investigated to gain a better understanding of the coating performance. This chapter addresses the first, second, third, and fifth objective of this research and resulted in the following publication: M.S.I. Chowdhury, B. Bose, S. Rawal,

G.S. Fox-Rabinovich, and S.C. Veldhuis, "Investigation of the wear behaviour of PVD coated carbide tools during Ti6Al4V machining with intensive built up edge formation", Coatings, V. 11, pp. 266, 2021.

Chapter 4 investigates the effect of coating hardness and coating thickness during rough turning of Ti6Al4V alloy. The wear performances of the various TiB_2 coated carbide tools with varying hardness and thickness were evaluated using tool life studies and the 3D volumetric wear measurements of the worn tool. The micro-mechanical properties of the coatings were also studied in detail to correlate with the coatings' performances. In this chapter, the third objective of this research was addressed, and the following journal article was published: M.S.I. Chowdhury, B. Bose, G.S. Fox-Rabinovich, and S.C. Veldhuis, "Investigation of the wear performance of TiB_2 coated cutting tools during the machining of Ti6Al4V alloy", Materials, Vol. 14, I. 11, pp. 2799, 2021.

Chapter 5 summarizes the major observations and findings of the current research and highlights the research's contributions along with recommendations for future research work.

Appendix A studies tool wear mechanisms during the rough and finish turning of Ti6Al4V alloy. The effectiveness of self-adaptive TiB_2 and CrN coatings for both rough and finish turning operations were also investigated and compared to uncoated and AlTiN coated tools. All the research objectives were partially addressed here. Part of the findings were published in the following journal article: J.M. Paiva, M.A.M. Shalaby, M. Chowdhury, L. Shuster, S. Chertovskih, D. Covelli, EL Junior, P. Stolf, A. Elfizy, C.A.S. Bork, G.S. Fox-Rabinovich GS, and S. Veldhuis "Tribological and wear performance of

carbide tools with TiB_2 PVD coating under varying machining conditions of TiAl6V4 aerospace alloy", Coatings, V. 7, I. 11, pp. 187, 2017.

Appendix B investigates the effect of deposition parameters on the performance of CrN coatings. There are three main deposition process parameters that effect the properties of the deposited coatings: nitrogen gas pressure, bias voltage, and coating thickness. This appendix addresses the second, third, and fifth objective of this research.

1.6. Note to Reader

It is important to note here that since this dissertation adopts a sandwich thesis format and has been compiled from peer-reviewed published and submitted journal articles, similarities may be present, especially in the introduction and experimental detail sections. However, the reader is highly encouraged to read them as they contain valuable information that is relevant to each study.

1.7. References

1. Veiga, C.; Davim, J. P.; Loureiro, A. J. R. Proprties and Applications of Titanium Alloys. Rev. Adv. Mater. Sci. 2012, 32, 133–148.
2. Chowdhury, M. S. I.; Chowdhury, S.; Yamamoto, K.; Beake, B. D.; Bose, B.; Elfizy, A.; Cavelli, D.; Dosbaeva, G.; Aramesh, M.; Fox-Rabinovich, G. S.; Veldhuis, S. C. Wear Behaviour of Coated Carbide Tools during Machining of Ti6Al4V Aerospace Alloy Associated with Strong Built up Edge Formation. Surf. Coatings Technol. 2017, 313, 319–327. https://doi.org/10.1016/j.surfcoat.2017.01.115.
3. Paiva, J. M.; Shalaby, M. A. M.; Chowdhury, M.; Shuster, L.; Chertovskikh, S.; Covelli, D.; Junior, E. L.; Stolf, P.; Elfizy, A.; Bork, C. A. S.; Fox-Rabinovich, G.; Veldhuis, S. C. Tribological and Wear Performance of Carbide Tools with TiB_2 PVD Coating under Varying Machining Conditions of TiAl6V4 Aerospace Alloy. Coatings 2017, 7 (11), 187. https://doi.org/10.3390/coatings7110187.
4. Dearnley, P. A.; Grearson, A. N. Evaluation of Principal Wear Mechanisms of Cemented Carbides and Ceramics Used for Machining Titanium Alloy IMI 318. Mater. Sci. Technol. 1986, 2 (1), 47–58. https://doi.org/10.1179/026708386790123611.
5. Boyer, R. R. An Overview on the Use of Titanium in the Aerospace Industry. Mater. Sci. Eng. 1996, 213, 103–114.
6. Hosseini, A.; Kishawy, H. A. Cutting Tool Materials and Tool Wear. In Machining of Titanium Alloys; Davim, J. P., Ed.; Springer Berlin Heidelberg: Berlin, Heidelberg, 2014; pp 31–56. https://doi.org/10.1007/978-3-662-43902-9_2.

7. Bouzakis, K. D.; Michailidis, N.; Skordaris, G.; Bouzakis, E.; Biermann, D.; M'Saoubi, R. Cutting with Coated Tools: Coating Technologies, Characterization Methods and Performance Optimization. CIRP Ann. - Manuf. Technol. 2012, 61 (2), 703–723. https://doi.org/10.1016/j.cirp.2012.05.006.
8. Fox-Rabinovich, G.; Gershman, I.; Hakim, M.; Shalaby, M.; Krzanowski, J.; Veldhuis, S. Tribo-film Formation as a Result of Complex Interaction at the Tool/Chip Interface during Cutting. Lubricants 2014, 2 (3), 113–123. https://doi.org/10.3390/lubricants2030113.
9. Australian Standard, Appendix B P35.
10. ISO 3685: 1993(E). Tool-Life Testing with Single-Point Turning Tools; International Organization for Standardization: Geneva, Switzerland, 1993.
11. Modern Metal Cutting, A Practical Handbook. Sandvik Coromant.
12. Shaw, M. C. Metal Cutting Principles. Oxford University Press, Inc., 2005.
13. Klocke, F. Manufacturing Processes 1: Cutting; Springer Berlin Heidelberg, 2010. https://doi.org/10.1007/978-3-642-11979-8.
14. Jehn, H. A. Multicomponent and Multiphase Hard Coatings for Tribological Applications. Surf. Coatings Technol. 2000, 131 (1–3), 433–440. https://doi.org/10.1016/S0257-8972(00)00783-0.
15. German S. Fox-Rabinovich; Kovalev, A. I. Self-Organization and Structural Adaptation during Cutting and Stamping Operations. In Self-Organization During Friction: Advanced Surface-Engineered Materials and Systems Design; CRC Press, Taylor and Francis Group, Boca Raton, NW, USA, 2006.

16. Hosseini, A.; Kishawy, H. A.; Hussein, H. M. Machinability of Titanium and Its Alloys. In Machinability of Advanced Materials; ISTE Ltd and John Wiley & Sons, Inc., 2014; pp 95–118. https://doi.org/10.1002/9781118576854.ch3.
17. Nabhani, F. Machining of Aerospace Titanium Alloys. Robot. Comput. Integr. Manuf. 2001, 17 (1–2), 99–106. https://doi.org/10.1016/S0736-5845(00)00042-9.
18. Freeman, R. M. The Machining of Titanium and Some of Its Alloys, Ph.D Thesis, University of Birmingham, UK, 1974.
19. Ezugwu, E. O.; Bonney, J.; Yamane, Y. An Overview of the Machinability of Aeroengine Alloys. J. Mater. Process. Technol. 2003, 134 (2), 233–253. https://doi.org/10.1016/S0924-0136(02)01042-7.
20. Myers, J. R.; Bomberger, H. B.; Froes. Corrosion Behaviour and Use of Titanium and Its Alloys. J. Miner. Met. Mater. Soc. 1984, 36 (10), 50–60.
21. Ezugwu, E. O.; Wang, Z.M. Titanium Alloys and Their Machinability. J. Mater. Process. Technol. 1997, 68 (3), 262–274.
22. Schwartz, M. M. Encyclopedia of Materials, Parts, and Finishes. CRC Press LLC. 2nd ed., 2002.
23. Machado, A. R.; Wallbank, J. Machining of Titanium and Its Alloys-a Review. Proc Instn Mech Engrs, Part B J. Eng. Manuf. 1990, 204, 53–60.
24. Trent, E.M. Metal Cutting. Butterworths & Co (Publishers) Ltd. 1984.
25. Jaffery, S. H. I.; Mativenga, P. T. Wear Mechanisms Analysis for Turning Ti-6Al-4V Towards the Development of Suitable Tool Coatings. Int. J. Adv. Manuf. Technol. 2012, 58 (5–8), 479–493.

26. Komanduri, R.; Turkovich, B. F. V. O. N. New Observations on the Mechanism When Machining Titanium Alloys of Chip Formation. Wear. 1981, 69, 179–188,
27. Yang, X.; Richard Liu, C. Machining Titanium and Its Alloys; 1999; Vol. 3. https://doi.org/10.1080/10940349908945686.
28. Rahman, M.; Wong, Y. S.; Zareena, A. R. Machinability of Titanium Alloys. JSME International Journal Series C. 2003, 46 (1), 107–115.
29. Pramanik, A.; Islam, M. N.; Basak, A.; Littlefair, G. Machining and Tool Wear Mechanisms during Machining Titanium Alloys. Adv. Mater. Res. 2016, 65, 338–343.
30. Ulutan, D.; Ozel, T. Machining Induced Surface Integrity in Titanium and Nickel Alloys: A Review. Int. J. Mach. Tools Manuf. 2011, 51 (3), 250–280.
31. Vaughn, R. L. Modern Metals Machining Technology; 1966.
32. Amin, A. K. M. N.; Ismail, A.F.; Khairusshima, M. K. N. Effectiveness of Uncoated WC–Co and PCD Inserts in End Milling of Titanium Alloy - Ti–6Al–4V. J. Mater. Process. Technol. 2007, 192–193, 147–158.
33. Chakraborty, A.; Ray, K. K., Bhaduri, S. B. Comparative Wear Behavior of Ceramic and Carbide Tools During High Speed Machining of Steel. Mater. Manuf. Process. 2000, 15 (2), 269–300.
34. Kramer, B. M. On Tool Materials for High Speed Machining. J. Eng. Ind. 1987, 109 (2), 87–91.
35. Narutaki, N.; Murakoshi, A.; Motonishi, S.; Takeyama, H. Study on Machining of Titanium Alloys. CIRP Ann. - Manuf. Technol. 1983, 32 (1), 65–69. https://doi.org/10.1016/S0007-8506(07)63362-9.

36. Naerheim, Y.; Trent, E. M. Diffusion Wear of Cemented Carbide Tools When Cutting Steel at High Speeds. Metals Technol. 1977, 548–556.
37. Dearnley, P. A.; Trent, E. M. Wear Mechanisms of Coated Carbide Tools. Met. Technol. 1982, 9 (1), 60–75. https://doi.org/10.1179/030716982803285909.
38. Hartung, P. D.; Kramer, B. M. Tool Wear in Machining Titanium. Ann. CIRP 1982, 30 (1), 75–80.
39. Che-Haron, C. H. Tool Life and Surface Integrity in Turning Titanium Alloy. J. Mater. Process. Technol. 2001, 118 (1–3), 231–237.
40. Cselle, T.; Barimani, A. Today's Applications and Future Developments of Coatings for Drills and Rotating Cutting Tools. Surf. Coatings Technol. 1995, 76–77 (PART 2), 712–718. https://doi.org/10.1016/0257-8972(96)80011-9.
41. Jawaid, A.; Sharif, S.; Koksal, S. Evaluation of Wear Mechanisms of Coated Carbide Tools When Face Milling Titanium Alloy. J. Mater. Process. Technol. 2000, 99 (1–3), 266–274. https://doi.org/10.1016/S0924-0136(99)00438-0.
42. E.O. Ezugwu and Z.M. Wang. Tool Life and Workpiece Surface Integrity Evaluation When Machining Ti6Al4V with PVD Coated Tools. Surf. Modif. Technol. 1997, IOM 10, 414–426.
43. Wang, Z. M.; Ezugwu, E. O. Performance of PVD-Coated Carbide Tools When Machining Ti-6Al-4V©. Tribol. Trans. 1997, 40 (1), 81–86. https://doi.org/10.1080/10402009708983632.
44. Özel, T.; Sima, M.; Srivastava, A. K.; Kaftanoglu, B. Investigations on the Effects of Multi-Layered Coated Inserts in Machining Ti-6Al-4V Alloy with Experiments and

Finite Element Simulations. CIRP Ann. - Manuf. Technol. 2010, 59 (1), 77–82. https://doi.org/10.1016/j.cirp.2010.03.055.

45. Corduan, N.; Himbart, T.; Poulachon, G.; Dessoly, M.; Lambertin, M.; Vigneau, J.; Payoux, B. Wear Mechanisms of New Tool Materials for Ti-6AI-4V High Performance Machining. CIRP Ann. - Manuf. Technol. 2003, 52 (1), 73–76. https://doi.org/10.1016/S0007-8506(07)60534-4.
46. Jin, L. Adhesion Mechanisms of Ti-6Al-4V to PVD Coatings, University of Windsor, Canada, 2015.

Chapter 2. Development of Coating for Finish Turning Operation

Chowdhury, M.S.I, Bose, B., Yamamoto, K., Shuster, L.S., Paiva, J., Fox-Rabinovich, G., & Veldhuis, S.C. (2021). Wear performance investigation of PVD coated and uncoated carbide tools during high-speed machining of TiAl6V4 aerospace alloy. Wear, Volume 446-447, pp. 203168.

Author's Contribution

Mohammad Shariful Islam Chowdhury	Designed the research methodology. Performed the experiments. Analyzed the results. Wrote the manuscript.
Bipasha Bose	Assisted with designing the research methodology. Assisted with analyzing the data. Assisted with writing and editing the manuscript.
Kenji Yamamoto	Assisted with designing the research methodology. Deposited the coating.
Lev Shuster	Assisted with data collection for coefficient of friction study at the tool-workpiece interface.
Jose Paiva	Assisted with designing the research methodology.
German Fox-Rabinovich	Assisted with designing the research methodology. Edited the manuscript. Supervised the project.
Stephen Veldhuis	Assisted with designing the research methodology. Edited the manuscript. Supervised the project.

Abstract

Selection of hard PVD coatings for the machining of Ti6Al4V alloy should be based on the dominant tool wear mechanism and tribological phenomena occurring at the chip-tool-workpiece interface. The present work investigates the effect of AlTiN and CrN hard coatings on the wear performance of cemented carbide cutting tools during high-speed finish turning of Ti6Al4V. The wear characteristics of the tools were evaluated by SEM and 3D wear volume measurements. The in-situ tribological performance of the coatings was characterized by chip morphology analysis, in combination with coefficient of friction measurements using a high temperature/heavy load tribometer that mimics actual machining conditions. Micro-mechanical characteristics of the coatings were also studied in detail. The results obtained show that the application of a CrN coating significantly improves tool performance due to a combination of the micro-mechanical properties of the coating and the tribological characteristics of the surface engineered layer.

Keywords

Finish turning, Ti6Al4V alloy, PVD coating, built up edge (BUE), crater wear, tribo-films.

2.1. Introduction

Developing a wear resistant PVD coating for the machining of TiAl6V4 presents a significant challenge. One of the main difficulties is posed by intensive sticking of the titanium workpiece to the tool surface that often results in the detachment of the coating layer [1]. Therefore, an uncoated tool often outperforms a coated one. Wear phenomena during the machining of a TiAl6V4 alloy are very complex [2–5]. Intensive adhesive interaction takes place at the workpiece-tool interface combined with built up edge (BUE) formation [5,6]. BUE plays a dual role in the wear performance of coated cutting tools. It predominantly forms at lower speeds and protects the surface of the tool [7,8]. However, BUE is an unstable structure with a temporal avalanche-like performance that eventually causes severe surface damage once the structure is destroyed during cutting [9]. Moreover, a dynamic thermal barrier TiC interlayer forms at the built up carbide tool interface [7,8] which makes the phenomenon even more complicated. However, the dominant wear mechanism significantly changes with increase in cutting speed [9]. The intensity of BUE formation is lower at higher speeds, since the built up wears out at an accelerated rate [10]. Therefore, the thermal barrier TiC layer is no longer capable of performing its protective role at the tool/chip interface, and the dominant wear mechanism shifts to cratering due to the rapid (thermally enhanced) diffusion of the cutting tool material into chips [11]. For this reason, the cratering wear mechanism begins to control overall tool life.

The selection of coatings in the present study was based on industrial practice and previously published data on coatings used for the machining of titanium alloys [12]. Two major categories of coatings are considered in literature: AlTiN-based [13] and CrN-based

[14,15]. The AlTiN family of coatings are the most widely used in industry [12]. The CrN coating, is generally a good candidate for the machining of non-ferrous alloys due to its very low affinity to non-ferrous workpieces [16]. CrN is also known to have high chemical stability, which results in good corrosion and oxidation resistance [14], improved tribological properties (low coefficient of friction) and toughness [15,17–19]. These properties are of great importance during the machining of sticky titanium alloys. It was previously shown that for some cutting tool applications, CrN coating delivers better results, especially at low speeds, compared to (Ti, Al) N coatings due to strong adhesion to the tool substrate and high resistance to adhesive wear [20]. The major focus of this research is the selection of the optimal PVD coating for wet finish turning of Ti6Al4V alloy at high speeds of 150 m/min, where the crater tool wear mechanism is predominant.

2.2. Experimental Details

2.2.1. Coating deposition

All coatings were deposited on polished cemented carbide CNGG432FS inserts from Kennametal. The tested AlTiN commercial coating was supplied by Kennametal and designated as KC5010 grade. It is an advanced PVD coating whose applications range from finishing to general machining of most steels, stainless steels, non-ferrous materials, cast irons and super alloys. The CrN coating was deposited by arc evaporation using a AIP-S20 PVD coater (Kobelco, Japan) from a 100 mm diameter Cr target (99.9% purity). The mirror polished cemented carbide substrates were ultrasonically cleaned in acetone prior to deposition. After the pumping-down procedure (reaching a pressure of 1 × 10-2 Pa), in-situ cleaning of the substrate was performed by argon ion etching using a substrate bias voltage

of 400 V at 1.33 Pa pressure for 7.5 min. The Cr target was powered in arc mode. The working table rotated at 5 rpm during the process. During coating deposition, a constant working pressure of 4.0 Pa was maintained with N_2 as process gas. The substrate temperature was 500 °C. The coating deposition was conducted at a bias voltage of -50V for 20 mins.

2.2.2. Coating characterization

Coating thicknesses were determined using Calotest and reconfirmed with measurements on the fractured sections of the coatings. X-ray diffraction (Proto AXRD Benchtop Powder Diffraction System, Proto Manufacturing) with Cu-Kα radiation was performed to determine the preferred orientation and crystal structure of the coating. Residual stresses were evaluated with a conventional X-Ray diffractometer (Proto LXRD Stress Analyzer, Proto Manufacturing), using the $\sin^2 \psi$ method. A 1.0 mm round aperture was used to perform residual stress measurements with total collection time of about 80 seconds by a multiple exposure technique at 4 second per step for 22 ψ (psi) tilts. Measurements were carried out using Cu-Kα (1.541 Angstroms) radiation on the (422) plane at a diffraction angle of around 130°. A Gaussian function was used to fit the diffraction peaks. Fluorescence was suppressed by Ni filters.

Generation and chemical nature of tribo-oxides were determined using X-Ray Photoelectron Spectroscopy (XPS). A Physical Electronics (PHI) Quantera II (Physical Electronics Inc., Chanhassen, MN, USA) spectrometer equipped with an Al anode source for generating X-rays and a hemispherical energy analyzer was used to collect the XPS spectra. The generated X-rays were focused with a quartz crystal mono-chromator. The

mono-chromatic Al-Kα X-ray (1486.7 eV) source was operated at 50W and 15 kV. The system base pressure was as low as 1.33 × 10−7 Pa with an operating pressure not exceeding 2.67 × 10−6 Pa. The samples were sputter-cleaned for 4 min using a 4-kVAr+ beam before any spectra was collected. All data were obtained using a 200-μm beam. All survey spectra were gathered at a pass energy of 280 eV and high-resolution spectra at a pass energy of 55 eV. All spectra were collected at a 45° take off angle. Neutralization of all samples was ensured by a dual-beam charge compensation system. The equipment was calibrated by setting the C1s C–C peak to 284.8 eV and the Ag 3d5/2 peak to 368 eV in a freshly cleaned Ag reference foil. PHI Multipak version 9.4.0.7 software was used to analyze all the data.

The micro-mechanical properties of the coatings were measured using a Micro Materials NanoTest P3 system on polished WC-Co samples. Nano-indentation was performed using a Berkovich diamond indenter in a load-controlled mode. Following the ISO14577–4 procedure, the indenter was calibrated in terms of shape, displacement, load and frame compliance. 40 indentations at a peak load of 50 mN were performed per coating. The load was selected to ensure that the indentation contact depth was within 1/10 of the film thickness and to minimize the influence of the sample's surface roughness. This ensures that only the coating (load-invariant) hardness was measured alongside coating-dominated elastic modulus. The indentations were performed with a dwell period of 5 seconds at maximum load and room temperature, followed by 60 seconds of post indentation thermal drift correction.

Micro-scratch tests were performed by an Anton Paar-RST3 Revetest® Scratch Tester. A 200 μm end radii Rockwell diamond indenter was used. The test was performed in a 3-scan procedure progressive mode. The 3-scan procedure of the scratch test consisted of an initial topography scan, followed by a ramped scratch scan in which the load was ramped up from a minimum load of 0.5 N to a maximum load of 150 N and then completed with a post topography scan. The ramping load rate was 498.33 N/min with a scan speed and total scan length of 10 mm/min and 3 mm, respectively. At least 3 scratch tests were performed on all samples. The Anton Paar-RST3 Revetest® Scratch Tester was used to assess the toughness of the two coatings using a modified Palmqvist toughness method (ISO 28709). The load applied for the test was 100 N and the toughness values were given by the quotient of the load and the total crack lengths (from crack tip to indentation corner) from all four corners of each indent.

A specially designed apparatus described in [21] was used to determine the relationship between the coefficient of friction and temperature at the tool-workpiece interface. The apparatus mimics the adhesive interaction at the tool-workpiece interface during machining conditions. The apparatus operates by rotating a coated pin between two polished discs of workpiece material (TiAl6V4 alloy). The discs were resistively heated to a temperature range of between 25 °C to 1000 °C to simulate friction conditions at the tool-workpiece interface. Plastic strain in the contact zone was generated by applying a force of 2400 N. The friction coefficient value was calculated by the ratio amongst the shear strength of the adhesive bonds and the normal contact stress generated at the interface. Three tests were

conducted for each coating and the estimated magnitude of error of the coefficient of friction was approximately 5%.

2.2.3. Machining studies

Progressive tool wear studies were conducted under a wet turning condition of an ASTM B265 Grade 5 Ti6Al4V aerospace alloy. According to ISO 3685:1993 and ISO 8688-2:1989, the tool life criterion was set to be a maximum flank wear of 0.3 mm. The flank wear measurements were taken by a Keyence optical microscope (model VHX-5000 Series, KEYENCE America, Elmwood Park, NJ, USA). Detailed inspections of the inserts were carried out after every 600 m length of cut with an Alicona Infinite Focus G5 3D surface measurement system (Alicona Manufacturing Inc., Bartlett, IL, USA) and a scanning electron microscope, SEM (Vega 3-TESCAN, Brno Kohoutovice, Czech Republic). 3D topographic images of the cutting inserts with real color information were generated by the Alicona 3D optical system with focus-variation technology. Cutting tool topography was characterized by a 3D-motif analysis at a magnification of 10x. According to ISO 25178-2 [22], a 3D-motif is defined as a valley and/or peak (hill) that includes the critical points (peaks, valleys and saddle points) and the critical lines (ridge lines and course lines). The 3D-motif analysis compared the worn and the new cutting edge.

All turning tests were performed on CNGG432FS cemented carbide (WC, 6% Co) grade K313 turning inserts from Kennametal. The turning tests were conducted in a NAKAMURA SC450 turning machining center (Nakamura company, Hakusan Ishikawa, Japan) in an MCLN-5° Kennametal KenlocTM tool holder under flood coolant condition. The cutting fluid was directed at the tool tip via a nozzle at a flow rate of 14 L/min. An

XTREME CUT 290 (Qualichem, Salem, VA, USA) semi-synthetic cutting fluid, typically recommended for machining aerospace alloys, was used during machining. The cutting conditions (Table 2.1) were selected based on industrial recommendations. The cutting tests were repeated at least 3 times for each coating. The scatter of the tool life measurements was approximately 10%. Chip characteristics was analyzed using standard procedures [23]. EBSD analysis of chip cross sections was conducted by a JEOL JSM-7000F high-resolution SEM, operating at 20kV and 60 µm aperture size. A CCD detector was used at a 181 mm insertion distance. The sample was tilted by 70 degrees and working distances ranged from 8 to 12 mm.

Table 2.1. *Cutting data for the experiments performed.*

Cutting data							
Machining operation	**Cutting tool substrates**	**Workpiece material**	**Workpiece hardness, HRC**	**Speed, m/min**	**Feed, mm/rev**	**Depth of cut, mm**	**Coolant Condition**
Turning	Kennametal CNGG432FS Grade K 313 Turning inserts	TiAl6V4 alloy	37-38	150	0.1225	0.25	Flood

2.3. Results and discussion

2.3.1. Structural and mechanical properties of the coatings

The mechanical properties and structure of the coatings were thoroughly investigated in this paper. Figure 2.1 shows the fracture sections of the coatings. The thickness of the monolayer AlTiN coating with cubic microstructure is 1.94 µm (Table 2.2). The CrN coating has a similar thickness of 1.80 µm (Table 2) as well as a monolayer cubic microstructure. XRD data for CrN are shown in Fig. 2. The coating shows distinct diffraction peaks in the (111), (200) and (220) crystallographic planes, with other peaks

being less intense. The intensity of the (200) peak was the highest, indicating a preferred (200) orientation. The residual stress values, as well as micro-mechanical properties of the coatings are given in Table 2.2. The CrN coating has higher compressive residual stresses values than the AlTiN coating. However, the CrN coating has a lower hardness and increased plasticity index compared to the AlTiN coating. Plasticity index is the ratio between the plastic work done during indentation and the total plastic and elastic work done during indentation [24]. It was observed that during applications featuring heavy loads typical of titanium machining, a higher plasticity index indicates higher toughness and durability of the coating [25]. Toughness is the capability of a material to absorb energy during the deformation leading up to fracture as well as its ability to resist crack propagation [26]. A modified Palmqvist toughness test shows that the CrN coating has higher toughness (Table 2.2). Since both AlTiN and CrN coatings were deposited on the same substrate, it can be concluded that the difference in the toughness values is entirely associated with the coatings.

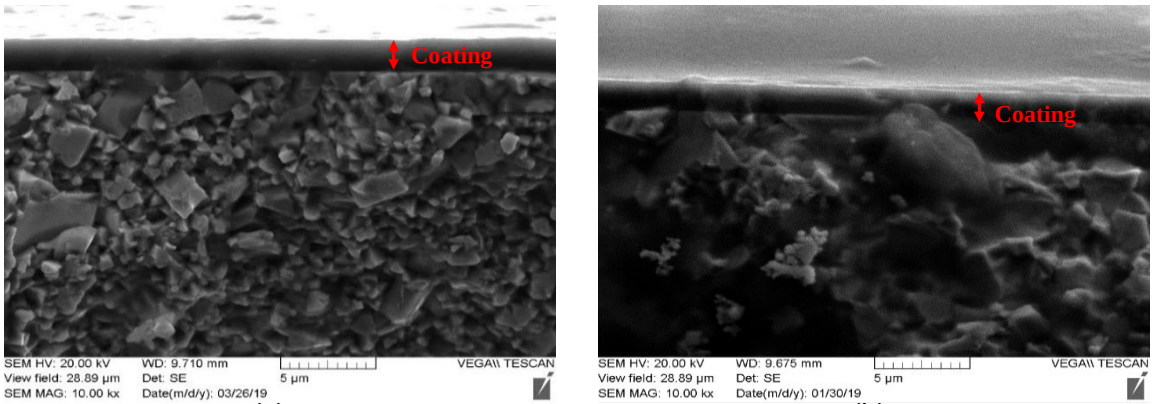

Figure 2.1. *SEM images of fracture sections of coatings: a) AlTiN; b) CrN.*

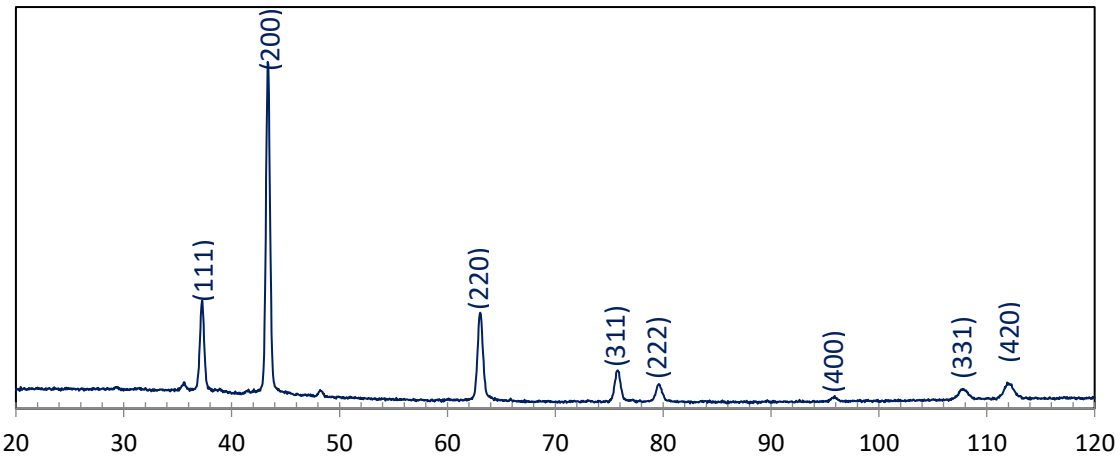

Figure 2.2. *XRD data of monolayer CrN coating.*

Table 2.2. *Micro-mechanical properties of the coatings.*

Coating	Architecture	Properties							Modified Palmqvist Toughness, N/µm
		Thickness, µm	Hardness, GPa	Elastic modulus, GPa	Plasticity index	H/E ratio	H^3/E^2 ratio	Residual stresses, MPa	
AlTiN	Monolayer	1.94	28.9 ± 2.0	516.52	0.46	0.056	0.09	-599 ± 168	1.37
CrN	Monolayer	1.80	21.1 ± 2.4	534.5	0.63	0.039	0.033	-955 ± 68	1.5

A scratch test is an effective method of analyzing the responses of a coating under a variety of loads. It can be used to investigate microscopic plastic deformation performance, frictional and wear characteristics as well as micro-cracking behaviour of the subsurface/surface layers [27]. Scratch test results of CrN and AlTiN show that the deformation mechanism during highly loaded sliding contact is quite different in the two coatings. Coefficient of friction data reveal resistance to scratching within the coating layer. The lower value of coefficient of friction in the CrN coating indicates better resistance of the coating against peeling during friction. The scratch tracks, illustrated in Figure 2.3 and Figure 2.4, show that the AlTiN coating fails in a brittle manner with substrate exposure even outside the scratch track, whereas in the CrN coating, failure occurs by plastic flow.

In the CrN coating, the deformation is localized with no substrate exposure outside the scratch track. Such scratch test behaviour of the coatings could be related to their hardness, H/E, H^3/E^2 ratios and residual stress. The H/E ratio of a coating indicates the elastic strain to failure characteristics of the coating and the H^3/E^2 ratio indicates the coating's resistance to plastic deformation [28]. Compared with the AlTiN coating, H/E and H^3/E^2 ratios are lower in the CrN coating. The elastic modulus of both coatings is quite comparable. Therefore, the lower H/E and H^3/E^2 ratios can be attributed to the significantly lower hardness of the CrN coating. Lower hardness and lower H^3/E^2 ratio indicate that CrN has less brittleness. Also, combined with the fact that CrN coating has higher compressive stress, it can undergo greater plastic deformation under the applied load. The aforementioned characteristics of the CrN coating are extremely important for machining applications where BUE formation is present, since they inhibit coating detachment when BUE is removed during cutting, which provides better substrate protection. Thus, the improved performance of the CrN coating could be associated with the lower hardness and tougher behaviour of the coating.

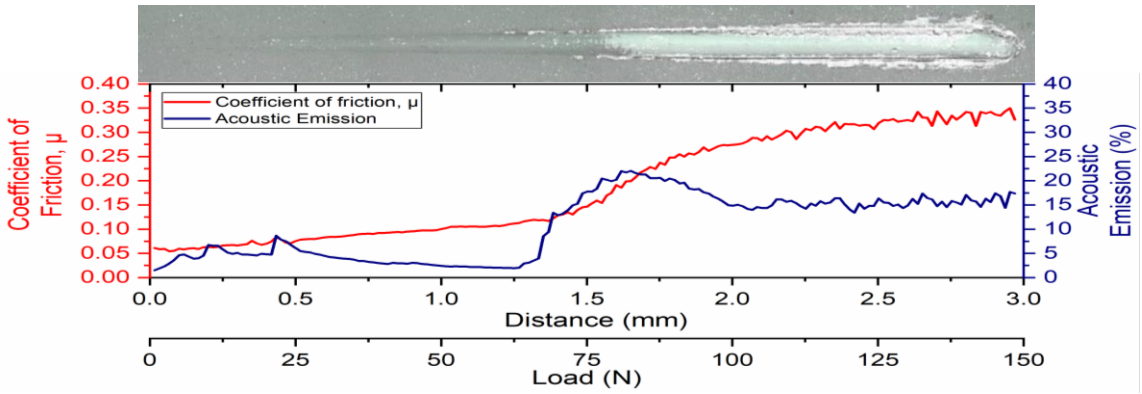

Figure 2.3. *Scratch track data for AlTiN coating.*

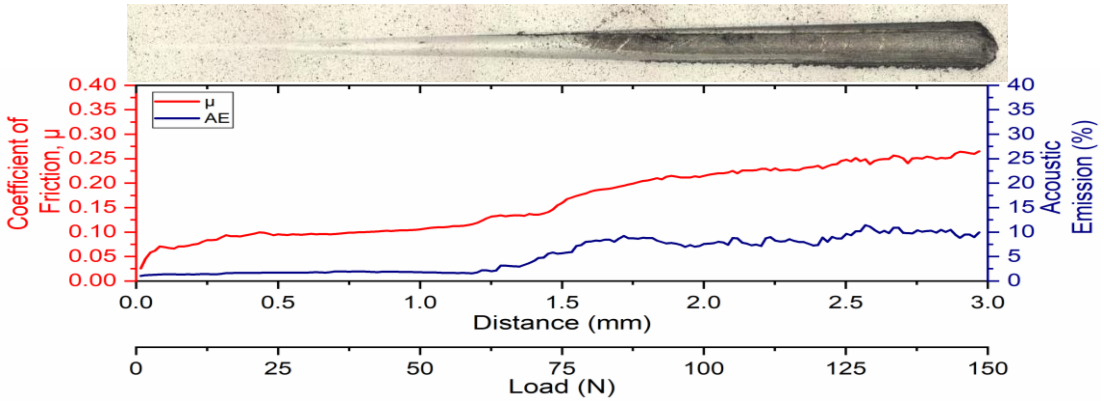

Figure 2.4. *Scratch track data for CrN coating.*

It is known that in machining applications where the adhesive wear mechanism is present, a coating with a high H/E ratio has less wear resistance [21,29]. Thus, under heavy loaded tooling applications where intensive surface deformation of surface layers occurs during friction, a so-called elastic strain to failure (H/E) is crucial for achieving better tool life [21,29]. This should be considered in combination with plasticity index values (Table 2.2). Under heavy loaded applications, coatings also need to have an increased ability to dissipate frictional energy that arises from severe deformation of the surface layers. The more energy is dissipated, the less of it is spent on deformation and damaging of the carbide material. Higher values of plasticity index, in this case for the CrN coating, are associated with higher energy dissipation under loading. The plasticity index parameter has similar implications as the H/E parameter [30,31]. Both parameters could be used to evaluate the wear behaviour of heavy-loaded tribo-systems under conditions of intensive adhesive wear, typical during titanium alloy machining. Therefore, a CrN coated carbide with lower hardness and H/E ratio, as well as higher plasticity index and toughness, demonstrates better wear performance as well as longer tool life.

2.3.2. Tool wear studies

Tool life and wear performance studies were carried out at a speed of 150 m/min, where BUE formation was diminished [8], but tool life was short due to the intensive crater wear [8]. Figure 2.5 presents flank wear vs. length of cut data for wet turning of both coated and uncoated tools at a cutting speed of 150 m/min. The tool wear intensity is ranked from the highest being present in the AlTiN coated tool to the lowest in the CrN coated tool with that of the uncoated being in between. The CrN coated tool outperformed the AlTiN coated tool by ~129% and the uncoated tool by ~45%.

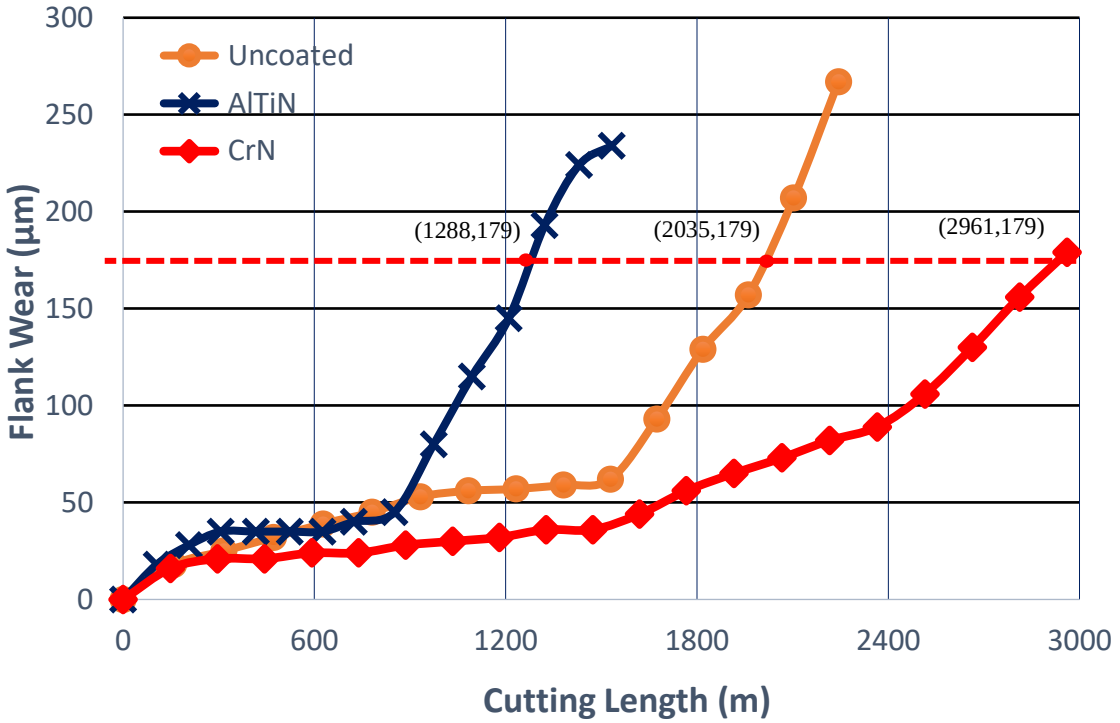

Figure 2.5. *Flank wear vs. length of cut data under wet conditions at 150 m/min for coated and uncoated tools.*

To explain why the CrN coating outperformed the others and to understand the tool wear mechanism, progressive wear studies were performed following every 600 m length of cut using 3D optical imaging combined with SEM wear pattern studies (Figure 2.6 and

Figure 2.7). Two wear phenomena are prevalent under the outlined machining conditions: crater wear and intensive adhesive interaction at the tool/chip interface. The red color on the 3D images (Figure 2.6 and Figure 2.7) represents BUE, while the blue color represents crater wear formation. 3D and SEM images of the uncoated tools show significant BUE formation along with crater wear formation that propagate with cutting. At elevated cutting speeds present during Ti6Al4V machining, the diffusion wear mechanism begins to prevail due to high cutting temperature generation, which generates severe cratering on the rake face of the tool [32].

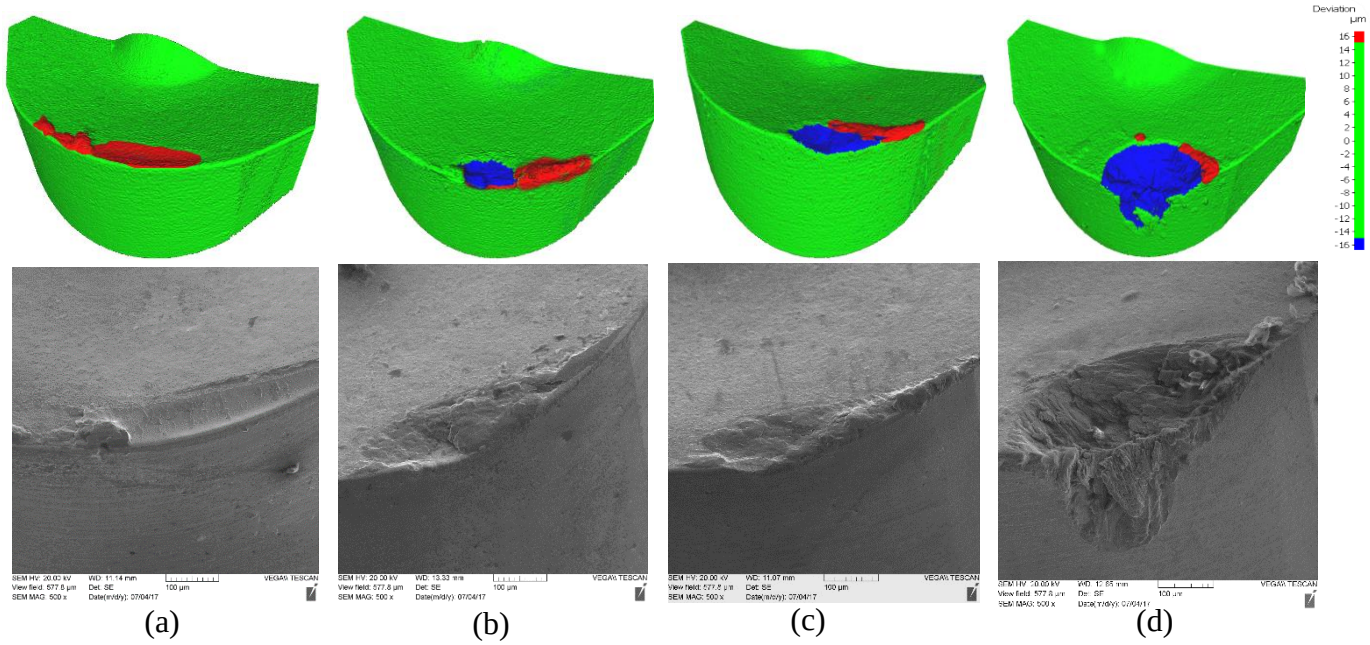

Figure 2.6. *3D progressive wear data for uncoated tool after every 600 m length of cut: (a) 600 m; (b) 1200 m; (c) 1800 m; (d) 2400 m.*

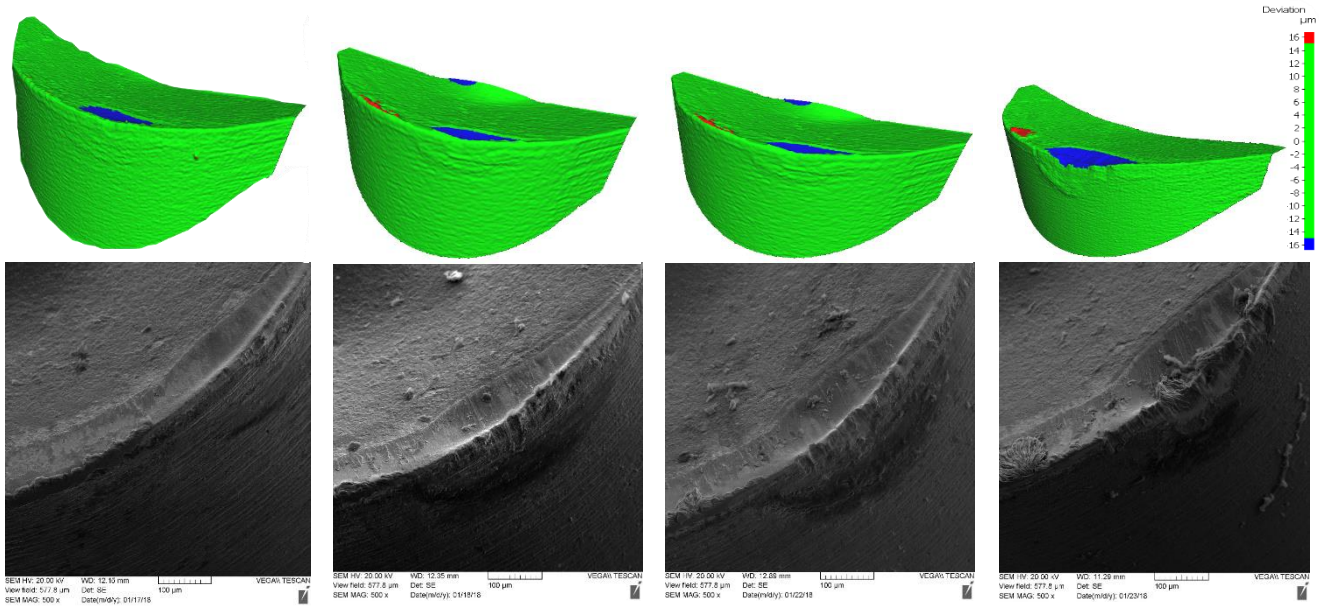

(a) (b) (c) (d)

Figure 2.7. *3D progressive wear data for CrN coated tool after every 600 m length of cut: (a) 600 m; (b) 1200 m; (c) 1800 m; (d) 2400 m.*

It is interesting to note that all tools show a very stable form of wear up to a certain point, before beginning to rapidly fail (Figure 2.5). The onset of this rapid failure can be linked to the moment when crater wear expands to the flank edge of the cutting tool. Figure 2.8 and Figure 2.9 show the progression of BUE and crater wear vs. length of cut for uncoated and coated tools. Significant BUE formation is observed in the uncoated tool compared to the coated tools. The BUE instability is also demonstrated by the increment and decrement of the peak volume in relation to previous passes (Figure 2.8). Compared to an uncoated and a AlTiN coated tool, the CrN coated tool has less BUE formation, which decreases the possibility of tool edge chipping following BUE removal. The CrN coating also has reduced crater wear intensity, as well as delayed propagation of crater wear with the length of cut. This results in a more uniformly increasing wear, which prevents the rapid failure of the CrN coated tool (Figure 2.7 and Figure 2.9). It should be noted here that the

reduced crater wear values of the uncoated tool (Figure 2.9) are caused by the BUE covering the crater wear on its rake surface. This is confirmed by the SEM images (Figure 2.6 (c) and Figure 2.7 (c)).

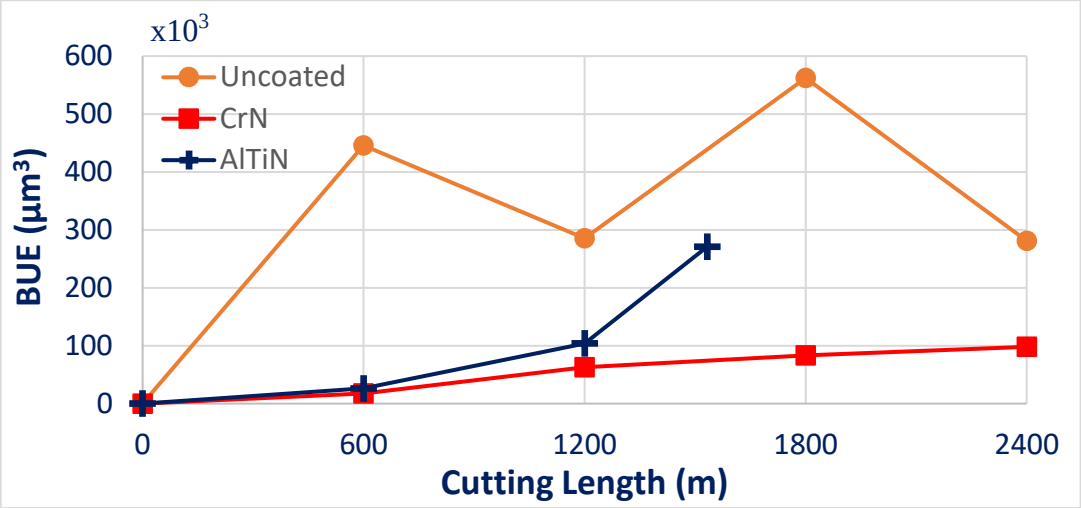

Figure 2.8. *Built up volume for coated and uncoated tools considering the peaks above reference surface of the original tool.*

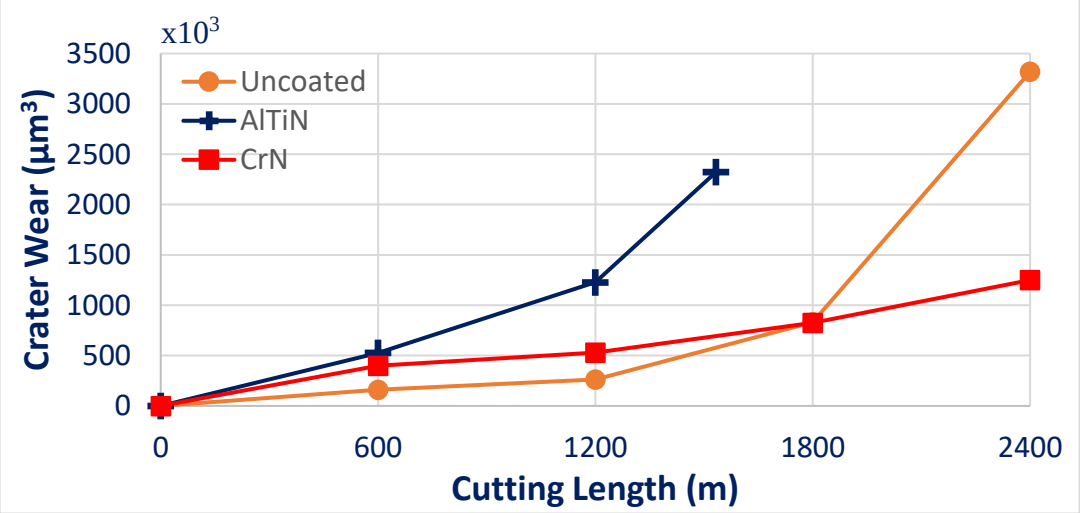

Figure 2.9. *Crater wear volume for coated and uncoated tools considering the peaks below reference surface of the original tool.*

2.3.3. Tribological analysis

Analysis of the CrN coated tool reveals that the crater wear intensity and overall sticking of the workpiece material to the friction surface of the tool has been diminished compared to the uncoated tool (see Figure 2.6 and Figure 2.7). The tool life improvement of the CrN coated tool could be attributed to two groups of characteristics: micro-mechanical (see section 3.1) and tribological. Compared to the AlTiN coating, the CrN coating shows lower hardness and an increased plasticity index (Table 2.2). Scratch tests (Figure 2.3 and Figure 2.4) reveal that under loaded sliding contact, the AlTiN coating fails in a much more brittle manner compared to the CrN coating, with higher substrate exposure being indicated by acoustic emission data. The sliding contact friction is also much higher in the AlTiN coating, as shown by the coefficient of friction data during the scratch test. Thus, for the outlined application, the softer and tougher CrN coating features superior performance due to its ability to sustain intensive sticking without peeling off and better tribological behaviour under loaded conditions typical of Ti6Al4V alloy machining.

Tribological behaviour of the coatings in contact with the Ti6Al4V alloy were assessed via: 1) the investigation of tribo-film formation on the tool/chip interface during cutting; 2) evaluation of the coefficient of friction vs. temperature of the coatings, and 3) evaluation of the chip characteristics (Table 2.3). All analyses show that the uncoated and AlTiN coated tool feature worse tribological properties compared to the CrN coated tool.

Tribological performance is strongly associated with the adaptive behaviour of the coating. This is directly related to the formation of tribo-films on the friction surface [9]. In general, tribo-films affect the wear behaviour of cutting tools in two ways: (1) they serve

as a thermal barrier due to the lower thermal conductivity of the corresponding tribo-oxides; and (2) they provide in-situ lubrication to reduce the intensity of workpiece material sticking to the tool [9]. During cutting, a strong temperature gradient is created, with the highest temperature being present on the rake surface of the tool, where the crater wear intensity is at its maximum. XPS analysis of tribo-film formation on the worn surface of the tool helps explain the superior performance of the CrN coating (Figure 2.10). The data obtained show that the CrN coating layer undergoes tribo-oxidation, forming a Cr_2O_3 tribo-ceramic on the rake surface of the tool. These films have a corundum structure [33] and provide thermal barrier properties at high cutting temperatures [34]. The temperature at the tool/chip interface during cutting under the outlined conditions is around 900-950 °C [8], at which these tribo-films function with a fair degree of efficiency. This is supported by coefficient of friction vs. temperature data shown in Figure 2.11. The apparatus used to determine the relationship mimics the adhesive interaction that occurs during machining. It can be seen that the coefficient of friction values in the CrN coating are significantly lower compared to the uncoated and the AlTiN coated tool. Thus, these tribo-films can serve as a functional substitute for the thermal barrier TiC interlayer that forms at lower speeds [35], reducing the crater wear intensity and friction at the tool/chip interface.

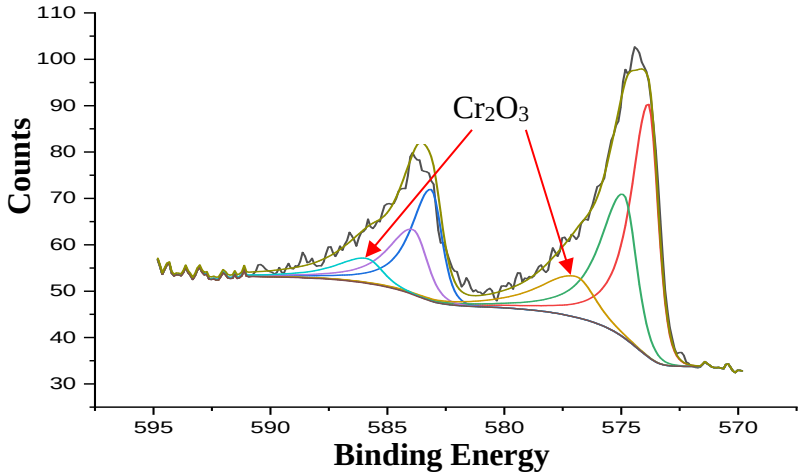

Figure 2.10. *High resolution XPS data of worn rake surface of CrN coated insert, Cr2p spectrum.*

Tribological conditions at the tool/chip interface play a significant role during the chip formation process. To evaluate chip characteristics, the chips were collected at the beginning of the cut (approximately 50 m cutting length). The data are presented in Table 2.3. The tribological characteristics of the coating layer show good correlation with coefficient of friction data (Figure 2.11) and indicate the same trend. The chip compression ratio is greater in the CrN coating, which yields a higher shear plane angle. This signifies that the shearing force acting on the CrN chips is lower, which results in the reduction of cutting and frictional forces at the tool/chip interface. CrN chips have higher chip sliding velocity, indicating a lower tool/chip contact length and a consequently lower rise in temperature at the cutting zone. Higher chip sliding velocity also confirms lower friction at the tool/chip interface. The chip characteristics thus demonstrate lower friction being present at the tool/chip interface, which increases tool life in the CrN coating.

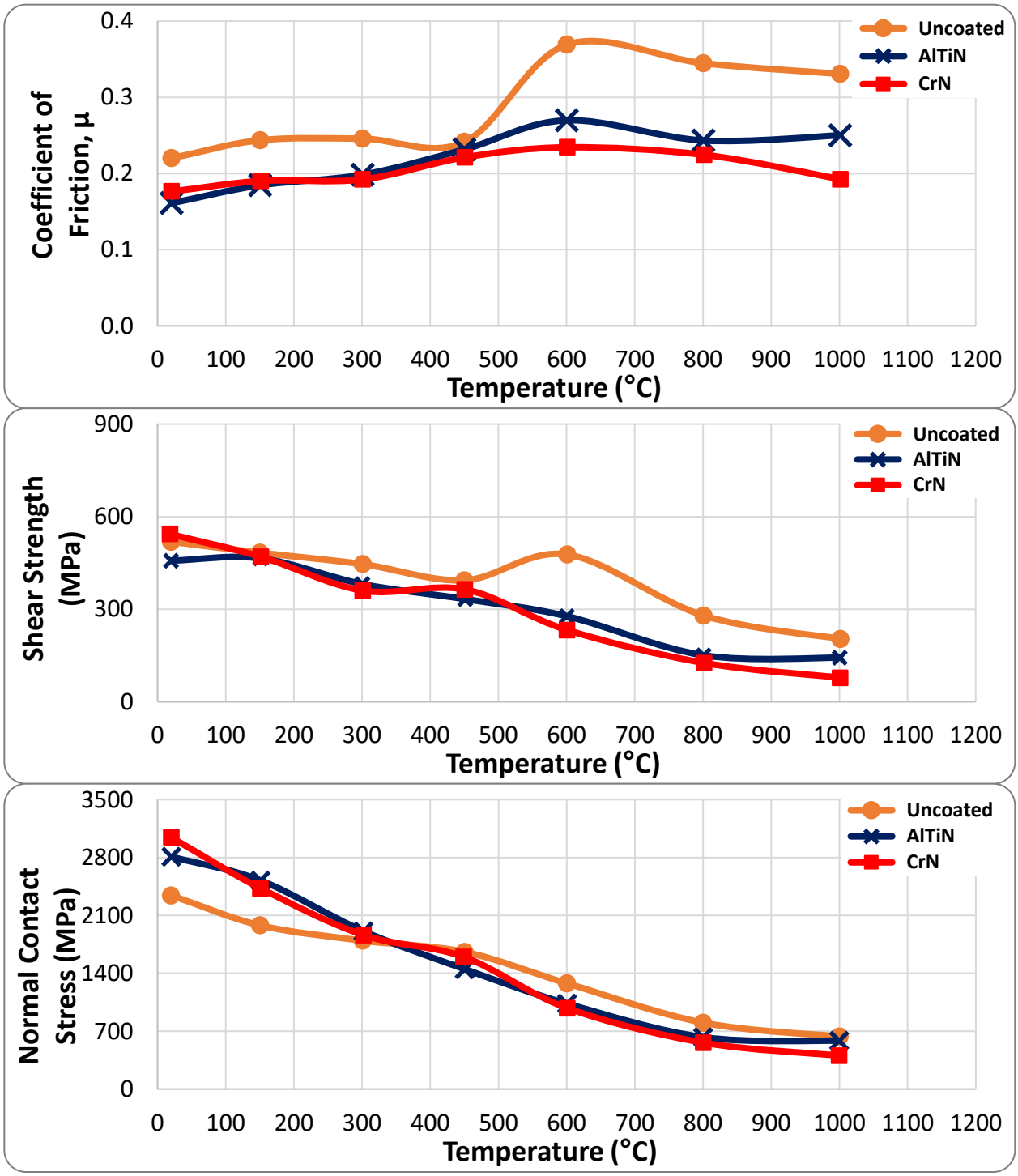

Figure 2.11. *Coefficient of friction, shear strength and normal contact stress vs. temperature data for uncoated and coated tools.*

Table 2.3. *Tribological performance evaluated through chip characteristics.*

Coating	Chip Compression Ratio - CCR	Φ - Shear Angle (°)	(ϒ) Shear Strain	Chip sliding Velocity (m/min)
AlTiN	1	48.50	0.66	150
CrN	1.4	59.17	0.37	210

To confirm that the chip flow process is improved in the CrN coating, cross sectional EBSD analysis was performed on the chips of the coated tools collected during cutting. Results presented in Figure 2.12 show the microstructure and texture orientation of the chips. Overall, the images display the main deformed zone on the edge close to the interface between the cutting tool and the chip. Both chips present a grain refinement in this zone. However, the chips produced by CrN coating show a tendency to nucleate to an ultrafine grain on the shear boundaries, which confirms the enhancement of the chip flow process. It has also been observed that the accelerated chip flow promotes dynamic recrystallization, where new grain orientation takes place as shown in the orientation maps. This probably increases the slip planes which enhances the plasticity of the chips.

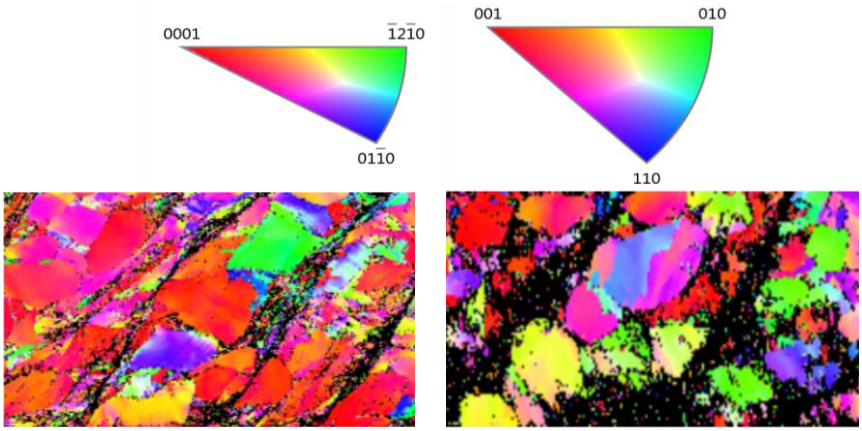

Figure 2.12. *EBSD analysis of chip cross section showing orientation and phase map: (a) AlTiN; (b) CrN.*

2.4. Conclusions

Selection of the best hard PVD coating for the machining of a Ti6Al4V aerospace alloy strongly depends on the tool wear mechanisms and the tribological phenomena occurring at the chip-tool-workpiece interfaces. The wear performance of the PVD coatings evaluated in this work are considered and explained in relation to the mechanical and tribological conditions that develop at the tool/chip interface.

Different compositions of PVD coatings were tested under conditions of high-speed finish turning of TiAl6V4 aerospace alloy. The best tool life was exhibited by the CrN monolayer coating. This coating has a beneficial combination of micro-mechanical and tribological properties, which prevent intensive detachment of the coating layer under operation. Application of a CrN coating addresses the challenges posed by major wear mechanisms present in the high-speed machining of TiAl6V4 alloy, especially severe cratering. Due to the enhanced ability of the CrN coating to form thermal barrier Cr_2O_3 tribo-films under operation, the intensity of crater wear is strongly diminished, and the tool life is increased. The major novelty presented in this research consists of the demonstration of integral characteristics (adaptive performance, as well as the combination of micro-mechanical and tribological properties) of the CrN coating layer, which are mostly responsible for its superior wear performance under specific machining conditions.

2.5. References

1. M'Saoubi, R.; Axinte, D.; Soo, S. L.; Nobel, C.; Attia, H.; Kappmeyer, G.; Engin, S.; Sim, W. M. High Performance Cutting of Advanced Aerospace Alloys and Composite Materials. CIRP Ann. - Manuf. Technol. 2015, 64 (2), 557–580. https://doi.org/10.1016/j.cirp.2015.05.002.
2. Dearnley, P. A.; Grearson, A. N. Evaluation of Principal Wear Mechanisms of Cemented Carbides and Ceramics Used for Machining Titanium Alloy IMI 318. Mater. Sci. Technol. 1986, 2 (1), 47–58. https://doi.org/10.1179/026708386790123611.
3. Ezugwu, E. O.; Wang, Z. M. Titanium Alloys and Their Machinability. J. Mater. Process. Technol. 1997, 68 (3), 262–274. https://doi.org/10.1016/S0924-0136(96)00030-1.
4. Hartung, P. D.; Kramer, B. M. Tool Wear in Machining Titanium. Ann. CIRP 1982, 30 (1), 75–80.
5. Machado, A. R.; Wallbank, J. Machining of Titanium and Its Alloys-a Review. Proc Instn Mech Engrs, Part B J. Eng. Manuf. 1990, 204, 53–60.
6. Narutaki, N.; Murakoshi, A.; Motonishi, S.; Takeyama, H. Study on Machining of Titanium Alloys. CIRP Ann. - Manuf. Technol. 1983, 32 (1), 65–69. https://doi.org/10.1016/S0007-8506(07)63362-9.
7. Qi, H. S.; Mills, B. Formation of a Transfer Layer at the Tool-Chip Interface during Machining. Wear 2000, 245 (1–2), 136–147. https://doi.org/10.1016/S0043-1648(00)00474-9.

8. Paiva, J. M.; Shalaby, M. A. M.; Chowdhury, M.; Shuster, L.; Chertovskikh, S.; Covelli, D.; Junior, E. L.; Stolf, P.; Elfizy, A.; Bork, C. A. S.; Fox-Rabinovich, G.; Veldhuis, S. C. Tribological and Wear Performance of Carbide Tools with TiB_2 PVD Coating under Varying Machining Conditions of TiAl6V4 Aerospace Alloy. Coatings 2017, 7 (11), 187. https://doi.org/10.3390/coatings7110187.
9. Fox-Rabinovich, G. S.; Kovalev, A. I. Self-Organization and Structural Adaptation during Cutting and Stamping Operations. In Self-Organization During Friction: Advanced Surface-Engineered Materials and Systems Design; CRC Press, Taylor and Francis Group, Boca Raton, NW, USA, 2006.
10. Kabaldin, Y. G. The Structure-Energetic Approach to the Friction Wear and Lubricating Phenomenon at Cutting. J. Frict. Wear 1989, 10 (5), 800–801.
11. Trent, E. M.; Wright, P. K. Chapter 7 - Cutting Tool Materials II: Cemented Carbides. In Metal Cutting; Trent, E. M., Wright, P. K., Eds.; Butterworth-Heinemann: Woburn, 2000; pp 175–226. https://doi.org/https://doi.org/10.1016/B978-075067069-2/50009-7.
12. Biksa, A.; Yamamoto, K.; Dosbaeva, G.; Veldhuis, S. C.; Fox-Rabinovich, G. S.; Elfizy, A.; Wagg, T.; Shuster, L. S. Wear Behaviour of Adaptive Nano-Multilayered AlTiN/MexN PVD Coatings during Machining of Aerospace Alloys. Tribol. Int. 2010, 43 (8), 1491–1499. https://doi.org/10.1016/j.triboint.2010.02.008.
13. Sharif, S.; Rahim, E. A. Performance of Coated- and Uncoated-Carbide Tools When Drilling Titanium Alloy-Ti-6Al4V. J. Mater. Process. Technol. 2007, 185 (1–3), 72–76. https://doi.org/10.1016/j.jmatprotec.2006.03.142.

14. Milosev, I.; Strehblow, H. H.; Navinsek, B. Comparison of TiN, ZrN, and CrN Coatings under Oxidation. Thin Solid Films 1997, 303 (303), 246–254.
15. Berg, G.; Friedrich, C.; Broszeit, E.; Berger, C. Development of Chromium Nitride Coatings Substituting Titanium Nitride. Surf. Coatings Technol. 1996, 86–87 (PART 1), 184–191. https://doi.org/10.1016/S0257-8972(96)03042-3.
16. Lupicka, O.; Warcholinski, B. The Adhesion of CrN Thin Films Deposited on Modified 42CrMo4 Steel. Adv. Mater. Sci. Eng. 2017, 2017, 1–14. https://doi.org/10.1155/2017/4064208.
17. Sato, T.; Tada, Y.; Ozaki, M.; Hoke, K.; Besshi, T. A Crossed-Cylinders Testing for Evaluation of Wear and Tribological Properties of Coated Tools. Wear 1994, 178 (1–2), 95–100. https://doi.org/10.1016/0043-1648(94)90133-3.
18. Navinšek, B.; Panjan, P.; Milošev, I. PVD Coatings as an Environmentally Clean Alternative to Electroplating and Electroless Processes. Surf. Coatings Technol. 1999, 116–119, 476–487. https://doi.org/10.1016/S0257-8972(99)00145-0.
19. Bertrand, G.; Mahdjoub, H.; Meunier, C. A Study of the Corrosion Behaviour and Protective Quality of Sputtered Chromium Nitride Coatings. Surf. Coatings Technol. 2000, 126 (2–3), 199–209. https://doi.org/10.1016/S0257-8972(00)00527-2.
20. Kondo, A.; Oogami, T.; Sato, K.; Tanaka, Y. Structure and Properties of Cathodic Arc Ion Plated CrN Coatings for Copper Machining Cutting Tools. Surf. Coatings Technol. 2004, 177–178, 238–244. https://doi.org/10.1016/j.surfcoat.2003.09.039.
21. Fox-Rabinovich, G. S.; Shuster, L. S.; Beake, B. D.; Veldhuis, S. C. Physical and Mechanical Properties to Characterize Tribological Compatibility of Heavy Loaded

Tribo-Systems (HLTS). In Self-Organization During Friction: Advanced Surface-Engineered Materials and Systems Design; CRC Press, Taylor and Francis Group, Boca Raton, NW, USA, 2006.

22. ISO 25178-2:2012 Geometrical Product Specifications (GPS)—Surface Texture: Areal—Part 2: Terms, Definitions and Surface Texture Parameters; International Organization for Standardization: Geneva, Switzerland, 2012.
23. Shaw, M. C. Metal Cutting Principles; Oxford University Press, Inc., 2005.
24. Beake, B. D.; Fox-Rabinovich, G. S.; Veldhuis, S. C.; Goodes, S. R. Coating Optimisation for High Speed Machining with Advanced Nanomechanical Test Methods. Surf. Coatings Technol. 2009, 203 (13), 1919–1925. https://doi.org/10.1016/j.surfcoat.2009.01.025.
25. Zhang, X.; Beake, B. D.; Zhang, S. Toughness Evaluation of Thin Hard Coatings and Films. In Thin Films and Coatings: Toughening and Toughness Characterization; CRC Press, Taylor and Francis Group, Boca Raton, NW, USA, 2015; p 52.
26. Zhang, S.; Zhang, X. Toughness Evaluation of Hard Coatings and Thin Films. Thin Solid Films 2012, 520 (7), 2375–2389. https://doi.org/10.1016/j.tsf.2011.09.036.
27. Zhang, F.; Meng, B.; Geng, Y.; Zhang, Y.; Li, Z. Friction Behaviour in Nanoscratching of Reaction Bonded Silicon Carbide Ceramic with Berkovich and Sphere Indenters. Tribol. Int. 2016, 97, 21–30. https://doi.org/10.1016/j.triboint.2016.01.013.
28. Leyland, A.; Matthews, A. On the Significance of the H/E Ratio in Wear Control: A Nanocomposite Coating Approach to Optimised Tribological Behaviour. Wear 2000, 246 (1–2), 1–11. https://doi.org/10.1016/S0043-1648(00)00488-9.

29. Sato, K.; Ichimiya, N.; Kondo, A.; Tanaka, Y. Microstructure and Mechanical Properties of Cathodic Arc Ion-Plated (Al,Ti)N Coatings. Surf. Coatings Technol. 2003, 163–164, 135–143. https://doi.org/10.1016/S0257-8972(02)00610-2.
30. Fox-Rabinovich, G. S.; Veldhuis, S. C.; Scvortsov, V. N.; Shuster, L. S.; Dosbaeva, G. K.; Migranov, M. S. Elastic and Plastic Work of Indentation as a Characteristic of Wear Behaviour for Cutting Tools with Nitride PVD Coatings. Thin Solid Films 2004, 469–470 (SPEC. ISS.), 505–512. https://doi.org/10.1016/j.tsf.2004.07.038.
31. Chowdhury, M. S. I.; Chowdhury, S.; Yamamoto, K.; Beake, B. D.; Bose, B.; Elfizy, a.; Cavelli, D.; Dosbaeva, G.; Aramesh, M.; Fox-Rabinovich, G. S.; Veldhuis, S. C. Wear Behaviour of Coated Carbide Tools during Machining of Ti6Al4V Aerospace Alloy Associated with Strong Built up Edge Formation. Surf. Coatings Technol. 2017, 313, 319–327. https://doi.org/10.1016/j.surfcoat.2017.01.115.
32. Hatt, O.; Crawforth, P.; Jackson, M. On the Mechanism of Tool Crater Wear during Titanium Alloy Machining. Wear 2017, 374–375 (December), 15–20. https://doi.org/10.1016/j.wear.2016.12.036.
33. Kramer, A.; Bignardi, L.; Lacovig, P.; Lizzit, S.; Batzill, M. Comparison of Surface Structures of Corundum Cr_2O_3 (0 0 0 1) and V2O3 (0 0 0 1) Ultrathin Films by x-Ray Photoelectron Diffraction. J. Phys. Condens. Matter 2018, 30 (7), 74002. https://doi.org/10.1088/1361-648x/aaa5ed.
34. Wang, D. Y.; Lin, J. H.; Ho, W. Y. Study on Chromium Oxide Synthesized by Unbalanced Magnetron Sputtering. Thin Solid Films 1998, 332 (1–2), 295–299. https://doi.org/10.1016/S0040-6090(98)01266-8.

35. Taylor, R. E. Thermal Conductivity of Titanium Carbide at High Temperatures. J. Am. Ceram. Soc. 1961, 44 (10), 525. https://doi.org/10.1111/j.1151-2916.1961.tb13718.x.

Chapter 3. Development of Coating for Rough Turning Operation

Chowdhury, M.S.I, Bose, Rawal, S., Fox-Rabinovich, G., & Veldhuis, S.C. (2021). Investigation of the Wear Behaviour of PVD Coated Carbide Tools during Ti6Al4V Machining with Intensive Built Up Edge Formation. Coatings, Volume 11, pp. 266.

Author's Contribution

Mohammad Shariful Islam Chowdhury	Designed the research methodology. Performed the experiments. Analyzed the results. Wrote the manuscript.
Bipasha Bose	Assisted with designing the research methodology. Assisted with analyzing the data. Assisted with writing and editing the manuscript.
Sushant Rawal	Deposited the coating.
German Fox-Rabinovich	Assisted with designing the research methodology. Edited the manuscript. Supervised the project.
Stephen Veldhuis	Assisted with designing the research methodology. Edited the manuscript. Supervised the project.

Abstract

Tool wear phenomena during the machining of titanium alloys are very complex. Severe adhesive interaction at the tool chip interface, especially at low cutting speeds, leads to intensive Built Up Edge (BUE) formation. Additionally, a high cutting temperature causes rapid wear in the carbide inserts due to the low thermal conductivity of titanium alloys. The current research studies the effect of AlTiN and CrN PVD coatings deposited on cutting tools during the rough turning of a Ti6Al4V alloy with severe BUE formation. Tool wear characteristics were evaluated in detail using a Scan-ning Electron Microscope (SEM) and volumetric wear measurements. Chip morphology analysis was conducted to assess the in situ tribological performance of the coatings. A high temperature–heavy load tribometer that mimics machining conditions was used to analyze the frictional behaviour of the coatings. The micromechanical properties of the coatings were also investigated to gain a better understanding of the coating performance. It was demonstrated that the CrN coating possess unique micromechanical properties and tribological adaptive characteristics that minimize BUE formation and significantly improve tool performance during the machining of the Ti6Al4V alloy.

Keywords

PVD coating; Ti6Al4V, crater wear; built up edge (BUE); tribo-films.

3.1. Introduction

Titanium alloys are widely used in many industries, especially the aerospace and automotive sectors, due to their superior mechanical properties such as high corrosion resistance, biocompatibility, and good strength-to-weight ratio. However, they are considered to be difficult-to-cut materials due to a set of unique characteristics that severely affect machinability [1,2]. Titanium alloys retain strength even at elevated temperatures, leading to work hardening or strain hardening of the workpiece during machining. Their low thermal conductivity results in high cutting zone temperatures and consequent rapid tool wear [1,3]. They also have a high chemical affinity which causes intensive Built Up Edge (BUE) formation, especially during rough turning at low cutting speeds, contributing to premature tool failure and chipping [1,4,5].

Cemented carbide tools are the most widely used tools for titanium machining. Tool wear of cemented carbide tools during titanium machining is controlled mainly by two wear mechanisms: the first is adhesion wear that results in BUE formation and the second is diffusion wear causing crater wear formation. Adhesion caused BUE formation on both the flank and the rake surfaces of the cutting tool plays a significant role in flank wear [1,6]. Due to the diffusion of tool material into the workpiece mate-rial as it passes over the tool surface, crater wear ensuing from the high cutting temperature generated during titanium machining determines the degree of wear on the rake surface of the tool [7,8]. The predominant wear mechanism, however, can vary depending on the machining conditions. Typically, rough turning of the titanium alloys at lower cutting speeds is associated with severe BUE formation [9–11]. However, during finish turning at high speeds crater wear

becomes the predominant wear mechanism due to significantly higher cutting temperature generation [10–12].

Many research studies have considered the use of PVD coated tools to address these issues. However, in most cases, PVD coated tools perform worse than uncoated tools, since the unstable structure of the formed BUE facilitates detachment and sur-face damage of the coating layer [13,14]. Multiple research studies [1,12,15] have concluded that coatings such as TiN, TiC, TiCN, TiN-TiC, TiN–Ti(C,N)–TiC, Al_2O_3/TiC, Al_2O_3, and HfN feature higher tool wear rates than uncoated tools. However, several researchers [16,17], have reported a slight improvement in the tool performance of a single layer PVD TiN or a multilayer PVD TiN/TiCN/TiN and TiAlN coating at high cutting speeds compared with uncoated tools. Although coated carbide tools have had significant success in the machining of cast irons, steels, and many superalloys, they are yet to achieve the same level of efficiency when it comes to titanium machining. Extensive research is still required to address the tool wear issues during Ti6Al4V machining especially at a combination of low cutting speeds with a high depth of cut (i.e., rough turning) that promotes significant BUE formation. Since the performance of the cutting tool is strongly associated with the conditions of the machining process, PVD coatings used for Ti6Al4V machining must be selected according to the tribological interactions taking place at the tool–chip interface. The micromechanical and tribological characteristics of the coatings must be tailored to address the underlying predominant wear mechanism.

For machining applications with intensive BUE formation, the coating's lubricity [6] becomes a significant factor in determining its overall performance. A CrN coating is

generally used to machine nonferrous alloys due to its low chemical affinity with nonferrous materials [18]. CrN is known for its high chemical stability, good corrosion and oxidation resistance [19], improved toughness, and lower friction coefficient [20–23]. These properties are highly beneficial for the machining of sticky titanium alloys. It was previously shown that the CrN coating performs better compared to (Ti, Al) N coatings in some cutting tool applications, especially at low cutting speeds, due to its high resistance to adhesive wear and strong coating–substrate adhesion [24]. There-fore, a self-lubricating CrN coating was developed in the present study to minimize BUE formation during the rough turning of a Ti6Al4V alloy and improve tribological interaction at the tool–chip interface. The performance of this CrN coating was com-pared with that of uncoated tool and the widely used commercial AlTiN coating recommended in industry.

The authors, in a previous research paper [11], have shown that CrN coating, de-posited by Fine Cathode (FC) arc deposition process, improves tool performance during high-speed machining (finish turning) of Ti6Al4V alloy. This was due to the formation of Cr_2O_3 tribo-film with thermal barrier characteristics that reduced the propagation of crater wear. The authors also found evidence of the lubricating properties of Cr_2O_3 tribo-film. In the current research paper, detailed investigation of a CrN coating deposited by an advanced plasma-enhanced arc Superfine Cathode Process (SFC) [25] is conducted to assess tool performance during the rough turning of a Ti6Al4V alloy. The main goal of this research is to demonstrate that the unique micromechanical and tribological characteristics of the developed CrN coating can improve tool performance during the rough turning of a Ti6Al4V alloy associated with strong BUE formation giving maximum economic benefit

to the industries by reducing machining downtime and tooling cost. This investigation also suggests that CrN coating can possibly be considered as a general-purpose coating to be used for a wider cutting range condition.

3.2. Experimental Methods

3.2.1. Coating Deposition and Characterization

All the coatings investigated in the present study were deposited on Kennametal CNMG432 and polished Sandvik Coromant SPGN120308 cemented carbide uncoated inserts. The Kennametal CNMG432 were used to conduct the machining tests whereas all coating characterization were done on the flat polished Sandvik Coromant SPGN120308 inserts. Both the inserts have the same cemented carbide grade and have same microstructural composition. The commercial AlTiN coating was supplied by Kennametal. This advanced PVD coating is designated as KC5010 grade and is recommended for machining non-ferrous metals and superalloys. The CrN coating was deposited by a cathodic arc ion plating process using an AIP-S20 PVD (Kobe Steel Ltd., Kobe, Japan) deposition system. This coating system uses an advanced plasma-enhanced arc superfine cathode process (SFC) [25], which is a novel, magnetically controlled cathodic arc source. The SFC process enables the deposition of smooth coatings with low compressive residual stresses. A 105 mm diameter Cr target with 99.9% purity powered in the arc mode was used to deposit the CrN coating. The substrates were cleaned with acetone in an ultra-sound bath for 16 minutes before the deposition process. After pumping-down to a pressure of 1×10^{-2} Pa, the substrate was cleaned in situ by argon ion etching for 7.5 minutes at a substrate bias voltage of 400 V and pressure of 1.33 Pa. The substrate was heated to 500°C

and rotated at 5 rpm during the process. The CrN coating was deposited at a bias voltage of −50 V for 20 minutes at 4.0 Pa pressure, using nitrogen as a process gas.

The coating thicknesses were determined on the polished Sandvik Coromant SPGN120308 cemented carbide inserts using a BC-2 Miba Coating Group ball crater system and a steel ball with a diameter of 25 mm. The thicknesses were confirmed with optical measurements of the coatings' fractured sections done on a Vega 3-TESCAN scanning electron microscope (SEM) (Brno Kohoutovice, Czech Republic). The surface morphology of the coatings was evaluated using an Anton Parr Tosca^{TM} 400 atomic force microscope (AFM) (Graz, Austria). The system was operated in the tapping mode using commercial silicon probes with a resonant frequency of 285 kHz and a force constant of 42 N/m. The scan size was maintained at 25 μm x 25 μm. The image processing and data analyses were performed using Tosca^{TM} analysis software (Version-7.4.8341).

An XRD X-ray Diffraction System from Proto Manufacturing Limited (LaSalle, Ontario, Canada) with Cu-Kα (1.544 Å) radiation was used to determine the crystal structure and preferred orientation of the CrN and AlTiN coatings. Residual stresses were measured via a $\sin^2 \psi$ technique with a LXRD Stress Analyzer from Proto Manufacturing. These measurements were performed with a 1.0 mm round aperture in (422) and (200) planes identified at 2θ angles of 130° and 80° for CrN and AlTiN coat-ings, respectively. A Gaussian function was used to fit the diffraction peaks.

X-Ray Photoelectron Spectroscopy (XPS) was used to determine the formation and chemical composition of the tribo-oxides. A Kratos AXIS Supra (Kratos Analytical, Manchester, UK) spectrometer with a hemispherical energy analyzer collected the XPS

spectra. X-rays were generated with an Al anode source. The Al-Kα X-ray source was operated at a constant acceleration voltage of 15 keV and an emission current of 25 mA. The system's base pressure was not higher than 2×10^{-9} Torr and the operating pressure did not exceed 2×10^{-8} Torr. A 4 kV Ar+ beam was used to sputter-clean the samples for 5 minutes before any spectra were collected. A 50 μm beam was used to obtain all the data. All survey and high-resolution spectra were collected at pass energies of 160 eV and 40 eV, respectively. All spectra were obtained with the Kratos' pa-tented charge neutralization system. High-resolution data was calibrated by setting the C1s C–C peak to 284.8 eV. Analysis of the data was performed by CasaXPS Version 2.3.18 software.

The micromechanical properties of the coatings were evaluated using a Micro Materials NanoTest P3 system (Micromaterials, Wrexham, UK). Nanoindentation was performed in a load-controlled mode at a peak load of 50 mN and a dwell period of 5 seconds. A Berkovich diamond indenter was used to perform 40 indents per coating. The indenter was calibrated according to ISO14577–4 [26]. The load was adjusted to minimize the influence of the sample's surface roughness and to keep the indentation contact depth within 1/10 of the coating's thickness. This was to ensure that coating-only (load-invariant) hardness was measured in combination with the coating-dominated elastic modulus. The same instrument was used to perform nanoimpact tests on the coatings. The tests were done at room temperature using a cube-corner indenter. The indenter was accelerated 12 μm away from the coating surface with a 20 mN force that was used to produce an impact every 4 seconds for a total duration of 300 seconds. Five tests were performed at different locations for each coating.

Scratch tests were conducted with an Anton Paar-RST3 Revetest® Scratch Tester (Graz, Austria). A Rockwell diamond indenter with a 20 μm end-radius was used for the tests, which were performed in progressive mode. A 3-scan procedure was adopted for all tests. This procedure consisted of a pre topography scan at a 0.5 N load, a progressive load scratch scan in which the load was steadily increased from 0.5 N to 5 N, and a post topography scan at 0.5 N load. The total scratch length was 0.5 mm with a ramping load rate of 7.02 N/min and scan speed of 0.78 mm/min. Three scratch tests were performed for each sample. Multi-pass wear tests were also per-formed with the same RST3 system. Each wear test was carried out at a constant load of 0.75 N for 5 passes with a Rockwell diamond indenter with a 20 μm end-radius. The track length was maintained at 1 mm. The toughness of the coatings was evaluated by means of a modified Palmqvist toughness method with the RST3 system, as per ISO 28079 standard [27]. A load of 100 N was used for the test. The tough-ness values were calculated by dividing the load with the summation of the total crack lengths from crack tip to indentation corner from all four corners of the indent.

To investigate the correlation between the temperature and the friction coefficient at the tool workpiece interface, a specially designed instrument, described in [28], was used. This apparatus can mimic the adhesive interaction that occurs during machining at the tool–workpiece interface. The test is performed by rotating a coated pin in between two polished Ti6Al4V alloy discs. To simulate the friction conditions at the tool–workpiece interface, the discs were progressively heated from 25°C to 800°C. A load of 2400 N was applied to create plastic strain at the contact surface. The friction coefficient was calculated using the ratio between the shear strength of the adhesive bonds and the normal contact stress

generated at the interface. Three tests were conducted for each coating, and the estimated magnitude of error for the coefficient of the friction value was approximately 5%.

3.2.2. Cutting Tests and Chip Morphology Analysis

To evaluate the wear behaviour, progressive tool wear studies were performed within a NAKAMURA SC450 turning machine under wet turning conditions. An ASTM B265 Grade 5 Ti6Al4V aerospace alloy was used as the workpiece material. All tests were conducted on cemented carbide (WC, 6% Co) grade K313 CNMG432 turning inserts supplied by Kennametal. A MCLN-5° Kennametal KenlocTM tool holder un-der a flood coolant condition was used for the tests. XTREME CUT 290 semisynthetic cutting fluid, which is designed for machining aerospace alloys, was used during cutting. The coolant was maintained at a flow rate of 14 L/min. Table 3.1 outlines the cut-ting parameters used to conduct the machining tests. The selected cutting conditions chosen were based on industry recommendations. Figure 3.1 shows the experimental setup for the turning operation. A maximum flank wear of 300 μm was set to be the tool life criterion, as per ISO 3685:1993 [29]. The flank wear measurements were made with a Keyence optical microscope (model VHX-5000 Series, KEYENCE America, Elmwood Park, NJ, USA) during the cut-ting tests. The scatter of tool life measurements was approximately 10%.

Table 3.1. *Cutting parameters for machining of Ti6Al4V alloy.*

Machining Operation	Cutting Tool Substrates	Workpiece Material	Workpiece Hardness, HRC	Speed, m/min	Feed, mm/rev	Depth of Cut, mm	Coolant Condition
Turning	Kennametal CNMG432 Grade K 313 Turning inserts	ASTM B265 Grade 5 Ti6Al4V alloy	37-38	45	0.15	2	Flood

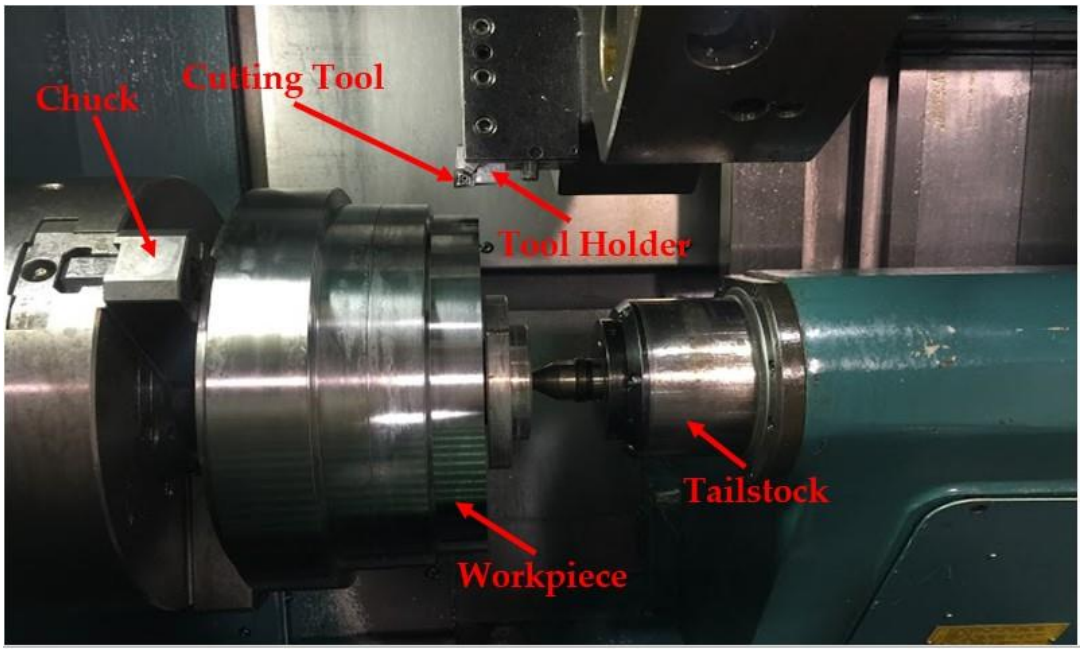

Figure 3.1. *Experimental setup for turning operation.*

After every 600 m of cutting length, the tools were inspected with a SEM and an Alicona Infinite Focus G5 3D surface measurement system (Alicona Manufacturing Inc., Bartlett, IL, USA). The focus-variation technology of the Alicona system was used to generate 3D topographic images of the cutting inserts and measure the volumetric difference between the worn and new tool. To measure the built up volume and crater wear volume, 3D volume dataset of a worn tool after every 600 m of cutting length were compared against a reference 3D volume dataset of the same tool corner collect-ed prior to machining using the Alicona

system. A postprocessing software package Measure Suite aligns the two datasets and calculates the built up and crater wear volume by measuring the difference in volume of the worn tool above and below the reference dataset. Chip analysis was conducted using standard practices [30]. A JEOL JSM-7000F high-resolution SEM was used to perform EBSD analysis of the chip cross sections. The SEM was operated at a 25 kV accelerating voltage and 60 μm aperture size. The sample was tilted to 70°, and a working distance of be-tween 10 to 12 mm was maintained. The CCD detector was kept at an insertion distance of 186 mm.

3.3. Results and Discussions

3.3.1. Tool Wear Performance Studies

Tool wear performance was investigated under wet rough turning conditions. The tool wear progression with respect to cutting length for uncoated, AlTiN coated, and CrN coated tools is illustrated in Figure 3.2. The highest tool wear intensity was observed for the AlTiN coating, followed by the uncoated tool and the CrN coated tool. The tool life of the CrN coated tool improved by approximately 232% compared to the AlTiN coated tool and 155% compared to the uncoated tool.

Progressive tool wear studies were conducted after every 600 m of cutting length using an SEM combined with 3D imaging by Alicona. The progression of tool wear for uncoated, AlTiN coated, and CrN coated tools is shown in Figures 3.3–3.5, respectively. Two tool wear phenomena were observed: intensive adhesive interaction at the tool/chip interface and crater wear. Both the 3D and SEM images of the uncoated and AlTiN coated tools showed significant BUE formation and propagation of crater wear as cutting progressed.

Figures 3.6 and 3.7 show the formation of BUE and crater wear with respect to cutting length for uncoated, AlTiN coated, and CrN coated tools. Both the uncoated and the AlTiN coated tools show significant BUE formation compared to the CrN coated tool. The instability of the BUE formation is also evident by the strong fluctuation in peak volume compared with the previous passes (Figure 3.6). The lower BUE formation in the CrN coated tool decreased the possibility of tool edge chipping following its removal. The CrN coating also showed a reduction in the crater wear in-tensity and delay in the propagation of crater wear as machining progressed. Thus, lower BUE formation and delayed crater wear resulted in a much more uniform in-crease in tool wear, which, in turn, prevented rapid failure of the CrN coated tool. It is important to note here that the reduced crater wear values obtained for the uncoated tool (Figure 3.7) were due to the BUE covering the crater wear on the tool. This can be confirmed by the 3D and SEM images (Figure 3.3 a, b) and (Figure 3.5 a, b).

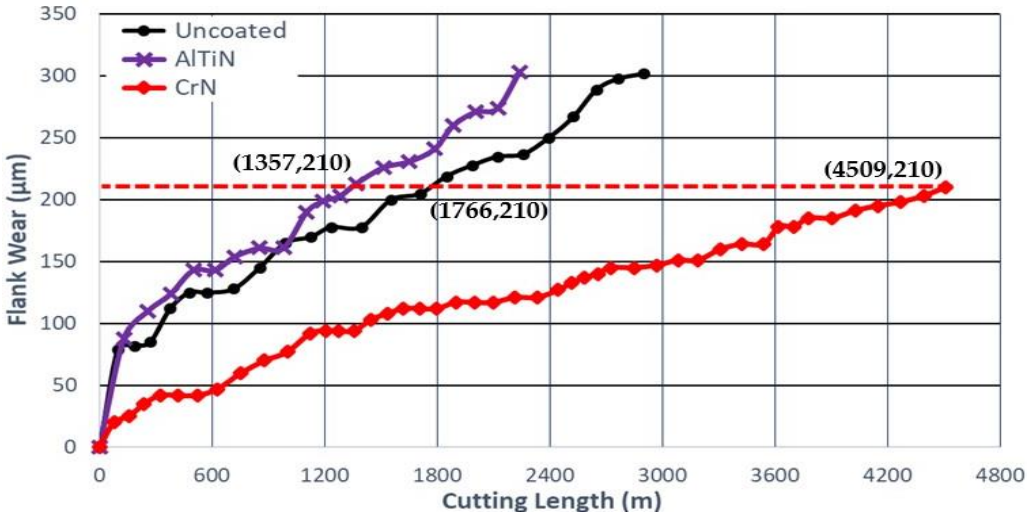

Figure 3.2. *Flank wear vs. length of cut data of wet rough turning for uncoated, AlTiN and CrN coated tools showing significant tool life improvement for CrN coated tool.*

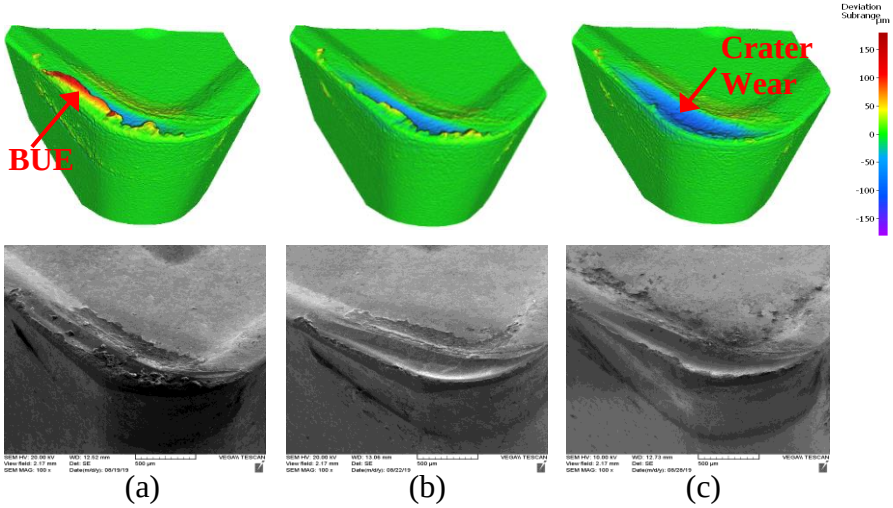

Figure 3.3. *3D progressive wear data for uncoated tool highlighting progression of built up layer and crater wear after different length of cut: (a) 600 m; (b) 1200 m; (c) 1800 m.*

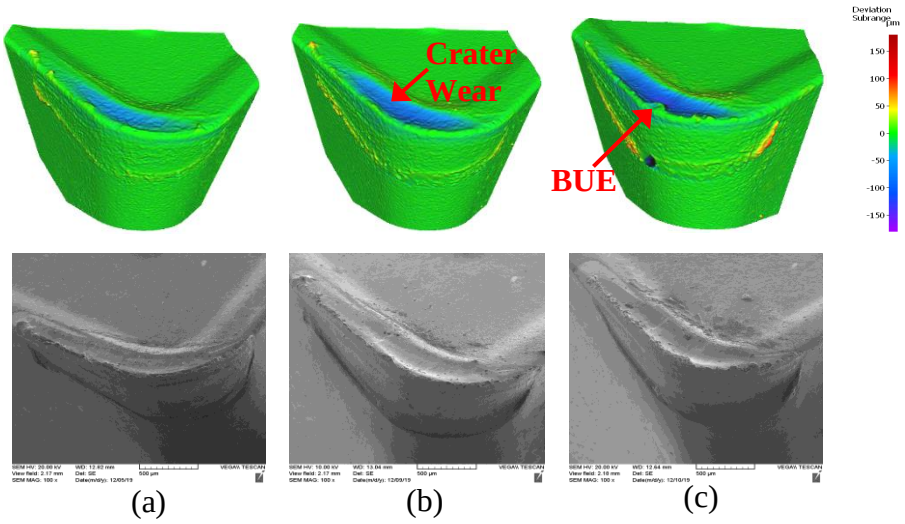

Figure 3.4. *3D progressive wear data for AlTiN coated tool highlighting progression of built up layer and crater wear after different length of cut: (a) 600 m; (b) 1200 m; (c) 1800 m.*

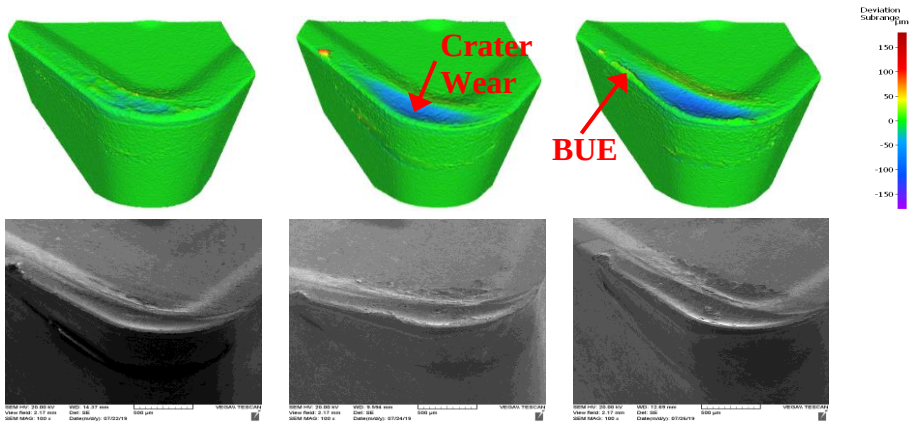

Figure 3.5. *3D progressive wear data for CrN coated tool highlighting progression of built up layer and crater wear after different length of cut: (a) 600 m; (b) 1200 m; (c) 1800 m.*

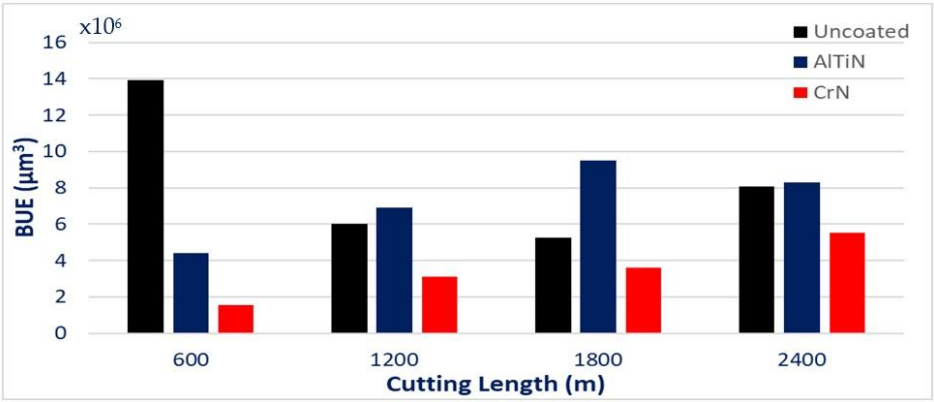

Figure 3.6. *Built up volume progression vs. length of cut for uncoated, AlTiN and CrN coated tools considering the peaks above reference surface of the original tool.*

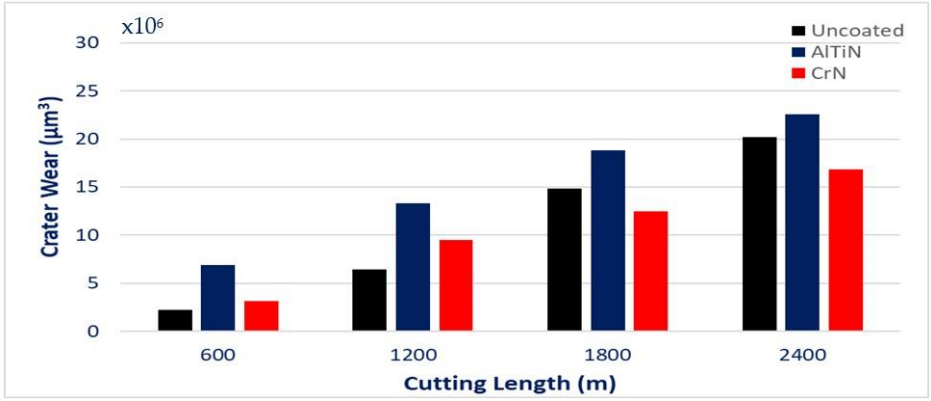

Figure 3.7. *Crater wear volume progression vs. length of cut for uncoated, AlTiN and CrN coated tools considering the peaks below reference surface of the original tool.*

3.3.2. Coating Characterization

Detailed investigations were conducted to assess the mechanical properties and structure of the coatings. The SEM images of the fracture sections of the coatings are shown in Figure 8. Both the AlTiN and CrN are monolayer coatings with a cubic microstructure, with the thickness of the AlTiN coating being 1.94 µm and that of the CrN coating being 1.83 µm (Figure 3.8; Table 3.2). Figure 3.9 shows the XRD data for both AlTiN and CrN coatings. Three distinct diffraction peaks for the (111), (200), and (220) crystallographic planes were observed in both coatings. The intensity of the (200) peak was the highest in both the AlTiN and CrN coatings, indicating that they have a preferred (200) orientation. The micromechanical properties and residual stress values of the coatings are shown in Table 3.2. It is evident that the CrN coating has a higher compressive residual stress, lower hardness, and higher plasticity index than the AlTiN coating. The plasticity index is given by the quotient of the plastic work and the total plastic and elastic work during indentation [31]. For the high tool load characteristic of titanium machining, a higher plasticity index indicates a coating's higher toughness and durability [32]. Toughness is a material's ability to resist crack propagation as well as its energy absorption during the deformation that leads to fracture [33]. The modified Palmqvist toughness test confirmed the higher toughness of the CrN coating (see Table 3.2). Since the substrates were the same in both cases, the differences in the toughness values were solely due to the composition of the coatings. As reported in the literature, higher compressive residual stress also helps prevent crack propagation in the coatings [34]. The fatigue fracture resistance properties of the coatings were evaluated using nano-impact testing in relation to the final depth of the penetration

during impact. The lower depth of the penetration in CrN indicates the superior performance of this coating under repeated loading, in addition to better fatigue resistance (Figure 3.10).

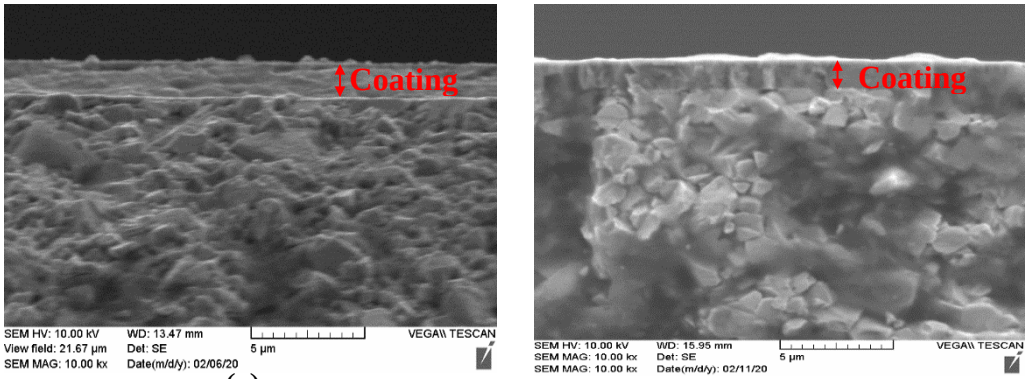

(a) (b)

Figure 3.8. *SEM images of fracture sections of the studied PVD coatings highlighting coating thickness: (a) AlTiN; (b) CrN.*

Table 3.1. *Micromechanical properties of AlTiN and CrN coatings.*

		Properties							
Coating	**Architecture**	**Thickness, µm**	**Hardness (H), GPa**	**Elastic Modulus (E), GPa**	**Plasticity index**	**H/E ratio**	**H^3/E^2 ratio**	**Residual Stresses, MPa**	**Modified Palmqvist Toughness, N/µm**
AlTiN	Monolayer	1.94	28.9 ± 2.0	516.52	0.46	0.056	0.090	−599 ± 168	1.37
CrN	Monolayer	1.83	20.37 ± 2.5	591.87	0.66	0.034	0.024	−979 ± 81	1.51

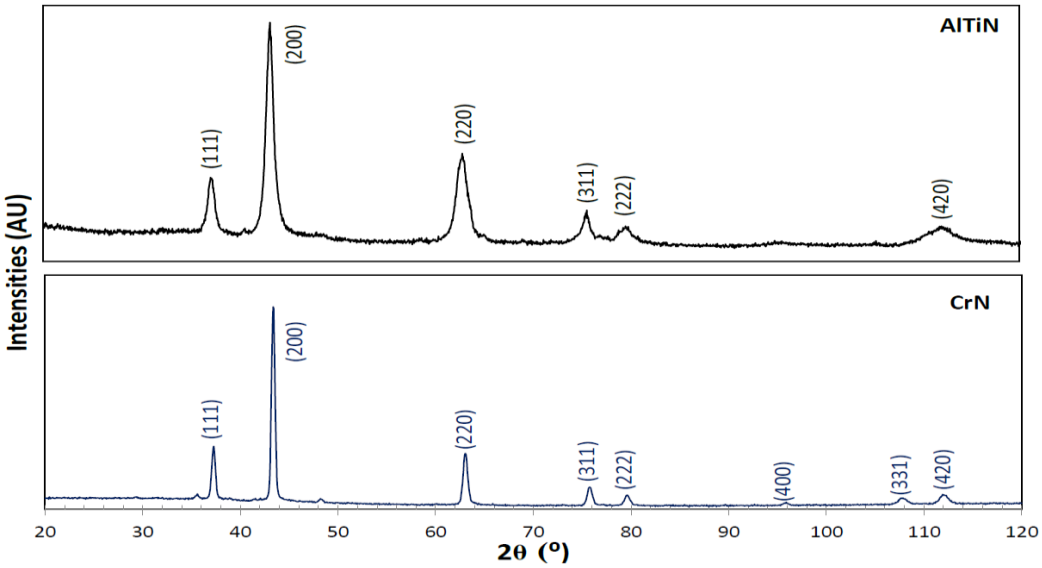

Figure 3.9. *X-ray diffraction patterns of monolayered AlTiN and CrN coatings.*

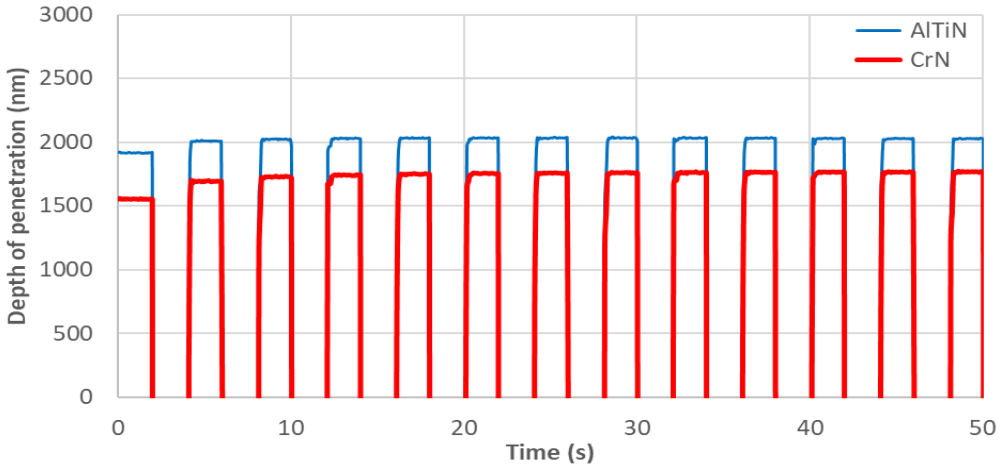

Figure 3.10. *X-ray diffraction patterns of monolayered AlTiN and CrN coatings.*

The AFM images of 3D surface morphologies of the AlTiN and CrN coatings are illustrated in Figure 3.11. The arithmetical mean height (Sa) values were obtained from a scan size of 25 µm × 25 µm. As shown, the overall surface roughness of the CrN coating was lower than that of AlTiN. The lower roughness of the CrN coating contributes to its superior frictional properties. Scratch tests were conducted to analyze the be-havior of the coatings under progressive loads. Wear tests, which are basically multi-pass constant load

scratch tests, were also performed at a subcritical load of 0.75 N with the objective of studying the gradual deformation of the coatings. These studies provided information about frictional and wear characteristics, microscopic plastic deformation performance, and microcracking behaviour at the subsurface/surface interface [35]. Figure 3.12 shows how the coefficient of friction changes for the coatings after one pass, three passes and five passes during repetitive wear test. It shows that that although each of the coatings initially have a similar coefficient of friction, it increases less drastically in the CrN coating with further wear test passes, which indicates the more gradual deformation of this coating. The scratch test results showed that the deformation mechanism under a heavily loaded sliding contact was considerably different for the AlTiN and CrN coatings. The scratch test results for AlTiN and CrN coatings are illustrated in Figure 3.13 and Figure 3.14, respectively. The coefficient of friction data obtained during the scratch test demonstrated the ability of the coatings to resist scratching within the layers. The CrN coating had a lower coefficient of friction, which signifies its superior ability to withstand peeling during friction. The scratch track of the CrN coating showed that the failure was caused by the plastic flow, and the deformation was highly localized, with little substrate exposure outside of the scratch track. In comparison, brittle failure with widespread substrate exposure outside of the scratch track was observed for the AlTiN coating. The performance of the coatings in the scratch test can be described in terms of their hardness, H/E, H^3/E^2 ratios, and residual stress, as summarized in Table 2. The H/E and H^3/E^2 ratios were calculated from coating's hardness (H) and coating's elastic modulus (E) obtained from nanoindentation tests. The H/E ratio signifies the elastic strain to failure characteristics of a coating, and the H^3/E^2

ratio refers to a coating's ability to resist plastic deformation [36]. The H/E and H^3/E^2 ratios of the CrN coating were lower than those of the AlTiN coating. The elastic modulus of both coatings was very similar. The lower H/E and H^3/E^2 ratios of the CrN coating can be thus ascribed to its considerably lower hardness. This combination of properties suggests that CrN is less brittle. The soft CrN coating, combined with its overall lower compressive residual stress, can thus undergo greater plastic deformation under the given load. For machining applications in which BUE formation is prominent, such qualities of the CrN coating are very important since they prevent coating delamination when BUE is re-moved during machining, providing better tool protection. Thus, the enhanced performance of the CrN coating can be related to its lower hardness and toughness characteristics. It was previously shown that a coating with a low H/E ratio delivers better wear resistance in machining applications that feature adhesive wear. Thus, the elastic strain to failure characteristic (H/E ratio) is critical for attaining better tool life under heavy loaded tooling applications where severe surface layer deformation occurs during friction [28,37]. However, such behaviour must be evaluated in conjunction with the coating's plasticity index values (Table 3.2). For heavy loaded applications, the coatings must have an enhanced capability to dissipate the frictional energy generated by severe surface layer deformation. The greater the energy dissipation, the lower the amount of energy expended on the deformation and damage of the substrate material. A higher plasticity index indicates greater energy dissipation under loading. Thus, the high plasticity index CrN coating exhibited better performance than the AlTiN coating. The plasticity index and the H/E parameter both have similar ramifications [4,38]. These parameters could be applied to

assess the wear performance of a heavily loaded tribo-system under the severe adhesive wear conditions typical of titanium machining. Therefore, the CrN coated tool, which had a higher plasticity index and toughness combined with a lower hardness and H/E ratio, demonstrated superior tool wear performance and longer tool life.

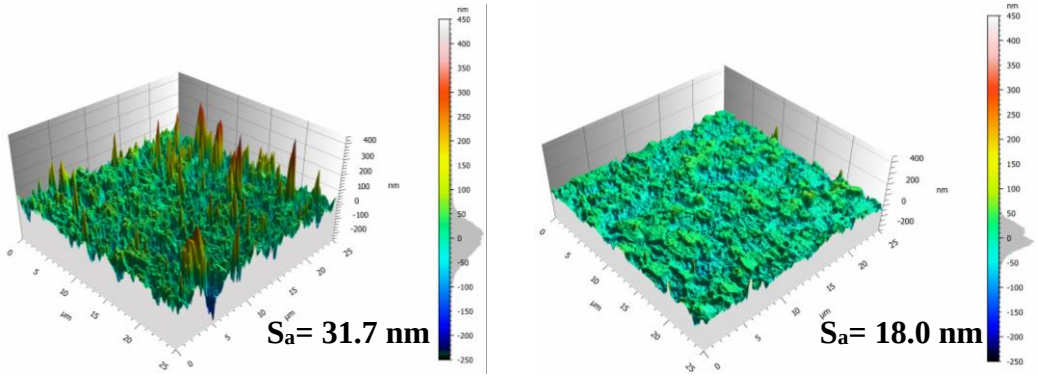

Figure 3.11. *Atomic force microscope (AFM) images of surface topography of the coatings with arithmetic mean height (Sa) values: (a) AlTiN; (b) CrN.*

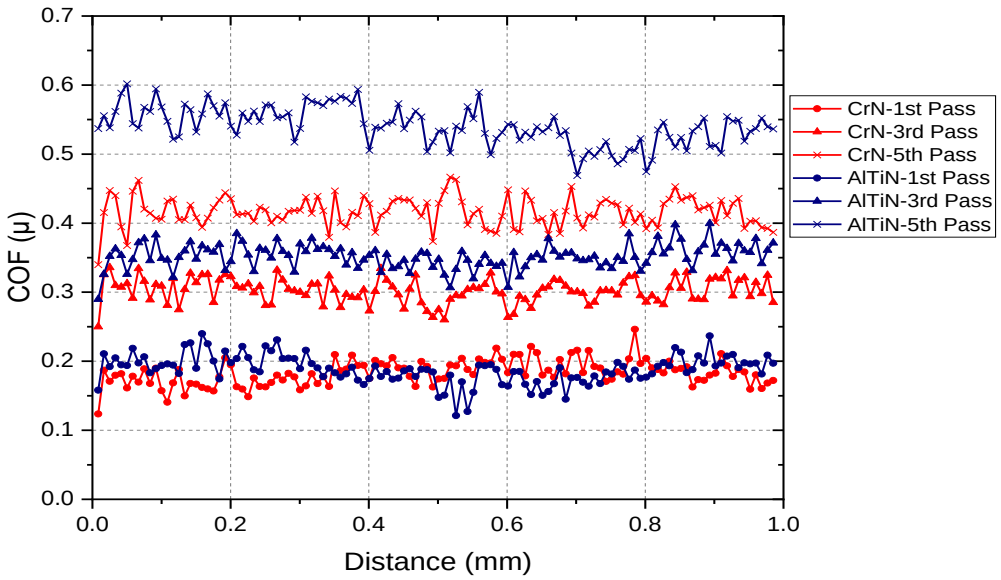

Figure 3.12. *Evolution of coefficient of friction at different passes during repetitive wear test at 0.75 N for AlTiN and CrN coatings.*

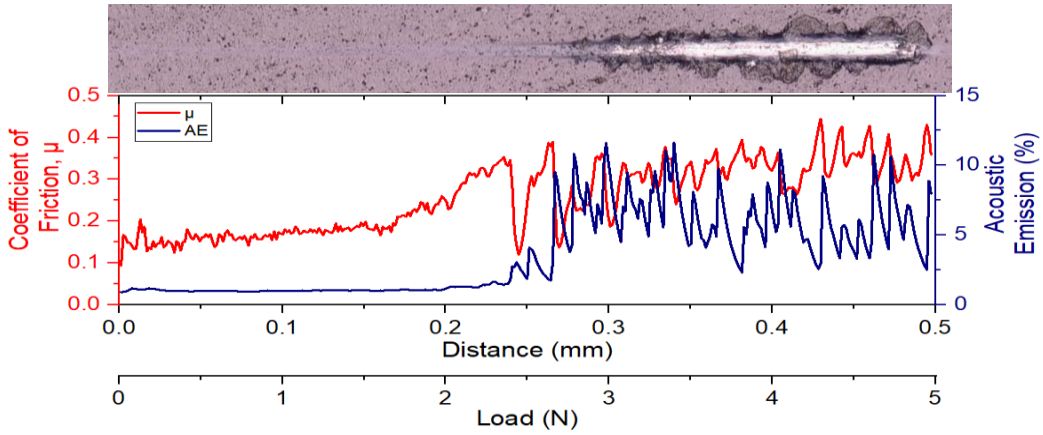

Figure 3.13. *Optical images of the ramped load scratch test track with coefficient of friction and acoustic emission data for the AlTiN coating.*

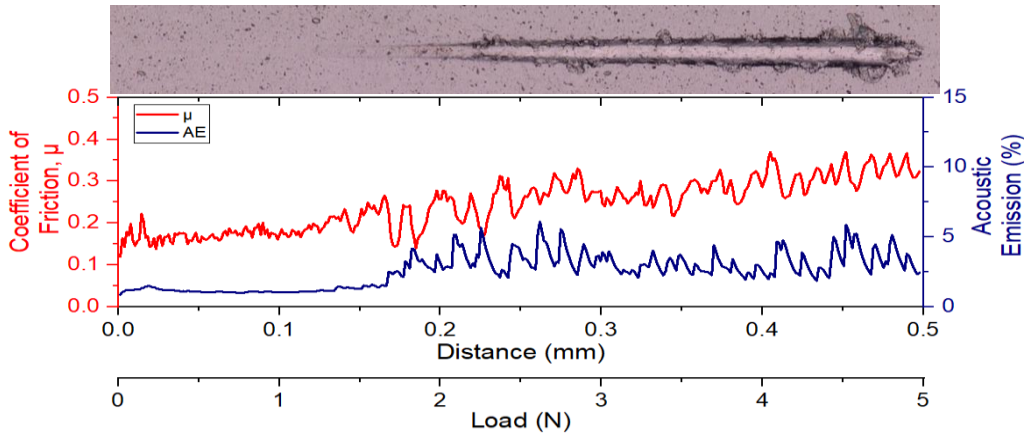

Figure 3.14. *Optical images of the ramped load scratch test track with coefficient of friction and acoustic emission data for the CrN coating.*

3.3.3. Assessment of Tribological Performance

It is evident from Figures 3.3–3.5 that the BUE resulting from titanium adhesion and crater wear intensity is significantly reduced in the CrN coated tool compared with the uncoated and AlTiN coated tools. This wear behaviour and subsequent tool life improvement could be attributed to the micromechanical (section 3.2) and tribological characteristics of the CrN coating, which include lower hardness, H/E and H^3/E^2 ratios, and

higher plasticity index compared to the AlTiN coating (Table 3.2). A lower H^3/E^2 ra-tio and hardness indicate the low brittleness of CrN, which also has a higher tough-ness. The scratch test revealed that the CrN coating failed due to localized plastic flow deformation and had a lower sliding contact friction. Such a combination of micro-mechanical properties provides the softer and tougher CrN coating with an enhanced capability to withstand intensive sticking without delamination, and improved tribo-logical characteristics under heavy loaded tooling applications.

The tribological performance of the coatings, discussed in the following paragraphs, was evaluated through: 1) an analysis of tribo-film formation at the tool–chip interface during machining; 2) an evaluation of the coefficient of friction of the coatings with respect to temperature; and 3) an assessment of the chip characteristics (Table 3.3). All analyses confirmed that the CrN coated tool provided better tribological performance.

The tribological performance of a coating is strongly dependent on its self-adaptive behaviour. This is directly related to the coating's ability to form beneficial tribo-oxides at the tool–chip interface during cutting [14]. Tribo-films influence tool wear behaviour in two ways: by providing in situ lubrication that reduces the intensity of BUE formation and by serving as a thermal barrier on account of the low thermal conductivity of the generated tribo-oxides [14]. Figure 3.15 shows the coefficient of friction versus temperature data for the uncoated, AlTiN coated, and CrN coated tools. The instrument used to determine this correlation mimics the adhesive interaction present during cutting under a heavy load. The coefficient of friction values for the CrN coating were considerably lower than both the uncoated and the AlTiN coated tool, especially at temperatures between 550–700 °C, which

are typical for the outlined machining conditions [10]. Such superior tribological performance from the CrN coating can be attributed to its ability to form lubricious and thermal barrier tribo-oxides during cutting. The XPS analysis on the worn tool confirmed tribo-film formation, as evident in Figure 3.16. The obtained data reveal that the CrN coating under-went tribo-oxidation and formed a Cr_2O_3 tribo-ceramic layer on the surface of the tool. These tribo-layers have a corundum structure [39] and provide lubricating characteristics [40] and enhanced thermal barrier properties at high cutting temperatures [41]. Cr_2O_3 tribo-films thus decrease friction at the tool–chip interface, thereby significantly reducing BUE formation as well as crater wear intensity during the machining of a Ti6Al4V alloy.

Table 3.3. *Tribological performance evaluation through chip characteristics for AlTiN and CrN coatings.*

Coating	Chip Compression Ratio - CCR	Φ - Shear Angle (°)	(ϒ) Shear Strain	Chip Sliding Velocity (m/min)
AlTiN	1.11	51.90	0.56	50.0
CrN	1.36	58.23	0.39	61.1

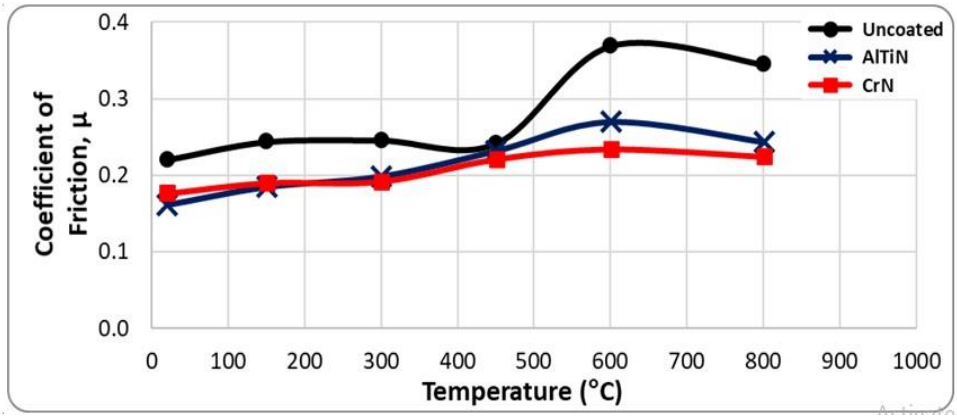

Figure 3.15. *Coefficient of friction vs. temperature data for uncoated, AlTiN and CrN coated tools obtained from high temperature/heavy load tribometer.*

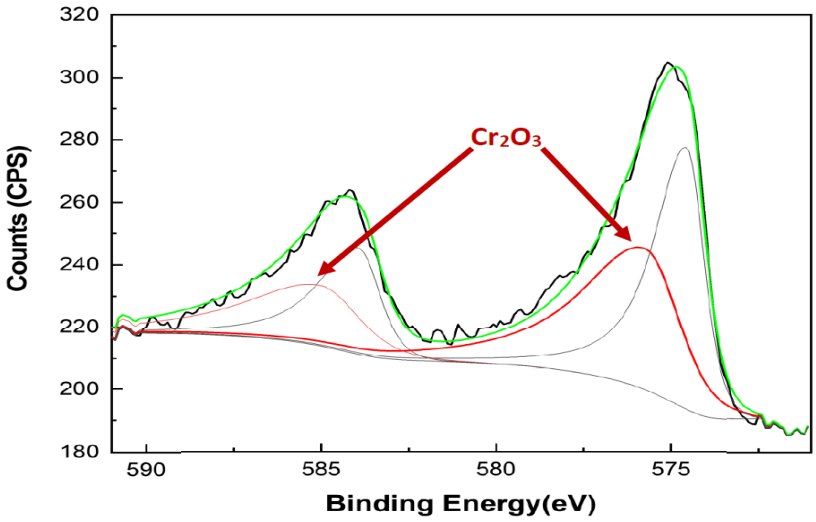

Figure 3.16. *High resolution XPS data (Cr 2p spectrum) of worn rake surface of CrN coated insert confirming formation of Cr_2O_3 tribo-oxides.*

Tribological interactions occurring at the tool–chip interface play a considerable role in forming the chips. The characteristics of the chips collected after approximately 50 m of machining length were evaluated, and the results are summarized in Table 3.3. The tribological characteristics of the AlTiN and CrN coatings compliment the coefficient of friction data shown in Figure 3.15. The chip compression ratio and shear plane angle were greater for the CrN coating. This indicates that a low shearing force acted on the chips produced by the CrN coated tool, which resulted in reduced cutting and frictional forces at the tool–chip interface. The chip sliding velocity was also higher in the CrN coated tool, which reduced the tool–chip contact length and friction at the tool–chip interface. This consequently impeded temperature rises at the cutting zone. The analysis of the coated tool's chip characteristics thereby confirms that the reduction of friction at the tool–chip interface leads to increased tool life in the CrN coated tool.

In order to analyze the chip flow process, a cross sectional EBSD analysis was performed on chips collected during machining. Figure 3.17 shows the texture orientation maps and microstructure of the chips. The images demonstrate that the main deformed zone was largely close to the edge of the chip–tool interface, and both chips depict grain refinement in this region. However, the chips produced by the CrN coated tool showed the formation of ultrafine grains along the shear boundaries. This confirms the superior chip flow process in the CrN coated tool. The accelerated chip flow process also resulted in dynamic recrystallization of the grains with new grain orientation taking place as observed in the orientation maps. This may have increased slip planes and, consequently, enhanced chip plasticity.

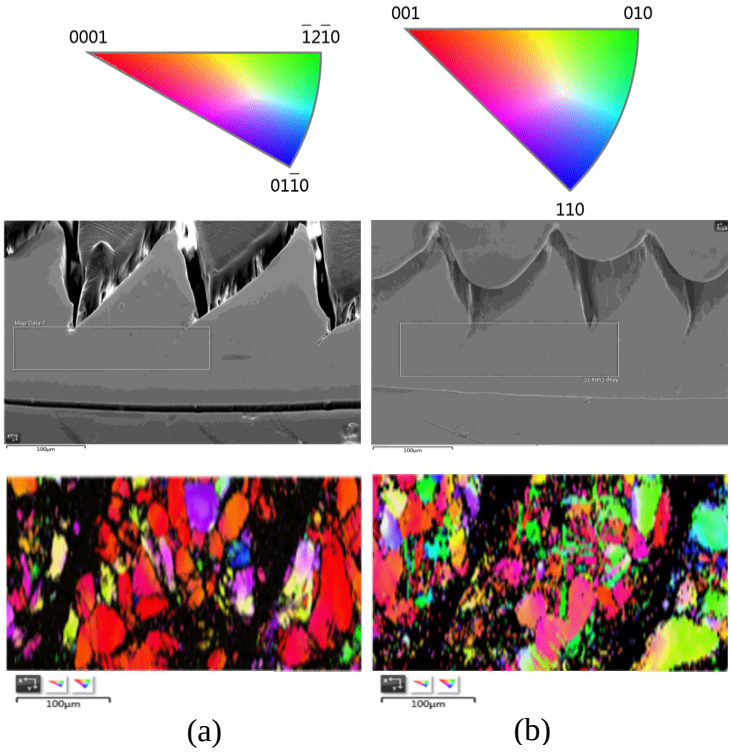

Figure 3.17. *EBSD orientation, chip cross sections and phase map of chip cross sections: (a) AlTiN; (b) CrN.*

3.4. Conclusions

Intense BUE formation occurs during the rough turning operation of a Ti6Al4V aerospace alloy. This phenomenon, combined with the high cutting temperatures generated during machining, results in rapid tool wear. An effective strategy for minimizing tool wear is the application of self-adaptive PVD coatings that generate lubricious and protective tribo-layers to counteract the underlying wear mechanisms. A monolayer SFC PVD CrN coating was demonstrated in the current research, which significantly improved tool life during Ti6Al4V machining as compared to commercial AlTiN coating. A CrN coating is capable of inhibiting the intensive detachment of the coating layer due to its unique combination of micromechanical and tribological characteristics. In addition, the coating generates Cr_2O_3 tribo-films during machining, which possess thermal barrier and lubricating characteristics. The developed CrN coating can impede the tool wear mechanism (cratering and adhesive interaction with the workpiece), thereby significantly prolonging tool life. The beneficial micromechanical and tribological properties, in conjunction with the adaptive behaviour of the developed CrN coating, were demonstrated to have delivered superior performance un-der the outlined machining conditions for a Ti6Al4V alloy.

3.5. References

1. Dearnley, P. A.; Grearson, A. N. Evaluation of Principal Wear Mechanisms of Cemented Carbides and Ceramics Used for Machining Titanium Alloy IMI 318. Mater. Sci. Technol. 1986, 2, 47–58. https://doi.org/10.1179/026708386790123611.
2. Boyer, R. R. An Overview on the Use of Titanium in the Aerospace Industry. Mater. Sci. Eng. 1996, 213, 103–114.
3. Hosseini, A.; Kishawy, H. A. Cutting Tool Materials and Tool Wear. In Machining of Titanium Alloys; Davim, J. P., Ed.; Springer Berlin Heidelberg: Berlin, Heidelberg, 2014; pp 31–56. https://doi.org/10.1007/978-3-662-43902-9_2.
4. Chowdhury, M. S. I.; Chowdhury, S.; Yamamoto, K.; Beake, B. D.; Bose, B.; Elfizy, A.; Cavelli, D.; Dosbaeva, G.; Aramesh, M.; Fox-Rabinovich, G. S.; Veldhuis, S. C. Wear Behaviour of Coated Carbide Tools during Machining of Ti6Al4V Aerospace Alloy Associated with Strong Built up Edge Formation. Surf. Coatings Technol. 2017, 313, 319–327. https://doi.org/10.1016/j.surfcoat.2017.01.115.
5. Jaffery, S. H. I.; Mativenga, P. T. Wear Mechanisms Analysis for Turning Ti-6Al-4V-towards the Development of Suitable Tool Coatings. Int. J. Adv. Manuf. Technol. 2012, 58, 479–493. https://doi.org/10.1007/s00170-011-3427-y.
6. Biksa, A.; Yamamoto, K.; Dosbaeva, G.; Veldhuis, S. C.; Fox-Rabinovich, G. S.; Elfizy, A.; Wagg, T.; Shuster, L. S. Wear Behaviour of Adaptive Nano-Multilayered AlTiN/MexN PVD Coatings during Machining of Aerospace Alloys. Tribol. Int. 2010, 43, 1491–1499. https://doi.org/10.1016/j.triboint.2010.02.008.

7. Naerheim, Y.; Trent, E. M. Diffusion Wear of Cemented Carbide Tools Vvhen Cutting Steel at High Speeds. 1977, No. December, 548–556.
8. Dearnley, P. A.; Trent, E. M. Wear Mechanisms of Coated Carbide Tools. Met. Technol. 1982, 9, 60–75. https://doi.org/10.1179/030716982803285909.
9. Armendia, M.; Garay, A.; Iriarte, L.-M.; Arrazola, P.-J. Comparison of the Machinabilities of Ti6Al4V and TIMETAL® 54M Using Uncoated WC–Co Tools. J. Mater. Process. Tech. 2010, 210, 197–203. https://doi.org/10.1016/j.jmatprotec.2009.08.026.
10. Paiva, J. M.; Shalaby, M. A. M.; Chowdhury, M.; Shuster, L.; Chertovskikh, S.; Covelli, D.; Junior, E. L.; Stolf, P.; Elfizy, A.; Bork, C. A. S.; Fox-Rabinovich, G.; Veldhuis, S. C. Tribological and Wear Performance of Carbide Tools with TiB_2 PVD Coating under Varying Machining Conditions of TiAl6V4 Aerospace Alloy. Coatings 2017, 7, 187. https://doi.org/10.3390/coatings7110187.
11. Chowdhury, M. S. I.; Bose, B.; Yamamoto, K.; Shuster, L. S.; Paiva, J.; Fox-Rabinovich, G. S.; Veldhuis, S. C. Wear Performance Investigation of PVD Coated and Uncoated Carbide Tools during High-Speed Machining of TiAl6V4 Aerospace Alloy. Wear 2020, 446–447 (December 2019), 203168. https://doi.org/10.1016/j.wear.2019.203168.
12. Corduan, N.; Himbart, T.; Poulachon, G.; Dessoly, M.; Lambertin, M.; Vigneau, J.; Payoux, B. Wear Mechanisms of New Tool Materials for Ti-6AI-4V High Performance Machining. CIRP Ann. - Manuf. Technol. 2003, 52, 73–76. https://doi.org/10.1016/S0007-8506(07)60534-4.

13. M'Saoubi, R.; Axinte, D.; Soo, S. L.; Nobel, C.; Attia, H.; Kappmeyer, G.; Engin, S.; Sim, W. M. High Performance Cutting of Advanced Aerospace Alloys and Composite Materials. CIRP Ann. - Manuf. Technol. 2015, 64, 557–580. https://doi.org/10.1016/j.cirp.2015.05.002.
14. German S. Fox-Rabinovich; Kovalev, A. I. Self-Organization and Structural Adaptation during Cutting and Stamping Operations. In Self-Organization During Friction: Advanced Surface-Engineered Materials and Systems Design; CRC Press, Taylor and Francis Group, Boca Raton, NW, USA, 2006.
15. Hartung, P. D.; Kramer, B. M. Tool Wear in Machining Titanium. Ann. CIRP 1982, 30 (1), 75–80.
16. Wang, Z. M.; Ezugwu, E. O. Performance of PVD-Coated Carbide Tools When Machining Ti-6Al-4V©. Tribol. Trans. 1997, 40 (, 81–86. https://doi.org/10.1080/10402009708983632.
17. Özel, T.; Sima, M.; Srivastava, A. K.; Kaftanoglu, B. Investigations on the Effects of Multi-Layered Coated Inserts in Machining Ti-6Al-4V Alloy with Experiments and Finite Element Simulations. CIRP Ann. - Manuf. Technol. 2010, 59, 77–82. https://doi.org/10.1016/j.cirp.2010.03.055.
18. Lupicka, O.; Warcholinski, B. The Adhesion of CrN Thin Films Deposited on Modified 42CrMo4 Steel. Adv. Mater. Sci. Eng. 2017, 2017, 1–14. https://doi.org/10.1155/2017/4064208.
19. Milosev, I.; Strehblow, H. H.; Navinsek, B. Comparison of TiN, ZrN, and CrN Coatings under Oxidation. Thin Solid Films 1997, 303, 246–254.

20. Berg, G.; Friedrich, C.; Broszeit, E.; Berger, C. Development of Chromium Nitride Coatings Substituting Titanium Nitride. Surf. Coatings Technol. 1996, 86–87 (PART 1), 184–191. https://doi.org/10.1016/S0257-8972(96)03042-3.
21. Sato, T.; Tada, Y.; Ozaki, M.; Hoke, K.; Besshi, T. A Crossed-Cylinders Testing for Evaluation of Wear and Tribological Properties of Coated Tools. Wear 1994, 178, 95–100. https://doi.org/10.1016/0043-1648(94)90133-3.
22. Navinšek, B.; Panjan, P.; Milošev, I. PVD Coatings as an Environmentally Clean Alternative to Electroplating and Electroless Processes. Surf. Coatings Technol. 1999, 116–119, 476–487. https://doi.org/10.1016/S0257-8972(99)00145-0.
23. Bertrand, G.; Mahdjoub, H.; Meunier, C. A Study of the Corrosion Behaviour and Protective Quality of Sputtered Chromium Nitride Coatings. Surf. Coatings Technol. 2000, 126, 199–209. https://doi.org/10.1016/S0257-8972(00)00527-2.
24. Kondo, A.; Oogami, T.; Sato, K.; Tanaka, Y. Structure and Properties of Cathodic Arc Ion Plated CrN Coatings for Copper Machining Cutting Tools. Surf. Coatings Technol. 2004, 177–178, 238–244. https://doi.org/10.1016/j.surfcoat.2003.09.039.
25. Yamamoto, K.; Abdoos, M.; Paiva, J. M.; Stolf, P.; Beake, B.; Rawal, S.; Fox-Rabinovich, G.; Veldhuis, S. Cutting Performance of Low Stress Thick TiAlN PVD Coatings during Machining of Compacted Graphite Cast Iron (CGI). Coatings 2018, 8 (1), 1–12. https://doi.org/10.3390/coatings8010038.
26. ISO 14577-4: 2016(E) Metallic Materials — Instrumented Indentation Test for Hardness and 746 Materials Parameters — Part 4: Test Method for Metallic and Non-

Metallic Coatings. International Organization for Standardization: Geneva, Switzerland.

27. ISO 28079: 2009 (E) Hardmetals — Palmqvist toughness test. International Organization for Standardization: Geneva, Switzerland.
28. Fox-Rabinovich, G.; Shuster, L.; Beake, B.; Veldhuis, S. Physical and Mechanical Properties to Characterize Tribological Compatibility of Heavily Loaded Tribosystems (HLTS). In Self-Organization During Friction: Advanced Surface-Engineered Materials and Systems Design; CRC Press, Taylor and Francis Group, Boca Raton, NW, USA, 2006; pp 121–147. https://doi.org/10.1201/9781420017861.ch5.
29. ISO 3685: 1993(E) Tool-life testing with single-point turning tools. International Organization for Standardization: Geneva, Swit-zerland.
30. Shaw, M. C. Metal Cutting Principles; Oxford University Press, Inc., 2005.
31. Beake, B. D.; Fox-Rabinovich, G. S.; Veldhuis, S. C.; Goodes, S. R. Coating Optimisation for High Speed Machining with Advanced Nanomechanical Test Methods. Surf. Coatings Technol. 2009, 203 (13), 1919–1925. https://doi.org/10.1016/j.surfcoat.2009.01.025.
32. Zhang, X.; Beake, B. D.; Zhang, S. Toughness Evaluation of Thin Hard Coatings and Films. In Thin Films and Coatings: Toughening and Toughness Characterization; CRC Press, Taylor and Francis Group, Boca Raton, NW, USA, 2015; p 52.
33. Zhang, S.; Zhang, X. Toughness Evaluation of Hard Coatings and Thin Films. Thin Solid Films 2012, 520 (7), 2375–2389. https://doi.org/10.1016/j.tsf.2011.09.036.

34. Zhang, L.; Yang, H.; Pang, X.; Gao, K.; Volinsky, A. a. Microstructure, Residual Stress, and Fracture of Sputtered TiN Films. Surf. Coatings Technol. 2013, 224, 120–125. https://doi.org/10.1016/j.surfcoat.2013.03.009.
35. Zhang, F.; Meng, B.; Geng, Y.; Zhang, Y.; Li, Z. Friction Behaviour in Nanoscratching of Reaction Bonded Silicon Carbide Ceramic with Berkovich and Sphere Indenters. Tribol. Int. 2016, 97, 21–30. https://doi.org/10.1016/j.triboint.2016.01.013.
36. Leyland, A.; Matthews, A. On the Significance of the H/E Ratio in Wear Control: A Nanocomposite Coating Approach to Optimised Tribological Behaviour. Wear 2000, 246 (1–2), 1–11. https://doi.org/10.1016/S0043-1648(00)00488-9.
37. Sato, K.; Ichimiya, N.; Kondo, A.; Tanaka, Y. Microstructure and Mechanical Properties of Cathodic Arc Ion-Plated (Al,Ti)N Coatings. Surf. Coatings Technol. 2003, 163–164, 135–143. https://doi.org/10.1016/S0257-8972(02)00610-2.
38. Fox-Rabinovich, G. S.; Veldhuis, S. C.; Scvortsov, V. N.; Shuster, L. S.; Dosbaeva, G. K.; Migranov, M. S. Elastic and Plastic Work of Indentation as a Characteristic of Wear Behaviour for Cutting Tools with Nitride PVD Coatings. Thin Solid Films 2004, 469–470 (SPEC. ISS.), 505–512. https://doi.org/10.1016/j.tsf.2004.07.038.
39. Kramer, A.; Bignardi, L.; Lacovig, P.; Lizzit, S.; Batzill, M. Comparison of Surface Structures of Corundum Cr_2O_3 (0 0 0 1) and V2O3 (0 0 0 1) Ultrathin Films by x-Ray Photoelectron Diffraction. J. Phys. Condens. Matter 2018, 30 (7), 74002. https://doi.org/10.1088/1361-648x/aaa5ed.

40. Zhang, C.; Gu, L.; Tang, G.; Mao, Y. Wear Transition of CrN Coated M50 Steel under High Temperature and Heavy Load. Coatings 2017, 7 (11), 202. https://doi.org/10.3390/coatings7110202.
41. Wang, D. Y.; Lin, J. H.; Ho, W. Y. Study on Chromium Oxide Synthesized by Unbalanced Magnetron Sputtering. Thin Solid Films 1998, 332 (1–2), 295–299. https://doi.org/10.1016/S0040-6090(98)01266-8.

Chapter 4. Effect of Coating Hardness and Thickness

Chowdhury, M.S.I, Bose, B., Fox-Rabinovich, G., & Veldhuis, S.C. (2021). Investigation of the wear performance of TiB_2 *coated cutting tools during the machining of Ti6Al4V alloy. Materials, Volume 14, Issue 11, pp. 2799.*

Author's Contribution

Mohammad Shariful Islam Chowdhury	Designed the research methodology. Performed the experiments. Analyzed the results. Wrote the manuscript.
Bipasha Bose	Assisted with designing the research methodology. Assisted with analyzing the data. Assisted with writing and editing the manuscript. Supervised the project.
German Fox-Rabinovich	Assisted with designing the research methodology. Edited the manuscript. Supervised the project.
Stephen Veldhuis	Assisted with designing the research methodology. Edited the manuscript. Supervised the project.

Abstract

The machining of Ti6Al4V alloy, especially at low cutting speeds, is associated with strong Built-Up Edge (BUE) formation. The PVD coatings applied on cutting tools to machine such materials must have the necessary combination of properties to address such an underlying wear mechanism. The present work investigates and shows that TiB_2 PVD coating can be designed to have certain mechanical properties and tribological characteristics that improve machining in cases where BUE formation is observed. Three TiB_2 coatings were studied: one low hardness coating and two high hardness coatings with varied coating thicknesses. Wear performances for the various TiB_2 coated carbide tools were evaluated while rough turning Ti6Al4V. Tool wear characteristics were evaluated using tool life studies and the 3D wear volume measurements of the worn surface. Chip morphology analyses were done to assess the in-situ tribological performance of the coatings. The micro-mechanical properties of the coatings were also studied in detail to co-relate with the coatings' performances. The results obtained show that during the rough turning of Ti6Al4V alloy with intensive BUE formation, the harder TiB_2 coatings performed worse, with coating delamination on the rake surface under operation, whereas the softer version of the coating exhibited significantly better tool life without significant coating failure.

Keywords

Rough turning; Ti6Al4V alloy; PVD coating; built-up edge (BUE), flank wear; tribo-films; magnetron sputtering

4.1. Introduction

Titanium alloys possess an exceptional combination of mechanical and chemical properties (high ductility, good toughness, high-temperature strength, corrosion resistance, and a good strength-to-weight ratio) making them very popular in the aerospace and automobile industries [1–5]. However, they are very difficult to machine owing to certain unique characteristics like low thermal conductivity and a high chemical affinity towards tool materials. These result in high cutting temperatures during machining and built-up edge formation due to intensive adhesive interaction at the tool-chip interface, causing the carbide tools to wear rapidly. Consequently, to have a reasonably long tool life, low cutting speeds are typically used when machining titanium, sacrificing productivity.

For almost all machining applications, tool coatings have had significant success at reducing tool wear rates and improving productivity. However, when it comes to machining titanium, coatings have not achieved the same level of success. In many cases, coated cemented carbide tools perform worse than uncoated tools, especially during rough turning at low cutting speeds where the major phenomenon dictating tool performance is intensive BUE formation [6]. Many researchers have used PVD coated tools to improve tool performance when machining titanium alloys. However, most widely used PVD coatings, such as AlTiN, Al_2O_3, HfN, TiC, TiN, TiCN, TiN/TiC, TiN/TiC/TiN, and Al_2O_3/TiC, exhibit lower efficiency than uncoated tools [4,7,8]. This is due to how BUE formation instigates cohesive debonding and peeling of the coating layer under load [9–11]. Some researchers [12,13], however, have reported a minor improvement in tool performance with TiN, TiAlN, cBN+TiAlN, and TiN/TiCN/TiN coated tools.

Although PVD coated tools have had limited success with machining titanium, coating technology has advanced considerably over the years, and with the evolution of coating deposition technologies and a better understanding of the unique tribological requirements of machining titanium, new coating designs are being proposed [14]. Amongst others, PVD boride coatings have shown significant promise for machining titanium alloys [15]. TiB_2 coatings have high thermal and chemical stability at room and elevated temperatures [15–19]. Such properties make TiB_2 coatings very promising candidates for machining applications where BUE formation is observed. However, TiB_2 coatings have high hardness and residual stresses making the coatings brittle with low substrate adhesion [16,17]. This is counterproductive for such applications. However, this issue can be resolved by varying coating deposition parameters and by using various deposition technologies like magnetron sputtering [19–21]. Recently, it has also been shown that TiB_2 coatings have strong self-lubricating properties within the cutting zone [2]. These properties develop due to the ability of the coatings to form beneficial tribo-films through interaction with their environment [22]. For machining applications where BUE formation occurs, it is of the utmost importance to enhance the lubricity of the coating since it can minimize BUE formation and prevent coating detachment under load [9,23].

For the present paper, three TiB_2 coatings deposited by magnetron sputtering were studied: two high hardness TiB_2 coatings of varied thicknesses and one low hardness TiB_2 coating. One of the main goals of this paper is to relate the wear performance of TiB_2 coated carbide tools during the rough turning of Ti6Al4V to their mechanical and adaptive characteristics. The novelty of the present study lies in identifying the best performing TiB_2

coating for machining applications where BUE formation is observed, and an in-depth analysis of the relevant properties which make it perform better than the other types.

4.2. Experimental Procedure

4.2.1. Coating Deposition and Characterization Analyses

As indicated in the introduction, a previous investigation done by the authors has shown that tool life is significantly improved by the application of a TiB_2 coating [2]. Thus, the same TiB_2 coating used in that investigation was selected for the current investigation (Coating A). The two other coatings chosen for this investigation (Coating B and Coating C) were the commercial TiB_2 coatings manufactured by Kennametal (designated as KC5410 grade). All the coating deposition conditions except deposition time were kept constant for Coating B and Coating C. The coating deposition times for Coating B and Coating C were changed to achieve varied coating thicknesses. Coating B had a similar thickness to Coating A, and Coating C was thicker. The coatings had different hardness levels, with Coating A having the lowest hardness. Table 4.1 highlights the nomenclature for the coatings, including the thickness, hardness, and other micromechanical properties of the coatings.

The coatings were deposited on Kennametal CNMP432 and polished Sandvik Coromant SPGN120308 tungsten carbide inserts in a 6% cobalt matrix. Turning experiments were conducted with the Kennametal CNMP432 inserts. All coating characterizations were performed on the flat, polished Sandvik Coromant SPGN120308 inserts for accurate measurements and ease of use. Coating thicknesses after deposition were measured using the Calotest method with a 25 mm steel ball on SPGN120308 flat

inserts. Coating thicknesses were verified with high resolution Scanning Electron Microscope (SEM) images of Focused Ion Beam (FIB) cross sections with a Zeiss NVision 40 (Carl Zeiss, Oberkochen, Germany) dual-beam FIB-SEM instrument. The thicknesses of Coatings A, B, and C were 1.79, 1.82, and 2.89 µm, respectively (Table 1). X-ray diffraction analyses using Cu-Kα (1.544427 Angstroms) radiation were performed on a Proto AXRD Powder Diffraction System (Proto Manufacturing Limited, LaSalle, ON, Canada) to determine the crystal structure and the preferred orientation of the TiB_2 coatings. Residual stresses in the coatings were calculated by a Proto LXRD Stress Analyzer (Proto Manufacturing Limited, LaSalle, ON, Canada), using the $\sin^2 \psi$ method. The measurements were performed with a multiple exposure technique at 11 ψ (psi) tilts, using a 2.0 mm round aperture with a collection time of 80 s for each diffraction peak. To carry out the measurements, Ti-Kα (2.7497 Angstroms) radiation was used on the (101) plane at a diffraction angle of around 84°. For diffraction peak fitting, a Gaussian function was applied.

Table 4.1. *Micro-mechanical properties of the three monolayer TiB_2 coatings.*

Nomenclature	**Coating A**	**Coating B**	**Coating C**
Thickness, µm	1.79	1.82	2.89
Hardness (H), GPa	9.49 ± 0.516	36.03 ± 2.156	34.18 ± 3.512
Elastic Modulus (E), GPa	413.51 ± 10.56	582.12 ± 11.50	581.14 ± 24.33
Plasticity Index	0.778	0.494	0.507
H/E ratio	0.023	0.062	0.059
H^3/E^2 ratio	0.005	0.138	0.118
Cutting edge radius of coated tools, µm	51.38 ± 3.17	49.77 ± 3.58	53.01 ± 5.20
Modified Palmqvist Toughness, N/µm	1.081	0.897	0.643
Yield Stress, MPa	4600	8007	7936
Residual Stress, MPa	−633 ± 53	−842 ± 79	−930 ± 36

X-ray Photoelectron Spectroscopy (XPS) measurements were performed on worn tools (after approximately 100 m cut) to assess the tribo-film formation in a SPECS system (Berlin, Germany) equipped with a Phoibos 150 1D-DLD analyzer and monochromatic radiation source Al Kα (1486.7 eV). An initial analysis was carried out to determine the elements present (wide scan: step energy 1 eV, dwell time 0.1 s, pass energy 80 eV) and detailed analyses of the detected elements were carried out (detail scan: step energy 0.08 eV, dwell time 0.1 s, pass energy 30 eV) with an electron exit angle of 90°. The spectrometer was previously calibrated with Ag (Ag 3d5/2, 368.26 eV). The spectra collected were adjusted using the CasaXPS 2.3.16 software using a Gaussian–Lorentzian function after background subtraction. The concentrations were calculated by correcting the values with relative atomic sensitivity factors.

A Micro Materials NanoTest P3 (Micro Materials, Wrexham, UK) system was used to measure the hardness and elastic modulus of the coatings deposited on the polished WC-Co samples. A Berkovich diamond indenter was used to perform the nanoindentation at room temperature. The indenter was calibrated for indenter shape, load, displacement, and frame compliance according to ISO14577-4 [24]. A minimum of 40 indentations were done at a load of 50 mN. The load was adjusted to diminish the effect of the samples' surface roughness and prevent the substrate effect by keeping the penetration depth during indentation to less than 10% of the overall coating thickness. Thermal drift correction was done by collecting 60 s of post-indentation data after each indentation. Nano-impact testing was also conducted at room temperature with the P3 system. Five tests were carried out at various locations for each coating with a cube-corner indenter. A load of 20 mN was used

to do the impact test after every 4 s for a total test time of 300 s. An Anton Paar-NHT3 Nanoindentation Tester (Buchs, Switzerland) was used to measure the yield stress of the coatings. The test was conducted in the sinus mode at a sinus frequency of 5 Hz and amplitude of 20 mN. A 20 μm end radii spherical diamond indenter was used to analyze the yield property at a load of 200 mN. Twenty tests were carried out at different locations for each coated tool at a loading and unloading rate of 400 mN/min.

An Anton Paar-RST3 Revetest® Scratch Tester (Buchs, Switzerland) was used to perform micro-scratch tests, multi-pass wear tests, and toughness measurements on all coatings. Micro-scratch tests were carried out to study the behaviour of the coatings under progressive loading. The tests were conducted with progressive loading from 0.5 N to 5 N over a scratch length of 0.5 mm at a scratching speed of 0.78 mm/min and loading rate of 7.02 N/min. The pre- and post-topography scans were done at a 0.5 N load. A 20 μm end radii Rockwell diamond indenter was used to perform all tests. Three scratch tests were performed on each coating. Multi-pass wear tests were also conducted with the same 20 μm end radii Rockwell diamond indenter. Each test was performed with 5 passes over a track length of 1 mm at a constant load of 0.75 N. Based on the ISO 28,079 standard [25], a modified Palmqvist toughness measurement method was used to calculate the toughness of the coatings. The test was done at a 150 N load with a Vickers diamond indenter. The toughness values were calculated using the ratio of the load to the sum of the total crack lengths at the indentation corners. The images of the imprints were taken with a Vega 3-TESCAN scanning electron microscope (SEM) (Brno Kohoutovice, Czech Republic).

The surface topography and morphology of the TiB_2 coatings were assessed using the tapping mode of an Anton Parr ToscaTM 400 atomic force microscope (AFM) (Graz, Austria). Commercial silicon probes with 285 kHz of resonant frequency and a force constant of 42 N/m were used to perform the scans. A scan size area of 1 μm × 1 μm was used. ToscaTM analysis software (Version-7.4.8341) was used for image processing and data analysis of the scans. The thermal diffusivity and thermal conductivity of the coatings were measured using the laser flash method with a Discovery Laser Flash DLF- 1200 system (TA Instruments, New Castle, USA). The measurements were done at 100°C increments up to 800 °C.

4.2.2. Experimental Setup and Tool Wear Analyses

Cutting tests were performed to analyze the wear behaviour of the coated tools. Wet turning experiments were conducted on an ASTM B265 Grade 5 Ti6Al4V alloy and done on a Nakamura Tome SC450 CNC turning machining center (Nakamura-Tome Precision Industry Co., Ltd., Hakusan, Ishikawa, Japan). The wet turning tests were carried out for roughing operations with industry recommended cutting conditions, as stated in Table 4.2. Coated CNMP432 carbide grade (WC, 6% Co) K313 Kennametal turning inserts put on a MCLN-5° KenlocTM tool holder were used for all tests. The tool holder was placed on a Kistler Type 9129AA 3-component piezoelectric dynamometer for measuring the resultant cutting forces during machining. The dynamometer was connected to a Kistler type 5010 charge amplifier. The analog to digital signal conversion was done by a National Instruments (NI) Type 9215 data acquisition card in a National Instruments (NI) cDAQ-9172 DAQ system. A 5 kHz sampling rate was used for collecting the data. The data were

processed using National Instruments (NI) LabVIEW 2014. All cutting tests were repeated 3 times for each coating to assess repeatability.

Table 4.2. *Cutting parameters for machining of Ti6Al4V alloy.*

Machining Operation	Cutting Tool Substrates	Workpiece Material	Workpiece Hardness, HRC	Cutting Speed, m/min	Feed, mm/rev	Depth of Cut, mm	Coolant Condition
Rough Turning	Kennametal CNMP432 Grade K 313 Turning inserts	ASTM B265 Grade 5 Ti6Al4V alloy	37–38	45	0.15	2	Flood coolant (Xtreme Cut 290)

Tool life was evaluated in terms of tool flank wear which was measured after each cutting pass using a VHX-5000 Keyence optical microscope (KEYENCE corporation of America, Itasca, IL, USA). The cutting tests were continued until each tool reached a maximum flank wear of 300 µm in accordance with the ISO 3685:1993 standard [26]. The scatter of the flank wear measurements was approximately 10%. Chip morphology analyses were conducted on chips collected after approximately 50 m of cutting using standard practices [27].

Volumetric wear measurements were conducted for all the worn tools after approximately every 600 m of cutting length. The analyses were performed using the focus-variation technology of the Alicona Infinite Focus G5 3D surface measurement system (Alicona Manufacturing Inc., Bartlett, IL, USA). The system is capable of generating 3D topographic images of the cutting tools and of measuring the volumetric difference between the new and worn tools using the Measure Suite module. Before any cutting tests were performed, a 3D volume dataset of the cutting edge of the new tool was collected for reference. It was then compared against the 3D volume dataset of the same cutting edge of

the worn tool after approximately every 600 m of cutting length. The Measure Suite module aligned the two datasets and measured the crater wear and built-up volume of the cutting tools by calculating the volumetric difference of the worn tool above and below the reference dataset. The cutting-edge radius of each tool was also measured using the Edge Master module of the Alicona system.

4.3. Results and Discussions

4.3.1. Machining Performance Analysis

To assess the performance of the coatings during the wet rough turning of Ti6Al4V, tool life studies were performed. Figure 4.1 presents the progression of tool flank wear on the coated tools during machining with respect to cutting length. The highest flank wear intensity was seen for Coating C, followed by Coating B and Coating A. Coating A had approximately 346% tool life improvement compared to Coating C and approximately 248% tool life improvement compared to Coating B. Coating A also showed the lowest BUE intensity.

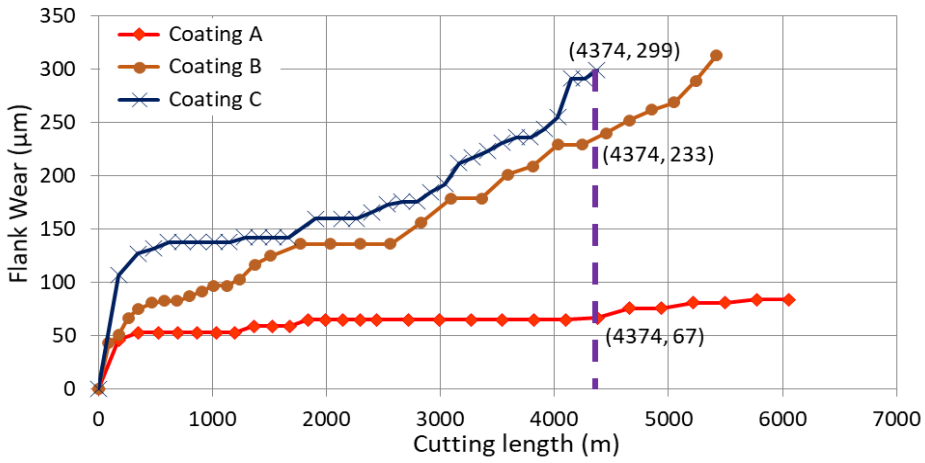

Figure 4.1. *Flank wear vs. cutting length data for the three TiB_2 coatings during wet rough turning of Ti6Al4V alloy.*

Figure 4.2 shows the progression of tool wear and the 3D difference measurement of the cutting edge after every 600 m of cutting length for the three TiB_2 coated tools. The tool wear was mainly concentrated on the cutting edge and dictated by two tool wear mechanisms: adhesion of the workpiece material leading to BUE formation at the cutting edge of the tool and crater wear occurring due to the generation of high cutting temperatures. As can be seen from the 3D images, the volume of BUE formation was significantly different for the various coated tools. The harder Coatings B and C showed substantial BUE formation, especially during the initial stages of the cut. Crater wear was also seen to be higher for Coatings B and C. The lowest BUE formation and crater wear progression was observed for Coating A, which had low hardness. Figures 4.3 and 4.4 illustrate the evolution of BUE formation and crater wear as cutting progressed for the three TiB_2 coatings. BUE formation is unstable and dynamic in nature. This behaviour is quite evident from the fluctuation in peak volume compared to previous machining passes, as seen in Figure 4.3. As BUE breaks off, it often leads to coating delamination and tool edge chipping. Coating A's lower BUE formation and lower progressive build-up while cutting therefore reduced the probability of tool edge chipping. Thus, the reduced BUE formation together with delayed and lower crater wear intensity led to uniform and stable tool wear for Coating A. It is important to point out here that the reduced crater wear value for Coating B at 600 m of cutting length (Figure 4.4) was due to the BUE covering the crater wear on the rake surface of the tool. This can be corroborated by the 3D images and BUE progressive volume data (Figures 4.2 and 4.3).

Figure 4.5 shows the variation in cutting forces for the three coated tools. The forces in all directions are lower for Coating A than for the others. This indicates that Coating A had lower cutting and frictional forces. All the coated tools had a similar cutting-edge radius (see Table 4.1) confirming that the variation in cutting forces was entirely due to the coating variations and not due to microgeometry changes in the tool. Chip characteristics provide valuable insights into the tribological interactions taking place at the tool-chip interface during machining. The characteristics of the chips collected after approximately 50 m of cutting length are presented in Table 4.3. Analysis of the chip characteristics showed an improvement in tribological behaviour for Coating A. Both the chip compression ratio and shear plane angle were higher for Coating A. These suggest that the cutting and frictional forces at the tool-chip interface were lower due to lower shearing forces acting on the chips. This complements the data on cutting forces. Coating A also had a higher chip sliding velocity which confirms that there was lower friction at the tool-chip interface and indicates that the tool-chip contact length was shorter. These led to lower cutting zone temperatures and consequently increased the tool life of Coating A.

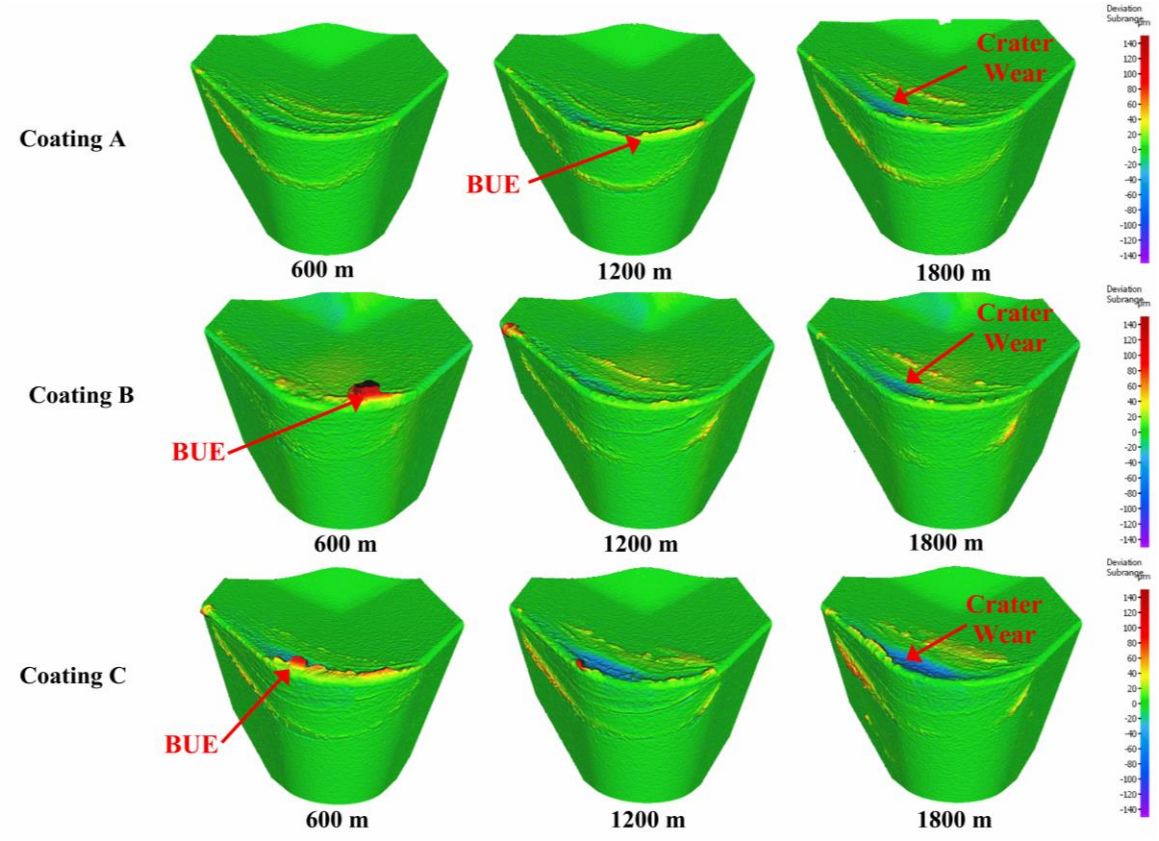

Figure 4.2. *3D progressive wear difference measurement of the coated tools highlighting evolution of built-up layer and crater wear during machining.*

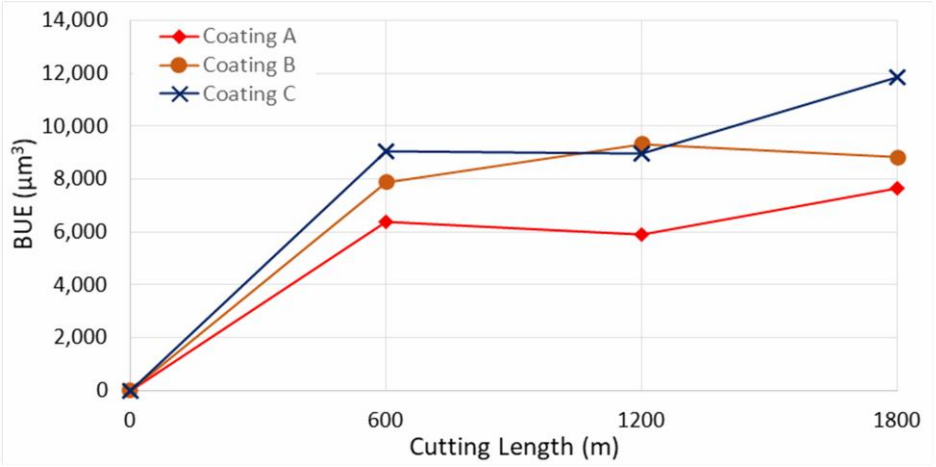

Figure 4.3. *Built-up volume progression vs length of cut for the three TiB_2 coated tools considering the peaks above reference surface of the original tool.*

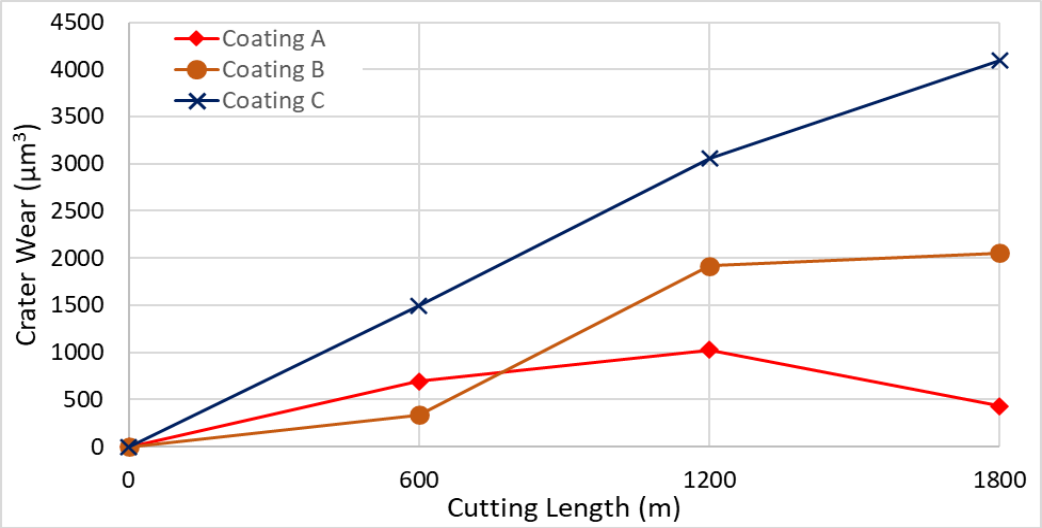

Figure 4.4. *Crater wear volume progression vs length of cut for the three TiB_2 coated tools considering the peaks below reference surface of the original tool.*

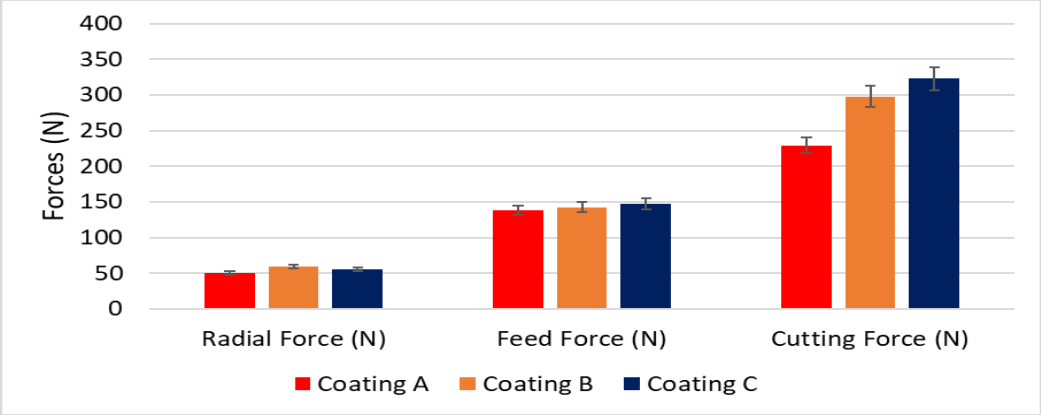

Figure 4.5. *Variation of cutting forces for the three TiB_2 coated tools.*

Table 4.3. *Tribological performance evaluated through chip characteristics for the TiB_2 coatings.*

Coating	Chip Compression Ratio - CCR	Φ - Shear Angle (°)	(ϒ) Shear Strain	Chip Sliding Velocity (m/min)
Coating A	1.18	53.7	0.50	52.9
Coating B	1.03	49.6	0.63	46.5
Coating C	1.07	50.7	0.59	48.2

4.3.2. Coating Characterization

Detailed micro-mechanical and structural analyses of the coatings were conducted to assess the wear behaviour of the coatings during machining. XRD patterns for all the coatings are shown in Figure 4.6. These indicate that the crystal orientations and structures of all the TiB_2 coatings were quite similar. Distinct peaks with varying intensities were observed for the coatings at crystallographic planes of (001), (100), (101), (002), and (110). For all the coatings, the (001) peak had the strongest intensity, suggesting that the coatings had a significant preferred orientation at the (001) crystallographic plane. The XRD analysis shows that all the deposited monolayer TiB_2 coatings have hexagonal crystal system (ICCD 00-035-0741). The irradiated area for the XRD analysis was the same for all three coatings. The XRD peaks are broader for coating B and C compared to Coating A suggesting higher dislocation density, which is contributing to the higher hardness of Coating B and C.

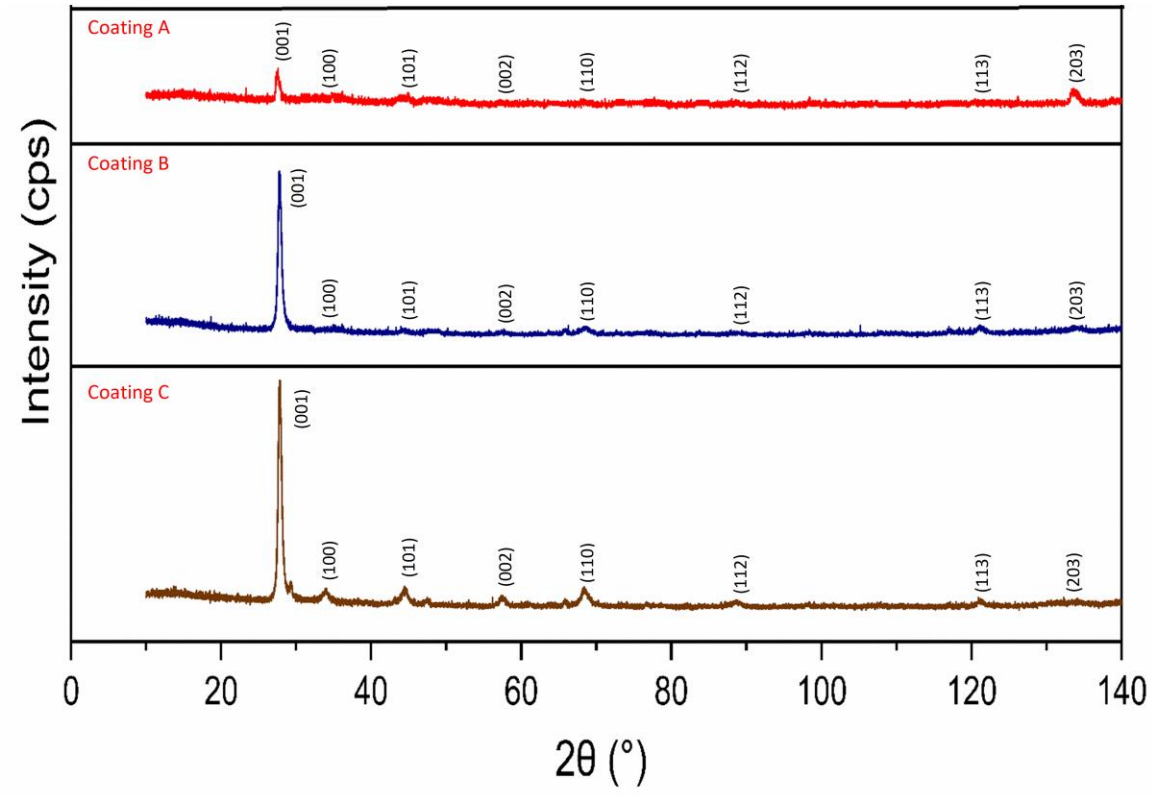

Figure 4.6. *X-ray diffraction patterns of the three TiB_2 coatings.*

Figure 4.7 shows high resolution SEM images of the structural characteristics and Figure 4.8 shows the cross sections of all three coatings. Both figures indicate that all three coatings have columnar structures. The AFM topography scans presented in Figure 4.9 also show that the size of the top of the columns [28,29] which in case of Coating A is the largest indicating the presence of thicker columns compared to Coatings B and C where the columns are found to be finer. Coating A also shows slightly increased roughness (Sa = 8.06 nm) in nanometer scale due to somewhat more curved column tops [28] compared to coating B (Sa = 5.21 nm) and C (Sa = 6.18 nm). Due to the thickness difference, although still much finer, Coating C has slightly larger column size than Coating B. The effects of

these differences in the coating structures are also evident through the differences in their properties and deformation behaviours, as discussed below.

Figures 4.7–4.9 also show that the column sizes, distributions, and inter-column spacings are different specially in case of Coating A. Previous in-depth investigations [28–32] have shown that these differences in columnar structures can affect coating properties and depending on the application, their performances. For example, inter-column spacings play an important role in effecting residual stress, hardness [28,30,31] and crack propagation [30]. Lower inter-column spacings or highly dense column boundaries result in higher compressive stress and hardness [28]. Therefore, the lower residual stress as well as the hardness (Table 4.1) in Coating A can be associated with the sub-dense column boundaries or higher inter-column spacings [28] as can be seen in the SEM images. XRD investigations, as discussed earlier, also indicated higher dislocation densities in Coatings B and C which can also contribute to their higher hardness values (Table 4.1).

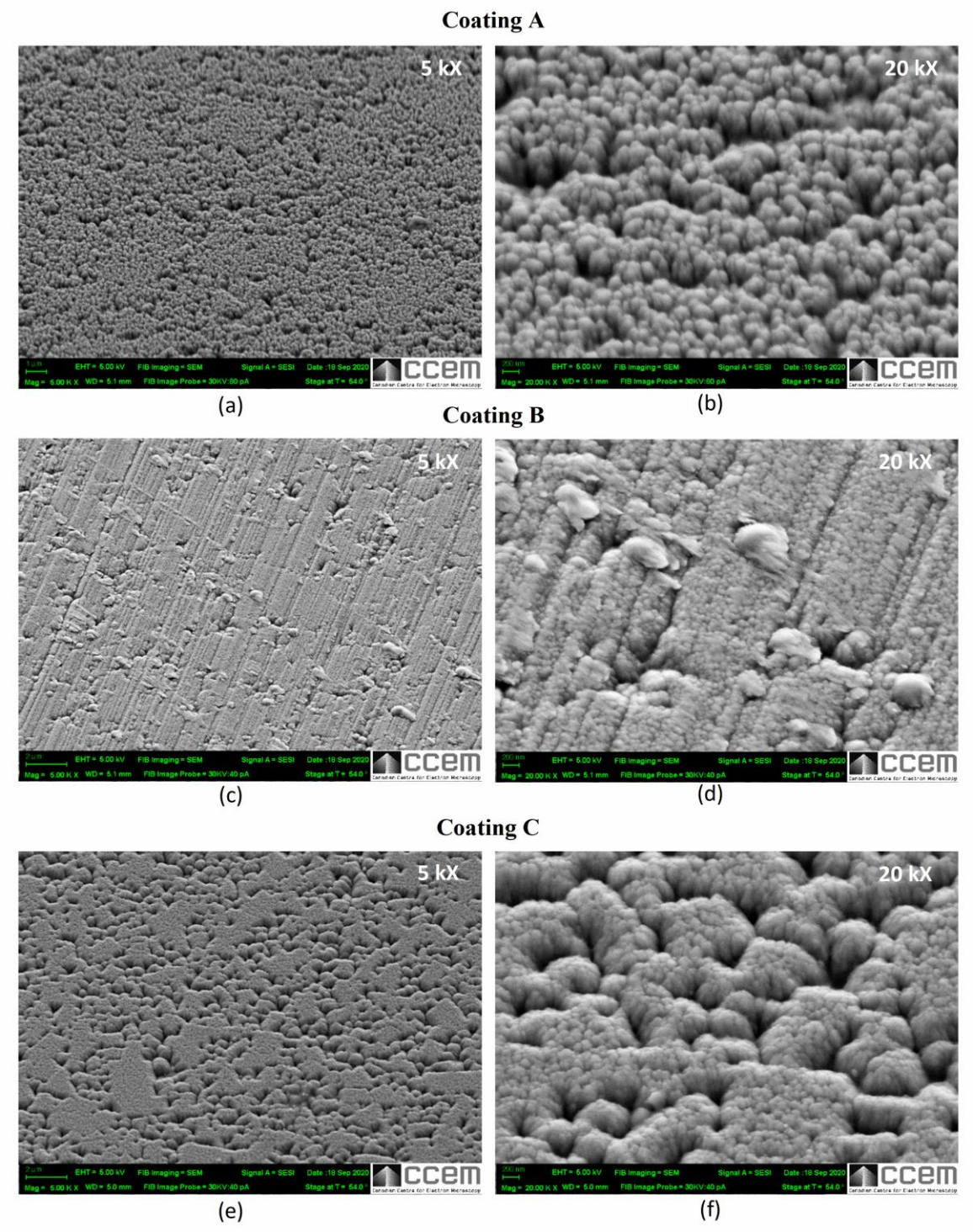

Figure 4.7. *SEM surface morphology of the three TiB_2 coatings: (a,c,e) at low magnification, (b,d,f) at high magnification.*

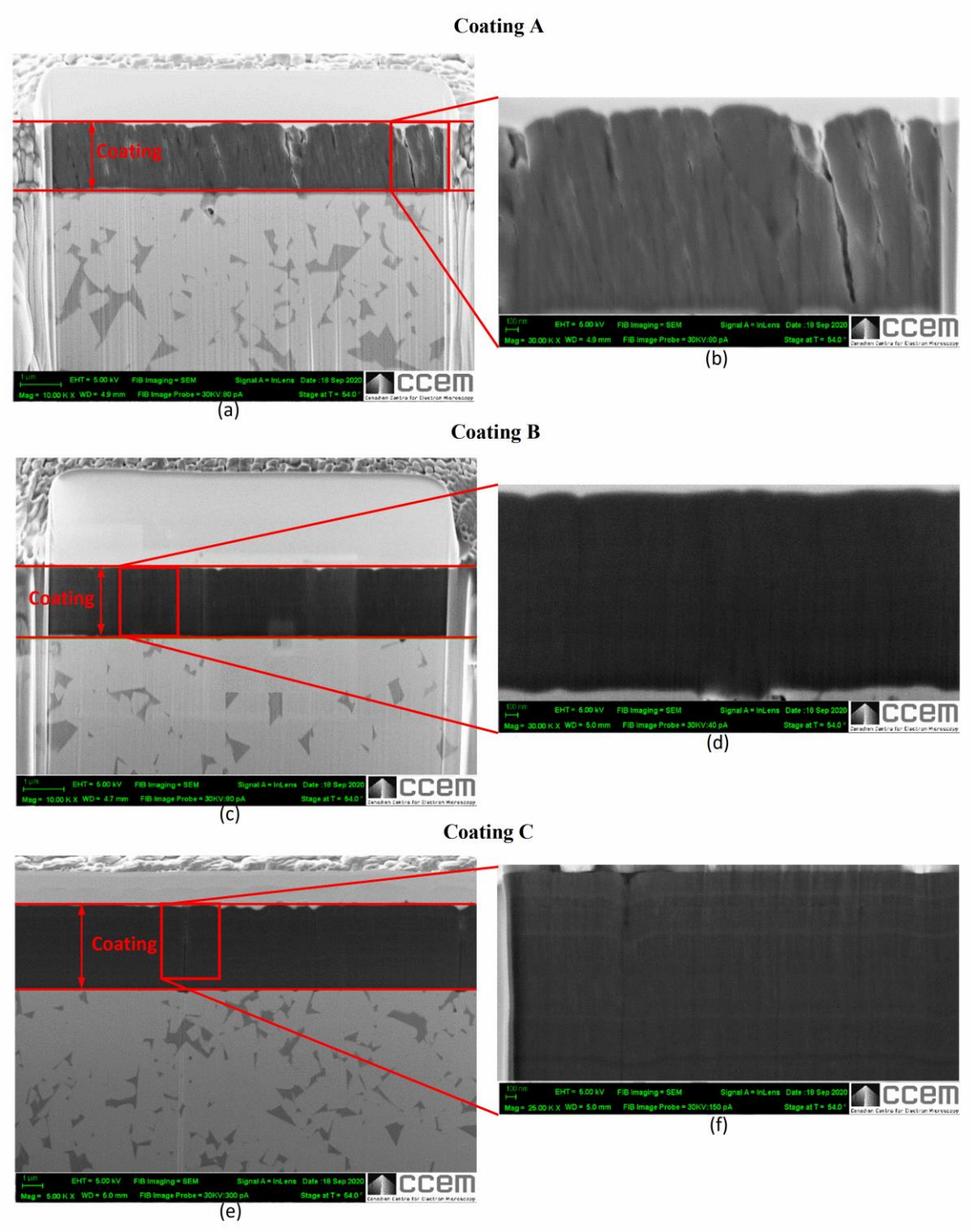

Figure 4.8. *SEM images of FIB cross-sections of the three TiB_2 coatings showing coating thickness and structure:* ***(a,c,e)*** *at low magnification,* ***(b,d,f)*** *at high magnification.*

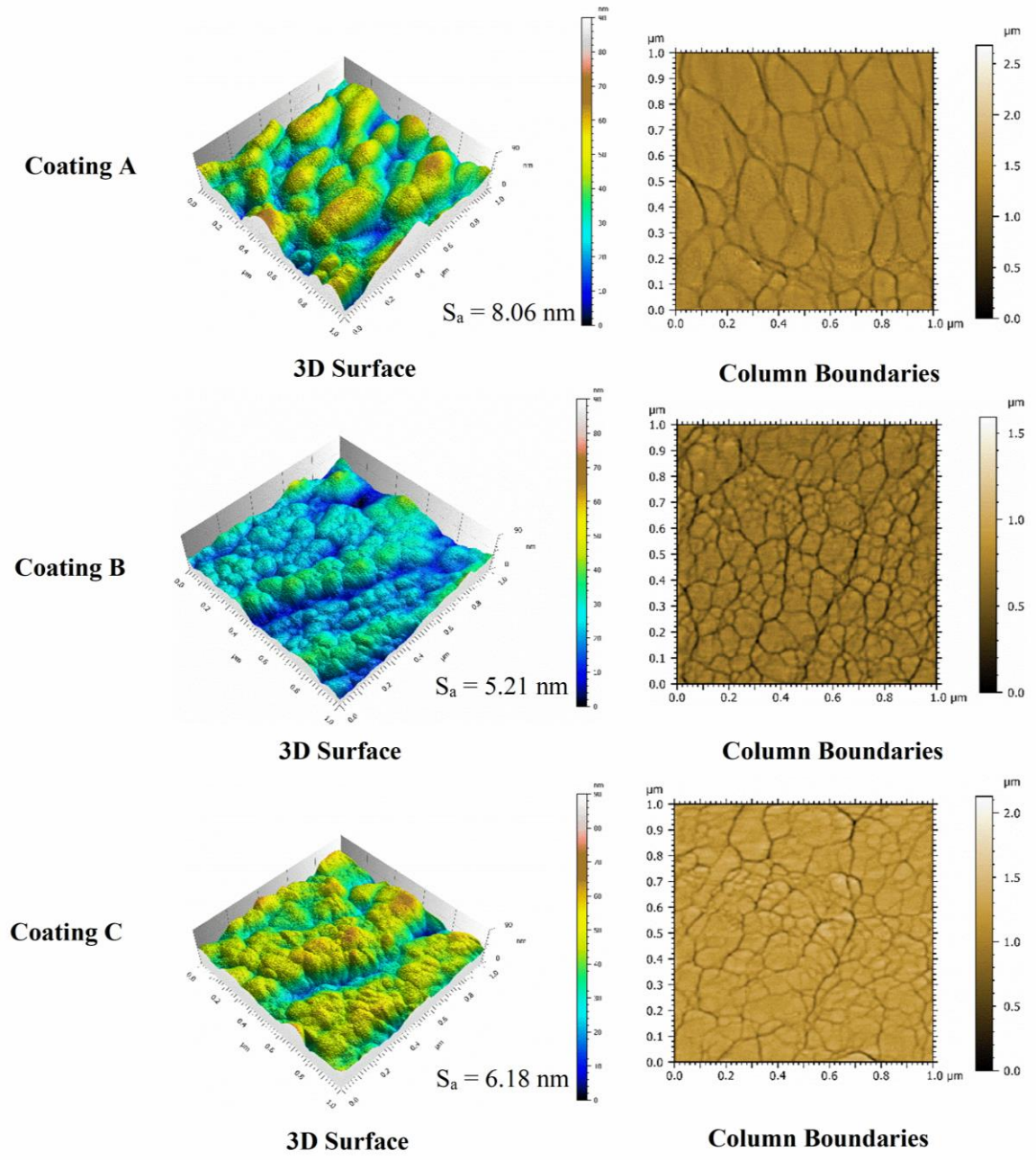

Figure 4.9. *AFM images of surface topography and column boundaries of the different TiB_2 coatings with arithmetic mean height (S_a) values.*

The coating thicknesses, micro-mechanical properties, and other related characteristics of the coatings are presented in Table 4.1. Coating A coating had considerably low hardness compared to the other coatings. The elastic modulus of Coating

A was also lower compared to the other two coatings but not as significantly lower as in the case of its hardness. The softer Coating A had lower H/E and H^3/E^2 ratios than the other harder TiB_2 coatings. The H/E and H^3/E^2 ratios of the coatings are calculated from the coating's hardness and elastic modulus. H/E is related to the elastic strain to failure and correlates well with how elastic the contact point of a coating stays during mechanical contacts [33,34]. The H^3/E^2 ratio indicates resistance to plastic deformation; a higher value of H^3/E^2 usually suggests that the likelihood of coatings to deform plastically is reduced [35]. The substantially lower hardness of Coating A was the main contributing factor for the coating's lower H/E and H^3/E^2 ratio. Such a combination of properties implies that Coating A was less brittle. Although Leyland et al. [33] suggest that coatings with a higher H/E ratio usually led to a reduction in wear, it is reported in the literature that for machining applications with an adhesive wear mechanism, as observed in the rough turning of Ti6Al4V, coatings with lower H/E ratios show better wear resistance [36,37]. Similar observations were also made in the current investigation, where Coating A showed the best wear resistance properties. Hence, for high tool load applications, typical when machining titanium, where severe deformation of the surface layers is possible, an optimized combination of H and E values is crucial for longer tool life.

It is also important for the applied coating in such applications to have an enhanced ability to dissipate the frictional heat energy that is produced due to intensive deformation of the surface layers. The more energy is dissipated, the less energy is absorbed into the tool effectively reducing deformation and damage to the tool substrate. The plasticity index, which is given by the ratio between the plastic work done and the total work done (plastic

and elastic) during indentation [38], can be used to assess a coating's ability to dissipate energy. Beake et al. [34] reported that a higher plasticity index improved the cutting behaviour in turning processes where adhesive wear dominates due to a greater ability to dissipate energy. Thus, a higher plasticity index, in this case for Coating A, indicates the coating's capability to dissipate higher energy when loaded [2,39]. Higher plasticity of a coating means that the coating releases absorbed energy through plastic deformation and not by brittle fracture, and higher H/E values result in higher critical loads for non-elastic deformation or the onset of yield during indentation or scratch testing [34]. The yield stress, determined from the indentation test, of Coating A (Table 4.1) was lower and therefore expected to yield early followed by a gradual plastic deformation. On the other hand, the higher yield stress of the harder Coatings B and C suggest that they could withstand higher stress but was followed by drastic brittle deformations. The residual stress data (Table 4.1) also support this fact, where higher compressive stress in the case of Coatings B and C may have delayed the yield a little, but the inherent higher stress was expected to cause drastic failure. This behaviour is also evident in the scratch test results (Figures 4.10–4.12, Table 4.4), where the scratch track for Coating A began to show signs of initial deformation or start of cohesive failure at a lower critical load (LC_1) but underwent plastic deformation without significant cracking and with more localized deformation (i.e., the only substrate exposed is within the scratch track, Figure 4.10), and the adhesive failure LC_2 (based on penetration depth data and scratch track analysis) was somewhat delayed compared to the other two. On the other hand, Coatings B and C did not show any gradual deformation or cohesive failure with clear LC_1 and started to deform drastically in a brittle manner

wherever the substrate was exposed, even outside of the scratch track (Figures 4.11 and 4.12). The acoustic emission data (Figures 4.11 and 4.12) also show clearly how drastic the deformation behaviour of Coatings B and C was compared to Coating A. Coating C underwent the worst deformation, indicating inferior tool performance (Figure 4.1). From a cutting tool life perspective, it could be highly beneficial that the softer Coating A does not chip in the same way as the harder Coatings B and C and less substrate is exposed when the coating fails. In this way, the surface is better protected by the coating layer. Therefore, the scratch test results, coupled with the micro-mechanical properties summarized in Table 4.1, help to explain why flaking off during cutting was avoided in the softer Coating A layer and why this coating has a potential for better tribological performance under operation. To study the frictional behaviour of the coatings, multi-pass constant load scratch tests, also known as wear tests, were performed at a subcritical load of 0.75 N. Figure 4.13 shows that for all the passes, the coefficient of friction was comparatively lower for Coating A and decreased slightly as the number of passes increased. This indicates that there was less friction at the cutting interface for Coating A than for the other two. A chip characteristics analysis also indicated improved tribological behaviour for Coating A (Table 4.3).

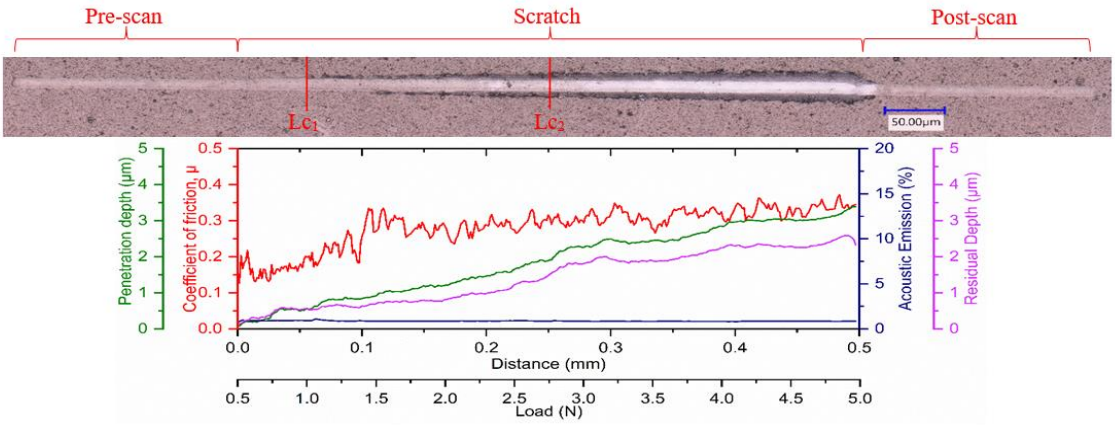

Figure 4.10. *Ramped load scratch test data with optical images of the scratch track for Coating A.*

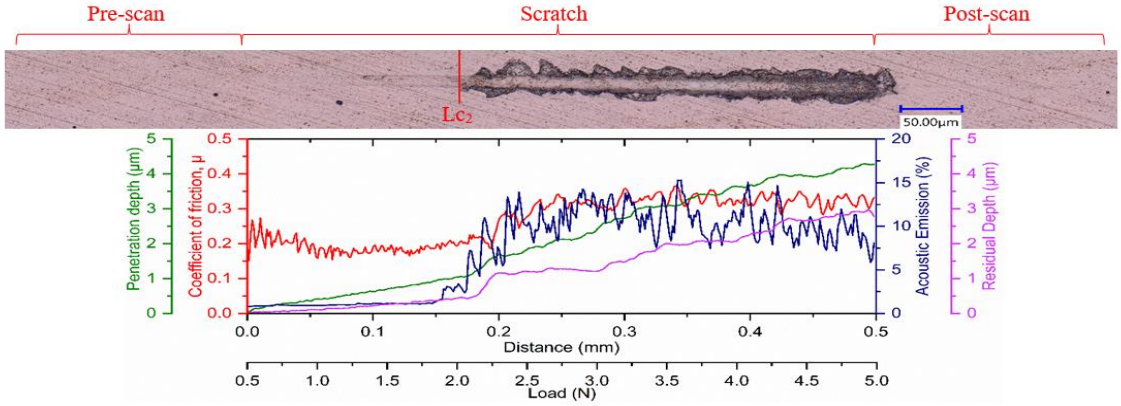

Figure 4.11. *Ramped load scratch test data with optical images of the scratch track for Coating B.*

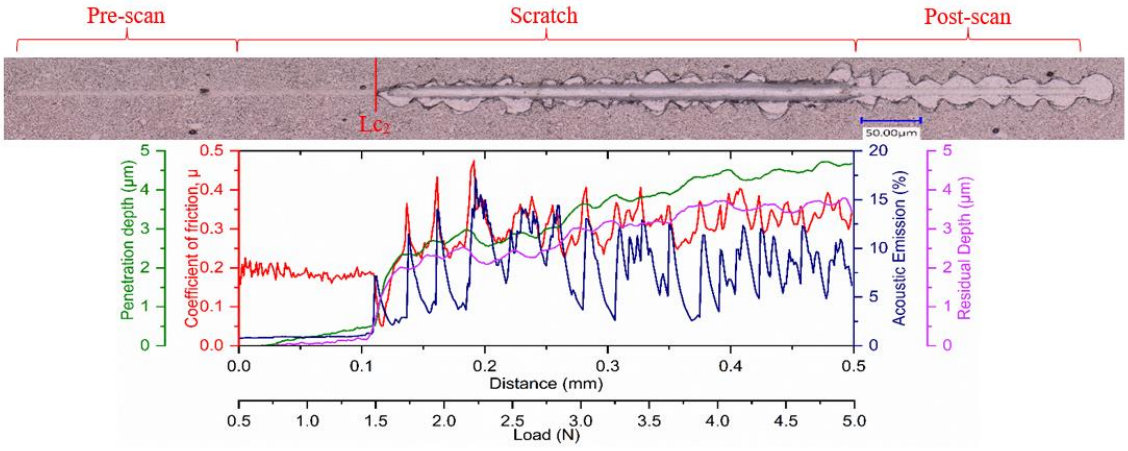

Figure 4.12. *Ramped load scratch test data with optical images of the scratch track for Coating C.*

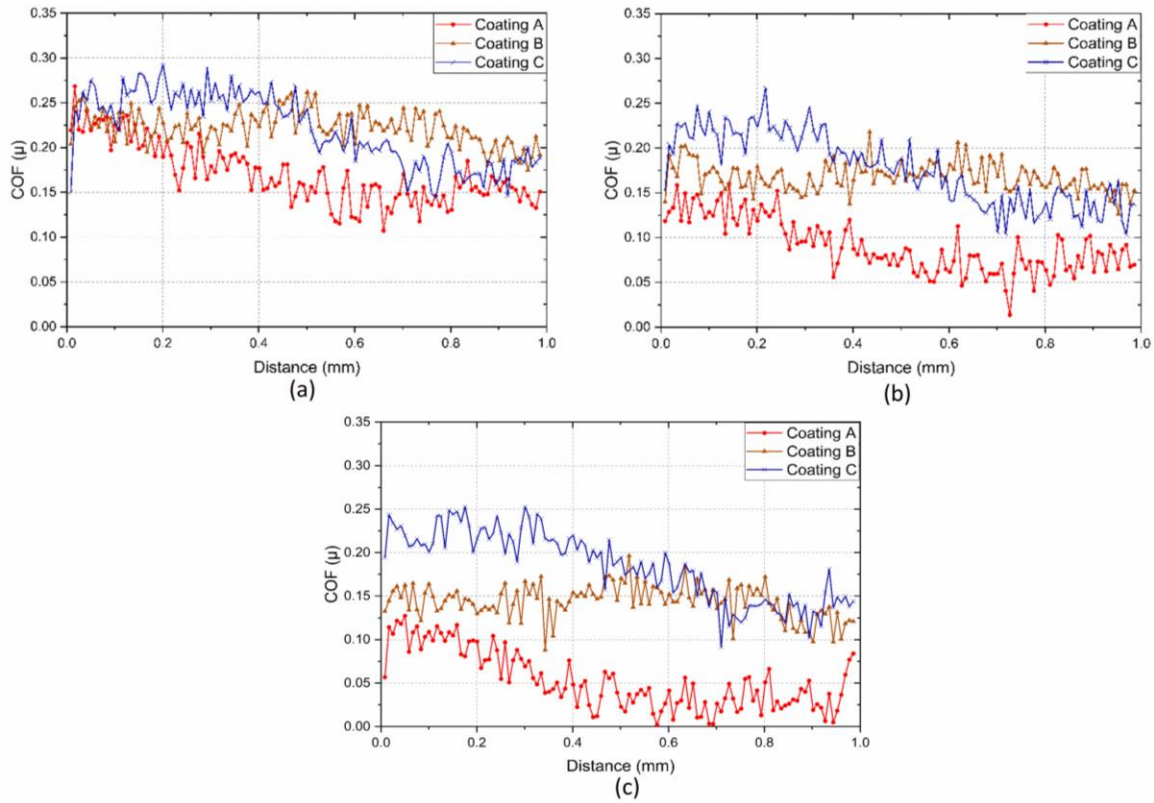

Figure 4.13. *Evolution of coefficient of friction at different passes during repetitive wear test at 0.75 N for the three TiB_2 coatings after: (a) 1 pass, (b) 3 passes and (c) 5 passes.*

Table 4.4. *Critical load for crack initiation in coating, LC_1 and critical load for coating failure, LC_2 obtained from ramped load scratch test for the three TiB_2 coatings.*

Coating	LC_1, N	LC_2, N
Coating A	1.00	2.75
Coating B	-	2.01
Coating C	-	1.50

It has been previously shown that a higher plasticity index (as seen for Coating A) is indicative of higher toughness and durability of the coatings [40]. Toughness refers to a coating's ability to absorb energy during deformation without fracturing and to resist crack propagation in the coating [41]. The modified Palmqvist toughness test confirmed that the softer Coating A had higher toughness than the harder Coatings B and C (Table 4.1). Since

all the coatings were deposited on the same substrate material, the variations in the toughness values obtained were entirely due to the applied coatings. Figure 4.14 shows SEM images of the imprints and the crack formations under indentation load. Cracks along the edges of Coatings B and C indicate the brittleness of these high hardness coatings compared to the softer Coating A. Nano-impact tests were carried out to study the coatings' fracture resistance under repetitive impact at the same spot with a 20 mN load every 4 s (Figure 4.15). The evolution of the impact penetration depths due to progressive coating damage was continuously monitored. The increase in penetration depth with repetitive impact was lowest for Coating A, indicating better fatigue fracture resistance. For Coatings B and C, the increase in penetration depth was significantly higher, indicating the inferior performance of these two coatings. Thus, the higher plasticity index, lower H/E ratio, higher modified Palmqvist toughness, and improved fatigue fracture resistance of the softer Coating A indicate that this coating has the ability to withstand more plastic deformation than the other two which, from the higher hardness values and higher H/E ratio, are more likely to fail in a brittle manner. For machining applications where an adhesive wear mechanism leading to BUE formation dictates tool wear, the coating properties that Coating A possesses are crucial. BUE is an unstable structure that breaks off intermittently during machining causing surface damage and coating delamination [42]. Coatings that fail in a brittle manner are more prone to coating delamination during BUE removal. Moreover, Coating A's increased thermal diffusivity and conductivity even at higher temperatures in comparison with the other two, as shown in Figure 4.16, will be beneficial for thermal

energy dissipation at the cutting zone, saving the tool from overheating. This also ensures that Coating A performs better, resulting in longer tool life (Figure 4.1).

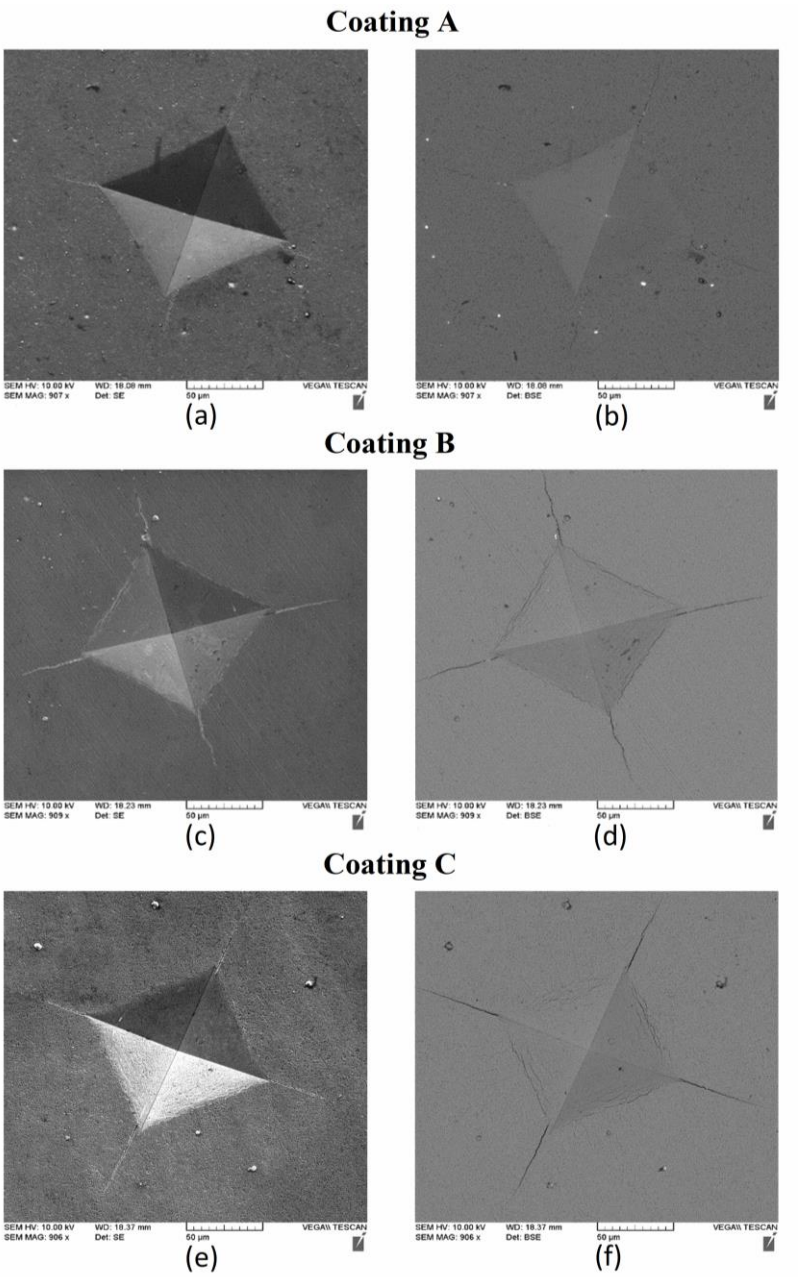

Figure 4.14. *SEM images of Vickers indentation and cracks of the three TiB_2 coatings from modified Palmqvist toughness test: (**a**,**c**,**e**) SE images, (**b**,**d**,**f**) BSE images.*

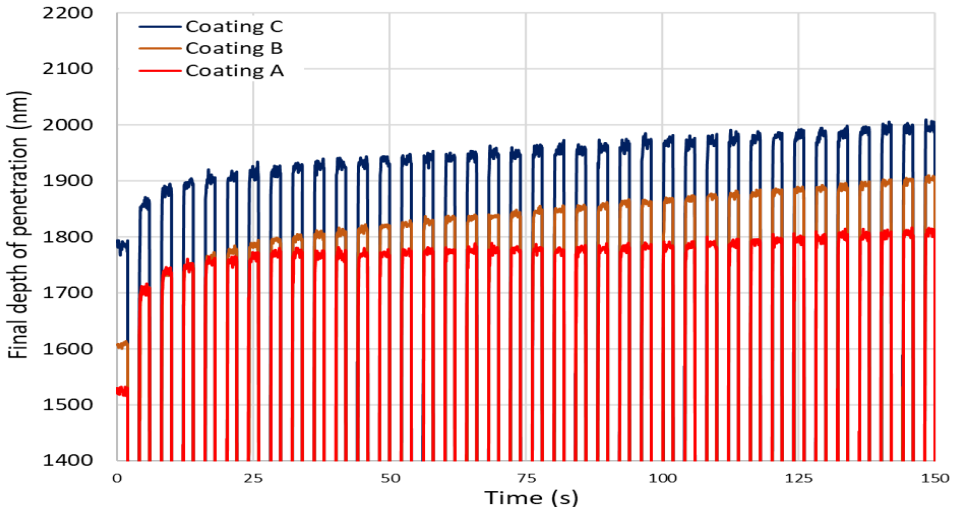

Figure 4.15. *First 150 s depth of penetration obtained from nano-impact testing at a load of 20 mN for the TiB_2 coatings.*

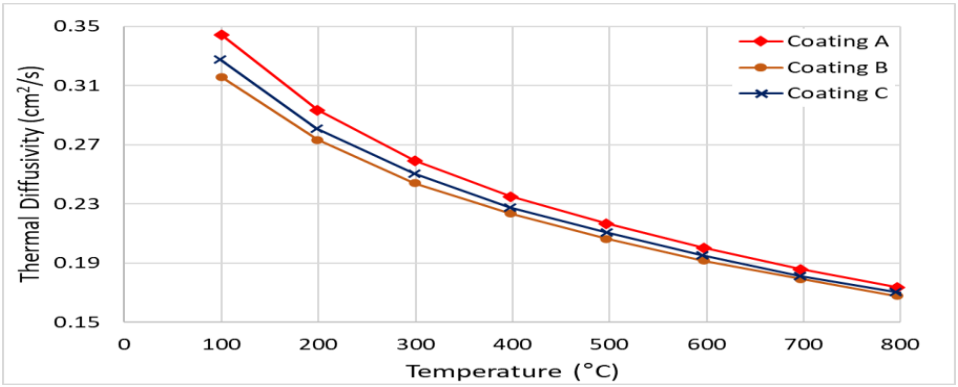

(**a**)

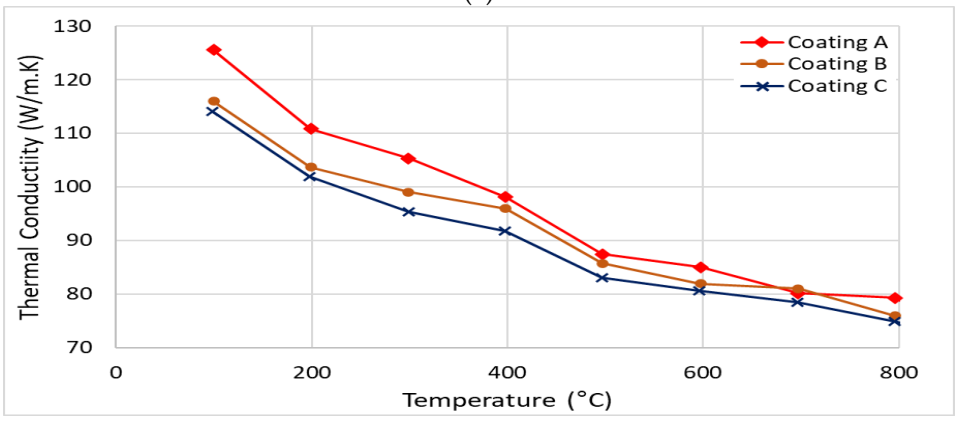

(**b**)

Figure 4.16. *Temperature dependent data of (a) thermal diffusivity and (b) thermal conductivity for the three TiB_2 coatings.*

XPS analysis on the worn tools showed B_2O_3 tribo-film formation (Figure 4.17). Table 4.5 shows the relative percentages of the tribo-films for the three TiB_2 coatings. These tribo-films form due to the self-lubricating nature of the TiB_2 coatings [2,22] and enhances lubriciousness of the coating thereby reducing friction at the tool-chip interface. As seen from Table 4.5, Coating A actually has the least amount of tribo-film formation although it gave the best tool performance (Figure 4.1). This suggests that the superior machining performance of Coating A is mostly attributed to its unique and superior micromechanical and tribological properties, not just due to the tribo-film formation. Therefore, Coating A, with a higher toughness and plasticity index combined with lower hardness, lower yield stress, lower H/E and H^3/E^2 ratios, and improved thermal properties, provides better tool protection and longer tool life by preventing coating delamination during cutting.

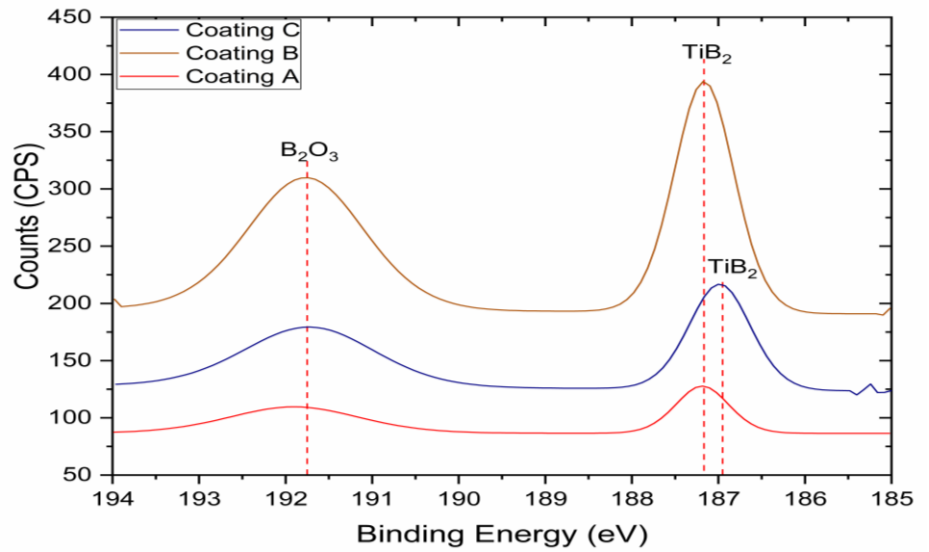

Figure 4.17. *High resolution XPS data (B 1s spectrum) of worn rake surface of the three TiB_2 coatings confirming B_2O_3 tribo-oxide formation.*

Table 4.5. *Relative percentages of the B_2O_3 phase present on the rake surface of the three TiB_2 coated tools after approximately 100 m cut obtained from High Resolution XPS.*

Coating	Binding Energy (eV)	Relative Atomic Percentage (%)
Coating A	191.9	2.348
Coating B	191.8	4.56
Coating C	191.7	3.815

4.4. Conclusions

Tool performance during the rough turning of Ti6Al4V alloy is mainly dictated by an adhesive wear mechanism leading to significant BUE formation. An effective strategy to improve tool performance in such cases is to use a lubricious tool coating that has its mechanical and adaptive characteristics tweaked to provide better tribological interaction at the tool-chip interface and reduce and minimize the effects of BUE formation. Amongst others, the TiB_2 family of coatings have shown great promise for the machining of titanium alloys.

The micromechanical and tribological properties of a coating have a direct relation to the wear performance of a tool under machining conditions associated with strong built-up edge formation. The properties of the coating strongly vary depending on the deposition parameters and techniques applied. In the current research, three TiB_2 coatings deposited by magnetron sputtering with varied coating thicknesses and hardness values were investigated. All the three TiB_2 coatings formed B_2O_3 tribo-films during machining which increased lubriciousness of the coatings reducing friction at the tool-chip interface. However, despite having lower amount of tribo-film formation, the thin TiB_2 coating with low hardness showed more significant tool life improvement during the rough turning of

Ti6Al4V alloy than the thin and thick TiB_2 coatings with high hardness. This could be attributed to the fact that the low hardness TiB_2 coating has the ability to minimize BUE formation and prevent coating delamination due to its unique blend of micromechanical and tribological properties. The low hardness TiB_2 coating under the tested machining conditions presents favorable combinations of mechanical and thermal properties and improved tribological properties with less substrate exposure, which ultimately leads to enhanced tool performance.

4.5. References

1. Veiga, C.; Davim, J.P.; Loureiro, A.J.R. Proprties and Applications of Titanium Alloys. Rev. Adv. Mater. Sci. 2012, 32, 133–148.
2. Chowdhury, M.; Chowdhury, S.; Yamamoto, K.; Beake, B.; Bose, B.; Elfizy, A.; Cavelli, D.; Dosbaeva, G.; Aramesh, M.; Fox-Rabinovich, G.; et al. Wear behaviour of coated carbide tools during machining of Ti6Al4V aerospace alloy associated with strong built up edge formation. Surf. Coatings Technol. 2017, 313, 319–327, doi:10.1016/j.surfcoat.2017.01.115.
3. Paiva, J.M.; Shalaby, M.A.M.; Chowdhury, M.; Shuster, L.; Chertovskikh, S.; Covelli, D.; Junior, E.L.; Stolf, P.; Elfizy, A.; Bork, C.A.S.; et al. Tribological and Wear Performance of Carbide Tools with TiB_2 PVD Coating under Varying Machining Conditions of TiAl6V4 Aerospace Alloy. Coatings 2017, 7, 187, doi:10.3390/coatings7110187.
4. Dearnley, P.; Grearson, A. Evaluation of principal wear mechanisms of cemented carbides and ceramics used for machining titanium alloy IMI 318. Mater. Sci. Technol. 1986, 2, 47–58, doi:10.1179/026708386790123611.
5. Boyer, R. An overview on the use of titanium in the aerospace industry. Mater. Sci. Eng. A 1996, 213, 103–114, doi:10.1016/0921-5093(96)10233-1.
6. Armendia, M.; Garay, A.; Iriarte, L.-M.; Arrazola, P.J. Comparison of the machinabilities of Ti6Al4V and TIMETAL® 54M using uncoated WC–Co tools. J. Mater. Process. Technol. 2010, 210, 197–203, doi:10.1016/j.jmatprotec.2009.08.026.

7. Corduan, N.; Himbart, T.; Poulachon, G.; Dessoly, M.; Lambertin, M.; Vigneau, J.; Payoux, B. Wear Mechanisms of New Tool Materials for Ti-6AI-4V High Performance Machining. CIRP Ann. 2003, 52, 73–76, doi:10.1016/s0007-8506(07)60534-4.
8. Hartung, P.D.; Kramer, B.M. Tool Wear in Machining Titanium. Ann. CIRP 1982, 30, 75–80.
9. Biksa, A.; Yamamoto, K.; Dosbaeva, G.; Veldhuis, S.; Fox-Rabinovich, G.; Elfizy, A.; Wagg, T.; Shuster, L. Wear behaviour of adaptive nano-multilayered AlTiN/MexN PVD coatings during machining of aerospace alloys. Tribol. Int. 2010, 43, 1491–1499, doi:10.1016/j.triboint.2010.02.008.
10. M'Saoubi, R.; Axinte, D.; Soo, S.L.; Nobel, C.; Attia, H.; Kappmeyer, G.; Engin, S.; Sim, W.-M. High performance cutting of advanced aerospace alloys and composite materials. CIRP Ann. 2015, 64, 557–580, doi:10.1016/j.cirp.2015.05.002.
11. Hatt, O.; Crawforth, P.; Jackson, M. On the mechanism of tool crater wear during titanium alloy machining. Wear 2017, 374-375, 15–20, doi:10.1016/j.wear.2016.12.036.
12. Wang, Z.M.; Ezugwu, E.O. Performance of PVD-Coated Carbide Tools When Machining Ti-6Al-4V©. Tribol. Trans. 1997, 40, 81–86, doi:10.1080/10402009708983632.
13. Özel, T.; Sima, M.; Srivastava, A.; Kaftanoglu, B. Investigations on the effects of multi-layered coated inserts in machining Ti–6Al–4V alloy with experiments and finite element simulations. CIRP Ann. 2010, 59, 77–82, doi:10.1016/j.cirp.2010.03.055.

14. Bouzakis, K.-D.; Michailidis, N.; Skordaris, G.; Bouzakis, E.; Biermann, D.; M'Saoubi, R. Cutting with coated tools: Coating technologies, characterization methods and performance optimization. CIRP Ann. 2012, 61, 703–723, doi:10.1016/j.cirp.2012.05.006.
15. Cherukuri, R.; Molian, P. Lathe Turning of Titanium Using Pulsed Laser Deposited, Ultra-Hard Boride Coatings of Carbide Inserts. Mach. Sci. Technol. 2003, 7, 119–135, doi:10.1081/mst-120018958.
16. Berger, M.; Hogmark, S. Evaluation of TiB_2 coatings in sliding contact against aluminium. Surf. Coatings Technol. 2002, 149, 14–20, doi:10.1016/s0257-8972(01)01361-5.
17. Park, B.; Jung, D.-H.; Kim, H.; Yoo, K.-C.; Lee, J.-J.; Joo, J. Adhesion properties of TiB_2 coatings on nitrided AISI H13 steel. Surf. Coatings Technol. 2005, 200, 726–729, doi:10.1016/j.surfcoat.2005.01.064.
18. Silva, M.F.; Hancock, P.; Nicholls, J. Multilayer Coating Techniques to Optimise the Properties of TiB_2-Based Coatings. Adv. Eng. Mater. 2000, 2, 666–671.
19. Berger, M.; Larsson, M.; Hogmark, S. Evaluation of magnetron-sputtered TiB_2 intended for tribological applications. Surf. Coatings Technol. 2000, 124, 253–261, doi:10.1016/s0257-8972(99)00638-6.
20. Kelesoglu, E.; Mitterer, C. Structure and properties of TiB_2 based coatings prepared by unbalanced DC magnetron sputtering. Surf. Coatings Technol. 1998, 98, 1483–1489, doi:10.1016/s0257-8972(97)00397-6.

21. Grancic, B.; Mikula, M.; Hruba, L.; Gregor, M.; Stefecka, M.; Csuba, A.; Dobročka, E.; Plecenik, A.; Kus, P. The influence of deposition parameters on TiB_2 thin films prepared by DC magnetron sputtering. Vacuum 2005, 80, 174–177, doi:10.1016/j.vacuum.2005.08.013.
22. Fox-Rabinovich, G.S.; Gershman, I.; El Hakim, M.A.; Shalaby, M.A.; Krzanowski, J.E.; Veldhuis, S.C. Tribo-film Formation As a Result of Complex Interaction at the Tool/Chip Interface during Cutting. Lubricants 2014, 2, 113–123, doi:10.3390/lubricants2030113.
23. Chowdhury, M.; Bose, B.; Rawal, S.; Fox-Rabinovich, G.; Veldhuis, S. Investigation of the Wear Behaviour of PVD Coated Carbide Tools during Ti6Al4V Machining with Intensive Built Up Edge Formation. Coatings 2021, 11, 266, doi:10.3390/coatings11030266.
24. ISO 14577-4: 2016(E). Metallic Materials—Instrumented Indentation Test for Hardness and 746 Materials Parameters—Part 4: Test Method for Metallic and Non-Metallic Coatings; International Organization for Standardization: Geneva, Switzerland, 2016.
25. ISO 28079: 2009 (E). Hardmetals—Palmqvist Toughness Test; International Organization for Standardization: Geneva, Switzerland, 2009.
26. ISO 3685: 1993(E). Tool-Life Testing with Single-Point Turning Tools; International Organization for Standardization: Geneva, Switzerland, 1993.
27. Shaw, M.C.; Cookson, J. Metal cutting principles. Tribol. Int. 1985, 18, 55, doi:10.1016/0301-679x(85)90013-1.

28. Luo, Q.; Lewis, D.; Hovsepian, P.; Münz, W.-D. Transmission Electron Microscopy and X-ray Diffraction Investigation of the Microstructure of Nanoscale Multilayer TiAlN/VN Grown by Unbalanced Magnetron Deposition. J. Mater. Res. 2004, 19, 1093–1104, doi:10.1557/jmr.2004.0143.
29. Luo, Q.; Wang, S.C.; Zhou, Z.; Chen, L. Structure characterization and tribological study of magnetron sputtered nanocomposite nc-TiAlV(N,C)/a-C coatings. J. Mater. Chem. 2011, 21, 9746–9756, doi:10.1039/c1jm10707k.
30. Ganvir, A.; Joshi, S.; Markocsan, N.; Vassen, R. Tailoring columnar microstructure of axial suspension plasma sprayed TBCs for superior thermal shock performance. Mater. Des. 2018, 144, 192–208, doi:10.1016/j.matdes.2018.02.011.
31. Fan, Z.; Wang, K.; Dong, X.; Duan, W.; Mei, X.; Wang, W.; Cui, J.; Lv, J. Influence of columnar grain microstructure on thermal shock resistance of laser re-melted ZrO2-7wt.% Y2O3 coatings and their failure mechanism. Surf. Coatings Technol. 2015, 277, 188–196, doi:10.1016/j.surfcoat.2015.07.036.
32. Qiu, S.-Y.; Wu, C.-W.; Huang, C.-G.; Ma, Y.; Guo, H.-B. Microstructure Dependence of Effective Thermal Conductivity of EB-PVD TBCs. Materials 2021, 14, 1838, doi:10.3390/ma14081838.
33. Leyland, A.; Matthews, A. On the significance of the H/E ratio in wear control: A nanocomposite coating approach to optimised tribological behaviour. Wear 2000, 246, 1–11, doi:10.1016/s0043-1648(00)00488-9.

34. Beake, B.; Fox-Rabinovich, G. Progress in high temperature nanomechanical testing of coatings for optimising their performance in high speed machining. Surf. Coatings Technol. 2014, 255, 102–111, doi:10.1016/j.surfcoat.2014.02.062.
35. Tsui, T.Y.; Pharr, G.M.; Oliver, W.C.; Bhatia, C.S.; White, R.L.; Anders, S.; Anders, A.; Brown, I.G. Nanoindentation and Nanoscratching of Hard Carbon Coatings for Magnetic Disks. MRS Proc. 1995, 383, 447–452, doi:10.1557/proc-383-447.
36. Fox-Rabinovich, G.; Shuster, L.; Beake, B.; Veldhuis, S. Physical and Mechanical Properties to Characterize Tribological Compatibility of Heavily Loaded Tribosystems (HLTS). In Self-Organization during Friction: Advanced Surface-Engineered Materials and Systems Design; CRC Press, Taylor and Francis group: Boca Raton, FL, USA, UK, 2006; pp. 121–147.
37. Sato, K.; Ichimiya, N.; Kondo, A.; Tanaka, Y. Microstructure and mechanical properties of cathodic arc ion-plated (Al,Ti)N coatings. Surf. Coatings Technol. 2003, 163-164, 135–143, doi:10.1016/s0257-8972(02)00610-2.
38. Beake, B.; Fox-Rabinovich, G.; Veldhuis, S.; Goodes, S. Coating optimisation for high speed machining with advanced nanomechanical test methods. Surf. Coatings Technol. 2009, 203, 1919–1925, doi:10.1016/j.surfcoat.2009.01.025.
39. Fox-Rabinovich, G.; Veldhuis, S.; Scvortsov, V.; Shuster, L.S.; Dosbaeva, G.; Migranov, M. Elastic and plastic work of indentation as a characteristic of wear behaviour for cutting tools with nitride PVD coatings. Thin Solid Films 2004, 469-470, 505–512, doi:10.1016/j.tsf.2004.07.038.

40. Zhang, X.; Beake, B.D.; Zhang, S. Toughness evaluation of hard coatings and thin films. In Thin Films and Coatings: Toughening and Toughness Characterization; CRC Press, Taylor and Francis Group: Boca Raton, FL, USA, 2015; p. 52.
41. Zhang, S.; Zhang, X. Toughness evaluation of hard coatings and thin films. Thin Solid Films 2012, 520, 2375–2389, doi:10.1016/j.tsf.2011.09.036.
42. German S. Fox-Rabinovich; Kovalev, A.I. Self-Organization and Structural Adaptation during Cutting and Stamping Operations. In Self-Organization during Friction: Advanced Surface-Engineered Materials and Systems Design; CRC Press, Taylor and Francis group: Boca Raton, FL, USA, UK, 2006.

Chapter 5. Conclusions and Future Work

5.1. General Conclusion

Despite possessing an excellent combination of mechanical and chemical properties like high-temperature strength, high ductility, a favorable strength-to-weight ratio, desirable toughness, corrosion resistance, high wear resistance and fracture resistance, etc., the use of titanium alloys is limited due to its low machinability [1-5]. Titanium alloys are categorised as difficult-to-cut materials due to certain unique characteristics such as high chemical affinity towards tool materials, low thermal conductivity, high-temperature strength, low modulus of elasticity, etc. These properties result in rapid tool wear, making machining titanium alloys relatively expensive.

An effective strategy for reducing tool wear is to use appropriate tool coatings to help protect the tool by providing better wear resistance. However, uncoated straight grade carbide tools are still being used in industry for titanium machining due to a lack of effective coating [6]. But with the significant advancement of tool coating deposition technology in recent years, it is now possible to design new tool coatings that cater to the unique tribological requirements of machining titanium alloys [7].

In the current research, novel compositions of self-adaptive and self-lubricating PVD coatings were developed to address the machinability issues of Ti6Al4V alloy during turning operations. While turning Ti6Al4V, the adhesion wear mechanism, which leads to BUE formation and crater wear formation due to high cutting temperature generation, dictates tool performance. However, the severity and rate of these wear phenomena vary

widely based on machining conditions. Two PVD coatings, TiB_2 and CrN, were chosen based on the expected formation of beneficial tribo-films that counteract specific wear mechanisms during the rough and finish turning of Ti6Al4V alloy. In-depth experimental studies were conducted to assess the performance of both coatings against uncoated and industrially recommended commercial AlTiN coated tools during the rough and finish turning of Ti6Al4V alloy. Tool wear characteristics were evaluated via tool life studies that were coupled with SEM, 3D volumetric wear measurements of the worn tools, cutting force measurements, and chip morphology analyses. The micro-mechanical properties of the coatings were also studied thoroughly in correlation with the coatings' performances using coating characterization techniques such as nanoindentation, impact test, scratch test, tribometer test, thermal conductivity test, AFM, XRD, XPS, FIB-SEM etc. Based on these detailed experimental and analytical studies, the major findings of the current research are summarized below:

1. During Ti6Al4V turning, the adhesion wear mechanism, which leads to BUE formation and crater wear formation, dictates tool performance. However, one of either BUE or crater wear is dominant over the other depending on cutting conditions. The in-depth experimental studies revealed that BUE formation due to intensive sticking of titanium on the cutting tool dictates tool performance during rough turning whereas crater wear formation due to high cutting temperature generation was the dominant tool wear mechanism during finish turning.
2. Self-adaptive TiB_2 and CrN coatings were effective at improving tool performance for rough turning Ti6Al4V alloy compared to uncoated and AlTiN coated tools where

adhesion wear was the dominant tool wear mechanism. The TiB_2 coating had the best tool performance due to the formation of a B_2O_3 tribo-film which has lubricious characteristics leading to reduced BUE formation. The CrN coating provided the second-best tool performance for rough turning Ti6Al4V due to Cr_2O_3 tribo-film formation, which also has lubricating properties but has lower efficiency than B_2O_3 tribo-films within the rough turning temperature range.

3. A self-adaptive CrN coating improved tool performance for the finish turning of Ti6Al4V alloy compared to uncoated and AlTiN coated tools where crater wear formation dictates tool performance. This is due to Cr_2O_3 tribo-film formation that has thermal barrier characteristics in addition to lubricating characteristics. A TiB_2 coating, however, was found to be ineffective during finish turning operation due to a drop in the efficiency of the B_2O_3 tribo-film at high temperatures.
4. Detailed experimental investigations into the effect of the deposition parameters on the performance of a CrN coating revealed that the optimal deposition parameters for the best machining performance for finish turning operation were 4 Pa nitrogen gas pressure, -50V bias voltage, and 1.81 μm coating thickness.
5. Since a CrN coating improves tool performance for both the rough and finish turning of Ti6Al4V alloy, it can possibly be considered as a general-purpose coating for a wider range of cutting conditions for Ti6Al4V turning.
6. For machining applications where BUE formation is observed, coating hardness plays a significant role in tool performance. It was found that lower hardness coatings perform better than higher hardness coatings since they fail because of localized plastic

deformation and have lower sliding contact friction. Such behaviour provides the lower hardness coatings with the ability to withstand intensive sticking, preventing coating delamination, and improved tribological characteristics under heavy loaded tooling applications.

Thus, in the present research, the selection and design of the self-adaptive PVD coatings for the turning of Ti6Al4V alloy was based on the dominant tool wear mechanism and tribological phenomena occurring at the tool-chip-workpiece interface. The major focus of this research was to identify the coatings' unique combination of micromechanical properties and adaptive tribological characteristics that leads to improvement in tool wear performance by addressing the underlying dominant tool wear mechanism during the rough and finish turning of Ti6AL4V alloy.

5.2. Research Contributions

The main contributions of this research are listed below:

1. The dominant tool wear mechanism dictating tool performance during the rough and finish turning of Ti6Al4V was identified. Both adhesive wear leading to BUE formation and crater wear formation was prevalent during Ti6Al4V turning. However, one is dominant over the other depending on the cutting conditions. It was established that adhesive wear causing BUE formation dictates tool performance during the rough turning of Ti6Al4V, whereas crater wear formation determines tool behaviour during the finish turning of Ti6AlV4 alloy.

2. Two self-adaptive PVD coatings, TiB_2 and CrN, that can form beneficial tribo-films catering to specific wear mechanisms during the rough and finish turning of Ti6Al4V alloy, were designed. The TiB_2 coating formed a lubricous B_2O_3 tribo-film and lowered the tool wear rate during rough turning approximately 74% compared to an industry recommended AlTiN coated tool at the same cutting length. The CrN coating, on the other hand, which forms tribo-films with both lubricious and thermal barrier properties, provided an approximately 61% lower tool wear rate for rough turning compared to an AlTiN coated tool. The CrN coating also lowered the tool wear rate during finish turning of Ti6Al4V alloy by around 68%.
3. It was established that for machining applications where the adhesive wear mechanism prevails, lower hardness coatings perform better than higher hardness coatings due to their increased capacity to prevent coating delamination and better tribological characteristics.
4. A CrN coating was developed using a systematic coating development framework and was established to be a general-purpose coating for a wide range of cutting conditions for Ti6Al4V turning. The nitrogen gas deposition pressure, deposition bias voltage and coating thickness was systematically tuned for the CrN coating to achieve the best tool performance during a finish turning operation.

In this research, the role of coating properties and tribo-film formation on tool performance was investigated in detail. It was shown that significant tool life improvement can be achieved if PVD coatings are designed with micro-mechanical and tribological properties that are tailored to address the dominant wear mechanism and tribological

interaction taking place at the tool-chip interface. The knowledge gained and the research approach adopted can be implemented to design PVD coatings for other difficult-to-cut materials to achieve similar results.

5.3. Recommendations for Future Research

In the current study, it was shown that tool life can be significantly increased for turning operations by designing PVD coatings to have a certain combination of micro-mechanical and tribological properties that addresses the main tool wear mechanism. Two PVD coatings were developed that address the adhesive wear mechanism and crater wear formation during Ti6Al4V turning. Similar coatings and coating development strategies can therefore be implemented for other machining applications such as drilling, milling, or tapping especially where the abovementioned wear mechanisms occur.

Other monolayer or multilayer coatings with different alloying elements that can generate tribo-films must be experimented on in an attempt to further improve tool life. Since it was found that TiB_2 and CrN coatings form beneficial B_2O_3 and Cr_2O_3 tribo-films, it may be worthwhile to investigate a combination of these two coatings (e.g., a monolayer CrB_2 or a multilayer TiB_2/CrN coating). A very elementary investigation done with a monolayer CrB_2 and a multilayer TiB_2/CrN coating revealed that both coatings have potential, but each have their own challenges that need to be addressed. Preliminary deposition was done using arc and sputtering CrB_2 targets. However, deposition was not successful because both targets cracked during deposition. This may be due to the thermal shock and the target being brittle which is a common issue for boride targets. To solve this issue, extra measures need to be taken such as better target design with proper back plating

for more effective heat transfer away from the target or use an instrument with better cooling system or lower heat generation during deposition. Furthermore, deposition parameters can be adjusted to possibly avoid cracking. For the multilayer TiB_2/CrN coating, coating thicknesses of each layer must be optimized to obtain benefits from both layers. Compatibility and good adhesion between the two layers of the coating must also be ensured.

As this research has focused on coating development, the effect of the developed coating on the surface integrity of the machined surface was not fully investigated. Surface integrity studies should therefore be performed to better understand the effect of the developed coatings on the workpiece.

During cutting, mechanical and thermal stress distribution on the cutting tool significantly affects coating performance. In addition, temperature distribution on the tool also affects tribo-film formation. It is very difficult or nearly impossible to accurately measure the temperature and stress distribution on the tool during machining without finite element modelling. Therefore, to better understand and correlate the effect of temperature and stress distribution on the performance of the coated tools, a comprehensive finite element model needs to be developed.

Cutting edge preparation can significantly affect a tool's microgeometry and substrate properties. With edge preparation, it is possible to reduce the manufacturing defects of tools and improve coating adhesion and coating quality. Edge preparation can also be done after coating deposition, which can further enhance the coating quality and performance. Hence,

an in-depth study on the effect of different edge preparation techniques on the coating quality and tool performance needs to be done.

Appendix A: Tool Wear Mechanism During Rough and Finish Turning of Ti6Al4V Alloy

A.1. Preface

PVD coatings for the machining of Ti6Al4V alloy should be selected and designed with consideration for the unique tribological phenomena that occur at the tool-chip-workpiece interface and the dominant tool wear mechanism that dictates tool failure. During Ti6Al4V machining, significant BUE and crater wear formation is observed. However, one form of wear is dominant over the other depending on cutting conditions such as rough turning and finish turning. Since cutting tool performance is strongly dependent on machining conditions, it is of utmost importance to study in detail the underlying tool wear mechanisms under various machining conditions during Ti6Al4V turning. It has been previously shown that TiB_2 coatings provide strong self-lubricating properties at the cutting zone during the rough turning of Ti6Al4V alloy [1]. Hence, a preliminary study complementing the current research work was conducted to study the effect of different machining conditions on the tool wear mechanisms and wear performance of uncoated and TiB_2 coated cemented carbide tools while turning Ti6Al4V alloy. Part of the study was published in the following journal article: Paiva, J. M., Shalaby, M. A. M., Chowdhury, M., Shuster, L., Chertovskih, S., Covelli, D., Junior, E.L., Stolf, P., Elfizy, A., Bork, C. A. S., Fox-Rabinovich, G. S., & Veldhuis, S. C. (2017). Tribological and wear performance of carbide tools with TiB_2 PVD coating under varying machining conditions of TiAl6V4

aerospace alloy. Coatings, Volume 7, Issue 11, pp. 187. The goal of the paper was to relate different machining conditions during Ti6Al4V turning to the tribological and wear performance of cemented carbide tools and to the underlying dominant tool wear mechanisms. Rough turning at a low cutting speed of 45 m/min and finish turning at a high cutting speed of 150 m/min were studied in detail. It was found that BUE formation dictates tool performance during rough turning whereas crater wear formation was the dominant tool wear mechanism during finish turning. The study also showed that a TiB_2 coating is very efficient under rough turning conditions but practically useless at the higher cutting speeds of 150 m/min under finishing operations. This has been discussed in detail in Part A of this appendix.

Since, during the finish turning of titanium, crater wear dominates flank wear, it is necessary to investigate self-adaptive coatings that can furnish thermal barrier characteristics through tribo-film formation. With that in mind, a CrN coating was developed at the MMRI with the expectation that Cr-O tribo-films will form that can give thermal barrier properties at a high cutting temperature. Generally, a CrN coating is a good candidate for machining non-ferrous alloys because they have a very low affinity for nonferrous workpieces [2]. CrN is also known to have high chemical stability, resulting in good corrosion and oxidation resistance [3], and good tribological properties (low coefficient of friction) and toughness [4-7]. These properties are crucial for the machining of sticky titanium alloys. Cr-O tribo-films also have lubricating characteristics, making CrN a good candidate for machining applications with intensive BUE formation, such as the rough turning of Ti6Al4V alloy. The performance of the CrN coated tool during the rough

and finish turning of Ti6Al4V alloy was investigated and has been discussed in detail in Chapter 2 and Chapter 3, respectively. It was found that a CrN coated tool significantly improves tool performance compared to an uncoated tool and industry recommended AlTiN coated tool for both the rough and finish turning of Ti6Al4V alloy.

The performance of the CrN coated tool was also compared against a TiB_2 coated tool. It was found that a TiB_2 coated tool is superior in performance to a CrN coated tool during rough turning operations. However, for finish turning operations, a CrN coated tool is superior in performance to a TiB_2 coated tool. These findings are discussed in detail in Part B of this appendix.

A.2. Part A: Wear performance of TiB_2 coated carbide tools under varying machining conditions for TiAl6V4 alloy

This section highlights the preliminary investigation that was conducted to understand the underlying tool wear mechanism during the rough and finish turning of Ti6Al4V alloy. A detailed account of the FEM of the temperature profile of the tool-chip-workpiece interface, experimental studies conducted with uncoated and TiB_2 coated tools, and the effectiveness of tribo-films formed under varying machining conditions are presented.

A.2.1 Finite Element Process Modeling

The finite element process modeling (FEM) is essential in evaluating cutting conditions, such as temperature profiles within the cutting zone. This is a critical step in understanding tool wear mechanisms. During Finite Element Modeling (FEM) for metal cutting, difficulty arises from severe plastic deformation of the metal, which results in extreme tribological

conditions at the tool-workpiece interfaces [8]. The cutting temperature profile is critical for understanding and controlling the machining process [9].

The modeling was performed with Third Wave Systems AdvantEdge™ simulation software, which integrates advanced finite element models appropriate for machining operations. A continuous method for the formation of continuous chips was developed through cutting length of 3 mm. The workpiece material was Ti6Al4V, and its mechanical properties were obtained using the FEM program database. The input parameters entered into the code as well as the contact conditions are given in Table A.1.

Table A.1. *Workpiece, tool and coolant material properties and cutting contact conditions [10-12].*

Materials Properties and Contact conditions					
Materials	**Property**		**workpiece**	**Tool**	**Coolant**
	Density, ρ *(kg/m³)*		4430	15700	980
	Elastic modulus, *E (GPa)*		110	705	-
	Poisson's ratio, υ		0.33	0.23	-
	Specific heat, C_ρ *(J/kg°C)*		670	178	-
	Thermal conductivity, λ *(W/m°C)*		6.6	24.0	-
	Expansion Coefficient, α_d *W(µm/m/°C)*		9	5	-
	$T_{melt,}$ (°C)		1630	-	-
	$T_{room,}$ (°C)			20	
Contact	Heat transfer Coeff., *h (kW/m²K)*			10	
	Heat partition Coeff., α			0.5	
	Friction coefficient, μ			0.2	
	Coolant mode			Emulsion - Flood	
	Coolant Concentration			6%	
	Jet Coolant Radius *(mm)*			5	
	Friction energy transferred into heat, *E*			100%	
Johnson-Cook Constitutive model parameters for Ti-6Al-4V alloy	**A (MPa)**	**B (MPa)**	**C**	**n**	**m**
	782	498	0.028	0.28	1

The Johnson-Cook phenomenological constitutive model was used for FEM modeling of cutting temperature calculation modeling (2D model) [10]. This model describes the workpiece material behaviour, considering the separated effects of strain hardening and thermal softening (eq 1).

$$\bar{\sigma} = [A + B(\varepsilon)^n] \cdot \left[1 + C \ln\left(\frac{\dot{\varepsilon}}{\dot{\varepsilon}_0}\right)\right] \cdot \left[1 - \left(\frac{T - Tr}{Tm - Tr}^m\right)\right] \quad (1)$$

Where:

A - yield stress of the material under reference deformation conditions (MPa)

B - strain hardening constant (MPa)

n - strain hardening coefficient

C - strain rate strengthening coefficient

m - thermal softening coefficient

T - deformation temperature

Tr - room temperature

Tm - melting temperature of the material

ε - reference strain rate (1/s)

ε – equivalent plastic strain normalized with a reference strain rate

ε̇₀ - plastic equivalent strain

The cutting edge was defined ideally rigid, according with CNGG 432 Grade K313 (Kennametal). The cutting parameters and tool code geometry used in the simulation are listed in Table A.2.

Table A.2. *Cutting data for the experiments performed.*

Machining operation	Cutting tool substrates	Workpiece material	Hardness (HRC)	Speed (m/min)	Feed (mm/rev)	Depth of cut (mm)
Rough turning, Wet machining	Kennametal CNMG432 Grade K 313 turning inserts	Ti6Al4V alloy	37-38	45	0.15	2
Finish turning, Wet machining	Kennametal CNGG432FS Grade K 313 turning inserts			150	0.1225	0.25

The 2D models of temperature at the cutting zone are presented in Figure A.1. FEM modeling shows the cutting edge temperature distribution for the two different cutting conditions tested. It can be seen that temperatures on the both rake and flank surfaces for the area close to the cutting edge are around 650 - 700°C at rough turning conditions (Figure A.1, a). However, the maximum cutting temperature rises up to 950°C at a speed of 150 m/min (Figure A.1, b).

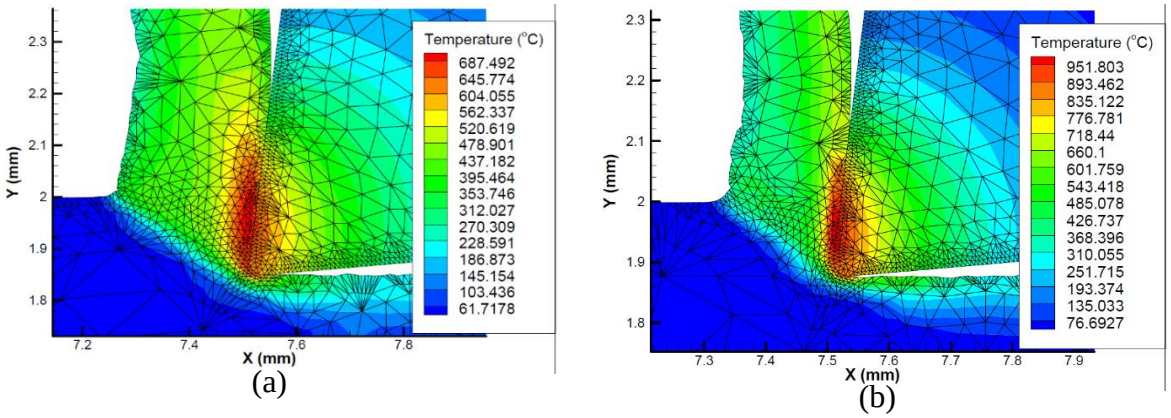

Figure A.1. *FEM temperature profile at: a) 45 m/min and b) 150 m/min.*

A.2.2 Experimental Procedure

The TiB_2 coating was deposited with DC magnetron sputtering from a stoichiometric TiB_2 target. The parameters of deposition are presented elsewhere [1]. The properties of the TiB_2 coating are shown in Table 3. The coating was deposited on cemented carbide (WC/6%Co) Kennametal turning inserts – grade K313 (CNMG432 and CNGG432FS), with the following geometry characteristics: back rake angle, $\lambda_0 = -5$; clearance angle, $\alpha_0 = 5°$; cutting edge angle, $\beta_0 = 90°$; rake angle, $y_0 = -5°$; side cutting edge angle, $\chi_r = 95°$; and nose radius, $R_\varepsilon = 0.8$ mm.

Table A.3. *Properties of the TiB_2 coating [1].*

Coating	Architecture	Properties		
		Thickness (μm)	**Hardness (GPa)**	**Residual stresses (GPa)**
TiB_2	Monolayer	1.79	15.5±4.3	-0.633 ± 0.0838

The machining experiments of Ti6Al4V aerospace alloy were performed in a NAKAMURA SC450 turning machining center. The turning tests were conducted for rough and finishing operations under wet cutting conditions. The cutting fluid was applied at a flow rate of 14 L/min via a nozzle positioned directly above the cutting tool and directed toward the tool lip. The cutting fluid was semi-synthetic XTREME CUT 290, typically recommended for machining aerospace alloys such as Ti6Al4V. The cutting conditions are presented in Table A.2. These cutting parameters were selected according to standards widely used in industry for the machining of aerospace alloys in roughing and finishing operations. The tool life criterion was set to a flank wear of 0.3 mm. During the cutting test, the tool flank wear was measured using an optical microscope (Mitutoyo™). Cutting tests

were repeated three times for each cutting test condition. Flank wear was measured three times for each insert. The scatter of the flank wear values was found to be approximately 5%.

The coefficient of friction vs. temperature was determined with the aid of a specially designed apparatus described in [13]. This apparatus was designed to mimic the adhesive interaction of the tool/workpiece interface that occurs during machining conditions. A rotating sample of the coated substrate was placed between two polished specimens made of work-piece material (Ti6Al4V alloy). To simulate tool/friction conditions, the specimens were heated by resistive heating to temperatures ranging from 25 to 1000 °C. A force of 2400 N was applied to achieve plastic strain in the contact zone. The coefficient of friction value was calculated, as a ratio between the shear strength of the adhesive bonds and the normal contact stress developed at the interface. Three trials were performed for each coating. The estimated magnitude of error in calculating the coefficient of friction was 5%.

Progressive wear studies have been performed for uncoated and coated cutting inserts under both roughing and finishing conditions. After each 600 m length of cut, the inserts were studied by Alicona Infinite Focus 3D optical microscope and scanning electron microscope (SEM). The 3D analysis of worn tools was performed on Alicona by plotting the profile of rake and flank surface wear of cutting inserts. Based on the combination of small depth and vertical scanning, the 3D optical system with Focus-Variated was used to generate a three-dimensional topography with real color information. In order to characterize the topography of cutting tools, a 3D-motif analysis was adopted to generate the regions of cutting tools out of the measured data. According to ISO 25178-2 [14], a 3D-

motif is defined as a valley and/or peak (hill) which includes the critical points (peaks, valleys and saddle points) and the critical lines (ridge lines and course lines). This analysis has been performed through of comparison between the worn and unworn cutting edge with a magnification of 50x. The Volume and square wear modes were measured and the total amount of BUE and its volume outlined with different colors. Besides the surface profiles and true color information, the whole areas of the cutting tool can be measured in 3D data. These values have been reported in the Origin analytical software system to stablish statistical data. The measurement was repeated three times for each insert. The average error was around 5%. In addition, the high-resolution scanning electron microscope (SEM) (Vega 3-TESCAN) was used for the detailed inspection of the worn cutting tools.

The formation of tribo-oxides was evaluated through of X-ray Photoelectron spectroscopic (XPS) analysis on both flank and rake surface for TiB_2 coated inserts. A Physical Electronics (PHI) Quantera II equipped with a hemispherical energy analyzer and an Al anode source for X-ray generation and a quartz crystal mono-chromator for focusing the generated X-rays was used to collect XPS data. A monochromatic Al K-α X-ray (1486.7 eV) source was operated at 50 W–15 kV. The system base pressure was as low as 1.0×10^{-9} Torr with an operating pressure that did not exceed 2.0×10^{-8} Torr. Before any spectra were collected, the samples were sputter-cleaned for 4 min using a 4-kVAr+ beam. A 200 μm beam was used for all data collected on the samples. A pass energy of 280 eV was used to obtain all survey spectra, while a pass energy of 55 eV was used to collect all high-resolution data. All spectra were obtained at a 45° take off angle. A dual beam charge compensation system ensured neutralization of all samples. All high-resolution data was

calibrated by setting the C1s C-C peak at 284.8 eV. All data analysis was performed using PHI Multipak version 9.4.0.7 software.

A.2.3 Results and discussion

Properties of the TiB_2 coating studied are presented in Table 3. We can see in the data that the TiB_2 coating has low residual stresses and low hardness. The coating is thus capable of sustaining harsh machining environments during the cutting of Ti6Al4V, especially at low speeds (lower cutting temperatures), under conditions of intensive buildup edge formation. However, its efficiency varies under different machining conditions (higher cutting temperatures).

A.2.3.1 Rough turning operation at low speed

Flank wear data is presented in Figure A. 2. The data indicate that TiB_2 coated carbide insert shows significant improvement in the wear rate, as soon as the uncoated insert demonstrates intensive wear rate above 300 microns. SEM images show strong buildup edge formation on the rake surface of the uncoated inset. In contrast, there is very low intensity of buildup edge formation on the surface of the TiB_2 coated insert.

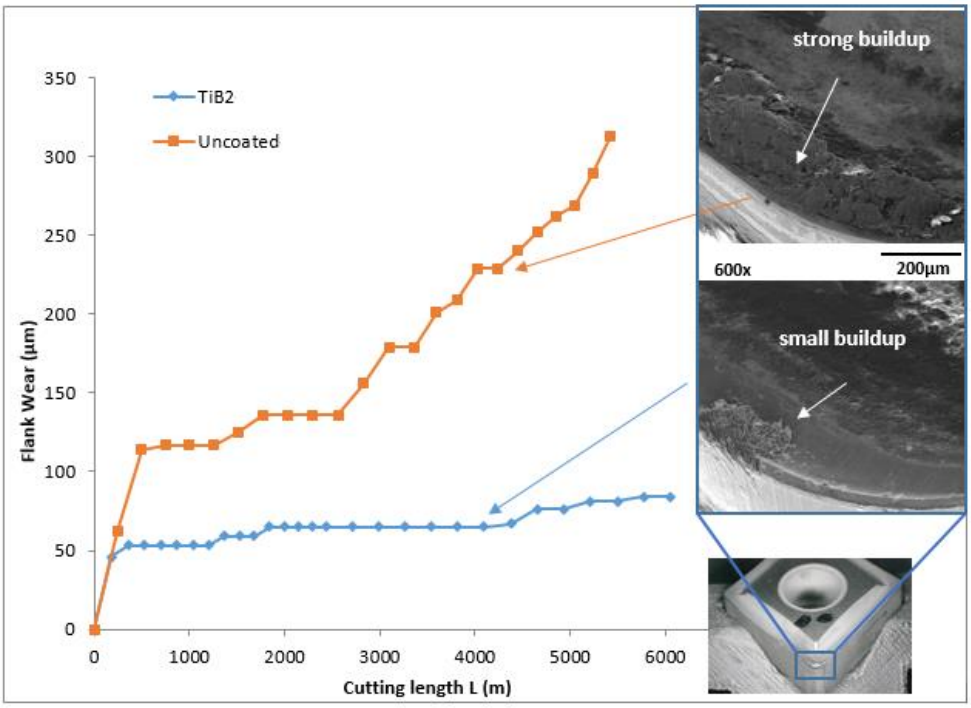

Figure A.2. *Flank wear data vs. length of cut for the uncoated and TiB_2 coating carbide turning inserts with SEM images of the worn surface (after length of cut of 4000 m).*

Figure A.3 demonstrates HR XPS data on the worn rake and flank surfaces of the cutting tool. It shows that complex phenomena are taking place during rough turning, which include:

- Formation of thermal barrier TiC interlayer at the chip/tool interface [13, 15] (Figure A.3a).
- Formation of a substantial amount (around 24.9 at. %) of B_2O_3 lubricating tribo-films which reduce intensity of buildup edge formation through surface lubrication on the rake surface (Figure A.3b).

• Formation of a smaller amount (only 6.5 %) of B_2O_3 lubricating tribo-films due to lower temperatures on the flank surface in correspondence to temperature profile presented in Figure A.1a.

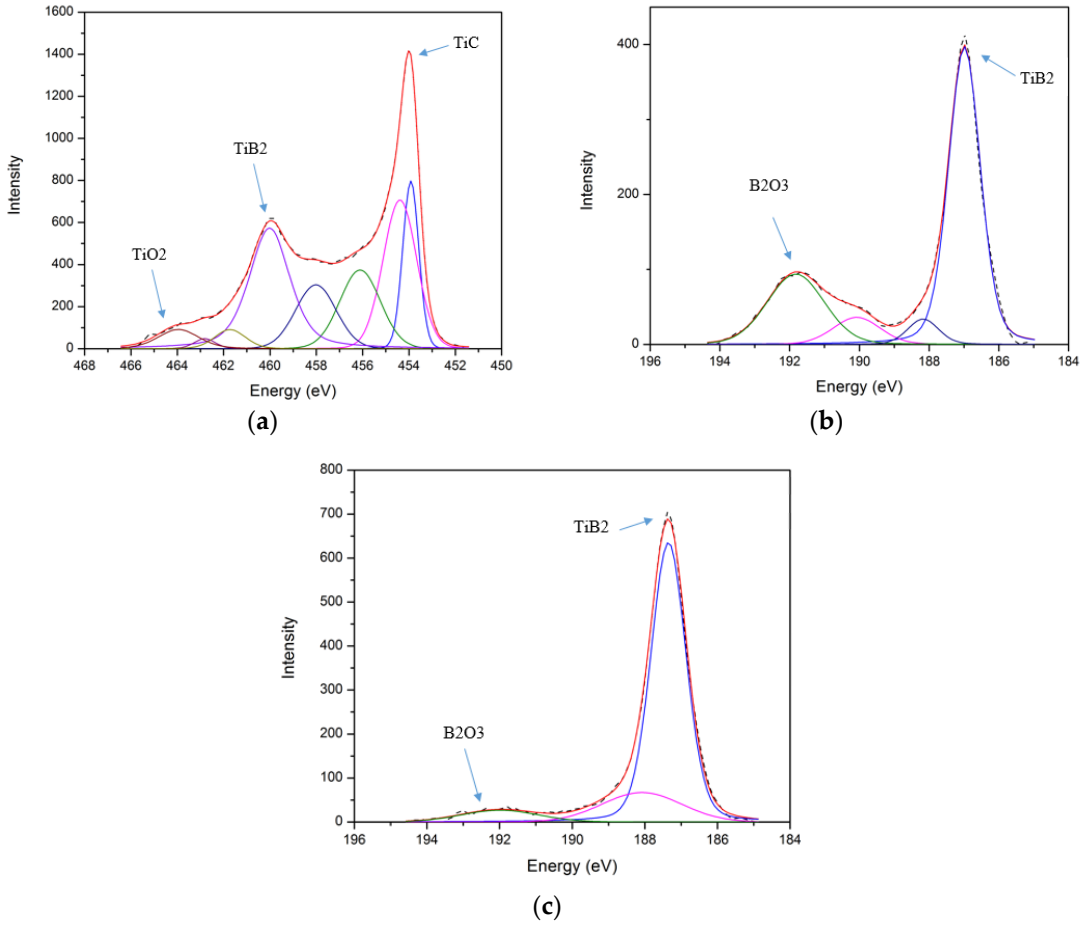

Figure A.3. *HR XPS data on the worn rake (a,b) and flank surfaces (c) after rough turning of Ti6Al4V alloy: (a) Ti2p;(b,c) B1s spectra.*

Figure A.4 exhibits COF vs. temperature data for the uncoated and TiB_2-coated inserts. The data presented indicates the formation of B_2O_3 tribo-films that melt at 450 °C [16] and serve as a liquid lubricant [1]. The temperature during rough turning is relatively low

(around 650–700 °C, Figure 1a) and these tribo-films are still fairly efficient [17] (see SEM images in Figure A.2).

At higher temperatures, (machining at higher speeds) they do not perform their lubricating role with similar efficiency (see Section A.2.3.2). This behaviour was observed and reported by Senda et al. [18] and Munro [19].

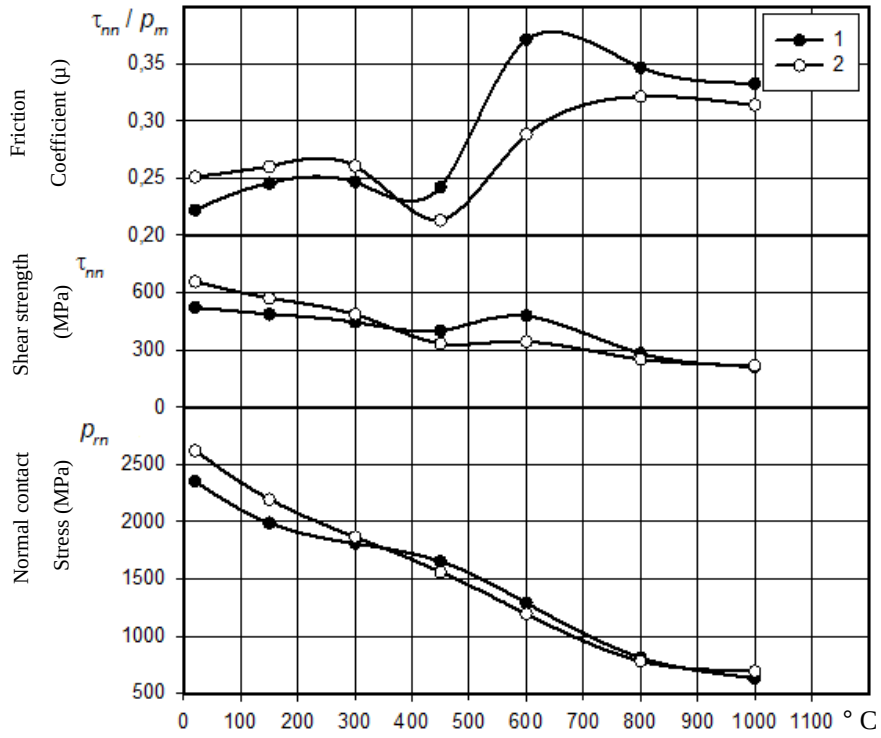

Figure A.4. *Coefficient of friction vs. temperature data for the uncoated and TiB_2 coated inserts: (1) uncoated; (2) TiB_2 coated.*

A.2.3.2 Finish turning operation.

Flank wear rate data are presented in Figure A.5. Tool life is very similar for the coated and uncoated inserts. According to FEM showed in Figure A.1b the temperature on the rake surface is around 900–950 °C.

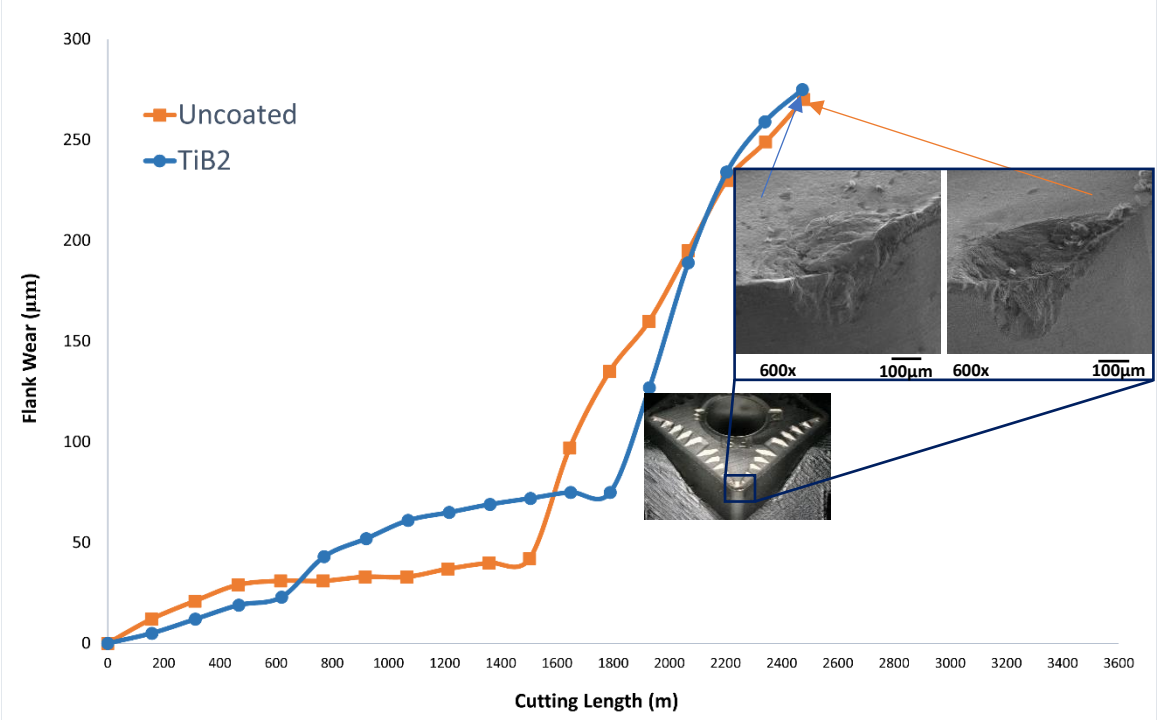

Figure A.5. *Flank wear data vs. length of cut for the uncoated and TiB_2 coated carbide turning inserts under finishing operations at 150 m/min.*

3D progressive wear volumes evaluation was performed by Alicona microscope. 3D images of worn inserts after 600 (Figure A.6 a,e), 1200 (Figure A.6 b,f), 1800 (Figure A.6 c,g), 2400 m (Figure A.6 d,h) length of cut are presented in Figure A.6. In this case, the red color represents a material adherent at cutting tool (BUE) while blue color shows damage generated at the cutting tool (crater wear).

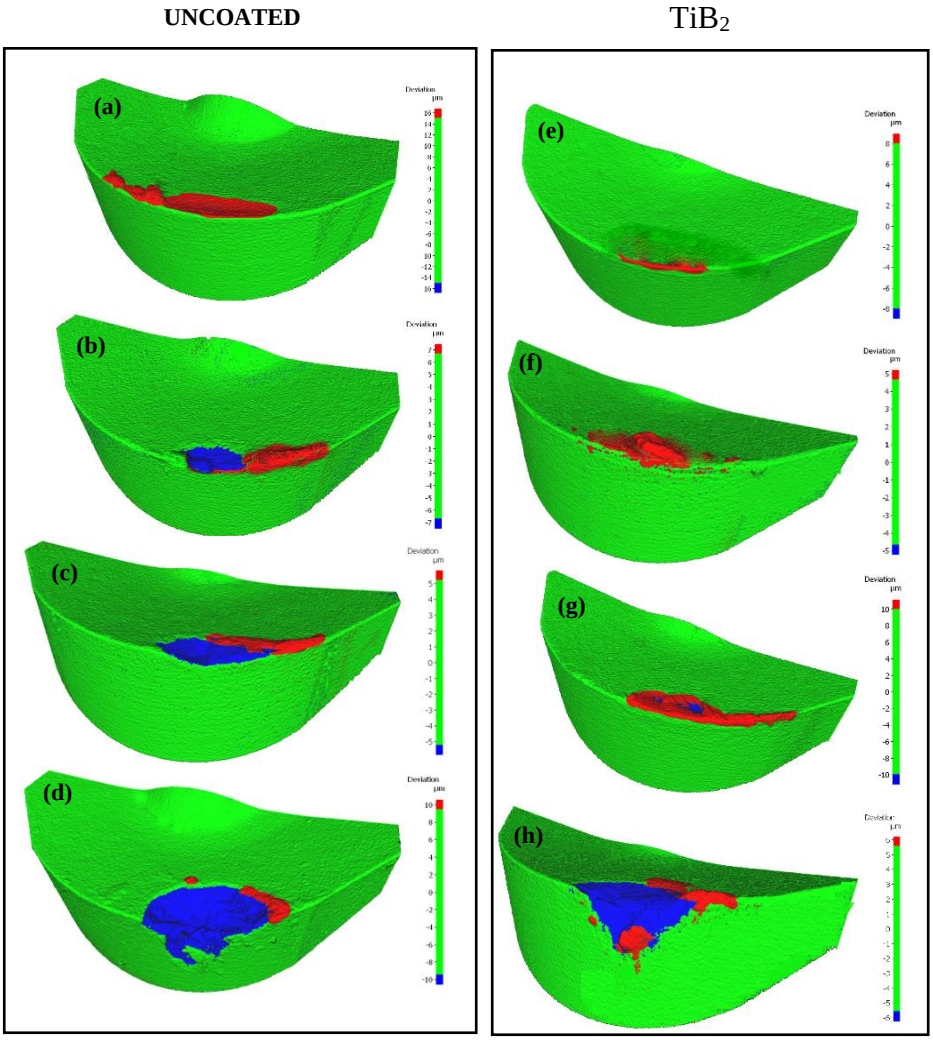

Figure A.6. *3D progressive wear volume data on uncoated (a–d) and TiB_2-coated (e–h) inserts, finish turning at 150 m/min. (a,e) 600 m length of cut; (b,f) 1200 m length of cut; (c,g) 1800 m length of cut; (d,h) 2400 m length of cut.*

Numerical data on the volumetric 3D wear measurement for uncoated and TiB_2-coated inserts is presented in Figure A.7.

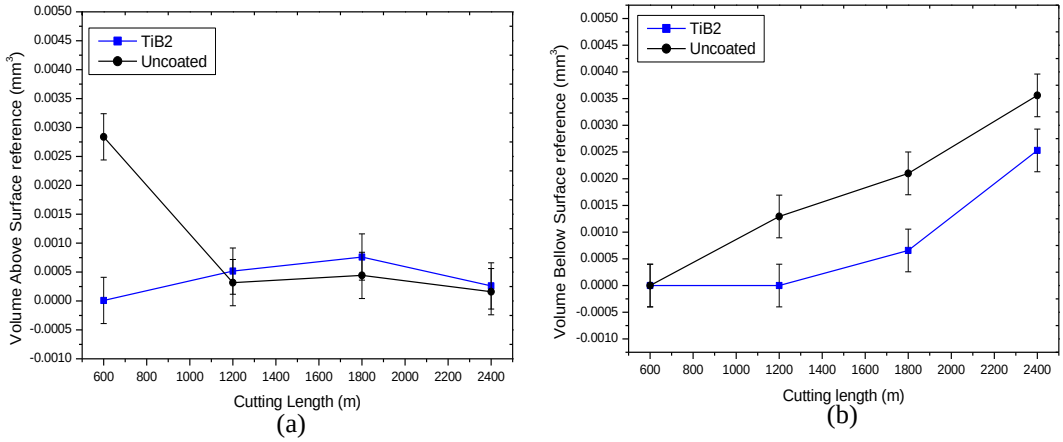

Figure A.7. *Numerical data on the volumetric 3D wear measurement for uncoated and TiB_2 coated inserts, finish turning at 150 m/min: a) rake surface square covered by buildup; b) volumetric 3D wear data.*

During the initial stage of wear, intensive adhesion of the workpiece material to the rake surface face can be observed (Figure A.6 a-b and e-f) for both uncoated and TiB_2 coated tools. Formation of the unstable buildup structure and its further tearing leads to the chipping on the cutting edge (see Figure A.6 c-d and g-h, as well as Figure A.6 b). Moreover, chipping of the cutting edge leads to an increase in the intensity of the buildup edge formation. This is because the buildup edge tearing also removes a part of the cutting edge, which correspondingly may intensify cutting edge chipping.

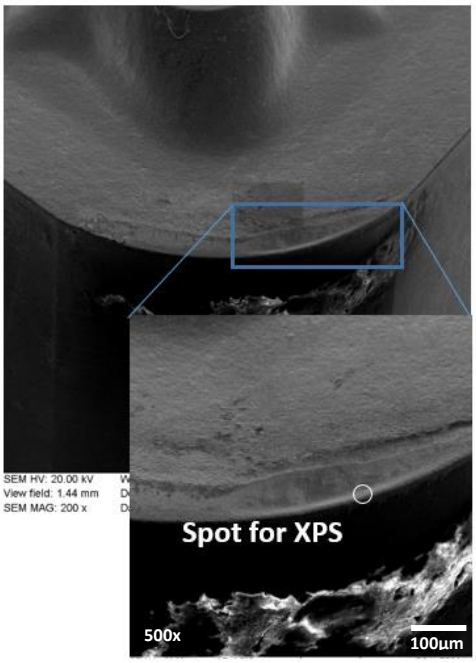

Figure A.8. *SEM images of the Coated tool worn surface at 150 m/min.*

XPS analysis was performed at the very cutting edge (see the spots marked at figure A.8). Figure A.9 presents XPS data under different speeds in the area of the cutting edge for both rake and flank worn surfaces. At the higher speeds of 150 m/min the mechanism of wear is changing: buildup is quickly worn out (Figure A.8) and therefore the TiC thermal barrier layer does not form [15] (Figure A.9 b). Higher temperatures under operation (above 900-950 °C, Figure A.1 b) [20] lead to intensive cratering (Figures A.1 b; A.6 b). Therefore, two simultaneously occurring phenomena affect flank wear rate (Figure A.5): a) the buildup edge tearing off and b) the crater wear. The flank wear intensity of TiB_2 coated tool is similar to the uncoated one. Formation of a large amount of lubricating B_2O_3 and WO_x tribo-films (Figure A.9 c) does not result in high tool life. This is probably due to a higher coefficient of friction of both the TiB_2 coating and uncoated tool at elevated temperatures

(Figure A.4) and dominating crater wear mechanism combined with intensive chipping. On the flank surface we can only see tribo-oxidation of both wearing-off coating layer and the substrate (Figure A.9 d).

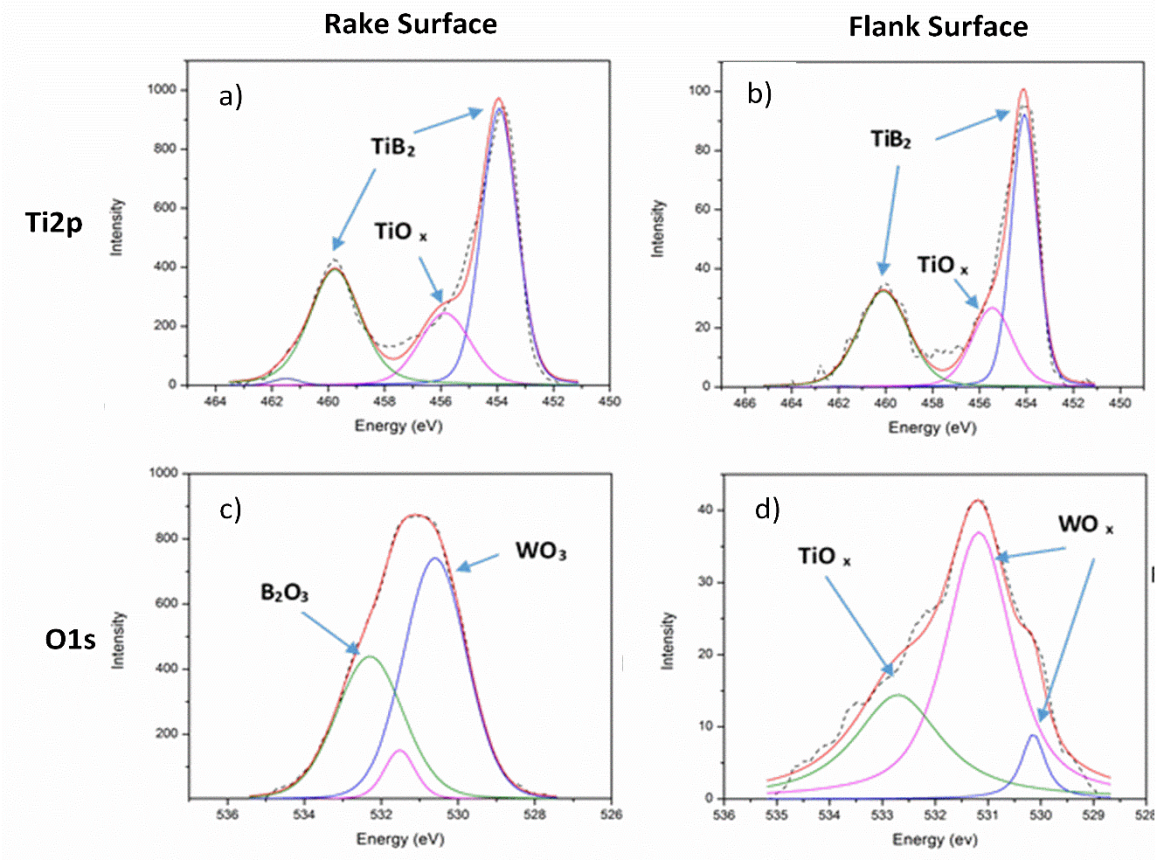

Figure A.9. *HR XPS data on the worn surfaces after finish turning of TiAl6V4 alloy (cutting edge area) at 150 m/min: (a,b) Ti2p spectra at rake and flank surface respectively, and (c,d) O1s spectra at rake and flank surface respectively.*

In addition to COF vs. temperature measurements, the tribological performance of the cutting tools at elevated temperatures was evaluated through chip characteristics. This was accomplished via the characterization of chip undersurface morphology using Alicona microscope with simultaneous evaluation of the surface roughness. The studies performed

show that there is no substantial difference in chip undersurface morphology (Figure A.10): application of both uncoated and TiB_2 coated tool results in visible stick-slip phenomenon [1], which is typical for the machining of Ti [20].

This means TiB_2 does not improve tribological conditions under higher speeds of 150 m/min and indirectly confirms that B_2O_3 tribo-films do not affect tribological performance of the tool.

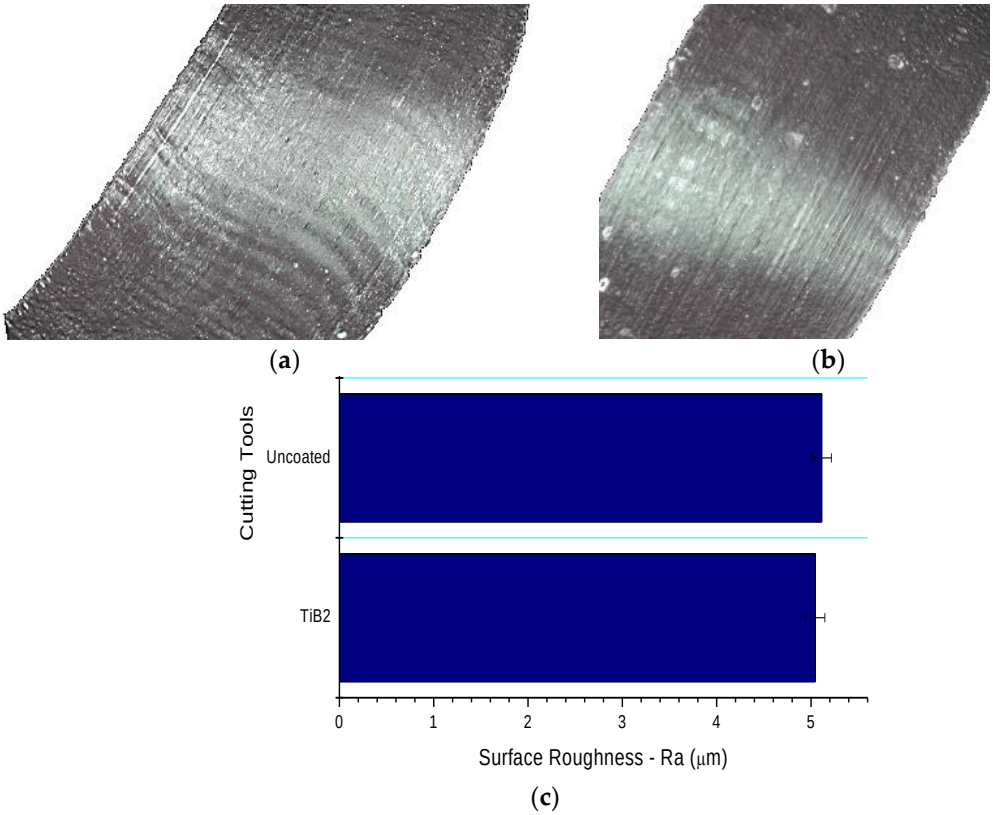

Figure A.10. *Chip undersurface morphology evaluated by Alicona 3D microscope: a) uncoated; b) TiB_2 coated and c) surface roughness values, (μm).*

A.2.4 Conclusions

The studies performed show that during machining of TiAl6V4 aerospace alloy the efficiency of TiB_2 coating application for carbide cutting tools strongly depends on the cutting conditions. FEM data on temperature profile obtained under real wet machining conditions is in strong agreement with tribological performance assessed through COF vs. temperature data as well as chip characteristic data. This allows us to evaluate the efficiency of the tribo-film formation on the friction surface, in particular TiC thermal barrier films as well as B_2O_3 lubricating films at different temperatures.

The comprehensive 3D wear evaluations combined with XPS and SEM studies of the worn surfaces show that the TiB_2 coating is very efficient under rough turning conditions (at low cutting speeds of 45 m/min and high depth of cut of 2 mm) when intensive buildup edge formation is addressed. Based on our analysis, it is proposed that this is due to the formation of a large amount of B_2O_3 tribo-oxide, which serves as a liquid lubricant. On the contrary, the TiB_2 coating shows practically no efficiency at the higher cutting speeds of 150 m/min under finishing machining operations (DOC 0.125 mm). This indicates that there is no universal solution for various machining conditions when different wear mechanisms are dominating. Therefore, a phenomena-based approach for coating design should be taken into consideration.

A.3. Part B: Comparison of wear performance of TiB_2 and CrN coated carbide tools

This section compares the performance of the self-adaptive TiB_2 and CrN coated tools investigated in the present research against uncoated and industry recommended AlTiN coated tools for both the rough and finish turning of Ti6Al4V alloy. A detailed account of tool performance, tribo-film formations, and their role in tool improvement are presented.

A.3.1 Tool wear performance

To address BUE formation during the rough turning of titanium, self-lubricating coatings that can form lubricious tribo-films are required to prevent titanium from sticking onto the tool. For finish turning, where crater wear formation caused by high cutting temperature generation dictates tool wear, a coating that can provide thermal barrier characteristics through tribo-film formation is necessary. Hence, the TiB_2 and CrN coatings were chosen based on the expected lubricious and thermal barrier tribo-film formation. Figure A.11 shows the tool wear performance of uncoated, AlTiN, CrN and TiB_2 coated tools for rough turning (Vc=45m/s, f=0.15mm/rev, DOC-2 mm). As can be seen, the TiB_2 coated tool gave the best tool life performance, followed by the CrN coating for rough turning. Both coatings significantly outperformed the uncoated cemented carbide tool and industrially recommended AlTiN coated tool. Figure A.12 shows the 3D images of the uncoated, CrN, and TiB_2 coated tool taken after every 600 m length of cut. It is evident from the 3D images that both the TiB_2 and CrN coatings significantly reduce BUE formation, thereby increasing tool life during rough turning.

Figure A.13 shows the tool wear performance of uncoated, AlTiN, CrN and TiB_2 coated tools for finish turning (Vc=150m/s, f=0.1225mm/rev, DOC-0.25 mm). As can be seen, the CrN coated tool performed the best, whereas the TiB_2 one performed almost the same as the uncoated and AlTiN coated one. It is interesting to note that all the tools show a very stable form of wear until a certain point after which the cutting edge rapidly starts to fail. Figure A.14 shows the 3D images of the uncoated, CrN, and TiB_2 coated tool taken after every 600 m length of cut. During the initial wear stage, significant BUE formation is seen. However, the BUE is unstable, which leads to chipping of the cutting edge. Crater wear formation is also observed and keeps propagating while cutting. It is evident from the 3D images that rapid tool failure occurs for both uncoated and TiB_2 coated tools due to the crater wear expanding to the flank edge of the cutting tool. This finding complements and explains the results of the tool wear studies for finishing (Figure A.11).

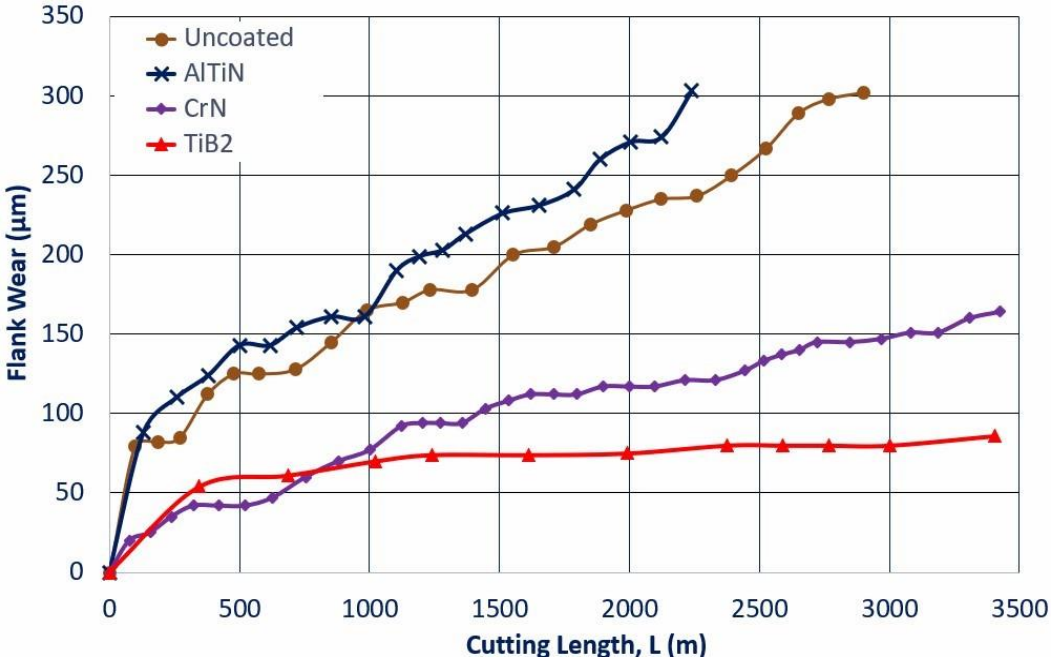

Figure A.11. *Flank wear vs. cutting length data during the wet rough turning of Ti6Al4V alloy.*

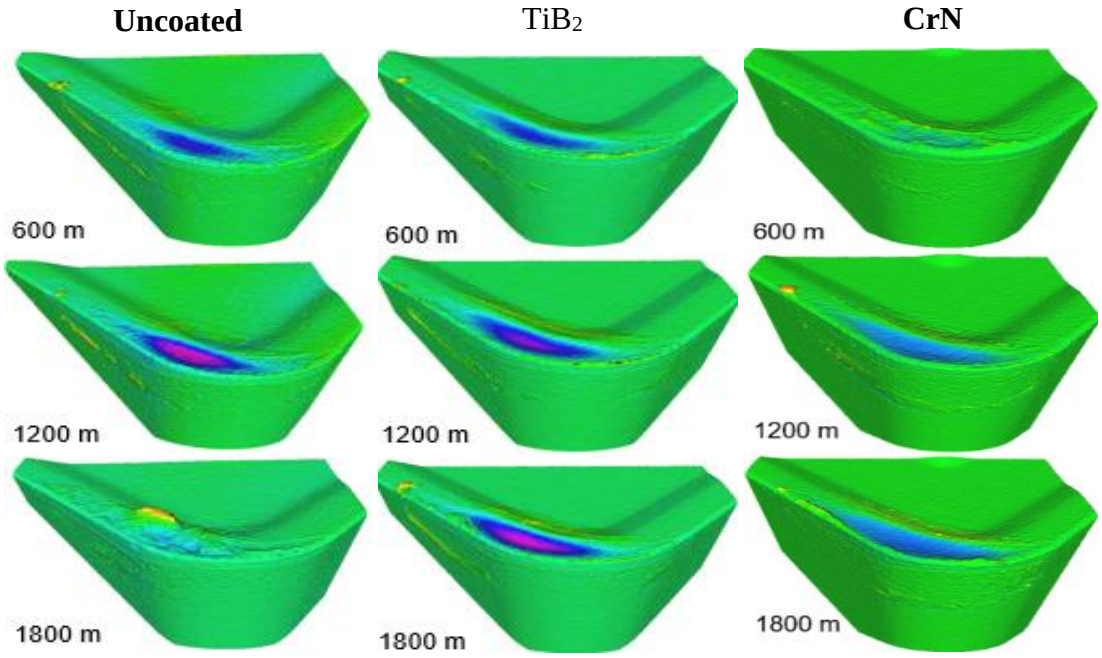

Figure A.12. *3D progressive wear difference measurement of the uncoated and coated tools, highlighting evolution of built-up layer and crater wear during the rough turning of Ti6Al4V alloy.*

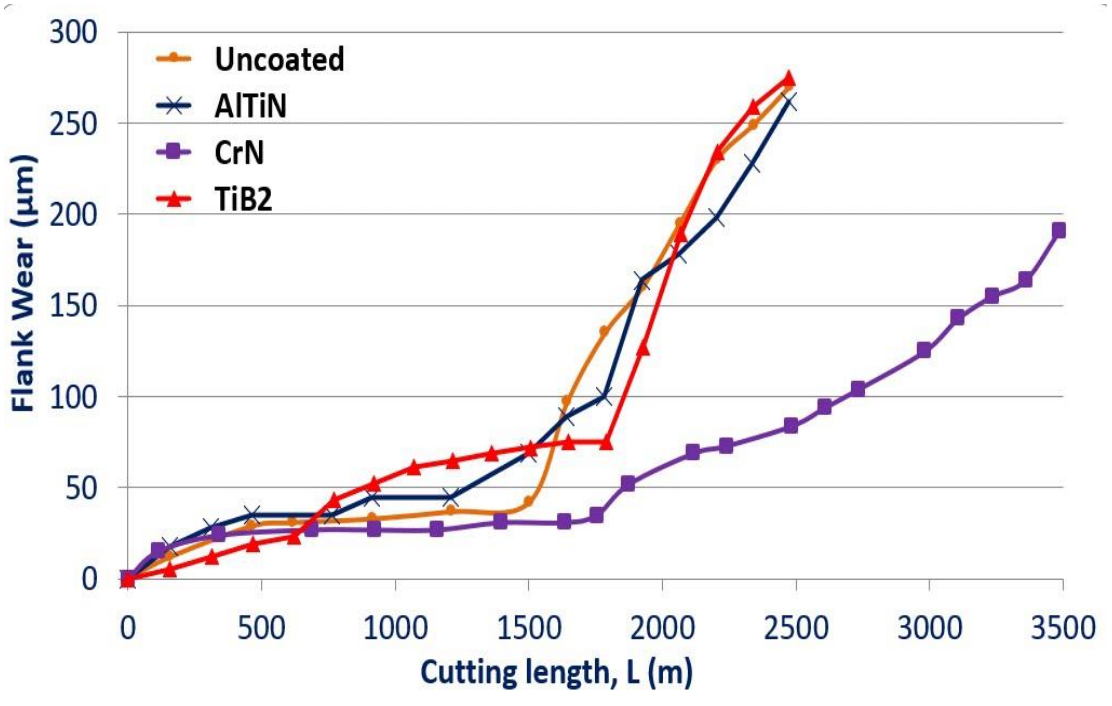

Figure A.13. *Flank wear vs. cutting length data during the wet finish turning of Ti6Al4V alloy.*

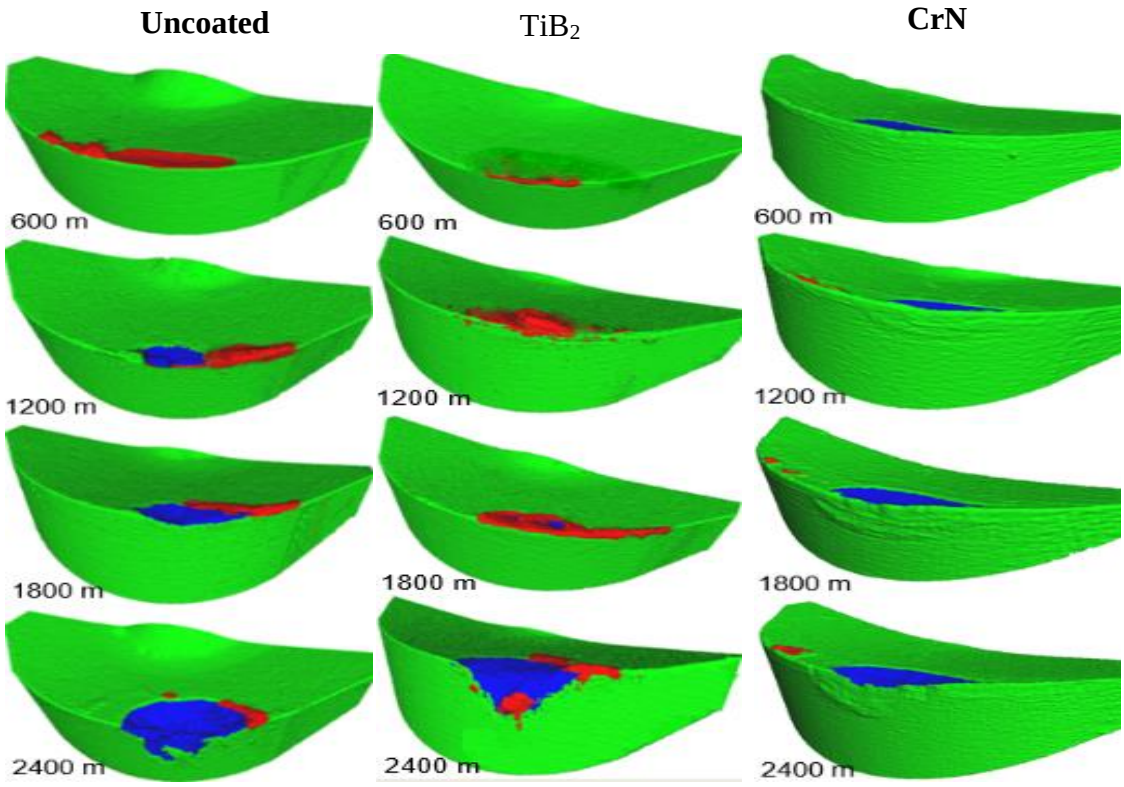

Figure A.14. *3D progressive wear difference measurement of the uncoated and coated tools, highlighting evolution of built-up layer and crater wear during the finish turning of Ti6Al4V alloy.*

A.3.2 Tribo-film formation and coating characterization

An XPS study was conducted on the rake surface of the tool to confirm tribo-film formation on both the TiB_2 and CrN coated tools (see Figure A.3, A.9, 3.10, and 4.16). It was found that a TiB_2 coating tribo-oxidizes to form a liquid lubricious B_2O_3 phase that reduces friction at the tool-chip and tool-workpiece interfaces, decreasing BUE formation and tool wear significantly for rough turning. However, the B_2O_3 tribo-film seems to be ineffective during finish turning, where crater wear is predominant. A CrN coating, on the other hand, tribo-oxidizes with the formation of Cr_2O_3 tribo-ceramic films. Cr_2O_3 films

provide thermal barrier properties and lubricating properties at high cutting temperatures, which helps to reduce crater wear intensity and BUE formation. Hence, a CrN coating reduces tool wear for both rough and finish turning, and crater wear intensity and built up edge formation is significantly diminished. However, a CrN coating performs worse than a TiB_2 coating for rough turning. 3D progressive wear volume studies complement these observations. To understand why TiB_2 and CrN coatings behave like this, high temperature tribometer studies were conducted to analyze the tribological characteristics of the coatings at different temperatures.

Figure A.15 shows the coefficient of friction vs. temperature data for the uncoated, TiB_2, and CrN coated tools. At temperatures around 550-700 °C (the typical temperature range for rough turning), the coefficient of friction value for the TiB_2 coating is significantly lower than that of the uncoated tool, indicating that the efficiency of the tribo-films at reducing friction is still fairly good in this temperature range. This is why a significant improvement in tool life is observed for rough turning operations. However, the coefficient of friction value is almost the same at higher temperatures indicating that the tribo-film's efficiency drops as the temperature gets higher, which is typically the case for finish turning. This explains why a TiB_2 coating is not effective during finish turning operations. Conversely, for the rough turning temperature range, the coefficient of friction value for the CrN coating is a little higher. This indicates that the B_2O_3 tribo-film has a higher efficiency and lubricity in this temperature range than the Cr_2O_3 tribo-film. However, at temperatures around 900-1000 °C (the typical temperature range for finish turning), the coefficient of friction value for the CrN coating is significantly lower than that of the

uncoated tool, signifying the high efficiency of the tribo-films at reducing friction in this temperature range. This could be attributed to the Cr_2O_3 tribo-film formation, which has lubricating properties in addition to thermal barrier characteristics.

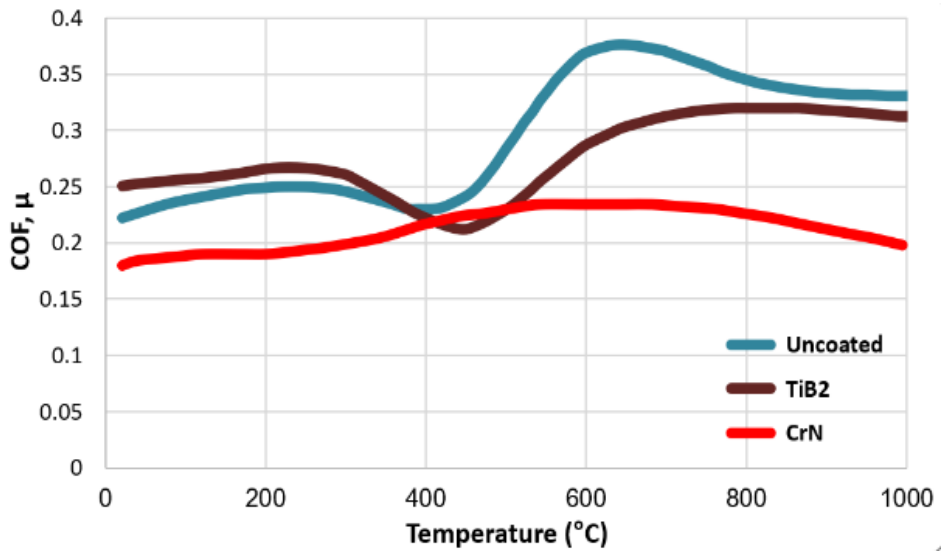

Figure A.15. *Coefficient of friction vs. temperature data for uncoated, TiB_2, and CrN coated tools.*

To analyze the behaviour of the coatings under progressive loads, scratch tests were conducted. Scratch test results showed that the deformation mechanism under a heavily loaded sliding contact was considerably different for AlTiN and the TiB_2 and CrN coatings. The scratch test results are illustrated in Figure A.16-A.18. The coefficient of friction data obtained during the scratch test demonstrates the ability of the coatings to resist scratching within the layers. Both the TiB_2 and CrN coatings had lower coefficients of friction than the uncoated tool, which signifies their superior ability to withstand peeling during friction. The scratch track of both the TiB_2 and CrN coatings showed that failure occurred from plastic flow and deformation was highly localized, with little substrate exposure outside of

the scratch track. In comparison, the AlTiN coating exhibited brittle failure with widespread substrate exposure outside the scratch track.

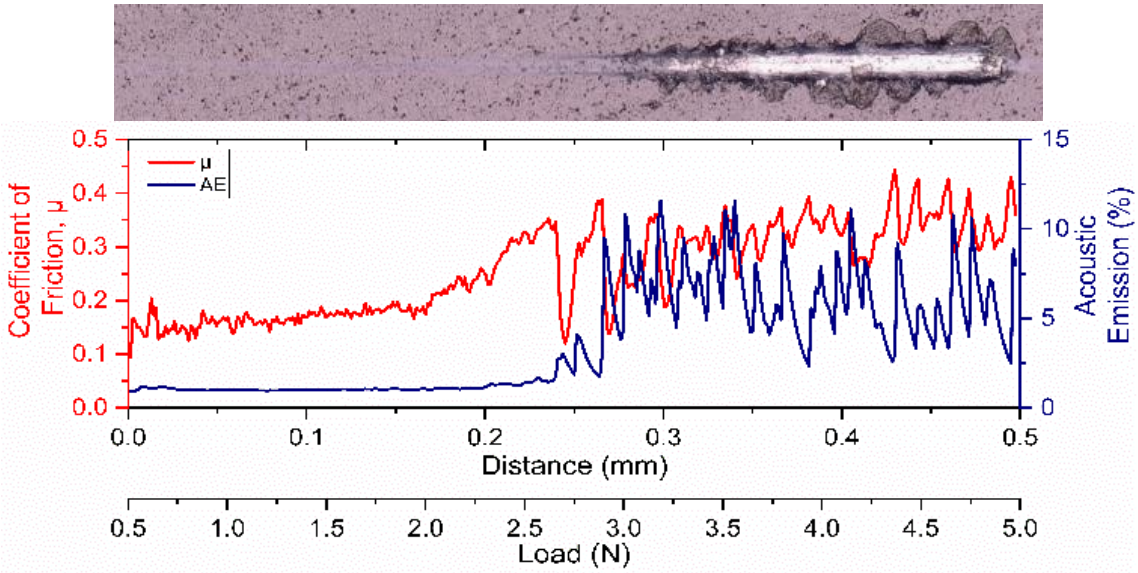

Figure A.16. *Optical images of the ramped load scratch test track with coefficient of friction and acoustic emission data for the AlTiN coating*

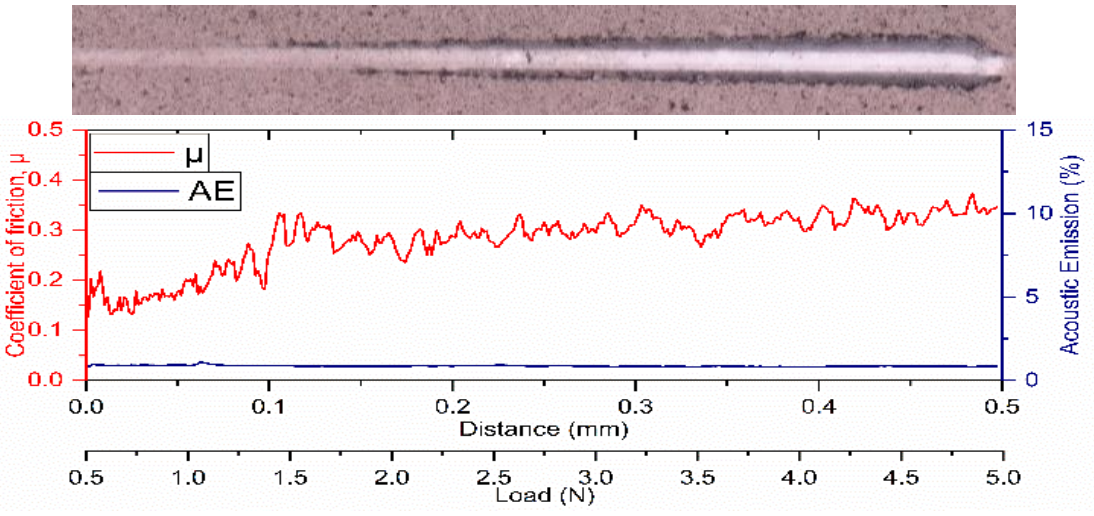

Figure A.17. *Optical images of the ramped load scratch test track with coefficient of friction and acoustic emission data for the TiB_2 coating*

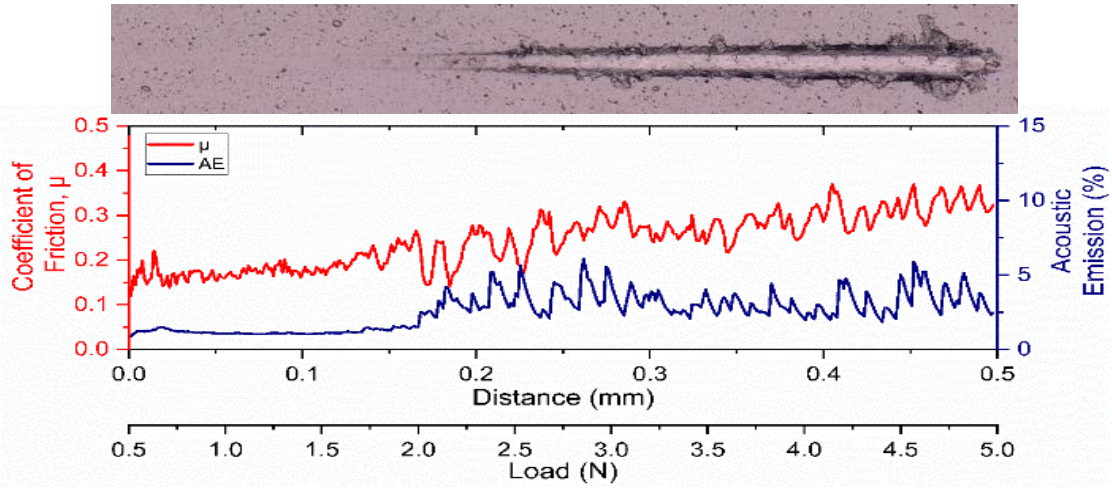

Figure A.18. *Optical images of the ramped load scratch test track with coefficient of friction and acoustic emission data for the CrN coating*

The micro-mechanical properties of the coatings are given in Table A.4. Both the TiB_2 and CrN coatings have lower hardness but increased plasticity index in comparison to the AlTiN coating. H/E and H^3/E^2 ratios are low for both the TiB_2 and CrN coatings. Under a heavy tool load, typical of titanium machining, surface layers are severely deformed, and therefore an increased ability to dissipate frictional energy is necessary. A higher plasticity index indicates greater energy dissipation under loading. A low H/E ratio delivers better wear resistance in machining applications that feature adhesive wear [21,22].

Table A.4. *Coating properties of the three coatings.*

Coating	**Coating Properties**						
	Thickness, μm	**Hardness, GPa**	**Elastic modulus, GPa**	**Plasticity index**	**H/E ratio**	**H^3/E^2 ratio**	**Residual stresses, MPa**
TiB_2	1.79	9.49 ± 0.52	413.51	0.78	0.023	0.005	-633 ± 53
CrN	1.8	21.1 ± 2.4	534.50	0.63	0.039	0.033	-955 ± 68
AlTiN	1.94	28.9 ± 2.0	516.52	0.46	0.056	0.090	- 599 ± 168

A.3.3 Conclusions

Detailed experimental investigations were conducted to compare the machining performance of the TiB_2 and CrN coated tools for the rough and finish turning of Ti6Al4V alloy. It was found that the TiB_2 coating was effective at improving tool performance for the rough turning of Ti6Al4V alloy, where the adhesion wear mechanism dominated due to lubricious B_2O_3 tribo-film formation. However, the TiB_2 coating was ineffective during finish turning operations where crater wear dictates tool performance due to a drop in the efficiency of the generated tribo-films. The CrN coating provided the second-best tool performance for the rough turning of Ti6Al4V alloy, but improved tool performance significantly for the finish turning of Ti6Al4V alloy. This was due to Cr_2O_3 tribo-film formation which had both lubricating and thermal barrier properties and was quite efficient in both low and high temperatures. Micro-scratch tests of the TiB_2 and CrN coatings revealed that both the coatings fail by plastic flow with localized deformation and no substrate exposure, providing better tribological performance.

A.4. References

1. Chowdhury, M.S.I.; Chowdhury, S.; Yamamoto, K.; Beake, B.D.; Bose, B.; Elfizy, A.; Cavelli, D.; Dosbaeva, G.; Aramesh, M.; Fox-Rabinovich, G.S.; et al. Wear behaviour of coated carbide tools during machining of Ti6Al4V aerospace alloy associated with strong built up edge formation. Surf. Coat. Technol. 2017, 313, 319–327.
2. Lupicka, O.; Warcholinski, B. The Adhesion of CrN Thin Films Deposited on Modified 42CrMo4 Steel. Adv. Mater. Sci. Eng. 2017, 2017, 1–14. https://doi.org/10.1155/2017/4064208.
3. Milosev, I.; Strehblow, H. H.; Navinsek, B. Comparison of TiN, ZrN, and CrN Coatings under Oxidation. Thin Solid Films 1997, 303 (303), 246–254.
4. Sato, T.; Tada, Y.; Ozaki, M.; Hoke, K.; Besshi, T. A Crossed-Cylinders Testing for Evaluation of Wear and Tribological Properties of Coated Tools. Wear 1994, 178 (1–2), 95–100. https://doi.org/10.1016/0043-1648(94)90133-3.
5. Berg, G.; Friedrich, C.; Broszeit, E.; Berger, C. Development of Chromium Nitride Coatings Substituting Titanium Nitride. Surf. Coatings Technol. 1996, 86–87 (PART 1), 184–191. https://doi.org/10.1016/S0257-8972(96)03042-3.
6. Navinsek, B.; Panjan, P.; Milosev, I. Industrial Applications of CrN (PVD) Coatings, Deposited at High. Surf. Coatings Technol. 1997, 97, 182–191.
7. Bertrand, G.; Mahdjoub, H.; Meunier, C. A Study of the Corrosion Behaviour and Protective Quality of Sputtered Chromium Nitride Coatings. Surf. Coatings Technol. 2000, 126 (2–3), 199–209. https://doi.org/10.1016/S0257-8972(00)00527-2.

8. Shaw, M.C. Metal Cutting Principles, 2nd ed.; Oxford University Press: Oxford, UK, 2005.
9. Melkote, S.N.; Grzesik, W.; Outeiro, J.; Rech, J.; Schulze, V.; Attia, H.; Arrazola, P.J.; M'Saoubi, R.; Saldana, C. Advances in material and friction data for modelling of metal machining. CIRP Ann. Manuf. Technol. 2017, 66, 731–754.
10. Johnson, G.R.; Cook, W.H. Fracture characteristic of three metals subjected to various strains, strain rate, temperature and pressure. Eng. Fract. Mech. 1984, 21, 31–48.
11. Lee, W.S.; Lin, C.F. High-temperature deformation behaviour of Ti6Al4V alloy evaluated by high strain-rate compression tests. J. Mater. Process. Technol. 1998, 75, 127–136.
12. Chen, G.; Ren, C.; Yang, X.; Jin, X.; Guo, T. Finite element simulation of high-speed machining of titanium alloy (Ti-6Al-4V) based on ductile failure model. Int. J. Adv. Manuf. Technol. 2011, 56, 1027–1038.
13. Fox-Rabinovich, G.S.; Kovalev, A.I.; Shuster, L.S.; Bokiy, Y.; Dosbaeva, G.K.; Wainstein, D.L. Characteristic features of alloying HSS-based deformed compound powdered materials with consideration for tool self-organization at cutting. Wear 1997, 206, 214–220.
14. ISO 25178-2:2012 Geometrical Product Specifications (GPS)—Surface Texture: Areal—Part 2: Terms, Definitions and Surface Texture Parameters; International Organization for Standardization: Geneva, Switzerland, 2012.
15. Qi, H.S.; Mills, B. Formation of a transfer layer at the tool-chip-interface during machining. Wear 2000, 245, 136–147.

16. Aouadi, S.M.; Gao, H.; Martini, A.; Scharf, T.W.; Muratore, C. Lubricious oxide coatings for extreme temperature applications: A review. Surf. Coat. Technol. 2014, 257, 266–277.
17. Narutaki, N.; Murakoshi, A.; Motonishi, S.; Takeyama, H. Study on Machining of Titanium Alloys. CIRP Ann. Manuf. Technol. 1983, 32, 65–69.
18. Senda, T.; Yamamoto, Y.; Ochi, Y. Friction and Wear Test of Titanium Boride Ceramics at Elevated Temperatures. J. Ceram. Soc. Jpn. 1993, 101, 461–465.
19. Munro, R.G. Material Properties of Titanium Diboride. J. Res. Natl. Inst. Stand. Technol. 2000, 105, 709–720.
20. Hartung, P.D.; Kramer, M.; Von Turkovich, B.F. Tool Wear in Titanium Machining. CIRP Ann. 1982, 31, 75–80.
21. Beake, B. D.; Fox-Rabinovich, G. S.; Veldhuis, S. C.; Goodes, S. R. Coating Optimisation for High Speed Machining with Advanced Nanomechanical Test Methods. Surf. Coatings Technol. 2009, 203 (13), 1919–1925. https://doi.org/10.1016/j.surfcoat.2009.01.025.
22. Zhang, X.; Beake, B. D.; Zhang, S. Toughness Evaluation of Thin Hard Coatings and Films. In Thin Films and Coatings: Toughening and Toughness Characterization; CRC Press, Taylor and Francis Group, Boca Raton, NW, USA, 2015; p 52.

Appendix B: Effect of Deposition Parameters on CrN Coating Properties and Performance.

B.1. Preface

In the present research, a self-adaptive CrN coating was designed and developed with the expectation that Cr-O tribo-films will form that can provide both thermal barrier and lubricating properties during machining. It has been previously mentioned that a CrN coating has unique micro-mechanical properties that are suitable in addressing machining issues during Ti6Al4V turning (see preface of Appendix A and Chapter 2 and 3). Detailed investigations in Chapters 2 and 3 suggested that a CrN coating could be considered as a general-purpose coating for a wider range of cutting conditions for Ti6Al4V turning.

In the process of developing the CrN coating, tuning of the deposition parameters was done. There are three main deposition process parameters that affect the properties of the deposited coatings: nitrogen gas pressure, bias voltage, and coating thickness. CrN coatings with various combinations of nitrogen gas pressure, bias voltage, and coating thicknesses were deposited, and tool life studies were conducted to assess the performance of the deposited CrN coatings. Coating characterizations were also done to gain a better understanding of the coating's performance. This appendix summarizes the key aspects of this investigation.

B.2. Experimental Details

The CrN coating was deposited at the MMRI's PVD coating facility by arc evaporation using an AIP-S20 PVD Coater (Kobelco, Japan) with a Cr target (99.9% purity) with a 100 mm diameter. Prior to deposition, the mirror-polished cemented carbide substrates were cleaned ultrasonically in acetone. After the pumping-down procedure (reaching a pressure of 10×10^{-3} Pa), in-situ cleaning of the substrates was done by argon ion etching using a substrate bias voltage of 400 V at 1.33 Pa pressure for 7.5 min. The Cr target was powered in the arc mode. The working table rotated at 5 rpm during the process. During coating deposition, the substrate temperature was maintained at 500 °C. N_2 gas was used as the process gas. The pressure of the process gas, bias voltage, and coating deposition time was varied to obtain CrN coatings with different combinations of deposition parameters. Table B.1 shows the variation of deposition parameters that was implemented to tune the CrN coating.

Table B.1. *Variation of deposition parameters.*

N_2 **Gas Pressure (Pa)**	**Bias Voltage (V)**	**Coating Thickness (µm)**
1.33, 4, 5.5	-20, -50, -100, -150	1.21, 1.81, 5.74, 7.52

The coatings were deposited on Kennametal CNGG432 and polished Sandvik Coromant SPGN120308 carbide cutting inserts. All coating characterizations were performed on the flat, polished SPGN120308 inserts, whereas finish turning experiments were conducted with the CNGG432 inserts. Calotest method with a 25 mm steel ball was used to measure the coating thicknesses of all coatings.

An Anton Paar-NHT3 Nanoindentation Tester (Buchs, Switzerland) was used to determine the coating's hardness, elastic modulus, and yield stress of the coatings. 40 nanoindentations were performed at room temperature with a Berkovich diamond indenter at a load of 50mN to determine the hardness and elastic modulus of the coatings. To determine the yield stress of the coatings, a spherical diamond indenter with 20 μm end radii was used. The test was performed in the sinus mode at a load of 200 mN at a frequency of 5 Hz and amplitude of 20 mN.

An Anton Paar-RST3 Revetest® Scratch Tester (Buchs, Switzerland) was used to conduct micro-scratch tests on the coatings to study their failure behaviour under progressive loading. The tests were performed with a 100 μm end radii Rockwell diamond indenter with loads increasing progressively from 0.5 N to 40 N for a scratch length of 3.5 mm. The scratching speed and loading rate was maintained at 4.43 mm/min and 50 N/min respectively. The tests were repeated three times for each coating.

Finish turning tests were conducted on an ASTM B265 Grade 5 Ti6Al4V alloy and done on a Nakamura Tome SC450 CNC turning center (Nakamura-Tome Precision Industry Co., Ltd., Hakusan, Ishikawa, Japan). The cutting conditions are provided in table B.2. All tests were repeated 3 times for each coating to ensure repeatability.

Table B.2. *Cutting data for the experiments performed.*

Machining operation	Speed, m/min	Feed, mm/rev	Depth of cut, mm	Coolant Condition
Finish Turning	150	0.1225	0.25	Flood

Tool flank wear was measured using a VHX-5000 Keyence optical microscope (KEYENCE corporation of America, Itasca, IL, USA). Volumetric wear measurements were done after approximately every 600 m of machining length for the worn tools. The evaluations were conducted using Alicona Infinite Focus G5 3D surface measurement system (Alicona Manufacturing Inc., Bartlett, IL, USA).

B.3. Results and Discussions

B.3.1 Tool Wear performance studies

Tuning of the deposition parameters (nitrogen gas pressure, bias voltage, and coating thickness) for the CrN coating was based on tool performance and were done in sequence. At first, tuning of the nitrogen gas pressure was done keeping the bias voltage and coating thickness constant. Then, tuning of bias voltage was done keeping the coating thickness constant and the nitrogen gas pressure at the determined optimal value. Finally, tuning of coating thickness was done at the determined optimal values of nitrogen gas pressure and bias voltage.

B.3.1.1 Tuning of Nitrogen Gas pressure

Three CrN coatings were deposited at nitrogen gas pressures of 1.33 Pa, 4 Pa, and 5.5 Pa. For all depositions, the bias voltage and coating thickness were kept fixed at -50V and approximately 1.8 μm, respectively. Figure B.1 shows the tool wear performance for the deposited coatings with varying nitrogen gas pressures. The lowest flank wear intensity was seen with nitrogen gas pressure of 4 Pa, followed by 1.33 Pa and then 5.5 Pa.

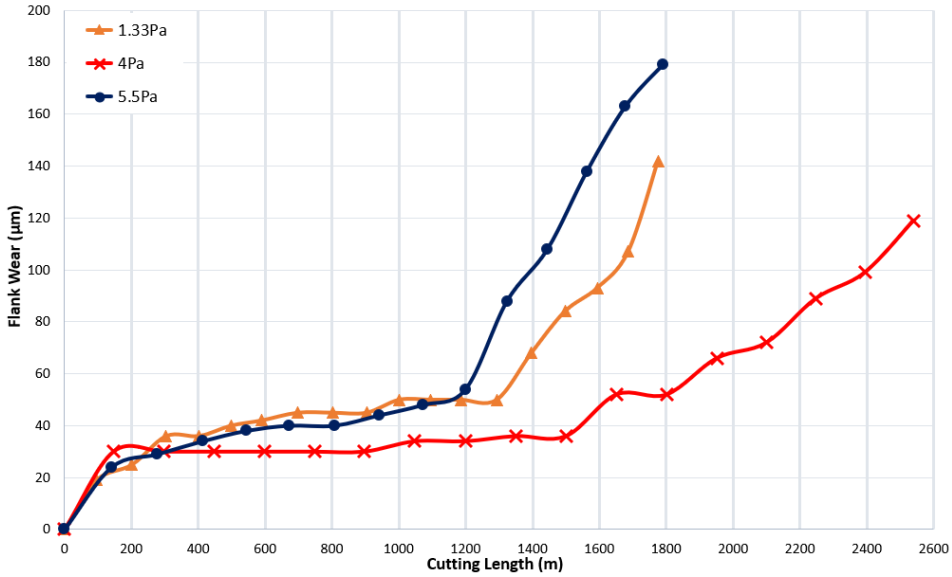

Figure B.1. *Flank wear vs. cutting length data during the wet finish turning of Ti6Al4V alloy with a CrN coating deposited under varying nitrogen gas pressures.*

Figure B.2 shows the tool wear progression and the 3D difference measurement of worn tool after every 600 m of machining length for the deposited coatings with varying nitrogen gas pressures. It is evident from the 3D images that tool wear was dictated by BUE formation and crater wear formation. Figures B.3 and B.4 show the variation of BUE formation and crater wear with cutting for the various coatings. As can be seen from Figures B.2-B.4, the CrN coating deposited at 4 Pa nitrogen gas pressure had the least BUE formation and crater wear progression. Less BUE formation and progressive build-up during machining reduces the propensity for tool chipping. The lower BUE formation, coupled with delayed and reduced crater wear intensity, led to stable, uniform, and minimal tool wear for the CrN coating deposited at 4 Pa nitrogen gas pressure. Thus, 4 Pa is found to be the optimal nitrogen gas pressure for a CrN coating deposition.

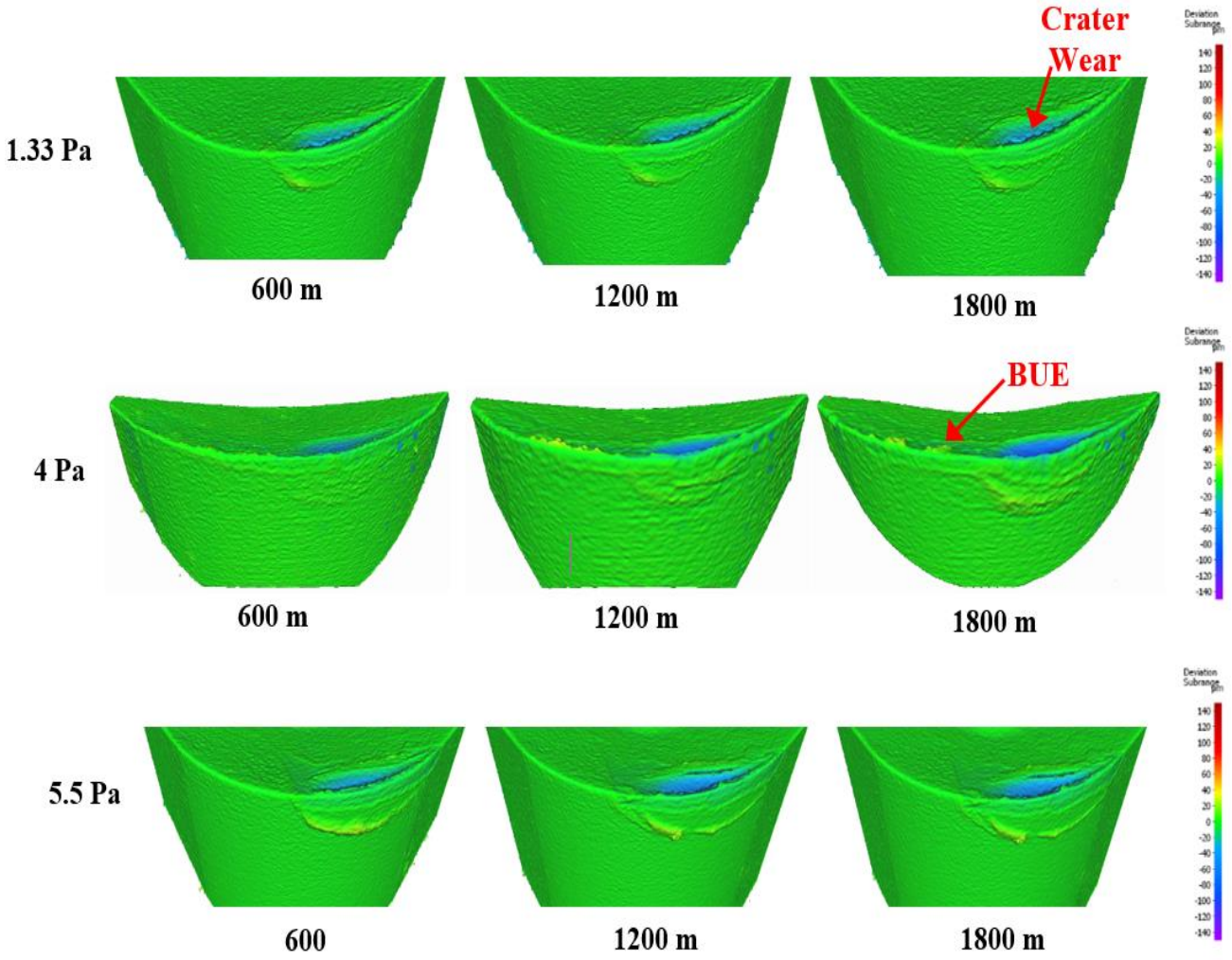

Figure B.2. *3D progressive wear difference measurement of the CrN coated tools deposited under varying nitrogen gas pressures, highlighting the evolution of built−up layers and crater wear during machining.*

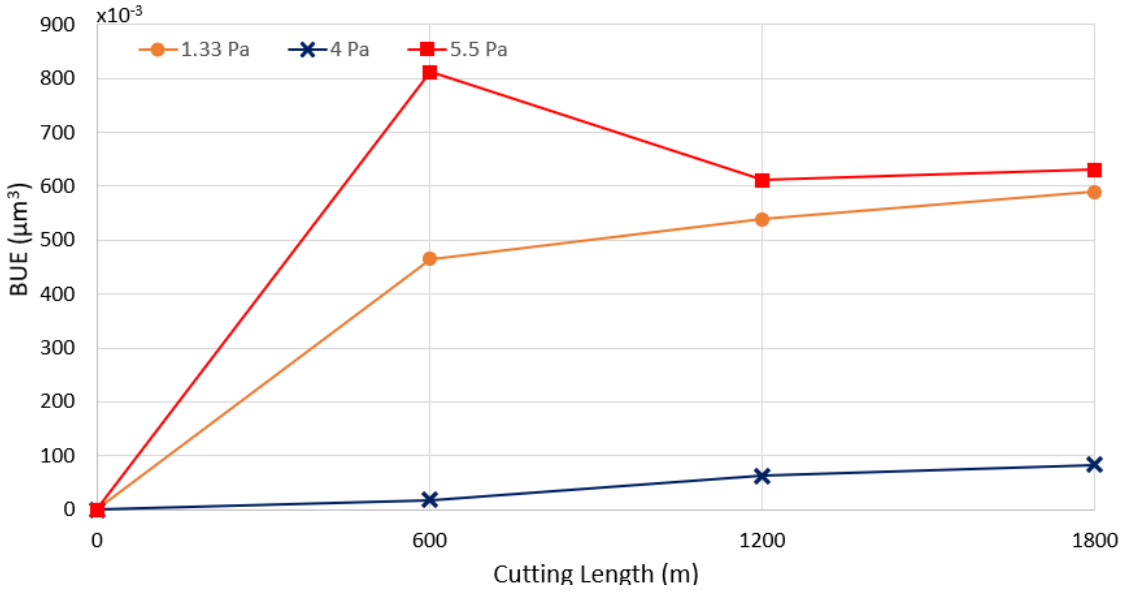

Figure B.3. *Built up volume progression vs. length of cut for the CrN coated tools deposited under varying nitrogen gas pressures, considering the peaks above the reference surface of the original tool.*

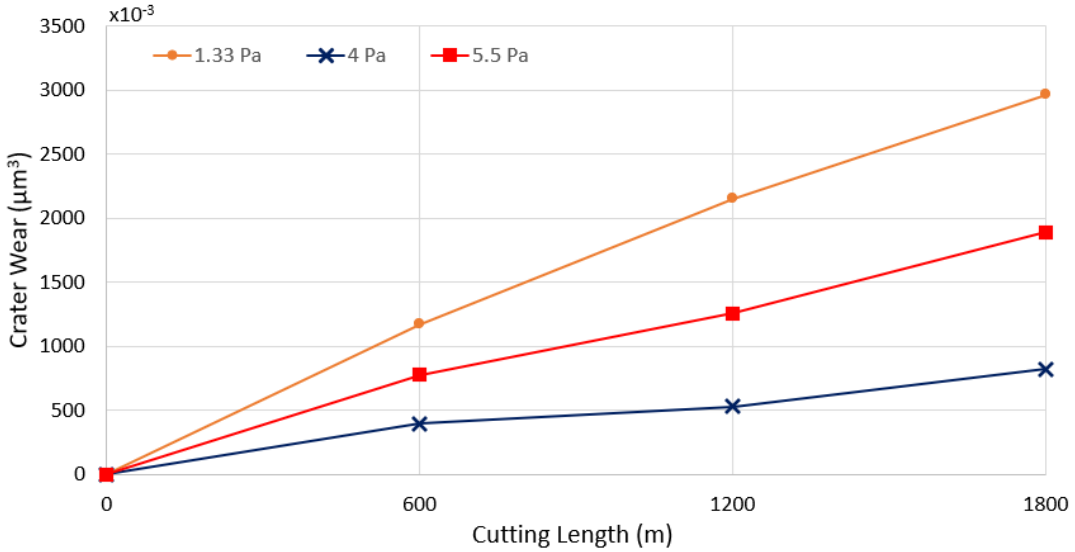

Figure B.4. *Crater wear volume progression vs. length of cut for the CrN coated tools deposited under varying nitrogen gas pressures, considering the peaks below the reference surface of the original tool.*

B.3.1.2 Tuning of bias voltage

To determine the optimal bias voltage for the CrN coating deposition, four CrN coatings were deposited at bias voltages of -20 V, -50 V, -100 V, and -150 V. All depositions were done at a nitrogen gas pressure of 4 Pa (since it was found to be optimal) and coating thickness of approximately 1.8 μm. Figure B.5 shows the tool wear performance for the deposited coatings with varying bias voltages. The best tool performance was given by the CrN coating deposited at a bias voltage of -50 V.

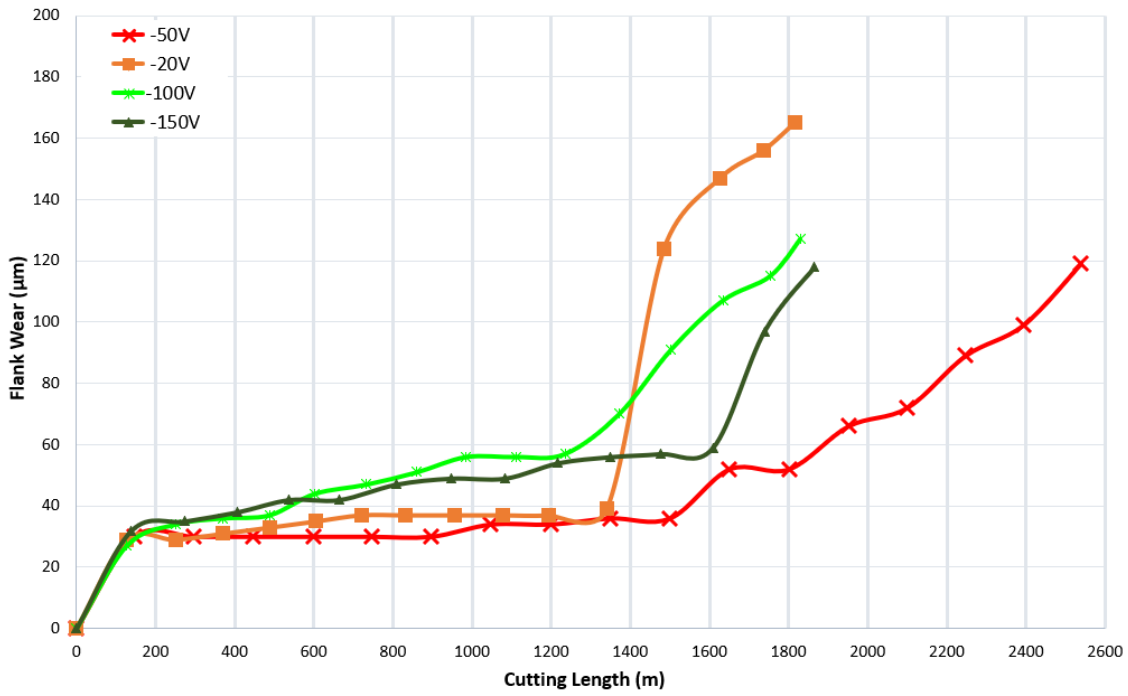

Figure B.5. *Flank wear vs. cutting length data during the wet finish turning of Ti6Al4V alloy with a CrN coating deposited under varying bias voltages.*

Figure B.6 shows the tool wear progression and the 3D volume measurement of the worn tool after approximately every 600 m of machining length for the deposited coatings with varying bias voltages. Figures B.6 and B.7 show the formation of BUE and crater wear

with respect to cutting length for the various coatings. As can be seen, the CrN coating deposited at -50 V bias voltage shows the least amount of BUE formation and crater wear propagation as cutting progressed. Minimal BUE formation and delayed crater wear resulted in a steady state of increase in tool wear, preventing rapid failure of the tool. This indicates that a bias voltage of -50 V is optimal for a CrN coating deposited by cathodic arc evaporation with an AIP-S20 PVD deposition system.

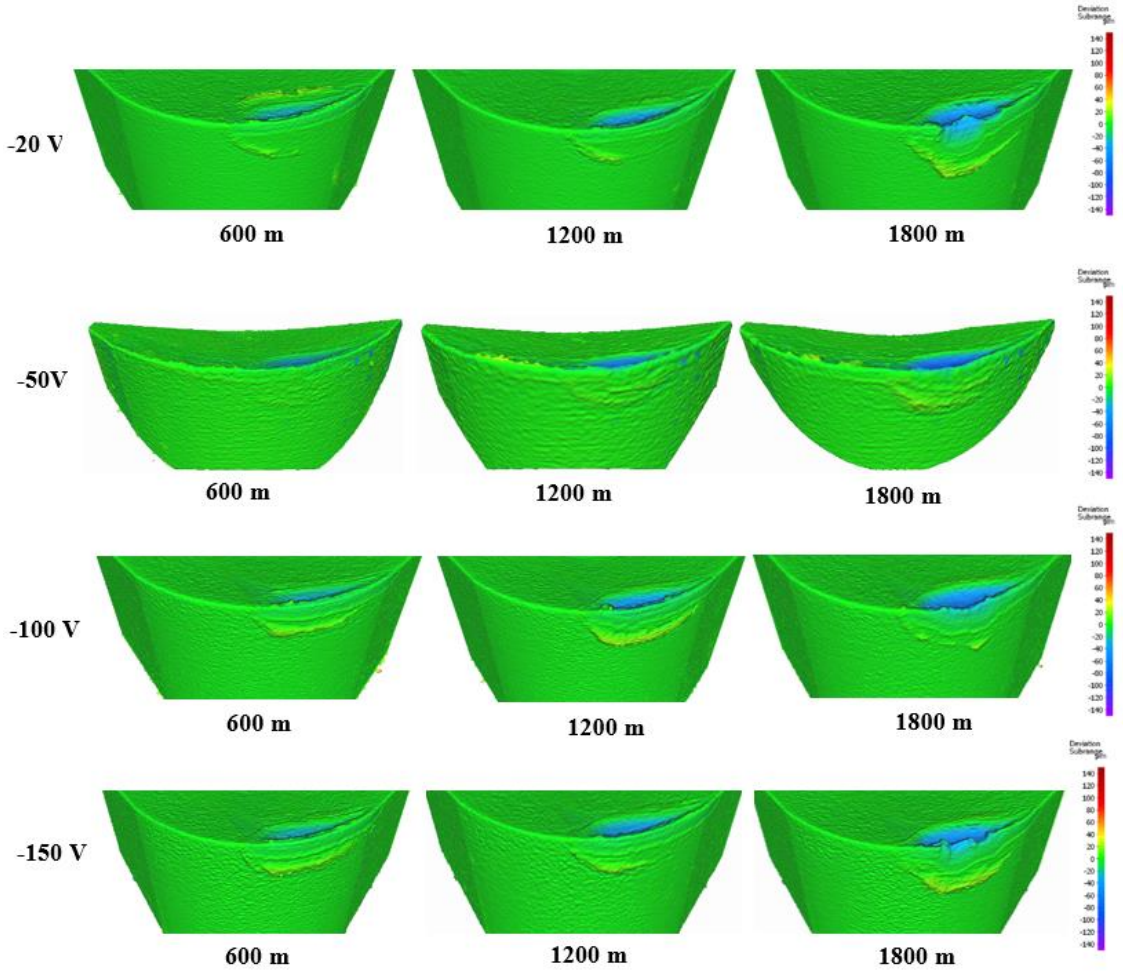

Figure B.6. *3D progressive wear difference measurement of the CrN coated tools deposited under varying bias voltages, highlighting the evolution of built−up layers and crater wear during machining.*

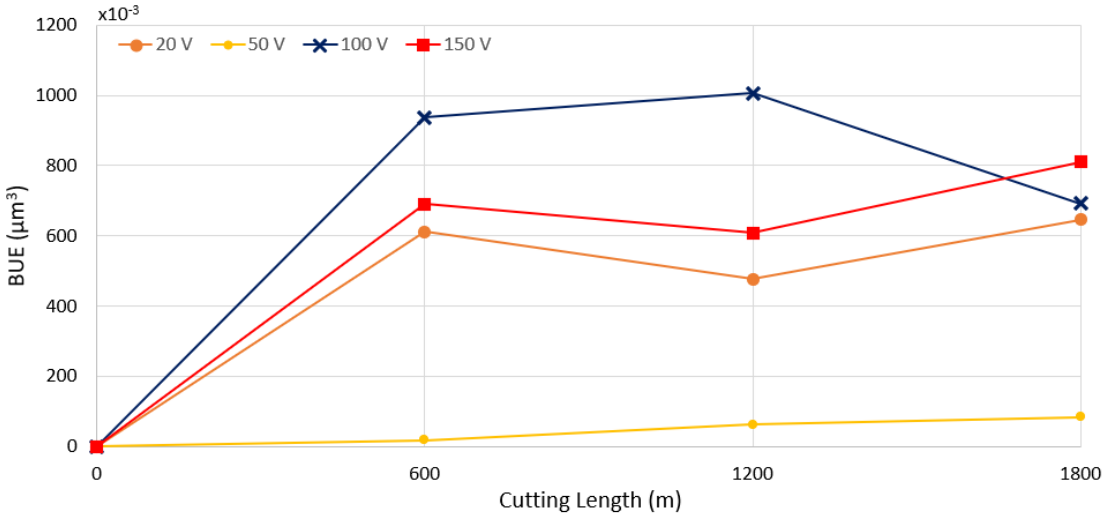

Figure B.7. *Built up volume progression vs. length of cut for the CrN coated tools deposited under varying bias voltages, considering the peaks above the reference surface of the original tool.*

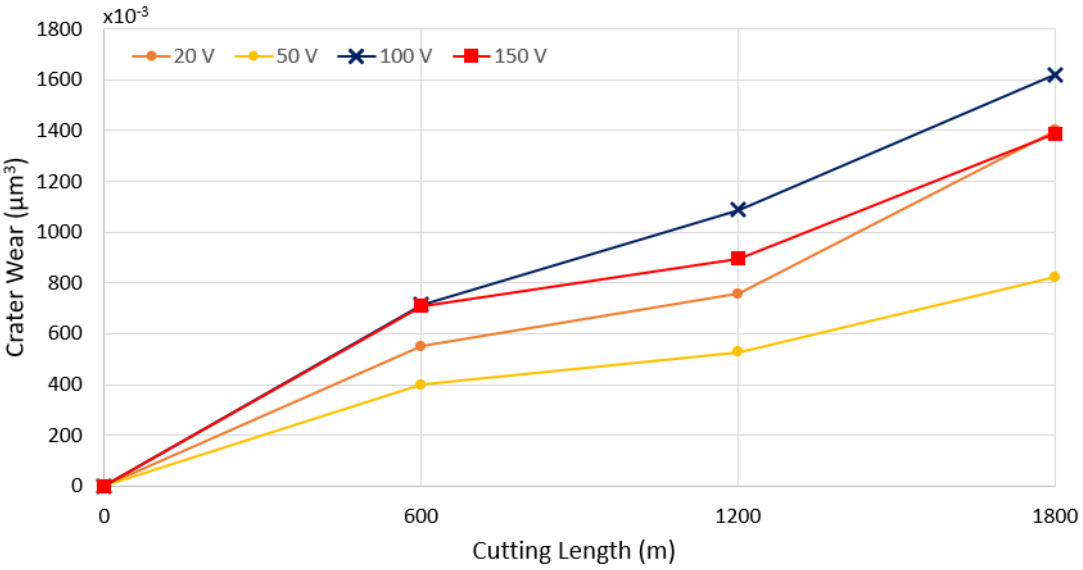

Figure B.8. *Crater wear volume progression vs. length of cut for the CrN coated tools deposited under varying bias voltages, considering the peaks below the reference surface of the original tool.*

B.3.1.3 Tuning of coating thickness

To determine the best possible coating thickness for the CrN coating to achieve improved machining performance, four CrN coatings were deposited with coating thicknesses of 1.21 µm, 1.81 µm, 5.74 µm, and 7.52 µm. All depositions were done at a nitrogen gas pressure of 4 Pa and bias voltage of -50 V (the optimal values as determined prior). Figure B.9 shows the tool wear performance for the deposited coatings with varying coating thicknesses. The best tool performance was given with a coating thickness of 1.81 µm.

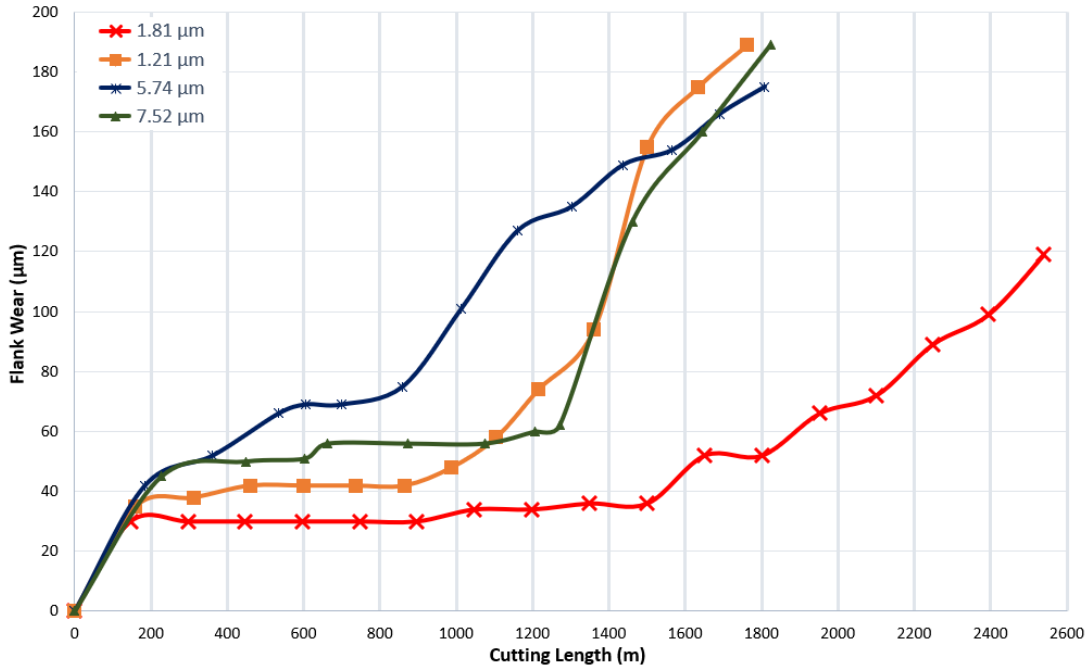

Figure B.9. *Flank wear vs. cutting length data during the wet finish turning of Ti6Al4V alloy with a CrN coating deposited with varying coating thicknesses.*

Figure B.10 shows the progression of tool wear and the 3D volume measurement of the cutting tool after every 600 m of cutting length for the deposited coatings with varying

coating thickness. Figures B.11 and B.12 show the formation of BUE and crater wear with respect to cutting length for the various coatings. As can be seen, CrN coating having 1.81 μm coating thickness shows the least amount of BUE formation and crater wear propagation as cutting progressed. Significant delamination of the coating occurs for the CrN coatings with 5.74 μm and 7.52 μm coating thicknesses. Thus, a coating thickness of around 1.81 μm is optimal for CrN coating for this particular application.

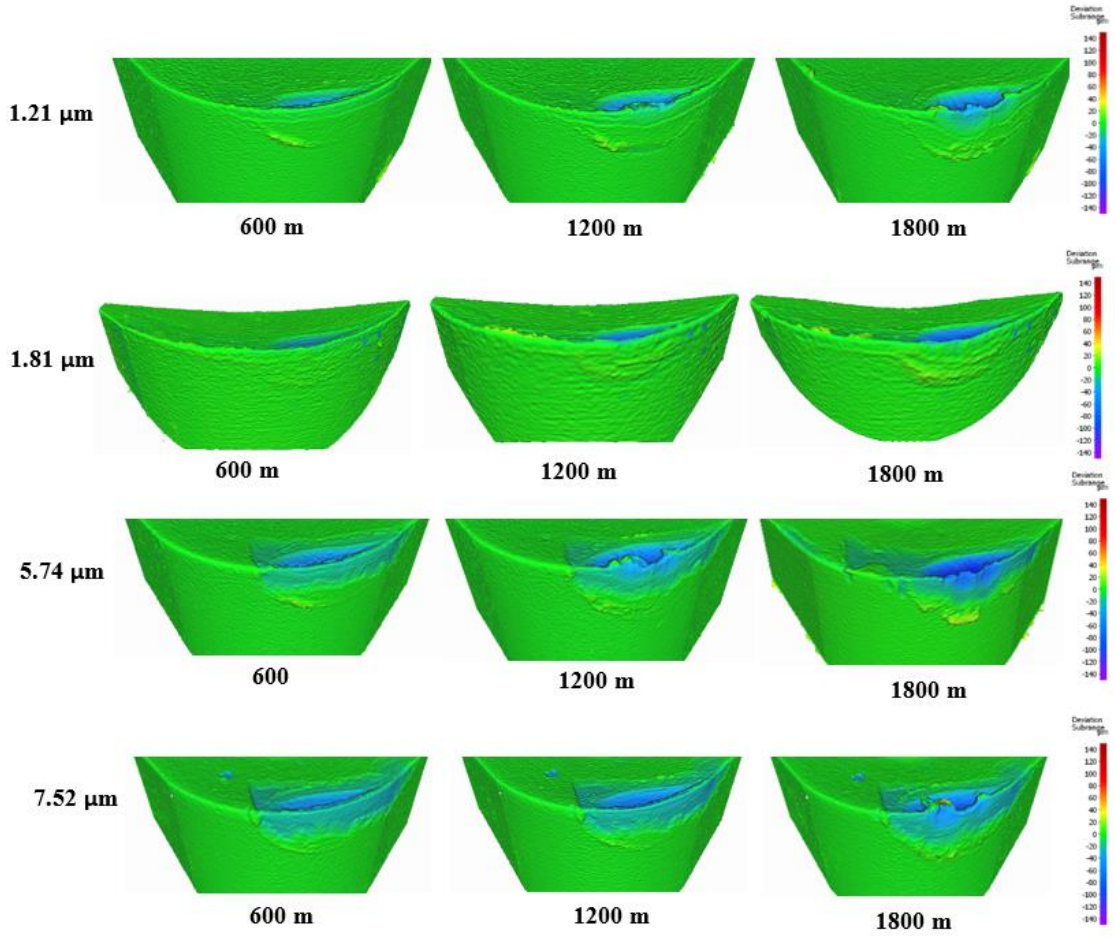

Figure B.10. *3D progressive wear difference measurement of the CrN coated tools deposited with varying coating thicknesses, highlighting the evolution of built−up layer and crater wear during machining.*

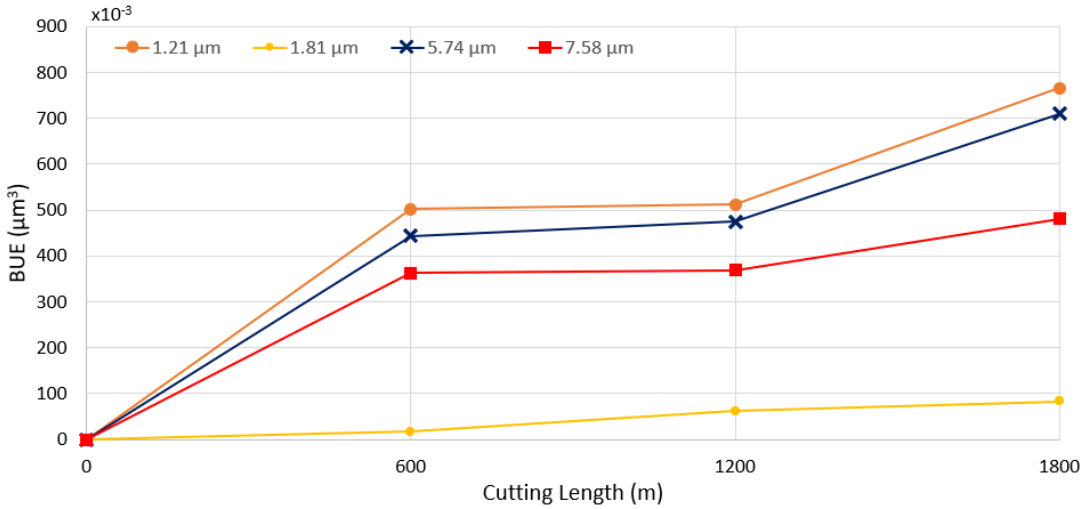

Figure B.11. *Built up volume progression vs. length of cut for the CrN coated tools deposited with varying coating thicknesses, considering the peaks above the reference surface of the original tool.*

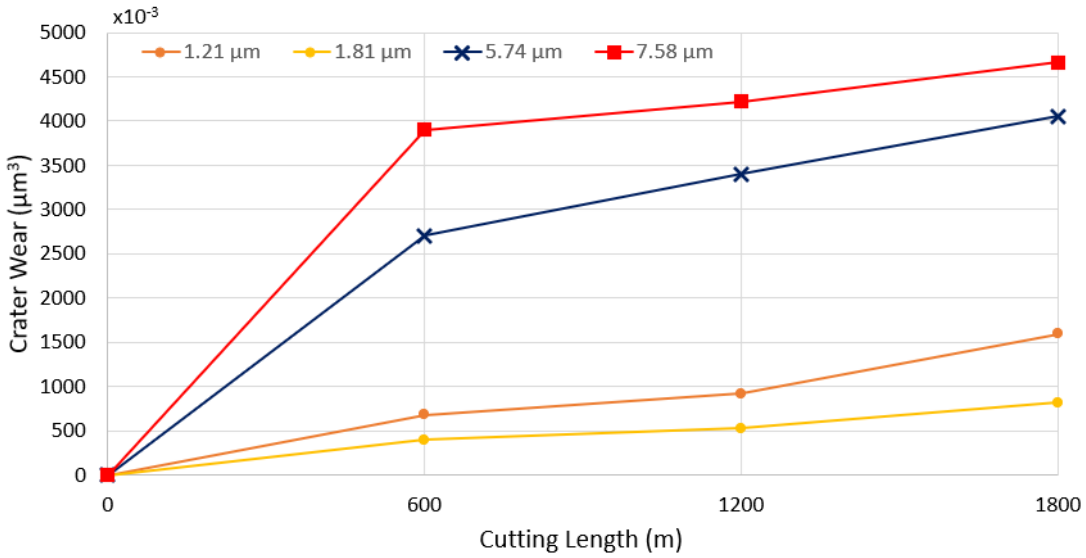

Figure B.12. *Crater wear volume progression vs. length of cut for the CrN coated tools deposited with varying coating thicknesses, considering the peaks below the reference surface of the original tool.*

Thus, based on machining performance, the CrN coating deposited at 4Pa nitrogen gas pressure, -50V bias voltage and with a coating thickness of 1.81 μm provided the best tool performance. This combination of deposition parameters for the CrN coating had the least formation of BUE on the coated tool, and it reduced crater wear progression.

B.3.2 Coating Characterization

As discussed in the previous section, the best tool performance was given by the CrN coated tool deposited at 4Pa nitrogen gas pressure, -50V bias voltage, and a 1.81 μm coating thickness. To assess the properties and failure behaviour of the various deposited CrN coatings under load, micromechanical studies were conducted. Figure B.13-B.15 show the variation in the hardness, elastic modulus, plasticity index, H/E ratio, and H^3/E^2 ratio for the deposited coatings with varying nitrogen gas pressures, bias voltages, and coating thicknesses. Considering independently the variation in nitrogen gas deposition pressure and bias voltage, coatings deposited at 4 Pa and -50V, which gives best tool performance, show higher elastic modulus values. It has been shown in previous investigations [1] that coatings which have slightly lower hardness values yet avoid sacrificing the elastic modulus (i.e., with a higher elastic modulus), usually perform better during Ti6Al4V machining. Researchers [2,3] have found that wear resistance increases with the elastic modulus. A similar trend is also observed when coating thickness variation is considered independently. As seen in Figure B.15 a and b, a coating thickness of 1.81 μm gives the lowest hardness value with a relatively high elastic modulus. The H/E and H^3/E^2 ratios are determined from the hardness (H) and elastic modulus (E) of the coatings. The H/E ratio indicates the elastic strain to failure characteristics of the coating and shows how elastic the

coating stays during mechanical contact [4,5]. The H^3/E^2 ratio shows the coatings resistance to plastic deformation. The plasticity index, the ratio between the plastic and the total work done during nanoindentation [6], assesses a coating's ability to dissipate energy. As can be seen from Figures B.13-B.15 c,d, and e, the values for the plasticity index, H/E, and H^3/E^2 ratios for the best performing coating with a 4 Pa deposition pressure, -50 V bias voltage, and 1.81 μm coating thickness are within two extremes, with neither the highest nor the lowest value. This indicates that the relationship between the hardness and elastic modulus of a coating needs to be optimized and not maximized for better tool performance. It has been previously shown in the literature [7] that for a coating with higher tool load applications where severe surface deformation occurs, such as during titanium machining, an optimized combination of coating hardness and elastic modulus is crucial for longer tool life.

The yield stress data shows that an increase in the nitrogen gas deposition pressure and coating thickness (Figure B.16) has a minor effect on yield stress. On the contrary, an increase in the negative bias voltage increases the yield stress of the coatings. The yield stress for the deposited coating at bias voltages of -100 V and -150 V is slightly increased compared to the coating deposited at -50 V bias voltage. A similar trend is found in the H/E data which is also a measure of brittleness. So, it can be said that the coatings deposited at bias voltages of -100 V and -150 V have higher yield stresses but are more brittle, which consequently makes them perform worse during machining than the coating deposited at -50V bias voltage (Figure B.16 b).

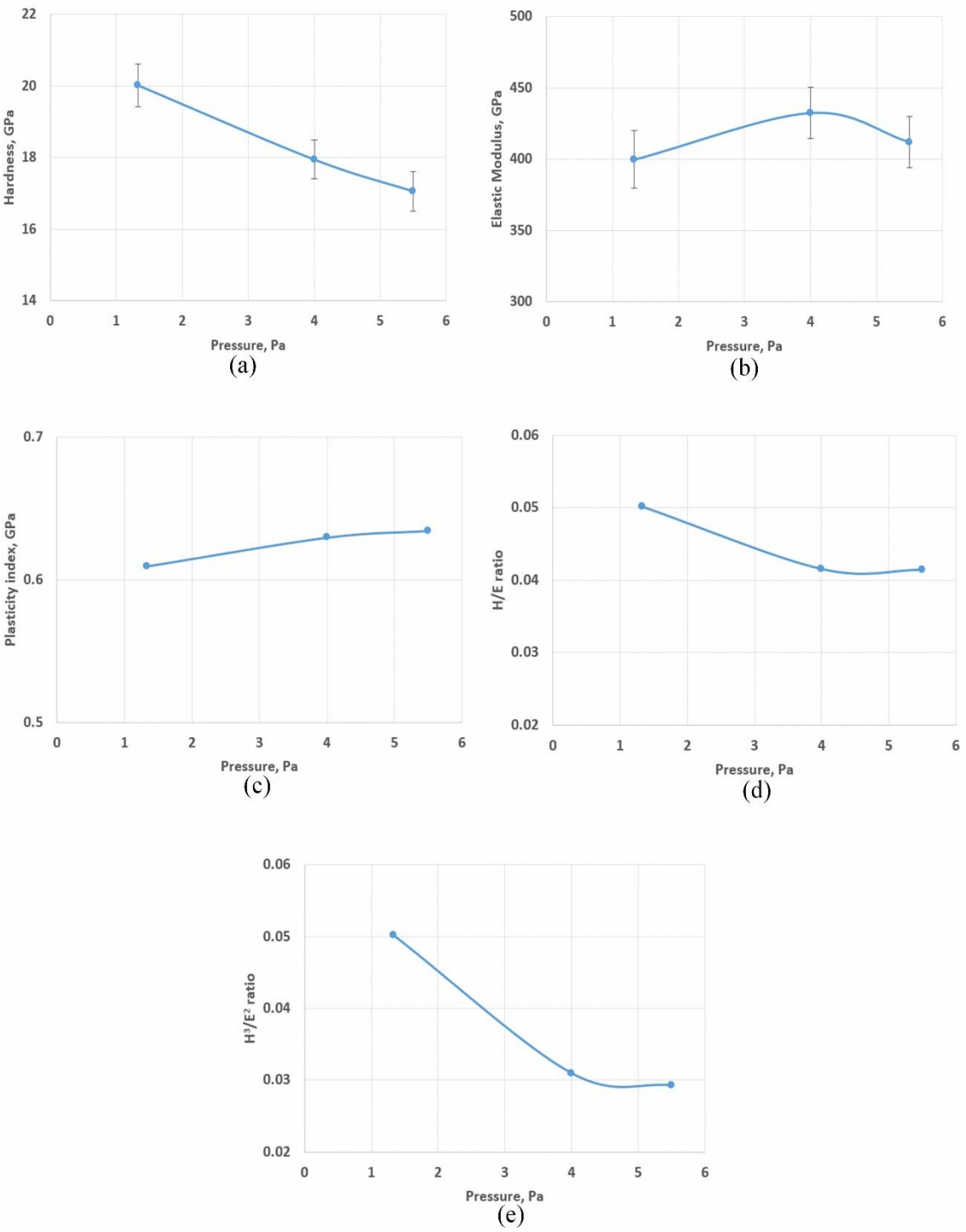

Figure B.13. *Variation of micromechanical properties of the CrN coatings deposited with varying nitrogen gas pressure: (a) hardness, (b) elastic modulus, (c) plasticity index, (d) H/E ratio, and (e) H^3/E^2 ratio.*

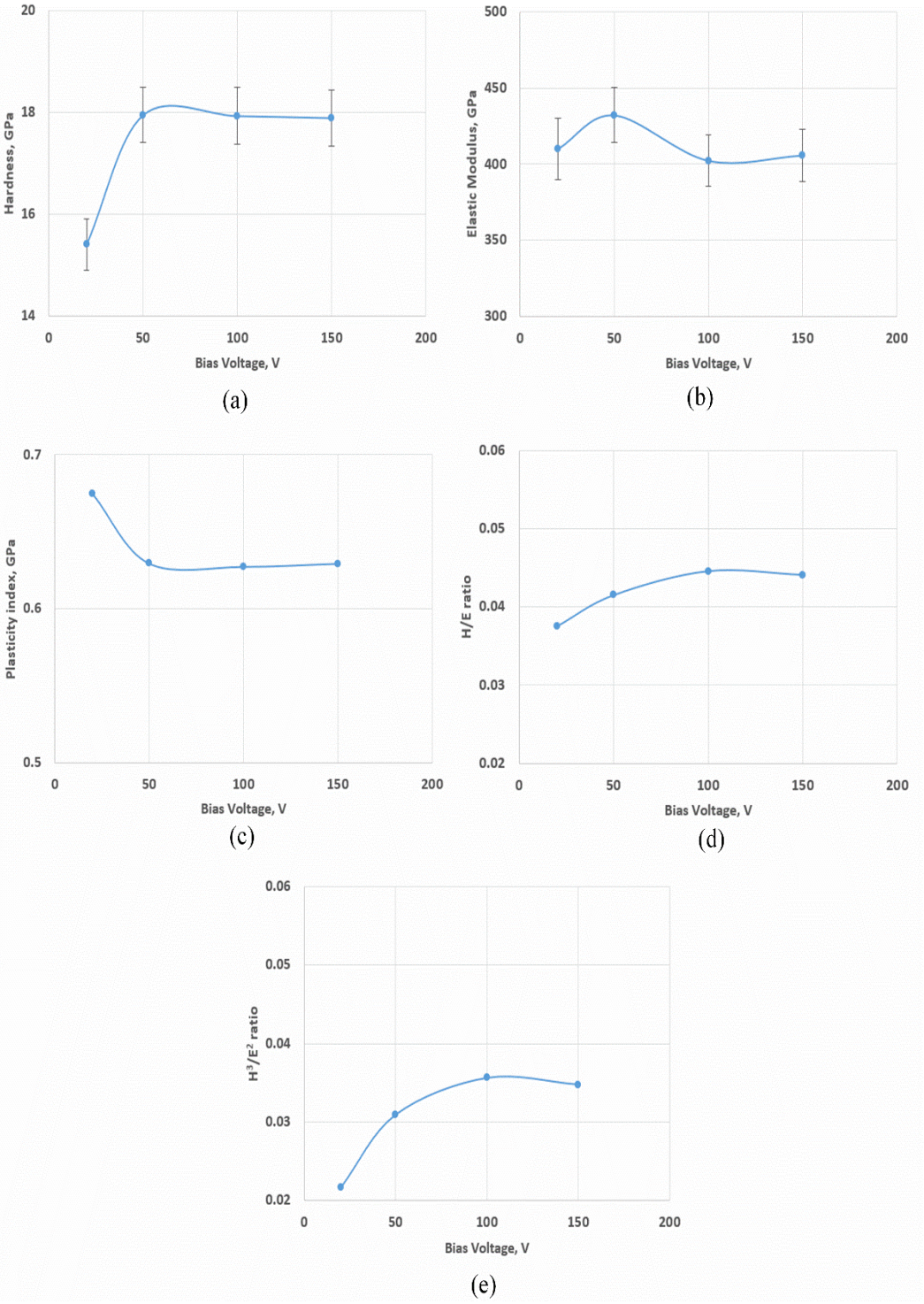

Figure B.14. *Variation of micromechanical properties of the CrN coatings deposited with varying bias voltage: (a) hardness, (b) elastic modulus, (c) plasticity index, (d) H/E ratio, and (e) H^3/E^2 ratio.*

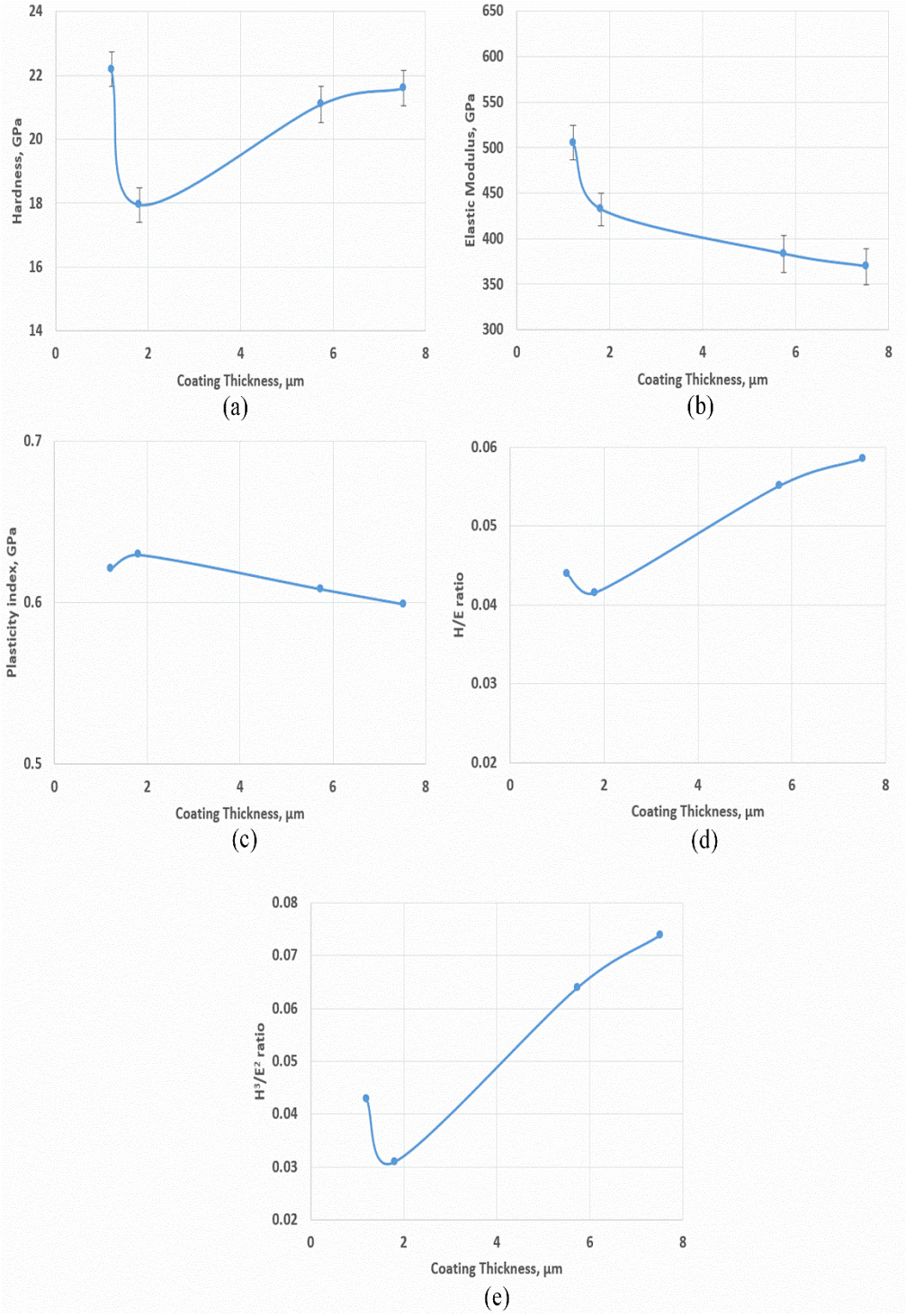

Figure B.15. *Variation of micromechanical properties of the CrN coatings deposited with varying coating thickness: (a) hardness, (b) elastic modulus, (c) plasticity index, (d) H/E ratio, and (e) H^3/E^2 ratio.*

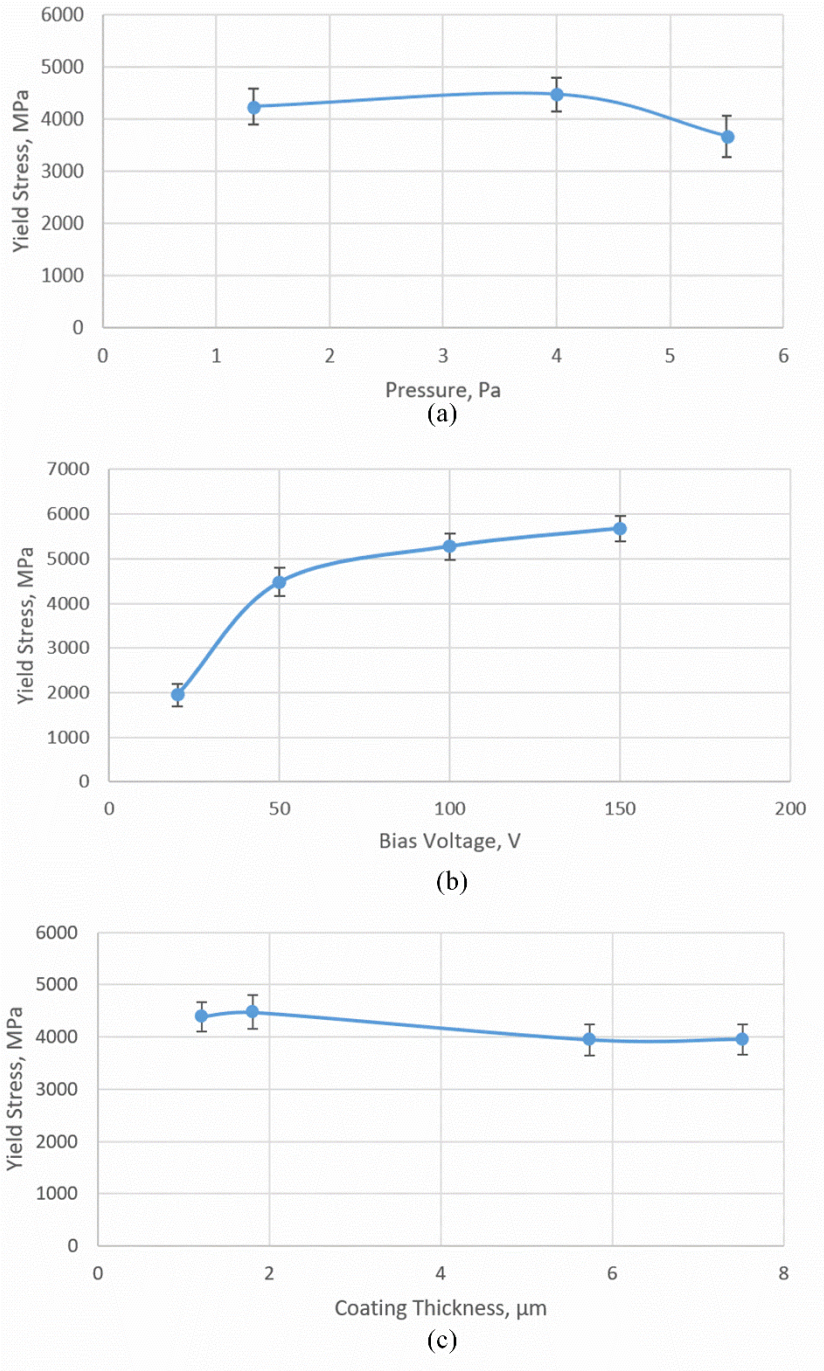

Figure B.16. *Variation of yield stress of the CrN coatings deposited with varying: (a) nitrogen gas pressure, (b) bias voltage, and (c) coating thickness.*

Figures B.17-B.27 and Table B.3 show the scratch test data for the CrN coatings deposited with various N_2 gas deposition pressures, bias voltages, and coating thicknesses. The failure behaviour of the coatings during the scratch test were defined by the critical loads of different failure modes. Two critical loads were identified for all the coatings: LC_1, the critical load showing signs of initial deformation, and LC_2, the critical load for coating failure. From the scratch test data (Figures B.17-B.19, Table B.3), it was found that variation in the N_2 gas deposition pressure does not have much effect on the failure behaviour of the coatings. However, a careful observation shows that for the 4Pa N_2 gas deposition pressure, the number of cracks on the side of the scratch track are somewhat smaller and fewer than the other two. The scratch tracks for the coatings deposited under varying bias voltages (Figures B.20-B.23, Table B.3) showed that the coating deposited at - 50V bias voltage had a higher critical load of deformation and comparatively smoother scratch track. On the other hand, coatings deposited at - 100V and - 150V bias voltages started to deform a bit earlier and show a little rough deformation due to their slightly higher brittle nature. Coatings deposited at -20V started to deform very early and clearly performed the worst during scratch testing. Scratch test data and the scratch tracks for the coatings with different coating thicknesses (Figures B.24-B.27, Table B.3) showed that the 1.81 μm coating thickness performed best. The thicker ones underwent drastic deformation and the thinnest one showed substrate exposure.

Table B.3. *Critical loads, LC_1 and LC_2, obtained from micro- scratch test for the coatings.*

	Coating deposition condition	LC_1, N	LC_2, N
N_2 gas pressure variation	1.33 Pa	22.07	28.2
	4 Pa	22.01	28.5
	5.5 Pa	22.04	28.54
Bias voltage variation	- 20 V	-	12.34
	- 50 V	22.01	28.5
	- 100 V	21.92	27.09
	- 150V	19.69	27.54
Coating thickness variation	1.21 µm	18.89	25.16
	1.81 µm	22.01	28.5
	5.74 µm	19.65	24.60
	7.52 µm	19.14	26.44

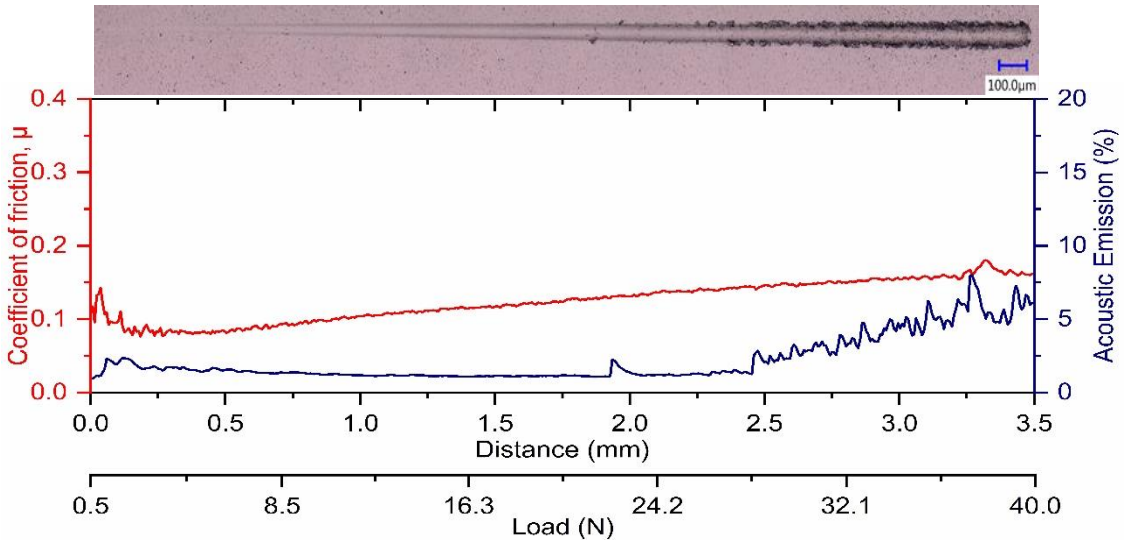

Figure B.17. *Micro-scratch test data with optical images of the scratch track for CrN coating deposited at 1.33 Pa nitrogen gas pressure, -50 V bias voltage and with approximately 1.8 µm coating thickness.*

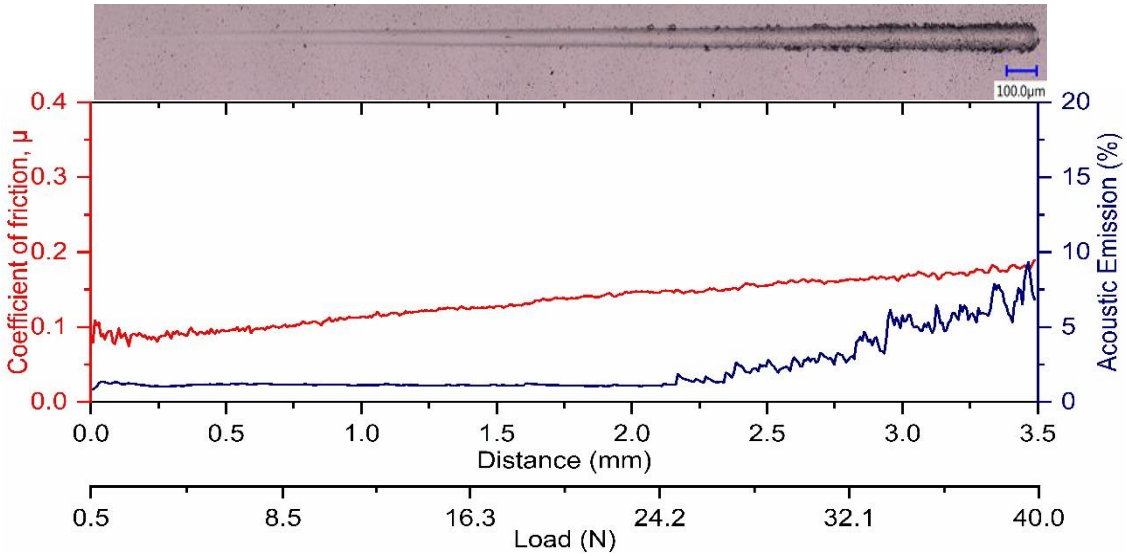

Figure B.18. *Micro-scratch test data with optical images of the scratch track for CrN coating deposited at 4 Pa nitrogen gas pressure, -50 V bias voltage and with 1.81 µm coating thickness.*

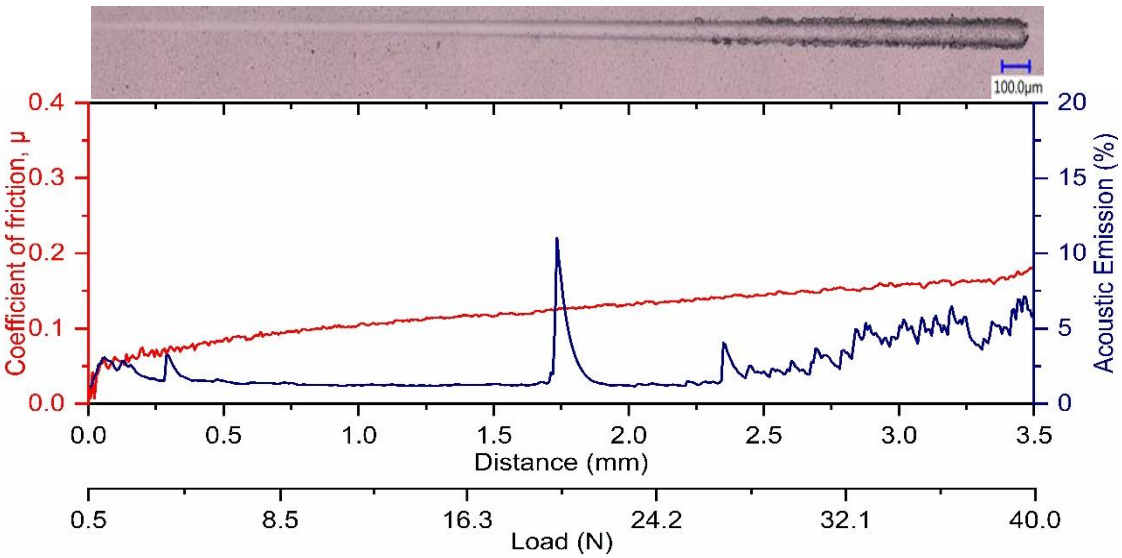

Figure B.19. *Micro-scratch test data with optical images of the scratch track for CrN coating deposited at 5.5 Pa nitrogen gas pressure, -50 V bias voltage and with approximately 1.8 µm coating thickness.*

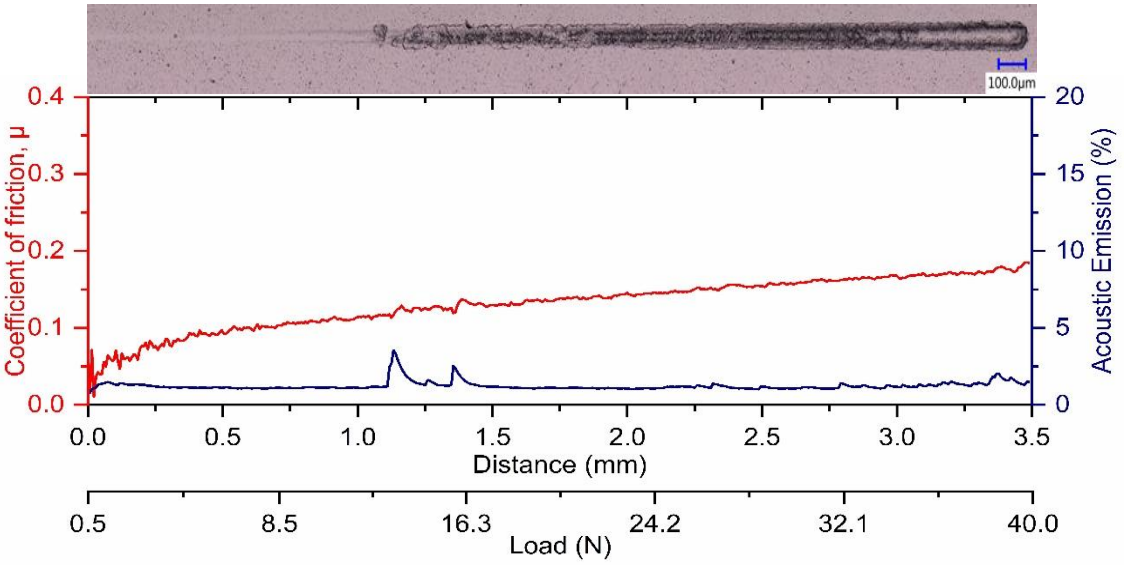

Figure B.20. *Micro-scratch test data with optical images of the scratch track for CrN coating deposited at -20 V bias voltage, 4 Pa nitrogen gas pressure and with approximately 1.8 µm coating thickness.*

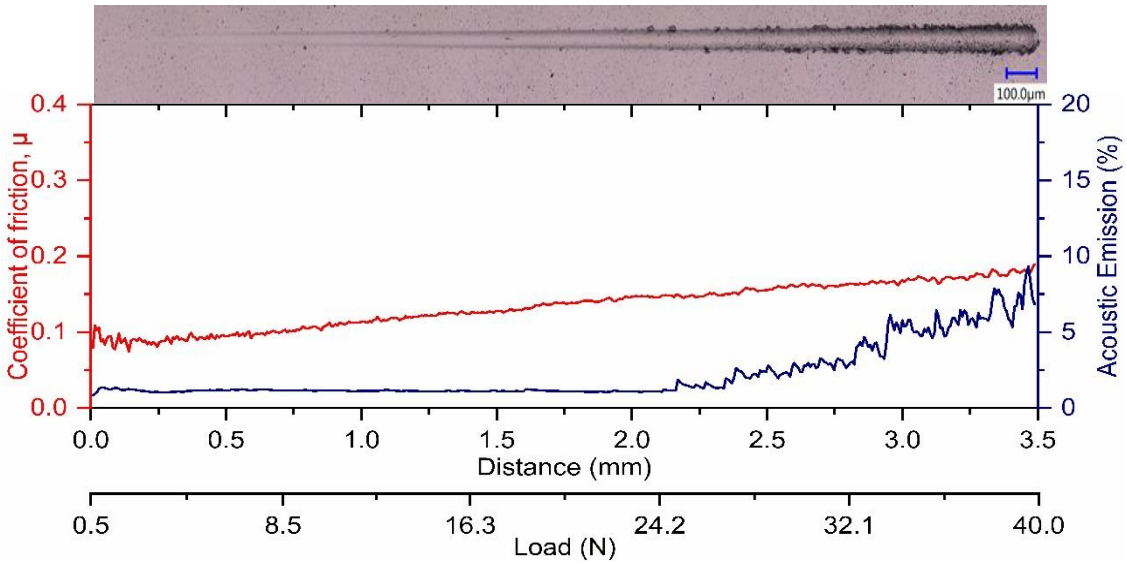

Figure B.21. *Micro-scratch test data with optical images of the scratch track for CrN coating deposited at -50 V bias voltage, 4 Pa nitrogen gas pressure and with 1.81 µm coating thickness.*

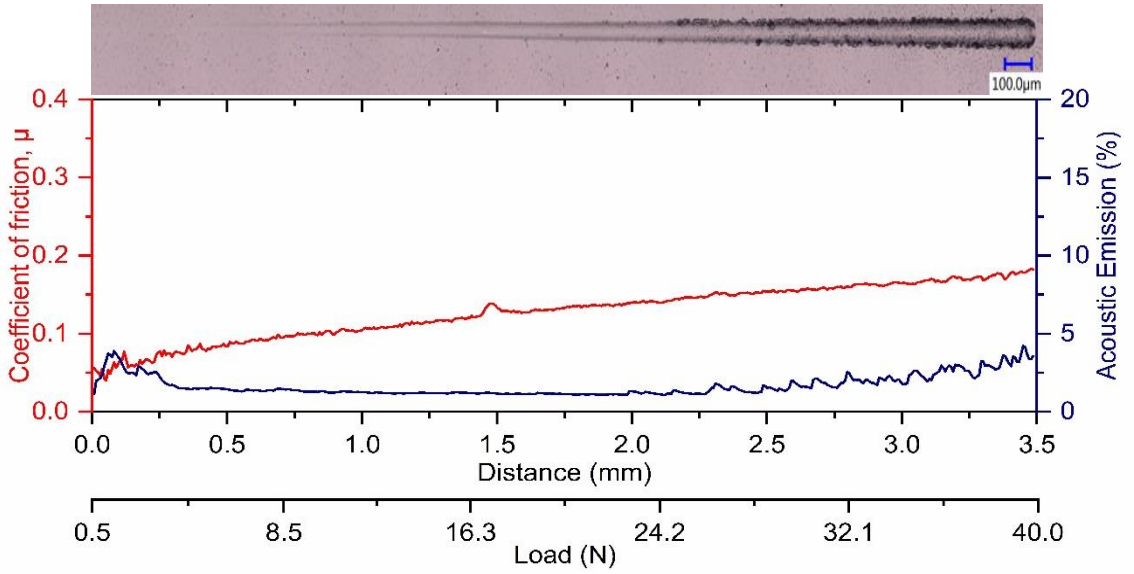

Figure B.22. *Micro-scratch test data with optical images of the scratch track for CrN coating deposited at -100 V bias voltage, 4 Pa nitrogen gas pressure and with approximately 1.8 µm coating thickness.*

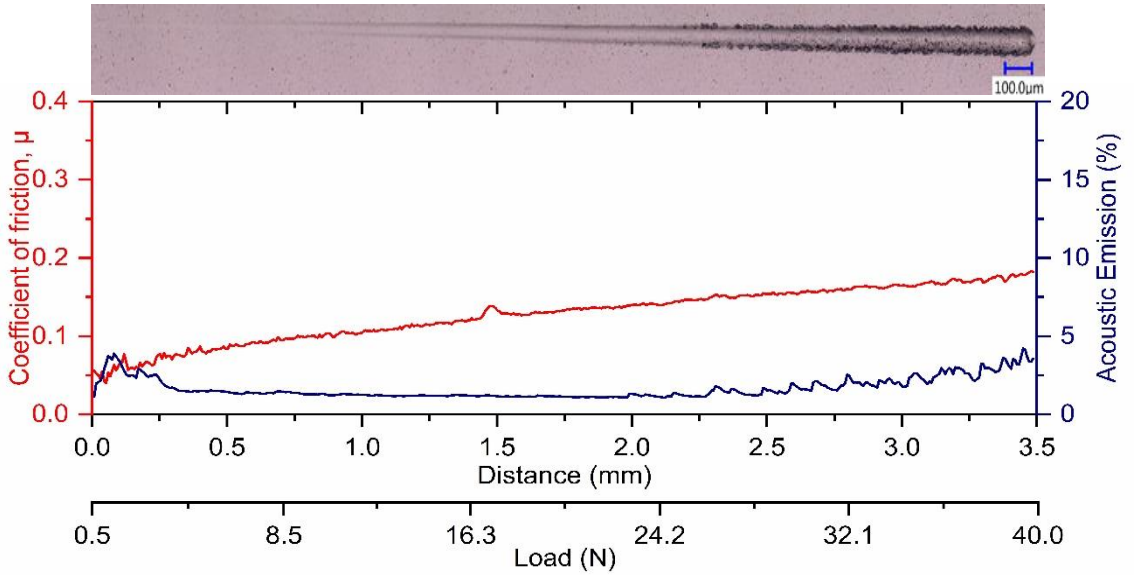

Figure B.23. *Micro-scratch test data with optical images of the scratch track for CrN coating deposited at -150 V bias voltage, 4 Pa nitrogen gas pressure and with approximately 1.8 µm coating thickness.*

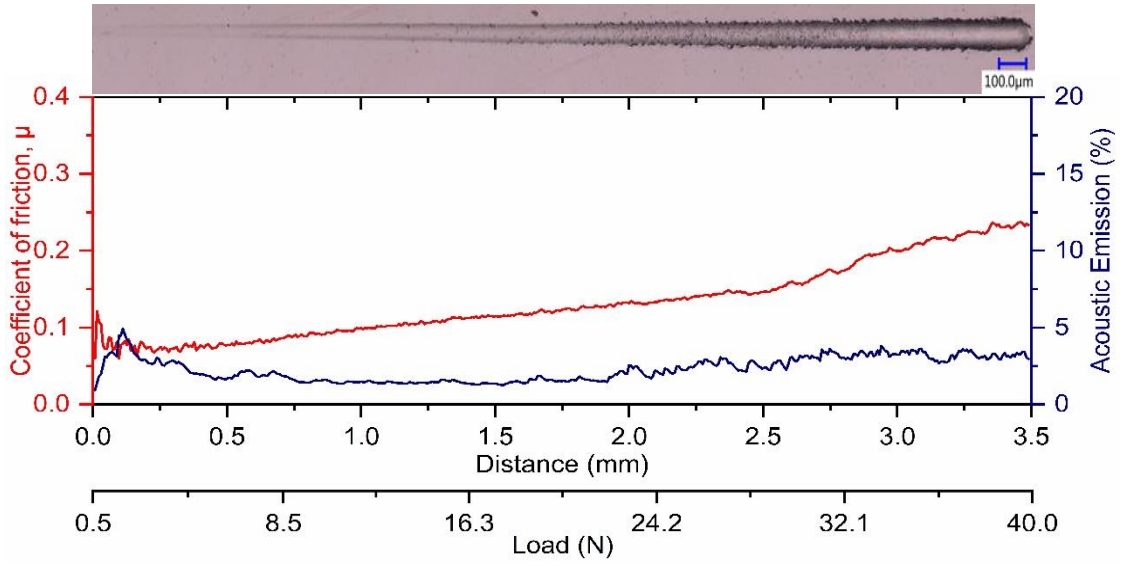

Figure B.24. *Micro-scratch test data with optical images of the scratch track for CrN coating deposited with 1.21 µm coating thickness at 4 Pa nitrogen gas pressure and -20 V bias voltage.*

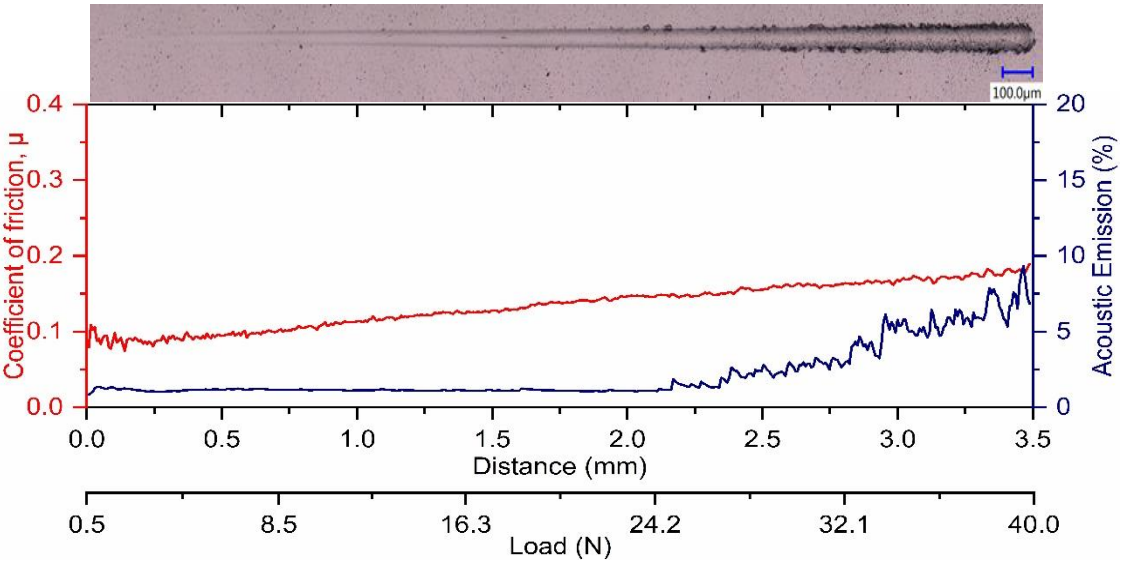

Figure B.25. *Micro-scratch test data with optical images of the scratch track for CrN coating deposited with 1.81 µm coating thickness at 4 Pa nitrogen gas pressure and -20 V bias voltage.*

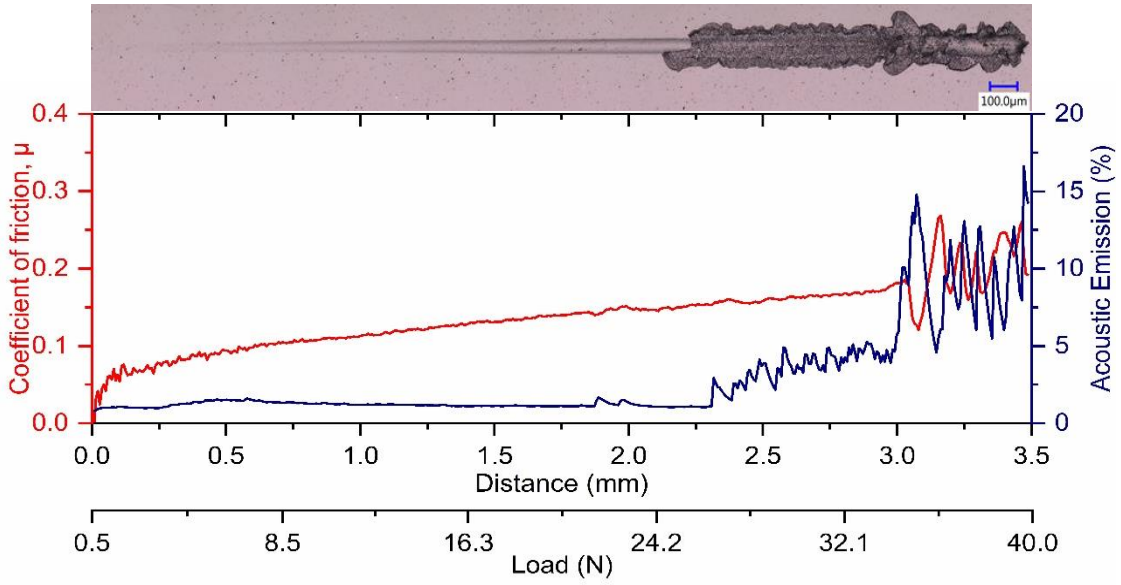

Figure B.26. *Micro-scratch test data with optical images of the scratch track for CrN coating deposited with 5.74 µm coating thickness at 4 Pa nitrogen gas pressure and -20 V bias voltage.*

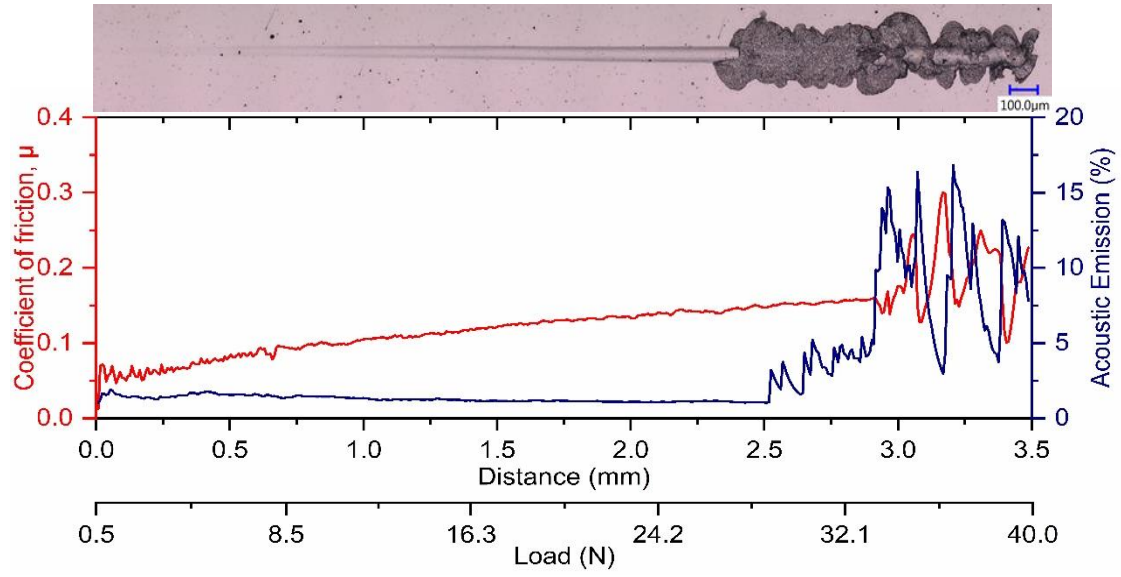

Figure B.27. *Micro-scratch test data with optical images of the scratch track for CrN coating deposited with 7.52 µm coating thickness at 4 Pa nitrogen gas pressure and -20 V bias voltage.*

B.4. Conclusions

In this research, a self-adaptive CrN coating was developed using a systematic framework. Tuning of the deposition parameters for the CrN coating was done methodically and its effects were studied in detail. CrN coatings with various combinations of nitrogen gas pressure, bias voltage, and coating thickness were deposited and their performances were evaluated through a tool life study. It was found that a 4Pa nitrogen gas deposition pressure, -50V bias voltage, and 1.81 μm coating thickness gave the best tool wear performance for the CrN coating. Detailed investigations of the micromechanical properties revealed that these deposition parameters provided an optimized combination of coating hardness and elastic modulus that led to better tool performance. It was also observed that an increase in negative bias voltage increases the yield stress of the coatings whereas variation in nitrogen gas pressure and coating thickness has little effect on yield stress. Micro-scratch tests showed that thicker coatings undergo more drastic deformation than thinner coatings and very low bias voltage leads to drastic failure of the coating. Nitrogen gas pressure variation showed minimal effects on the failure behaviour of the coatings.

B.5. References

1. Chowdhury, M. S. I.; Bose, B.; Fox-Rabinovich, G.; Veldhuis, S. C. Investigation of the Wear Performance of TiB_2 Coated Cutting Tools during the Machining of Ti6Al4V Alloy. Materials 2021, 14 (11). https://doi.org/10.3390/ma14112799.
2. Lancaster, J. K.; The relationship between the wear of carbon brush materials and their elastic moduli, Br. J. Appl. Phys. 1963, 14, 497–505. https://doi.org/10.1088/0508-3443/14/8/311.
3. Spurr, R.; Newcombe, T.; The friction and wear of various materials sliding against unlubricated surfaces of different types and degrees of roughness, in: Proceedings of the Conference on Lubrication and Wear Institution of Mechanical Engineers, in: Inst. Mech. Eng., London, UK 1957, 269.
4. Leyland, A.; Matthews, A. On the significance of the H/E ratio in wear control: A nanocomposite coating approach to optimised tribological behaviour. Wear 2000, 246, 1–11.
5. Beake, B.; Fox-Rabinovich, G. Progress in high temperature nanomechanical testing of coatings for optimising their performance in high speed machining. Surf. Coat. Technol. 2014, 255, 102–111.
6. Beake, B.; Fox-Rabinovich, G.; Veldhuis, S.; Goodes, S. Coating optimisation for high speed machining with advanced nanomechanical test methods. Surf. Coat. Technol. 2009, 203, 1919–1925.
7. Chowdhury, M.; Chowdhury, S.; Yamamoto, K.; Beake, B.; Bose, B.; Elfizy, A.; Cavelli, D.; Dosbaeva, G.; Aramesh, M.; Fox- Rabinovich, G.; et al. Wear behaviour

of coated carbide tools during machining of Ti6Al4V aerospace alloy associated with strong built up edge formation. Surf. Coatings Technol. 2017, 313, 319–327.